

University of Groningen

Modelling, simulation and analysis of security of supply scenarios in integrated gas and electricity transmission networks

Pambour, Kwabena Addo

IMPORTANT NOTE: You are advised to consult the publisher's version (publisher's PDF) if you wish to cite from it. Please check the document version below.

Document Version

Publisher's PDF, also known as Version of record

Publication date:
2018

[Link to publication in University of Groningen/UMCG research database](#)

Citation for published version (APA):

Pambour, K. A. (2018). Modelling, simulation and analysis of security of supply scenarios in integrated gas and electricity transmission networks [Groningen]: University of Groningen

Copyright

Other than for strictly personal use, it is not permitted to download or to forward/distribute the text or part of it without the consent of the author(s) and/or copyright holder(s), unless the work is under an open content license (like Creative Commons).

Take-down policy

If you believe that this document breaches copyright please contact us providing details, and we will remove access to the work immediately and investigate your claim.

Downloaded from the University of Groningen/UMCG research database (Pure): <http://www.rug.nl/research/portal>. For technical reasons the number of authors shown on this cover page is limited to 10 maximum.

Modelling, simulation and analysis of security of supply scenarios in integrated gas and electricity transmission networks

Kwabena Addo Pambour

Colophon

This PhD-project was partly funded by the European Commission's Joint Research Centre, Directorate (C) for Energy, Transport and Climate and supervised by the Center for Energy and Environmental Sciences (IVEM), which is part of the Energy and Sustainability Research Institute of the University of Groningen (ESRIG), the Netherlands.

The views expressed are purely those of the author, and may not in any circumstances be regarded as stating an official position of the European Commission.

ISBN: 978-94-034-0910-8

ISBN: 978-94-034-0909-2 (electronic version)

© 2018 Kwabena Addo Pambour. All rights reserved. No part of this publication may be reproduced, stored in a retrieval system, or transmitted, in any form or by any means, without prior permission in writing from the author.

Dutch translation: Dr. Tom van der Hoeven

Printed by Zalsman Groningen B.V.

Email: kwabena.pambour@gmail.com



/ university of
groningen

Modelling, simulation and analysis of security of supply scenarios in integrated gas and electricity transmission networks

PhD Thesis

to obtain the degree of PhD at the
University of Groningen
on the authority of the
Rector Magnificus Prof. E. Sterken
and in accordance with
the decision by the College of Deans.

This thesis will be defended in public on
Monday 17 September 2018 at 16.15 hours

by

Kwabena Addo Pambour

born on December 13, 1983
in Accra, Ghana

Supervisor

Prof. R. Herber

Co-supervisor

Dr. R. Bolado-Lavin

Assessment committee

Prof. A. Faaij

Prof. H. Saxen

Prof. X.-P. Zhang

Dedicated to the memory of Prof. Gerard P.J. Dijkema

Acknowledgment

This dissertation is the outcome of six years of research at the Joint Research Centre of the European Commission (EC-JRC), in Petten, the Netherlands, and the Center for Energy and Environmental Sciences Research Group of the Energy and Sustainability Institute of the University of Groningen (ESRIG-RUG). I would like to use this opportunity to express my gratitude to the people and organisations that contributed to the successful completion of this dissertation.

First of all, I would like to thank the EC-JRC for funding my research and for supporting me even after the end of my contract to complete this dissertation. I remain grateful for this opportunity that provided the platform to perform research in the area of security of energy supply. My sincere gratitude also goes to my research group at ESRIG-RUG for their academic support at the time when I was on the search for a research group interested in following my work. I would also like to thank my former employer Liwacom Informationstechnik GmbH (Liwacom), who gave me the opportunity to continue my research in part time while working as an engineer and software consultant in the natural gas industry.

I would like to express my greatest appreciation and my most special thanks to my co-supervisor Dr. Ricardo Bolado-Lavin for his continuous support and confidence in my research. The research presented in this thesis is the product of his daily guidance and knowledge in the energy field. I am most certainly also grateful to my former supervisor Prof. Gerard Dijkema, of blessed memory for his support and invaluable guidance. I also thank my supervisor Prof. Herber for enabling a seamless continuation and successful completion of my research.

My sincere appreciation and special gratitude also goes to Dr. Tom van der Hoeven for his support and for the productive meetings and discussions on modelling of gas transport systems. The simulation tool **SAInt** is a product of his excellent didactic skills and his great knowledge in modelling of energy systems.

While working for the EC-JRC and Liwacom, I was blessed to be surrounded by competent and helpful colleagues who provided guidance and support during my research. I am thankful to Dr. Marcelo Masera for his leadership and advice during my time at the EC-JRC. I would also like to thank Dr. Burcin Cakir Erdener, for many fruitful discussions and great collaborations, which resulted in a number of scientific publications. I would also like to thank my former colleagues Dr. Nuria Rodríguez Gómez and Dr. Nicola Zaccarelli for their support and expertise during my research. I am also grateful to Prof. Alfredo López and Prof. Francisco Javier Elorza from Universidad Politécnica de Madrid, Spain for their support and guidance at the start of my research. I am also thankful to Dr. Günter Wagner and my former colleagues at Liwacom, who were always supportive and encouraging. I am grateful to have been given the opportunity to gain experience in a private company and the natural gas industry.

Beside, the support from my former colleagues, I have been extremely lucky to have been surrounded by great friends, who have always been there in times of need. Many thanks to my friends Rostand, Dejoly, Esther and Carlo. Carlo was also my colleague and room-mate during my first two years at the EC-JRC. Thank you for your friendship, your encouragement and unconditional support.

Finally, I would like to express my special thanks to my wife Amma, my parents, my sister Constanze and all my relatives for their prayers, their patience and for always being present in times of need.

Kwabena Addo Pambour - September 2018

Contents

Nomenclature	V
List of Figures	XI
List of Tables	XVII
List of Listings	XIX
1. Introduction	1
1.1. Background and Motivation	1
1.1.1. Gas Supply to Power System Networks	2
1.1.2. Energy Storage through Power-to-Gas	3
1.1.3. Power Supply to Gas Pipeline Networks	3
1.1.4. Security of Supply in interconnected Gas and Electric Power Systems	4
1.2. Modelling of Gas and Electric Transmission Networks	5
1.2.1. Model Requirements	6
1.2.2. State of the Art	7
1.3. Research Questions	11
1.4. Thesis Outline	14
2. Dynamic Simulation Model for Gas Transmission Networks	17
2.1. Introduction	17
2.2. State of the Art	22
2.3. Methodology	24
2.3.1. Modelling of Pipelines	25
2.3.2. Modelling of Non-Pipe Facilities	32
2.3.3. Network Description	49
2.3.4. System of Equations for the Total Network	52
2.3.5. Boundary Conditions	54
2.3.6. Algorithm	57

2.4.	Model Benchmarking	59
2.4.1.	Simulation of a triangular Network	60
2.4.2.	Influence of the inclination term	64
2.4.3.	Simulation of a 30-Nodes Gas Network Model	65
2.5.	Model Application	67
2.6.	Conclusion	74
3.	Model Extension and Implementation into a Simulation Tool	77
3.1.	Introduction	77
3.2.	Definition of Risk	78
3.3.	Measures to Mitigate the Impact of Gas Disruptions	80
3.4.	Extended Model for Gas Infrastructures	83
3.5.	Modelling of Measures to Mitigate the Impact of Disruptions	95
3.6.	Model Application	96
3.7.	Conclusion	106
4.	Co-Simulation Framework for Gas and Electricity Networks	113
4.1.	Introduction	113
4.2.	Electric Power System Models	115
4.2.1.	AC-Power Flow Model	117
4.2.2.	Distributed Slack Bus Model	119
4.2.3.	AC-Optimal Power Flow Model	120
4.3.	Interconnection between Gas and Power Systems	122
4.4.	Integrated Co-Simulation Framework for Security of Supply Analysis . . .	123
4.5.	Model Application	127
4.6.	Conclusions	141
5.	Combined Simulation of integrated Gas and Electricity Networks	145
5.1.	Introduction	145
5.2.	Methodology	148
5.2.1.	Extended Power System Model	150
5.2.2.	Extended Coupling Equations	154
5.2.3.	Algorithm for solving the Combined Simulation Model	155
5.3.	Security of Energy Supply Parameters	157
5.4.	Model Application	160
5.4.1.	Case 0 - Base case scenario with intermittent wind power generation and backup by spinning reserve GFPP	164
5.4.2.	Case 1 - Disruption in compressor station CS.1	172

5.4.3. Case 2 - Full withdrawal capacity at gas storage facility to mitigate the impact of compressor station disruption	178
5.5. Conclusion	182
6. Conclusion	185
A. Input Data for 30-Nodes Gas Network	191
B. Combined Simulation of Gas and Electricity Networks	193
B.1. Primal Dual Interior Point Method	193
B.2. Data for sample gas and electricity network used in the case study	195
B.3. Simulation results for combined steady state simulation	199
B.4. Description of supplementary data available in the electronic version	199
B.4.1. SAInt Project files	199
B.4.2. Animation videos for the case studies generated with SAInt	203
B.4.3. Simulation protocol for the case studies generated with SAInt	203
B.4.4. Comparison between SAInt & MATPOWER for AC-OPF	204
Bibliography	XXI
Summary	XXXIII
Samenvatting	XLIII
List of Publications	LIII
Author Biography	LV

Nomenclature

Abbreviations

AC	Alternating current
AC-OPF	Alternating current -optimal power flow
AC-PF	Alternating current - power flow
ACS	Automatic control system
API	Application programming interface
CA	Competent authority
CBE	Cross border export
CBI	Cross border import
CCH	Constraints and control handling algorithm
CEI	Critical energy infrastructure
CGS	City gate station
CS	Compressor station
DC	Direct current
DC-OPF	Direct Current - optimal power flow
DFC	Dynamic event feasibility algorithm
DTA	Dynamic time step adaptation method
EC	European Commission
EDC	Electric driven compressor
ED	Economic dispatch
ENS	Energy not supplied
ENTSP	Energy not supplied per time span
EP	Emergency plan
EU	European Union
FMEA	Failure mode and effect analysis

GFPP	Gas fired power plants
GSUB	Subsystem of gas network
GTS	Gas transport system
GUI	Graphical user interface
HAZOP	Hazard and operability analysis
IND	Large industrial customer
KCL	Kirchhoff's current law
LNG	Liquefied natural gas
MOP	Maximum operating pressure
MS	Member state
NGTS	National gas transport system
OPF	Optimal power flow
P2G	Power to gas
PAP	Preventive action plan
PDE	Partial differential equation
PENS	Percentage of gas or energy not supplied
PI	Inlet pressure
PMIN	Minimum pressure
PNS	Power not supplied
PO	Outlet pressure
PRO	Production field
RA	Reserve allocation
RA	Risk assessment
RES	Renewable energy source
SAInt	Scenario analysis interface for energy systems
SCADA	Supervisory control and data acquisition
SCE	Simulation control evaluation algorithm
SCO	Simulation control object
SCUC	Security constrained unit commitment
SNG	Synthetic natural gas
STE	Slow transient equation
SVT	Survival time

TSO	Transmission system operator
TSP	Time span of energy not supplied
UC	Unit commitment
UGS	Underground gas storage

Mathematical Symbols

A	Pipe cross-sectional area	$[m^2]$
BP	Control mode bypass	
C	Control algorithm of controller	
c	Speed of sound	$[m \cdot s^{-1}]$
CV	Gas control volume	$[m^3]$
ρ	relative density	$[-]$
D	Pipe diameter	$[m]$
e	Euler's number	$[-]$
f	Fraction of driver power provided by electricity network	$[-]$
\mathbf{G}	Set of (differential) equations describing the physical processes at a station	
g	Gravitational acceleration $9.81 \ [m \cdot s^{-2}]$	$[m \cdot s^{-2}]$
GCV	Upper calorific value	$[J \cdot sm^{-3}]$
h_1	Elevation at inlet	$[m]$
h_2	Elevation at outlet	$[m]$
H_{ad}	Adiabatic head/specific enthalpy	$[J \cdot kg^{-1}]$
H_{real}	Specific enthalpy required for the actual compression process	$[J \cdot kg^{-1}]$
D	Number of grid segments per pipe	$[m]$
k	Pipe roughness	$[m]$
L	Load at supply or demand node	$[sm^3 \cdot s^{-1}]$
l	Pipe length	$[m]$
l_e	Effective pipe length	$[m]$
LP	Linepack	$[sm^3]$
M	Mass flow rate	$[kg \cdot s^{-1}]$
OFF	Control mode off	
P	Square gas pressure	$[bar^2]$

p	Gas pressure	[bar]
p_c	Critical gas pressure	[bar]
p_i	Inlet gas pressure	[bar]
$p_{i, set}$	Inlet pressure set point	[bar]
p_m	Mean pipeline pressure	[s]
p_{max}	Maximum delivery pressure	[bar]
p_{min}	Minimum delivery pressure	[bar]
p_o	Outlet gas pressure	[bar]
$p_{o, set}$	Outlet pressure set point	[bar]
PWD_{max}	Maximum available driver power	[W]
PWD_{set}	Driver power set point	[W]
PWD	Driver power	[W]
PWS	Shaft power	[W]
Q	Gas flow rate	[sm ³ · s ⁻¹]
Q_f	Required fuel gas for compression	[sm ³ · s ⁻¹]
Q_{in}	Gas inflow	[sm ³ · s ⁻¹]
Q_{out}	Gas outflow	[sm ³ · s ⁻¹]
Q_{set}	Flow rate set point	[sm ³ /s]
Q_{vol}	Volumetric gas flow	[m ³ · s ⁻¹]
$Q_{vol, max}$	Maximum volumetric gas flow rate	[m ³ · s ⁻¹]
$Q_{vol, min}$	Minimum volumetric gas flow rate	[m ³ · s ⁻¹]
$Q_{vol, set}$	Volumetric flow rate set point	[m ³ · s ⁻¹]
R	Specific gas constant	[J · (kg · K) ⁻¹]
R_f	Pipe resistance coefficient	[bar ² · (sm ³) ⁻²]
Re	Reynolds number	[−]
rpm	Revolutions per minute	[min ⁻¹]
SUMLP	Total linepack in network	[sm ³]
SUML	Flow balance, sum of supply minus demand	[sm ³ · s ⁻¹]
T	Gas temperature	[K]
t	Time	[s]
T_{amb}	Ambient temperature	[K]
T_c	Critical gas temperature	[K]

T_i	Inlet gas temperature	[K]
v	Gas flow velocity	[m · s ⁻¹]
V_{geo}	Geometric pipe volume	[m ³]
V_{max}	Maximum gas flow velocity	[m · s ⁻¹]
V_{set}	Flow velocity set point	[m · s ⁻¹]
x	Space coordinate along pipe length	[m]
\vec{X}	Set of state variables at station inlet and outlet	
\vec{X}_{lim}	Set of station constraints	
\vec{X}_{met}	Set of metered state variables	
\vec{X}_{set}	Set of control set points available to the dispatcher	
\vec{Y}_{act}	Set of actuators	
Z	Gas compressibility factor	[−]
\vec{Z}_{ext}	Set of external factors directly influencing the physical process	
Z_i	Inlet gas compressibility factor	[−]

Greek Symbols

Δp_{set}	Pressure difference set point	[bar]
Δt	Time step	[s]
ϵ	Residual tolerance	[−]
η	Dynamic viscosity	[kg · (m · s) ⁻¹]
η_{ad}	Adiabatic efficiency	[−]
η_e	Pipe efficiency	[−]
η_m	Mechanical efficiency of driver	[−]
κ	Isentropic exponent	[−]
λ	Friction factor	[−]
λ_e	Effective friction factor	[−]
Π	Compression ratio between outlet and inlet pressure	[−]
Π_{max}	Maximum compression ratio	[−]
Π_{min}	Minimum compression ratio	[−]
ρ	Gas density	[kg · m ⁻³]
ρ_n	Density at reference conditions	[kg · sm ⁻³]

τ Shear force $[N \cdot m^{-2}]$

List of Figures

2.1.	Natural Gas Infrastructure	19
2.2.	Forces acting on a control volume in a general gas pipeline	25
2.3.	Functional diagram of a control system in compressor or regulator station	32
2.4.	Compressor station with two stages and a parallel configuration of units .	34
2.5.	a) Typical operating envelope of a centrifugal compressor , b) Proposed aggregated operating region for the generic compressor station model . . .	36
2.6.	Typical schematic structure of a gas regulator and metering station	39
2.7.	Typical schematic structure of the above ground components of an underground gas storage facility	44
2.8.	Typical UGS envelopes for depleted gas fields, aquifer and salt cavern storage for the withdrawal process (top) and the injection process (bottom) .	45
2.9.	Typical schematic structure of a LNG regasification terminal	47
2.10.	Law of mass conservation for a nodal control volume in a gas network .	53
2.11.	Flow chart for transient simulation	58
2.12.	Topology of the 3 pipeline network	60
2.13.	Initial conditions and boundary conditions for the transient simulation of the 3 pipeline network a) pressure condition at the supply node 1 and b) Load profile at the demand nodes 2 and 3	62
2.14.	Computed pressure profiles at node 2 and node 3 compared to results from the literature and SIMONE	62
2.15.	a) average pipe flow rate in pipelines b) total line pack in network	63
2.16.	a) resulting load profile at supply node 1 b) load balance of the network .	63
2.17.	Computed pressure profiles at node 2 and node 3 for different elevations H_1 of node 1 compared to results from SIMONE	65
2.18.	Steady state solution for the sample network obtained with the developed gas model	66
2.19.	Steady state solution for the reference network obtained with SIMONE . .	67
2.20.	Comparison of simulation results for the sample network obtained with developed gas model and SIMONE	68

2.21. Steady state pressure and load distribution for the Bulgarian and Greek NGTS	69
2.22. Load profile assigned to city gate stations	70
2.23. Load balance and line pack evolution of the network	71
2.24. Load & pressure evolution at CBI Negru Voda	71
2.25. Load & pressure evolution at CBE Malcoclar	72
2.26. Load & pressure evolution at UGS Chiren	72
2.27. Load & pressure evolution at CBE Zidilova	72
2.28. Load & pressure evolution at CBI Kipi	73
2.29. Load & pressure evolution at LNG Terminal Revythoussa	73
3.1. Flow diagram of the transient hydraulic solver implemented in the simulation tool SAInt	84
3.2. Constraints and Control Handling Algorithm for compressor stations implemented in the simulation tool SAInt	91
3.3. Constraints and Control Handling Algorithm for entry and exit stations implemented in the simulation tool SAInt	93
3.4. Constraints and Control Handling Algorithm for UGS facilities implemented in the simulation tool SAInt	94
3.5. Constraints and Control Handling Algorithm for LNG Terminals implemented in the simulation tool SAInt	95
3.6. Snapshot of the network model of the Bulgarian-Greek NGTS in the graphical user interface of the simulation tool SAInt	97
3.7. Assigned subsystems in the Bulgarian-Greek simulation model	98
3.8. Snapshot of the SAInt -Node-Editor showing the assigned constraints to CBI-Negru Voda	100
3.9. Snapshot of the SAInt -Node-Editor showing the assigned constraints to CBI-Kipi	101
3.10. Snapshot of SAInt -Storage Editor (left) and LNG-Terminal-Editor (right) showing the assigned properties for UGS-Chiren (left) and LNG-Terminal-Revythoussa (right)	102
3.11. SAInt -Profile-Editor showing the relative 24 h load profile assigned to demand nodes representing city gate stations	103
3.12. Snapshot of the SAInt scenario definition table showing the defined boundary conditions disruption events and mitigation strategy for the case study	104
3.13. Time series of Line Pack (LP) and Minimum Pressure (PMIN) in the subsystems EL_NORTH (GSUB.0) and EL_SOUTH (GSUB.3)	105

3.14. Time series of delivered gas quantity, station control, load and pressure for the Cross Border Import Negru Voda	105
3.15. Time series of delivered gas quantity, station control, load and pressure for the Cross Border Import Kipi	106
3.16. Time series of station controls for compressor stations CS-Ihtiman (CS.8), CS-Petrich (CS.9) & CS-Nea Messimvria (CS.10)	107
3.17. Time series of inlet pressure (PI) and outlet pressure (PO) for compressor stations CS-Ihtiman (CS.8), CS-Petrich (CS.9) & CS-Nea Messimvria (CS.10)	108
3.18. Time series of flow rate (Q) for compressor stations CS-Ihtiman (CS.8), CS-Petrich (CS.9) & CS-Nea Messimvria (CS.10)	109
3.19. Time series of supply, storage inventory, delivered gas quantity, station control, pressure and storage envelope for the Underground Gas Storage Facility Chiren	110
3.20. Time series of supply, storage inventory, delivered gas quantity, station control, pressure and storage envelope for the LNG-Terminal Revythoussa	111
4.1. Generic branch model	116
4.2. Flow chart of the proposed Simulation Framework SAInt , showing the implemented algorithm.	125
4.3. Integrated gas and power network applied in the case study	128
4.4. Load profiles gas (left side) and power (right side) networks.	130
4.5. Timing of initial and cascading events for Scenario 1	134
4.6. Timing of initial and cascading events for Scenario 2	135
4.7. Time evolution of gas supply and pressure at the cross border import (CBI) node for the computed scenarios	136
4.8. Time evolution of gas supply and pressure at the production field for the computed scenarios.	136
4.9. Time evolution of regasification rate and pressure at the liquefied natural gas (LNG) terminal for the computed scenarios.	137
4.10. Time evolution of flow balance (sum of inflow minus sum of outflow) and linepack for the computed scenarios.	137
4.11. Time evolution of withdrawal rate and pressure at underground gas storage (UGS) facility for the computed scenarios.	138
4.12. Time evolution of load and pressure of failed GFPPs in scenario 1.	138
4.13. Time evolution of load and pressure of failed GFPPs in scenario 2.	139
4.14. Time evolution of bus voltage before load shedding and after for scenario 1	139
4.15. Time evolution of bus voltages before load shedding and after for Scenario 2	140

4.16. Load and pressure profile of CBE_1 for scenario 1.	140
5.1. Linear penalty function $f(P_{D,i})$ and constraints for dispatchable loads	152
5.2. Flow chart of the algorithm for solving the coupled gas and electric power system model	156
5.3. Security of supply indicators	158
5.4. 25-Node gas model used for the case studies	161
5.5. Modified version of IEEE 30-Bus power system model	162
5.6. Snapshot of SAInt-GUI showing results of the combined steady state computation for the gas network in the case study	165
5.7. Snapshot of SAInt-GUI showing results of the combined steady state computation for the electric network in the case study	166
5.8. Load profile assigned to CGS in gas network (left side) and active power load at buses in electric power network (right side)	167
5.9. Relative profile for variable and intermittent wind power generation assigned to bus GEN.22	167
5.10. SAInt scenario defintion table showing the defined boundary conditions for the electric network for case 0	168
5.11. Case 0 - Time plot for active power generation (PG) at buses GEN.12 and GEN.22	169
5.12. Case 0 - Time plot for Energy Not Supplied (ENS) for the total gas (blue curve) and total electric network (green curve)	169
5.13. Case 0 - Time plot for Percentage of Energy not Supplied (ENS) for the total gas (blue curve) and total electric network (green curve)	170
5.14. Case 0 - Time plot for linepack in subsystem GSUB.EAST (LP), nodal pressure (P) and fuel gas offtake for power generation (Q) at node NO.4	171
5.15. Case 1 - Time plot of the station control ($CTRL$) of compressor station CS.1	173
5.16. Case 1 - Time plot of the inlet and outlet pressure of compressor station CS.1	173
5.17. Case 1 - Time plot for active power generation (PG) at buses GEN.12 and GEN.22	174
5.18. Case 1 - Time plot for Energy Not Supplied (ENS) for the total gas (blue curve) and total electric network (green curve)	174
5.19. Case 1 - Time plot for Percentage of Energy Not Supplied (PENS) for the total gas (blue curve) and total electric network (green curve)	175
5.20. Case 1 - Time plot for Time Span of Energy Not Supplied (TSP) for the total gas (blue curve) and total electric network (green curve)	175

5.21. Case 1 - Time plot for Energy Not Supplied per Time Span of Energy Not Supplied (ENSTSP) for the total gas (blue curve) and total electric network (green curve)	176
5.22. Case 1 - Time plot for linepack in subsystem GSUB.EAST (<i>LP</i>), nodal pressure (<i>P</i>) and fuel gas offtake for power generation (<i>Q</i>) at node NO.4 .	177
5.23. Case 2 - Time plot of gas offtake (<i>Q</i>) gas pressure (<i>P</i>) station control (<i>CTRL</i>) and the operating gas storage envelope (withdrawal and injection rate versus working inventory) for the UGS facility connected to node NO.4	179
5.24. Case 2 - Time plot for Energy Not Supplied (ENS) for the total gas (blue curve) and total electric network (green curve)	180
5.25. Case 2 - Time plot for Percentage of Energy Not Supplied (PENS) for the total gas (blue curve) and total electric network (green curve)	180
5.26. Case 2 - Time plot for Time Span of Energy Not Supplied (TSP) for the total gas (blue curve) and total electric network (green curve)	181
5.27. Case 2 - Time plot for Energy Not Supplied per Time Span of Energy Not Supplied (ENSTSP) for the total gas (blue curve) and total electric network (green curve)	181
A.1. Relative Load profile assigned to demand nodes of the sample network . .	191

List of Tables

2.1.	Overview of available control modes and constraints settings for non-pipe facilities modeled as elements	37
2.2.	Overview of available control modes and constraints settings for non-pipe facilities modelled as nodes	41
2.3.	Basic elements comprising gas transport networks	50
2.4.	Classification and characteristics of nodes in the network	51
2.5.	Control modes for non-pipe facilities and their mathematical implementation	55
2.6.	Overview of available scenario parameter (control modes) for facilities modelled as demand, supply or storage nodes and their mathematical implementation	56
2.7.	Pipe data of the 3 pipeline network	60
2.8.	Input parameters for the transient simulation of the 3 pipeline network . .	61
2.9.	Inclination angles for different elevations of node 1	64
2.10.	Input parameter for transient simulation of the Bulgarian-Greek network model	71
3.1.	Security of gas supply measures	81
3.2.	Correspondence between EP measures and network facilities needed to implement them	82
3.3.	Overview of the properties of the scenario definition object and the simulation control object and their corresponding data types	85
3.4.	Overview of the properties of the profile object and their corresponding data types	85
3.5.	Properties of the Bulgarian-Greek NGTS	99
3.6.	Properties of the assigned subsystems	99
3.7.	Input parameter for transient simulation of the Bulgarian-Greek network model	99
4.1.	Basic components in an electric network model	118

4.2. Compressor station control (PRSET—Pressure Ratio Set Point) and constraints (PRMAX— Maximum Pressure Ratio, PWMAX—Maximum Available Driver Power, POMAX—Maximum Discharge Pressure, PIMIN—Minimum Suction Pressure).	130
4.3. Input data for facilities supplying the gas system with gas.	130
4.4. Input data for GFPPs connected to the gas and electric power system. Numbering of GFPPs corresponds to the numbering of the solid interconnection lines in Fig. 4.3	131
4.5. Input data for the gas simulator.	131
5.1. Input parameter for the sample combined gas and power transmission network	163
5.2. Summary of results for security of supply parameters for gas network . . .	178
5.3. Summary of results for security of supply parameters for electric network	178
A.1. Input parameter for the dynamic simulation of the 30-Nodes sample network and the combined model	191
A.2. Input data for the reference network	192
B.1. Input data for nodes in gas model	195
B.2. Input data for pipelines in gas model	196
B.3. Input data for compressor stations	196
B.4. Input data for electric power supply to LNG terminal	196
B.5. Input data for buses in power network. Priority factor λ is chosen such that buses connected to LDSs are less likely to be affected by load shedding than buses connected to INDs and CBEs.	197
B.6. Input data for transmission lines in power network	198
B.7. Input data for generation units in power model	199
B.8. Nodal control set points and results for initial combined steady state computation. Negative Q means gas supply, positive Q gas offtake.	200
B.9. Compressor stations control set points and results for initial combined steady state computation.	200
B.10. Results for power system buses for initial combined steady state simulation	201
B.11. Results for power system generation units for initial combined steady state simulation	201

List of Listings

3.1. Instantiating a simulation control object for modeling the transition of a compressor station from operating into bypass in SAInt using the object-oriented programming language VB.NET	87
3.2. Excerpt of the Simulation Control Evaluation Algorithm (SCE) for a compressor station implemented in SAInt using the object-oriented programming language VB.NET	88

1. Introduction

This chapter is based on the following published, peer reviewed journal articles:

- K. A. Pambour, B. Cakir Erdener, R. Bolado-Lavin, and G. P. Dijkema, “[SAInt - A novel quasi-dynamic Model for assessing Security of Supply in coupled Gas and Electricity Transmission Networks](#),” in *Applied Energy*, vol. 203, pp. 829 – 857, 2017.
- K. A. Pambour, B. Cakir Erdener, R. Bolado-Lavin, and G. P. Dijkema, “[Development of a simulation framework for analyzing Security of Supply in integrated gas and electricity systems](#),” in *Applied Sciences*, vol. 7, no. 1, pp. 47, 2017.
- B. Cakir Erdener, K. A. Pambour, R. B. Lavin, and B. Dengiz, “[An integrated simulation model for analysing electricity and gas systems](#),” in *International Journal of Electrical Power & Energy Systems*, vol. 61, no. 0, pp. 410 – 420, 2014.

1.1. Background and Motivation

Energy policies in the EU (European Union) and in many other regions in the world are aiming at reducing the emission of green house gases (GHG) to combat global warming and its impact on climate change. Among many if not all economic sectors, that of power is one of the largest emitters of GHG, with a share of 25% in total global GHG emission in 2010 [1]. Accordingly, this sector has been identified as one of the key economic sectors for enforcing low-carbon policies.

In its energy roadmap for 2050 [2], the European Commission set a target to reduce the emission of GHG in the power sector by 54-68% by 2030 and 93-99% by 2050 compared to 1990. One of the key measures to fulfilling this ambitious goal is to increase the share of renewable energy sources (RES), in particular, wind and solar energy in the primary energy mix for power generation. Germany, for instance, has asserted as part of its “En-

ergiewende” the goal to increase the share of power generation from RES to 35% by 2020 and 80% by 2050 [3].

The increased share of variable and intermittent RES comes with challenges mainly where the flexibility, reliability and sustainability of the electric power system are concerned. The stable operation of an electric power system requires a balance between total power generation, total power demand and total power losses incurred in lines and other components. The integration of RES introduces uncertainties in power generation which have to be compensated for by other generation units to ensure a stable operation of the electric power system. This requires the availability of flexible and reliable back-up generation units that can rapidly respond to reduced generation capacities and contingencies in the electric power system and the availability of energy storage capacities in case of need to store excess electric energy generated by RES.

1.1.1. Gas Supply to Power System Networks

The first requirement can be met by natural gas fired power plants (GFPP) which are known to be reliable and more flexible than conventional thermal power plants such as coal and nuclear plants. Gas fired generators typically have relatively short start up and shut down times, low start up and shut down costs and high ramp rates. Furthermore, the advancements in the gas turbine technology from single towards combined cycle machines has increased the overall efficiency of gas fired generators. GFPPs are typically connected to high pressure natural gas transmission networks, which supply the gas fired generators with the required quantity of gas at the desired pressure, since the storage of large volumes of gas on-site is not an option due to economic and security concerns. The gas generators in a GFPP require a specific fuel gas pressure in order to maintain operation [4]. If the fuel gas pressure goes below this threshold the gas generators have to either curtail the gas offtake or in the worse case shut down the entire station [5].

Another aspect that makes the use of GFPPs more attractive than other plant types, is the relatively small amount of GHG emitted when natural gas is combusted compared to other fossil fuels like coal and oil. Moreover, the improvements in shale gas exploitation and liquefaction technology has increased the attractiveness of natural gas from an economic point of view [6]. Due to this positive characteristics, natural gas is regarded as the main backup fuel for RES in case of shortage or loss of generation capacity.

As a result, the importance of natural gas in the global primary energy mix for power generation has increased in the last decade and is expected to increase further in the

future as more RES are integrated into the power system¹. According to a projection by the U.S. Energy Information Agency (EIA) [7], the global share of natural gas for power generation is expected to grow by 2.7% per year from 2012 to 2040, which is just 0.2 percent points less than the projected growth rate for RES, which have the highest growth rate among all primary energy sources for power generation [7]. In 2040 natural gas is expected to account for almost 30% of total global power generation, which is an increase of 8 percent points compared to 2012.

1.1.2. Energy Storage through Power-to-Gas

The connection to gas networks can also serve the purpose of storing a surplus of electric energy generated by RES. Unlike natural gas, electric energy cannot be stored economically in large quantities in current electric power systems. As a result, excess generation from RES is curtailed in order to avoid an imbalance between generation and demand. This energy losses can be avoided by using the capacities in gas pipeline networks as energy storage. Gas networks typically have large storage capacities available in pipelines and in underground gas storage facilities, especially in seasons of reduced gas demand, typically during summer time. The available storage capacities can be utilized by converting electric energy into chemical energy in the form of hydrogen (electric energy is used in water electrolysis to separate water into hydrogen and oxygen) and/or synthetic natural gas (SNG, methane is generated through a chemical reaction of hydrogen and carbon dioxide), which can be injected into the gas system and used for power production by GFPPs in periods of peak power demand or reduced generation by RES. This electro-chemical process, also referred to as Power-to-Gas, has gained great interest in recent years [8]. The first Power-to-Gas facilities are already in operation and several additional installations are planned across Europe [9]. The ongoing advancements in the P2G technology and the increasing number of installations of P2G facilities will increase the coupling between gas and electric power systems.

1.1.3. Power Supply to Gas Pipeline Networks

Not only is the importance of natural gas for the electric power system increasing, but also the gas system is increasingly dependent on reliable power supply from the electricity system. Many facilities in the gas system (e.g. electric drivers in gas compressor

¹This is not the case in the EU. In fact between 2010 and 2015 the drop in gas consumption for electricity production has resulted in a general drop in gas consumption.

stations and underground gas storage facilities, liquefied natural gas (LNG) regasification terminals, regulator and metering stations, valve stations etc.) rely on power supply from the electric system in order to operate. LNG regasification terminals, for instance, need electric power to cool down the LNG stored in storage tanks and to operate low and high pressure pumps required for increasing the pressure of the LNG to pipeline pressure before the vaporization process. Furthermore, compressor stations may rely on electric power supply from the electricity network to operate electric motors which drive the compressors, in order to increase the gas pressure for transportation. The use of electric drivers in gas compressor stations has increased in recent years [10]. Electric drivers are particularly attractive in situations where the use of conventional gas engines or turbines may be limited by emission restrictions or other environmental regulations [5]. Moreover, electric drivers outperform conventional gas turbines by higher mechanical efficiencies, lower operating and maintenance costs and a higher flexibility and controllability [11].

1.1.4. Security of Supply in interconnected Gas and Electric Power Systems

From the above discussion, it is apparent that the operation of gas and electric power systems is increasingly interdependent. This development is connected with challenges concerning security of energy supply. Security of energy supply is defined as the uninterrupted supply of energy to customers particularly in case of difficult climatic conditions and in the event of an unexpected disruption [12]. The growing interdependence between the two systems make the entire energy system more vulnerable to disruptions. A contingency triggered in one system may propagate to the other system or even back to the system where it originated. Therefore understanding the impacts of the interactions between the two systems is crucial for governments, system operators, regulators and operational planners, in order to ensure security of supply for the overall energy system.

The interactions between gas and electric systems make it increasingly difficult to separate security of gas supply from security of electricity supply. The changes in the overall energy system due to different types of incidents may affect the dynamic behaviour and vulnerability of the integrated gas/electricity system. The level of vulnerability depends on some external conditions like the level of power system dependency on GFPPs, power generation mix of a region, weather conditions, probabilities of natural disaster of a region, and failure probability of facilities in either of the systems, among other factors.

Generally, large disruptions in gas systems affecting both power and non-power consumers are not so common. The gas system is well known as reliable and safe. However, there

could be incidents resulting in curtailment of gas, which can cause problems in the power system, such as, unexpected increase in demand, freezing of well heads and disruption of pipelines among others. In such cases, the delivery pressure needed by the facilities has to be taken into account. This is particularly important in recently deployed GFPPs using modern combustion turbines, which need higher gas pressure to operate compared to conventional combustion turbines. It should be noted that, even if the gas system had enough capacity to deliver gas to GFPPs at peak demand, the coincidence of peak demand for GFPPs and for conventional use (household, commercial, industrial) may result in a significant diminished pressure in pipelines, which eventually may produce interruptions in the electricity generation because of insufficient pressure.

In case of lack of gas supply in a GFPP, the possible solutions that may help bridge the gap of gas availability could be dual fuel capabilities or/and a variety of storage options (linepack and UGS facilities close to consumption areas). However, the costs and feasibility of storage and fuel switching has to be analysed in detail since sometimes they cannot be used as a solution in practice. In fact, quite frequently because of the cost of fuel-oil storage a dual fuel GFPP cannot switch to the alternative fuel due to lack of fuel stored on-site.

When the consequences and cascading effects of a disruption originating in one system and propagating to the other system are compared, the gas system is more resilient to local and short-term disruptions compared to the electricity system. The main reason for this is that, in addition to the existence of linepack as short-term storage, the majority of compressor stations are still powered by gas turbines, which keeps the pressure profile within limits, allowing continued operation. Furthermore, in case electric driven compressors are installed, a back-up power system (typically diesel) is usually available to protect the system from power outages. A massive power failure would generally have no serious effect on the physical pipeline facilities, provided that it does not last too long. Compressor stations and underground gas facilities that utilize electric drivers would be the most affected and have to be analysed carefully.

1.2. Modelling of Gas and Electric Transmission Networks

The growing interactions between gas and electricity systems suggest the need for mathematical models and tools for planning and analysing the operation of the two systems in an integrated manner to understand better,

1. the depth and scope of these interdependencies,
2. how they may affect the operation of the two systems and
3. how to proactively approach the bottlenecks and challenges that may emerge.

When modelling integrated gas and electricity systems, there are several aspects to be addressed mainly due to the differences in the structure and physical behaviour of the two systems. For instance, the failure response of the power and gas system infrastructures is significantly different. A technical failure in the power system infrastructure can result in an immediate loss of service from a generating unit or a transmission line. Under some extreme conditions, this can propagate and eventually result in loss of service to electric customers due to cascading effects. On the contrary, most technical failures in gas systems (e.g. pipeline rupture, failure in compressor station or storage facilities etc.) result in a locally or regionally reduced network capacity rather than an entire loss of service to gas consumers [13]. This capacity reduction might result in curtailments of gas delivery to customers according to their priority level of service.

Another important distinction is the different dynamic behaviour of the two systems. Electricity travels almost instantaneously and cannot be stored economically in large quantities in current power systems, with the only exception of hydraulic pumping power stations, whose availability is very much limited in a significant number of countries. In case of disruptions, the response time of the power system is quite small and basically the transmission line flows satisfy the steady-state algebraic equations.

On the contrary, the gas flow in pipelines is a much slower process, with gas velocities below 15 m/s, resulting in a longer response time in case of disruptions. In particular, high-pressure transmission pipelines have much slower dynamics due to the large volumes of gas stored in pipelines. This quantity of gas cannot be neglected when simulating the dynamics in gas transmission systems; in fact the line pack in the pipeline increases the flexibility of the gas system to react to short term fluctuations in demand and supply. This information is important especially in the modelling stage, since different timing of the systems need to be considered during the simulation process.

1.2.1. Model Requirements

In order to capture appropriately the different characteristics of gas and electric power system discussed above and to assess the interdependencies between the two systems and how they may impact security of energy supply the following model requirements are proposed:

- (i) Dynamic model for describing the operation of gas transport networks (i.e. imbalance between gas supply and gas demand resulting in fluctuations in linepack), in order to reflect appropriately the changes in pressure and linepack, which cannot be captured by mass balance or steady state hydraulic models.
- (ii) AC model for the electric power system, in order to capture line losses, reactive power flow, voltage levels etc., which are neglected in DC models.
- (iii) Generic sub-models for the most important gas and power system facilities (e.g. compressor stations, UGS, LNG terminals, generation units, electric substations etc.) and their technical and contractual constraints (e.g. pressure limits, operating envelope of compressors, voltage limits, generator capability curves, transmission line capacity limits etc.), in order to reflect adequately the flexibility and operation of the two systems in scenarios, where both systems operate close to their limits.
- (iv) Consideration of the bidirectional interconnection between the two systems (i.e. gas offtake for power generation in GFPPs and power supply to EDCS and LNG terminals), in order to give a full picture of the interdependence between the two systems.
- (v) Simultaneous solution of the physical equations and coupling equations for the interconnected gas and electric power system for each simulation time step, in order to capture the direct impact of control changes or disruptions originating from one system and cascading to the other system.
- (vi) Possibility to implement conditional control changes, i.e. changing the set points in one system in respect to the conditions in the other system (e.g. the start up of a GFPP for power generation depends on the available linepack and pressure in the gas system), in order to model the coordination between the two systems and how they may improve the combined operation.
- (vii) Estimation of consequences of supply disruptions, in order to quantify how disruptions affect security of supply and to analyse the effectiveness of countermeasures to mitigate the impact of disruptions.

1.2.2. State of the Art

The research area of modelling the interdependencies between gas and electric power systems is relatively new. The models addressing this topic can be divided into the following four groups in terms of the area of application:

- economic and market analysis
- operation planning and control (e.g., optimization, demand response)
- design and expansion planning
- security analysis

Studies on the medium and long-term economic evaluations aiming at exploring the interactions between the mechanisms of pricing of each carrier are reported in [14–24], where the influence of technical constraints is often ignored or taken into account in a simplified way. Additionally in [25], the authors proposed a dynamic model representation of coupled natural gas and electricity network markets to test the potential interaction with respect to investments while considering network constraints of both markets. In [26], two methodologies for coupling interdependent gas and power market models are proposed in a medium-term scope, where the two systems are formulated separately as optimization problems and the obtained primal dual information is utilized.

From the operational viewpoint, unit commitment models relating to short term security constrained operation of combined gas and power systems are developed in [27–29]. In [28], the authors considered the natural gas network constraints in the optimal solution of security constrained unit commitment (SCUC). Additionally dual fuel units are modelled for analyzing different fuel availability scenarios. In [29], the model proposed in [28] is extended using a quadratic function of pressure for describing the gas flow in pipelines and also including the gas consumption of the compressors. In [30], an economic dispatch model (ED) is developed for integrated gas and power systems. The security constraints for the two systems are integrated in the ED which aims to minimize power system operating costs.

The optimal power flow (OPF) of the coupled gas and power systems are investigated in [31–36]. A method for OPF and scheduling of combined electricity and natural gas systems with a transient model for natural gas flow is investigated in [34] and the solutions for steady-state and transient models of the gas system are compared. A multi-time period OPF model was developed for the combined GB electricity and gas networks in [35,36].

The impact of uncertainties on integrated gas and power system operation caused by variable wind energy is discussed in [37–40]. In [37] the impacts of abrupt changes of power output from GFPPS, to compensate variable power output from wind farms, on the Great Britain (GB) gas network is analyzed. In [39], the authors developed partial differential equation (PDE) model of gas pipelines to analyze the effects of intermittent wind generation on the fluctuations of pressure in GFPPs and pipelines. The coordination

between the gas and power systems based on an integrated stochastic model for firming the variability of wind energy is presented in [40]. Gas transmission system constraints and the variability of wind energy is considered in the optimal short-term operation of stochastic power systems with a scenario based approach.

Studies considering the implementation of demand side response in order to mitigate the pressure of peak demand can be found in [41–44]. An operating strategy for short-term scheduling of integrated gas and power system is proposed in [43] while considering demand response and wind uncertainty. In [44], the impact of demand side response on integrated gas and power supply systems in GB is analysed for the time horizon from 2010 to 2050.

The problem of the design and expansion planning is addressed in [45,46] for the integrated gas and power systems at the distribution level and the transmission level, respectively.

Recently P2G has gained significant interest. A number of studies [47,48] have investigated the interdependencies introduced by P2G units on the integrated gas and power system operation in GB. The application of P2G for seasonal storage in gas networks was investigated in [49].

The security perspective including the reliability and the adequacy of integrated gas and power systems has gained significant interest due to increasing dependencies among the systems. Such studies may include the cascading effects of contingencies where the performance of the networks is reduced [15,50–53]. In [15], an integrated simulation model that aims at reflecting the dynamics of the systems in case of disruptions is proposed. While developing the integrated model, first gas and power systems are modelled separately and then linked with an interface.

Co-Simulation versus Combined Simulation

Another distinction between the available models is based on the different solution methods adopted for the integrated gas and electricity model. The following two methods are distinguished:

- Co-Simulation: The equations describing the operation of the gas and electricity network are solved successively in two separate simulation time frames and simulation environments (e.g. two different software applications, simulators or Solvers) and the two simulation environments communicate and exchange data through an interface that ensures the interconnections between the two systems are respected.

- Combined Simulation: The equations describing the operation of the gas and electricity network and the coupling equations describing the interconnection between the two networks are solved simultaneously for each simulation time step and in a single simulation environment (e.g. one software application, simulator, or solver that solves the combined model in a single simulation time frame). Thus, each computed state of the coupled network fulfills the coupling equations and the physical equations for the two networks.

The studies presented above are predominantly based on co-simulation methods. In the following, we give an overview of models in the literature that focus primarily on combined simulation.

Studies in the literature that use combined simulation to examine the interconnection between gas and power systems for planning purposes mainly focus on single or multi-time period operational optimisation methods based on steady state conditions [42, 54–59]. In [55], the authors investigate the short-term optimal operation of the integrated gas and electricity network with wind power and P2G facilities. The authors use a security-constraint bi-level ED model with an objective function that minimizes the day ahead costs of electricity and natural gas consumption, respectively. In [56], a multi-stage co-planning model is developed to identify the optimal expansion planning of integrated gas and electricity networks. In [58], a coupled steady state model is proposed to analyse the mitigation effects of integrated gas and electricity systems using a succession of steady state approach with time varying power demand and wind generation profiles. The authors use a steady state gas system model to address a dynamic problem. In [57], a unit commitment and ED model that considers the technical characteristics of power generation units is proposed. The authors include an energy flow model for the gas system taking into account pressure constraints.

In [59], the authors propose a probabilistic energy flow framework for investigating the impacts of uncertainties on the operation of the two systems using Monte-Carlo simulations. The authors use a combined steady state model for describing the gas and electric power system. Moreover, they consider the bi-directional coupling between the two systems at gas fired power plants and electric driven compressor stations taking into account the voltage and frequency dependency of electric power system loads. Additional stochastic optimization models are proposed in [21, 40, 43] in order to address the uncertainties of the integrated gas and electricity networks.

In the above studies, the dynamic behaviour of the gas system is neglected, which, however, is relevant when studying the combined operation of gas and electric power sys-

tems [60, 61]. The time evolution of linepack determines the level of flexibility the gas system can provide to the electric power system. In a steady state gas model the time derivative of the linepack is inherently zero, since total gas inflow and outflow are at equilibrium. Thus, the time evolution of the linepack cannot be captured appropriately by steady state gas models. To account for this aspect, researchers have developed models for combined optimization of gas and electricity networks considering the dynamics in gas pipeline systems [35, 60–63].

In [35], a multi-time period optimization model is proposed for analysing the coupling between the gas and power system network in Great Britain. The authors model key gas system facilities such as compressor stations and UGS facilities and their constraints. The power system model used in the study is based on a simplified DC-OPF model, where important power system constraints, such as thermal capacity limits of transmission lines and reactive power limits of generation units are disregarded. Moreover, the authors consider the ramping limits of generation units, but neglect their start-up and shut down time limits, which may restrict the availability and flexibility of these units. Furthermore, the bi-directional coupling between the gas and electric power system is neglected, since only the coupling through GFPPs is considered. In [62], the authors present a detailed optimal control model to capture spatio-temporal interactions between gas and electricity systems. The proposed model couples a dynamic gas model with an economic dispatch model for the power grid in order to investigate the economic and flexibility gains resulting from coordinating the dispatch of the two systems. Similar to [35] the power system model is based on a simplified DC model, which is connected with the limitations explained above.

In [61, 63], the authors introduce a coupled optimization model for the combined simulation of gas and electric power systems, where the two systems are coupled through gas fired power plants solely. The model is intended to assist gas and power TSOs in coordinating the scheduling of gas offtakes for power generation in GFPPs. Similar to the other studies the authors use a DC-OPF approach to model the electric power system.

1.3. Research Questions

The available models for analysing the interactions between gas and electricity systems do not fully cover the requirements proposed in Section 1.2.1. Most models use either mass balance or steady state models for describing the operation of the gas system, which is not suitable for security of supply studies, where a dynamic model for the gas system

is essential. Moreover, for the electric power system simplified DC models are considered, which neglect important power system constraints such as voltage limits, thermal capacities of lines, reactive power limits of generators etc. Furthermore, the majority of the models consider only a unidirectional coupling between the two systems at gas fired power plants.

This thesis covers the gaps in the state of the art by developing a mathematical model that respects the proposed requirements, and by implementing this model into a novel simulation tool that is designed for gas and power TSOs, researchers, regulatory agencies and governments to examine the interactions between gas and electric power systems and to assess the impact of disruption on security of supply in integrated gas and electric power systems. The developed model can be used to address the main research question of the thesis, which is:

- *How can the consequences of supply disruptions in an interconnected gas and electric power system be estimated?*

The quantification of the impact of disruptions on the operation of the combined energy system is crucial for assessing how severe a disruption event affects security of supply. In addition, the estimation of consequences is necessary to analyse the effectiveness of countermeasures and strategies to mitigate the impact of disruptions on security of supply. Furthermore, quantifying the consequences of disruptions is essential for performing a risk assessment of the combined system, which requires the identification of potential harmful scenarios, the estimation of their consequences and the probability of their occurrence.

In order to answer the main research question, an adequate mathematical representation of the physical behaviour of the two energy systems and their interconnection is required. To develop such a model, the following additional sub-research questions need to be addressed:

- *What are the most important facilities in the gas and electricity transmission networks in terms of security of supply?*
- *How can we develop a mathematical model that reflects appropriately their physical behaviour and their technical and contractual constraints?*
- *What are the most crucial interconnection points between the gas and electric power system?*
- *How can these interconnections be represented in the mathematical model?*

To answer these sub-questions the following approach is adopted. Firstly, a general description of the two energy systems is given, which helps identifying the most important facilities, their functions and their technical and contractual constraints. After identifying these facilities generic sub models are developed for each individual facility, which are eventually combined to an integrated network model for each energy system. The individual energy system models are validated against existing models to confirm their accuracy. Both energy systems are considered separately in the above approach.

Finally, the most important interconnections between the gas and electricity system are identified and reflected by mathematical coupling equations, which eventually combine both previously separated models to an integrated multi-vector energy system model with bi-directional interdependencies.

After developing the combined electricity and gas network model the following research sub-questions need to be addressed:

- *How do disruptions originating in the gas and/or electric network propagate from one network to the other and even back to the network where the disruption originated?*
- *How do disruptions triggered in one systems affect the operation of the other system?*
- *Which interconnections have more impact on the combined operation of the two systems?*

Addressing these research sub-questions is needed in order to demonstrate the capability of the combined electricity and gas network to capture the propagation of disruptions from one energy system to the other. Moreover, in the process of addressing this question a comparison between co-simulation and combined simulation is conducted and the advantages and disadvantages of both approaches are discussed.

After confirming the capability of the combined model, the model can be used to run different case studies to examine the impact of disruptions on security of supply. In order to analyse and compare results from the case studies a number of security of supply parameters are needed, which essentially address the following research sub-questions:

- *How can we quantify and compare the impact of supply disruptions on different gas customers?*
- *How can we quantify the grace period for gas and power TSOs to coordinate and react to supply disruptions?*

The capability to quantify the consequences of supply disruption on security of supply can be used to analyse the following follow-up research questions:

- *What countermeasures can be deployed to mitigate the impact of disruptions and how can these countermeasures be integrated into the combined model?*
- *How can we evaluate the effectiveness of different countermeasures to mitigate supply disruptions?*

To be able to implement countermeasures the concept of conditional control changes is utilized, which enables controlled facilities to change their control modes and/or control set points at a specific simulation time based on predefined conditions in the gas and electric network at previous simulation time steps.

1.4. Thesis Outline

The thesis follows the following structure.

Chapter 2

Chapter 2 gives an introduction to the structure of the natural gas transport system and elaborates the requirements for a transient hydraulic model for gas transmission networks, that is suitable for security of supply studies. The requirements are then used as an orientation to develop mathematical sub-models for the most important facilities comprising a gas transmission network, such as pipelines, compressor stations and underground gas storages. The models for the individual facilities are then combined to an integrated model for the entire gas transmission network. The developed model is then benchmarked against results from the scientific literature and a commercial gas simulation software. Finally, the model is applied to simulate the operation of a realistic gas transmission network of an European region in a disruption scenario.

Chapter 3

In Chapter 3, the gas network model developed in Chapter 2 is extended by an algorithm for processing control changes and constraints at controlled facilities in the course of the dynamic gas network simulation. The developed model and algorithm is then implemented

into a simulation software **SAInt**, which includes a graphical user interface for interacting with the user. The developed software application is used to perform a case study on a realistic gas transmission network of an European region.

Chapter 4

In Chapter 4, a framework for analysing security of supply in integrated gas and electricity networks is developed. The framework is based on a co-simulation platform between the developed gas simulation software **SAInt** and the Matlab-based power system simulation library MATPOWER, where the equations for the gas and electric power system are solved successively and in different simulation time frames considering the coupling equations at interconnection points.

Firstly, an introduction to the physical equations describing the operation of the electric power system is given, followed by the identification of the most relevant interconnections between the two systems and their corresponding coupling equations. Next, the co-simulation platform is developed, which is subdivided into a transient gas simulation model (**SAInt**), a multi time period steady state AC- power flow model (MATPOWER) and an interface that ensures the data exchange and communication between the two models. Finally, the platform is applied to perform a case study on a realistic interconnected gas and power system network of an European region.

Chapter 5

Chapter 5 is dedicated to combined simulation of interconnected gas and electricity networks, where the equations for the gas system, the electric power system and the coupling equations describing the interconnections between the two systems are solved simultaneously for each time step, considering the bi-directional interconnection between the two energy systems. The electric power system model from Chapter 4 is extended by a model for dispatchable power system loads and by time transitional constraints such as the ramp rate and the start-up time of different electric generators. Moreover, a number of security of supply parameter are developed which are used to quantify the impact of disruptions on security of supply. Finally, the developed model is implemented into the simulation software **SAInt** and applied to conduct a case study on a sample gas and power system network.

Chapter 6

Finally, Chapter 6 presents the conclusions and discusses how the developed models can be used and extended to address future research questions.

2. Dynamic Simulation Model for Gas Transmission Networks

This chapter is based on the following published peer reviewed journal article and conference papers:

- K. A. Pambour, R. Bolado-Lavin, and G. P. Dijkema, “[An integrated transient model for simulating the operation of natural gas transport systems](#),” in *Journal of Natural Gas Science and Engineering*, vol. 28, pp. 672 – 690, 2016.
- K. A. Pambour, R. Bolado-Lavin, and G. P. Dijkema, “[SAInt – A simulation tool for analysing the consequences of natural gas supply disruptions](#),” in *Pipeline Technology Conference (PTC) 2016*.
- K. A. Pambour, B. Cakir Erdener, R. Bolado-Lavin, and G. P. J. Dijkema, “[An integrated simulation tool for analysing the operation and interdependency of natural gas and electric power systems](#),” in *Pipeline Simulation Interest Group (PSIG) Conference 2016*.

2.1. Introduction

Natural gas plays a vital role in the energy portfolio of the EU. In 2013 it accounted for almost one quarter of the primary energy consumption in the EU-28 [64]. It is mainly used for power generation, heating, transportation and as a feed stock for industrial production.

Figure 2.1 shows a typical structure of the natural gas infrastructure. It basically consists of three subsystems, namely, the gas production system which includes the exploration, extraction and processing of natural gas, the national and/or regional gas transport system, which contains the transit, the transmission and storage of natural gas, and the local gas distribution system, which covers the distribution of natural gas to final consumers. The three subsystems differ in their pressure levels and may be operated by different independent entities. While in gas production systems the pressure can range from upto

450 bar-g at extraction to 80 bar-g at the exit point to the transport system, in gas distribution systems pressures are typically below 1 bar-g. The focus of this thesis is mainly on the operation of the gas transport system and the technical components and facilities connected to the transport system.

The location of natural gas deposits is usually many kilometres away from where it is demanded, therefore, natural gas is typically transported to market areas through a designated pipeline transport system. In cases where a direct pipeline connection between production and demand sites is inefficient or even infeasible natural gas is liquefied and then shipped as LNG in large vessels. At ports of destination, it is stored and finally regasified and injected into the pipeline system.

A large quantity of gas entering the transport system may be transmitted to neighbouring transport systems through a designated system of transit pipelines (see. Fig. 2.1), while the remaining quantity is either directly used to cover national demands or injected into storage facilities located close to consumption areas.

The driving force for the transport of natural gas in pipelines is the gas pressure. To balance pipeline capacity and cost, the system operates at elevated pressure. When gas is flowing, the pressure decreases (by approx. 0.1 bar/km) mainly due to friction between the gas and the inner surface of the pipeline. These losses are compensated for by compressor stations typically installed at 150-200 km intervals along the pipeline system. Compressor stations increase the inlet gas pressure to a higher outlet pressure in order to ensure a continuous transport and delivery of natural gas to its customers at the contracted nominations and delivery pressures. Natural gas arriving from the transport pipelines to consumption regions is either directly served to large customers connected to the transport pipeline, such as gas fired power plants and large industrial customers, or delivered to the local gas distribution system, where it is distributed to smaller customers (households, commercial customers, public services etc.). In both cases, the gas pressure and gas quantity exiting the transport system are metered and controlled by pressure reduction and metering stations, which consist of a number valves, regulators, metering devices and other components.

Natural gas may also be injected into UGS for later withdrawal. UGS may be for seasonal storage - store gas at long periods of gas surplus, usually during summer, and withdrawal at periods of increased or even peak demand in winter. Furthermore, the function of a UGS (e.g. salt cavern storage) can also be to facilitate market arbitrage - accommodating rapid cycles of storage and withdrawal, to let parties benefit from dynamic gas prices. This function to some extent can also be performed using line pack - the storage volume

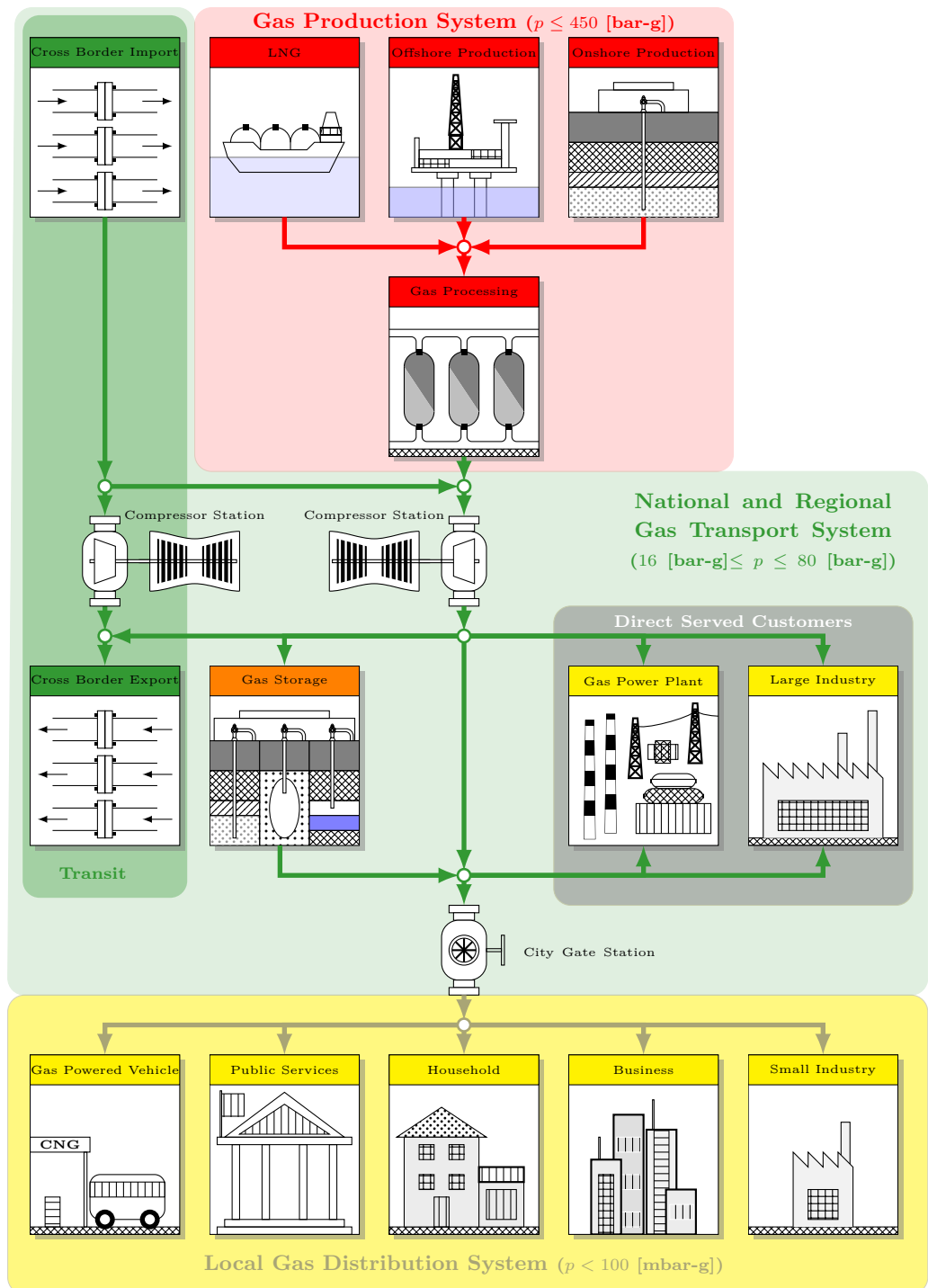


Fig. 2.1.: Natural Gas Infrastructure

available in the pipeline. UGS facilities increase the flexibility of the transport system to react to load fluctuations and supply disruptions.

The operation of natural gas transport systems is restricted by physical, technical and contractual constraints imposed by the different facilities and stakeholders involved in the gas supply chain. Pipelines, for instance, have a Maximum Operating Pressure (MOP), which if exceeded can cause great damage to the transport system. Compressor stations, on the other hand, have a limited compression power and usually require a minimum gas inflow for surge prevention, while gas fired power plants can only operate above a certain delivery pressure threshold [4]. In order to keep the network within its operational envelope and to meet the contractual nominations, TSO are usually equipped with a designated SCADA (Supervisory Control And Data Acquisition) - system together with software applications to monitor and control the facilities and components in their transport system. Controlling the system involves finding the most economical configurations and control set points for the facilities without violating technical and legal constraints.

While the TSO may have a good picture of the current and projected state of its network, it may however, not be fully aware of potential threats to security of gas supply originating from external sources. For instance, there may be a supply disruption from an important transit pipeline due to a failure in a facility located in an upstream transmission system, or an interrupted supply from a major LNG import terminal due to a geopolitical crises. Moreover, the growing dependency of the EU-28 upon gas imports from non-EU countries - mainly Russia, Norway and Algeria [64] - stresses the importance to examine the resilience and vulnerabilities of gas transport systems from an independent multinational perspective. By doing this, we can develop strategies to mitigate the potential threats to security of gas supply.

The examination of multinational gas transport systems in terms of security of gas supply requires the use of numerical models that are able to reflect the behaviour of gas transport systems and the reaction of the system to supply disruptions in adequate and accurate manner. The following three model requirements can be distinguished.

1. System Dynamic Behaviour:

The model should be able to capture accurately the reaction of (multi-) national transport systems to load variations (i.e. daily and seasonal changes of gas demands at offtake points) and disruption events (e.g. loss of supply from an entry point, failure in a compressor station etc.) with reasonable computation cost, taking into account the physical laws governing the dynamic behaviour of gas transport systems.

2. System Components:

The model should include reasonable sub models of all important facilities comprising a gas transport system, such as pipelines, compressor stations, production fields, cross-border entry and exit stations, city gate stations, stations of direct served customers, LNG terminals and UGS facilities.

3. System Constraints:

The model should implement appropriately the constraints imposed by major facilities and stakeholders (e.g. maximum operating pipeline pressures, maximum available compression power, maximum withdrawal rate from storages and production fields, minimum delivery pressures at offtake points etc.).

The goal of this chapter is to present an integrated transient hydraulic model that fulfils the criteria listed above. To achieve this goal the chapter follows the following pattern. In the first part, we present the state of the art of hydraulic models dealing with the simulation of gas transport systems and highlight the main contribution of this chapter. Secondly, we derive the equations describing the gas flow in pipelines and make use of commonly used assumptions in the state of the art to simplify and adapt the equations to the prevailing conditions in gas transport systems. In addition, we present a linearisation method for the pipe equations which has been used in the context of steady state computations for pipelines without inclination but not to the transient simulation of non-horizontal pipelines. The derivation and linearisation of the pipe equations is followed by a mathematical description of the network system and the basic non-pipe components included in the system, such as compressors, regulators, valves, resistors and nodes. Furthermore, we apply the integral form of the continuity equation to derive the equation system describing the integrated network model which includes generic sub models of all relevant facilities. The derivation is followed by a description of the algorithm for the solution of the system of equations based on an implicit time integration with an iterative linearisation of the pipe equation for each simulation time step.

In the last part of the Chapter, the accuracy of the model is demonstrated by benchmarking it against results from the literature and the commercial software SIMONE. Finally, the model is applied to perform a dynamic simulation on a real-world network, namely, the Bulgarian and Greek regional gas transmission system.

2.2. State of the Art

The hydraulic gas models in the literature can be divided into two groups, namely, steady state models and transient models. Steady state models are characterized by a balance between total gas inflow and outflow, since pressures and flows are assumed constant in time. Transient models in contrast, consider the time evolution of pressures and flows and the changes in line pack. Steady state models are primarily used for optimization and design purposes, mainly, due to their simplicity compared to transient models. While the simulation of transients involves the solution of a set of non-linear PDEs, a steady state problem requires only the solution of a set of non-linear algebraic equations. There are a number of references addressing both groups of models in the scientific literature, which are summarized in the following.

References mainly dealing with steady state models are [65–69]. Szoplik [65] applied a steady state model to perform a succession of steady state simulation to capture the behaviour of a low pressure distribution network for different air temperatures. The size of the investigated network amounts to 316 nodes, 319 branches. Woldeyohannes and Abd Majid [66] used a steady state approach with a detailed non-linear compressor model to simulate and analyze different configurations of an existing gas transmission network. The size and complexity of the simulated network is relatively low (1 source, 1 compressor station, 11 pipelines, 5 off take points, 1 loop). Mohring et al. [67] present a method to reduce the complexity of gas pipeline networks. The method is based on finding a bottleneck model using symbolic simplification, i.e. identifying and extracting dominant network components by combining computer algebra and numerical analysis. Finally, the method is applied on the transmission network of Belgium by comparing steady state simulations of the full network and the reduced network. Van der Hoeven [69] presented an approach for linearising the pressure drop equation for horizontal pipelines to perform steady state analysis on gas transport systems. The linearisation presented makes use of the positive slope of the pressure drop curve due to the positive sign of the pipe resistance. He presented three linearisation approaches which differ in the way the linear approximation of the pressure drop curve is obtained from the result of a previous iteration.

The majority of the references dealing with transient gas models either focus on the numerical schemes for solving the partial differential equations describing the gas flow through pipelines like for instance in [70–81] or on the comparison of different transient models obtained by simplifying the flow equations as it is done in [70, 82–85]. The numerical approaches adopted range from implicit finite difference methods to method of characteristics, finite element and finite volume methods. Herrán-González et. al. [70]

implemented the implicit Crank-Nicholson method and the method of characteristics to develop a Matlab-Simulink library which can be used to simulate the transient behavior of a gas network. Moreover, they stressed the importance of including the gravitational term in the momentum equation by comparing results for different pipe inclinations. The simulations they performed were applied to a single pipeline and a triangular network with three pipelines. Ke and Ti [86] presented a more unconventional method for solving transient flow in pipelines which is based on an analogy between the electrical grid and the gas network. The basic idea of this approach is the transformation of the gas model to a analogous electrical model with voltage, resistance, capacitance and inductance. Results computed with this method are benchmarked against those computed for the triangular network in other papers. Reddy et al. [72] developed a dynamic simulator based on a transfer function model to obtain an accurate on-line state estimation from measurements and to estimate the demands. The model is applied on an example pipeline network containing nine pipelines, one source node and two off-take points. Van der Hoeven [87] discussed the dynamics in gas transport pipeline based on a concept of distributing the dominant properties of a pipeline, namely, line pack and resistance by segmenting the pipeline into a succession of volumes and resistance. Using this approach he showed how the dynamics in gas transport systems can be described by a first order differential equation, which if solved yields an exponential function. Moreover, he presented the concept of a time constant which is an indicator for how long a pipeline may need to recover from a sudden change of demand at its outlet.

Furthermore, the suitability of steady state and transient methods for different applications have been discussed by a number of authors. Osiadazs [82] discussed the use of steady state and transient models in the industry. According to Osiadazs [82] steady state models are traditionally used for design purposes or in low pressure distribution networks where the dynamics are very rapid and steady state conditions are reached very fast, whereas in high pressure transmission networks where a very large amount of gas is stored in the pipeline the dynamics are much slower and therefore transient models are more appropriate. Modisette et al. [88] discussed the suitability of transient and succession of steady state models for different purposes like for instance product tracking, line balance, line pack distribution, pressure monitoring or deliverability. The suitability of each model depends on the application and the time step with which the information of the network is retrieved. Product tracking for instance can be adequately performed with succession of steady state due to large time step information points, while deliverability, pressure monitoring and line pack distribution cannot be captured correctly by steady state models due to the amplitudes in pressure and flows caused by short term changes in

the network (e.g. use of line pack at delivery points till demand is balanced by the supply source). Bachmann and Goodreau [89] discussed different sources of error causing steady state simulations to be unrealistic. One of these sources pointed out by these authors is the use of steady state models for solving problems of dynamic nature, like for instance, the use of line pack as short term gas storage to balance a ramp up of demand at industrial delivery points.

The state of the art of hydraulic gas models show that there are a number of hydraulic models addressing the steady state and transient simulation of gas network systems, however, the issue of security of gas supply has not been addressed in any of the hydraulic models in the literature. Since most of the models were not developed from a security of gas supply perspective they do not consider all relevant facilities which may play an important role in case of a gas supply disruption. UGS facilities and LNG terminals, for instance, have not been addressed in any of the hydraulic models in the literature. Moreover, the transient models in the literature are primarily applied to relatively small networks, without considering the technical and contractual constraints inherently present in a gas transport system. Thus, there is a gap in the literature which we would like to fill with the work in this chapter. The main contribution of this chapter is the development of an integrated transient hydraulic model for gas transport systems that includes all relevant facilities and their constraints and moreover enables the simulation of gas supply disruptions at a regional (multinational) level.

2.3. Methodology

In this Section, we develop the model to perform transient simulation in gas transmission networks. Firstly, we set the fundamental equations of gas flow and the corresponding simplifying assumptions for transport pipelines, including linearisation of equations. Then we describe the function of the different non-pipe facilities and develop generic models for the most important facilities, in terms of security of supply. Next, we elaborate the system of equations for the integrated network system and define the boundary conditions for controlled facilities, which we integrate into the system of equations. Finally, we present an algorithm for solving the developed model.

2.3.1. Modelling of Pipelines

The gas flow through pipelines is generally governed by the constitutional laws of fluid dynamics and thermodynamics, namely, the law of conservation of mass, Newton's second law of motion (conservation of momentum), the first law of thermodynamics (conservation of energy) and the real gas law. Applying these laws on an infinitesimal control volume

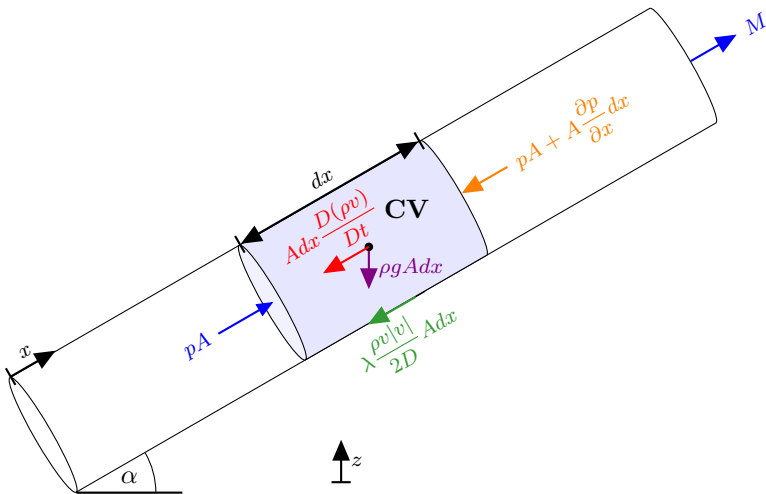


Fig. 2.2.: Forces acting on a control volume in a general gas pipeline

(*CV*) for a general pipeline with constant cross-sectional area A and an infinitesimal length dx (see Fig. 2.2) and moreover, assuming the parameters describing the gas flow along the pipe coordinate x are averaged over A , yields the following set of partial differential equations (PDEs)²:

Law of Conservation of Mass - Continuity Equation³:

$$\frac{\partial \rho}{\partial t} + \frac{\partial(\rho v)}{\partial x} = 0 \quad (2.1)$$

Newton's Second Law of Motion - Momentum Equation:

$$\underbrace{\frac{\partial(\rho v)}{\partial t}}_{\text{inertia}} + \underbrace{\frac{\partial(\rho v^2)}{\partial x}}_{\text{convective term}} + \underbrace{\frac{\partial p}{\partial x}}_{\text{pressure force}} + \underbrace{\frac{\lambda \rho v |v|}{2D}}_{\text{shear force}} + \underbrace{\rho g \sin \alpha}_{\text{force of gravity}} = 0 \quad (2.2)$$

²the assumption of averaging the flow parameters over the cross-sectional area can be justified as long as the pipe length L is much greater than the pipe diameter D which is the case in transmission networks where $\frac{D}{L}$ is of order $O(10^{-5})$ or lower.

³see nomenclature for variable definitions

First Law of Thermodynamics - Energy Equation :

$$\frac{\partial}{\partial t} \left[\left(c_v T + \frac{1}{2} v^2 \right) \rho A \right] + \frac{\partial}{\partial x} \left[\left(c_v T + \frac{p}{\rho} + \frac{1}{2} v^2 \right) \rho v A \right] + \rho v A g \sin \alpha = \dot{\Omega} \quad (2.3)$$

Real Gas Law - State Equation:

$$\frac{p}{\rho} = Z R T \quad (2.4)$$

The shear force term in the momentum equation is derived from the Darcy-Weisbach relation, which relates the frictional shear stress τ to the dynamic pressure $\rho v^2/2$.

$$\tau = \lambda \frac{dx}{D} \frac{\rho v |v|}{2} \quad (2.5)$$

For turbulent flow (typical flow condition in transport pipelines) the friction factor λ is generally described by the empirical Coolebrook-White correlation.

$$\frac{1}{\sqrt{\lambda}} = -2 \lg \left(\frac{2.51}{Re \sqrt{\lambda}} + \frac{k}{3.71D} \right) \quad (2.6)$$

where k is the integrated pipeline roughness and Re the Reynolds number, which is the ratio of inertia and frictional forces.

$$Re = \frac{\rho v D}{\eta} \quad (2.7)$$

where η is the dynamic viscosity of the flowing gas. The Coolebrook-White equation is implicit in λ , thus, it can only be solved iteratively. There are a number of explicit approximations for the Coolebrook-White equation which are applicable for a specific range of Reynolds numbers. One of these equations is the approximation by Hofer [90], which is valid for the turbulent flow regime in transport pipelines.

$$\lambda = \left[2 \lg \left(\frac{4.518}{Re} \lg \left(\frac{Re}{7} \right) + \frac{k}{3.71D} \right) \right]^{-2} \quad (2.8)$$

The friction factor λ is referred to a straight pipe without curvature. To account for the curvature and the form of the pipeline an efficiency factor η_e is typically introduced.

$$\sqrt{\frac{1}{\lambda_e}} = \eta_e \sqrt{\frac{1}{\lambda}} \quad (2.9)$$

where λ_e is the effective friction factor. Furthermore, the compressibility factor Z in the state equation is a correction factor for real gases, which accounts for the deviation from ideal gas behavior. Z depends on the gas pressure and temperature and can be approximated by the following equation derived by Papay [91], which is valid for natural gas upto a pressure of 150 bar.

$$Z = 1 - 3.52 \left(\frac{p}{p_c} \right) \exp \left[-2.260 \left(\frac{T}{T_c} \right) \right] + 0.274 \left(\frac{p}{p_c} \right)^2 \exp \left[-1.878 \left(\frac{T}{T_c} \right) \right] \quad (2.10)$$

where p_c and T_c are the critical pressure and temperature, respectively.

Simplifying Assumptions

As can be seen from the above derivations, the set of equations describing the gas flow in pipelines is very complex and can only be solved numerically. For large pipeline systems with hundreds or even thousands of interconnected pipeline elements the solution of the integrated PDE system may be very costly regarding computing time and storage. Therefore, it is reasonable to adapt the equations to the prevailing conditions in gas transport systems by means of neglecting some of the terms in the PDE system, but at the same time maintaining an appropriate level of accuracy. The process of simplifying the PDE system has been thoroughly discussed in the available literature, thus, we make use of some of the most common assumptions applied by a number of authors in the literature [70, 82, 92]. The following assumptions are generally accepted as reasonable approximations for the prevailing conditions in gas transport systems.

1. Isothermal Flow:

The changes in gas temperature are negligible, therefore we can assume isothermal flow, i.e. the gas temperature is constant in time and space and equal to the ground temperature.

2. Creeping Motion:

The influence of the convective term is negligible compared to the other terms in the momentum equation (2.2), due to the typically small velocities in transport pipelines ($v \leq 10$ m/s).

3. Slow Changes in Boundary Conditions:

The inertia term can be neglected if the boundary conditions in terms of pressures

and flows do not change rapidly, which is the case in a normal operation of gas transport systems, where load changes typically occur in a time scale of an hour.

The most common simplification is to assume isothermal flow, which means the gas temperature is constant along the pipeline at any time. Since pipelines are typically installed approx. two meters underneath the ground the gas temperature is assumed to be equal to the prevailing ground temperature. In reality the gas temperature may change along the pipeline, especially in submarine pipelines and in downstream pipelines of compressor stations (increase in gas temperature) and regulator stations (decrease in gas temperature), though these stations typically mitigate large temperature changes by cooling or preheating the gas. Changes in gas temperature along the pipeline are primarily caused by the Joule-Thompson-Effect and heat exchange between the pipeline and its surroundings. To capture this process adequately one would require a good knowledge of the thermal resistance and the distribution of the ground temperature, which is typically difficult to estimate. Moreover, due to the slow dynamics in transport pipelines ($v \leq 10$ m/s) the flowing gas typically has sufficient time to exchange heat with the ground and adapt its temperature to ground temperature. Thus, it is reasonable to neglect the temperature changes and assume a constant temperature equal to the ground temperature as it is done by many authors in the literature [70, 82, 92]. If the isothermal condition is applied to the set of PDEs the energy equation becomes redundant and can, therefore, be neglected. Furthermore, the following relation for the isothermal speed of sound c can be obtained from the state equation.

$$\frac{p}{\rho} = c^2 = ZRT \quad (2.11)$$

The PDEs can be further simplified by comparing the different terms in the momentum equation for typical conditions in transport pipelines. The convective term and the pressure term, for instance, are both partial derivatives of the space coordinate x , thus, it is reasonable to compare the magnitude of both terms for typical values for the flow velocity ($v = 10$ m/s) and the speed of sound ($c = 350$ m/s, assuming $p = 50$ bar & $T = 15$ °C).

$$\frac{\partial}{\partial x} [\rho v^2 + p] = \frac{\partial}{\partial x} \left[p \left(1 + \frac{v^2}{c^2} \right) \right] = \frac{\partial}{\partial x} \left[p \left(1 + \frac{10^2}{350^2} \right) \right] \quad (2.12)$$

$$= \frac{\partial}{\partial x} [p (1 + 8.16 \cdot 10^{-4})] \approx \frac{\partial p}{\partial x} \quad (2.13)$$

The convective term is negligible compared to the pressure term for typical flow conditions in gas pipelines, therefore, this term can be neglected. Applying the above assumptions

and the following relation for the flow rate Q and density ρ_n at standard conditions and the mass flow rate M ,

$$M = \rho_n Q = \rho v A \quad (2.14)$$

the PDEs are reduced to the following form referred to as fast transient equations (FTE).

$$\frac{\partial p}{\partial t} = -\frac{\rho_n c^2}{A} \frac{\partial Q}{\partial x} \quad (2.15)$$

$$\frac{\partial p}{\partial x} = -\frac{\rho_n}{A} \frac{\partial Q}{\partial t} - \frac{\lambda \rho_n^2 c^2}{2\eta_e^2 D A^2 p} |Q|Q - \frac{g \sin \alpha}{c^2} p \quad (2.16)$$

From these equations, we can conclude the following. A pipeline section has linepack (i.e. the amount of gas stored in the pipeline) which is proportional to the gas pressure. Pressure and linepack change in time whenever there is an imbalance between inflow and outflow at the boundary of the pipeline section (continuity equation). At steady state (i.e. time derivatives are equal to zero) there is a balance between incoming and outgoing flow and the flow rate Q is constant along the pipeline ($\partial Q / \partial x = 0$). The second equation explains the pressure drop along the pipeline as a result of inertia (force acting opposite to the direction of flow acceleration), resistance (frictional force acting opposite to the flow direction) and gravity (gravitational force due to pipeline inclination). Moreover, if we consider the third assumption, eq. (2.16) can be further simplified to the following ordinary differential equation with respect to the square pressure $P = p^2$, which we will refer to as slow transient equation (STE).

$$\frac{dP}{dx} + \frac{2g \sin \alpha}{c^2} P = -\frac{\lambda \rho_n^2 c^2}{\eta_e^2 D A^2} |Q|Q \quad (2.17)$$

The STE can be solved analytically if we assume the flow rate Q the compressibility factor Z and the friction factor λ are averaged over the pipe section with length $\Delta x = l$. The solution yields the pressure drop equation.

$$\Delta P = R_f \cdot |Q|Q \quad (2.18)$$

with

$$\Delta P = P_1 - P_2 e^s, \quad s = \frac{2g(h_2 - h_1)}{c^2}, \quad R_f = \frac{16\lambda \rho_n^2 c^2 l_e}{\pi^2 \eta_e^2 D^5}$$

$$l_e = \begin{cases} l, & h_1 = h_2 \\ \frac{e^s - 1}{s} l, & h_1 \neq h_2 \end{cases}$$

where ΔP is the (corrected) square pressure drop, R_f the pipe resistance coefficient, e Euler's number and h_1 and h_2 the elevation at the pipe inlet and outlet, respectively. The pressure drop equation (2.20) is parabolic and has a positive resistance R_f , i.e. the slope of the parabolic curve is always positive, which is a beneficial characteristic in terms of solving the set of equations for the entire network.

The assumption of slow transients may not be appropriate if the boundary conditions change rapidly. The most rapid change one can think of is the opening or closure of a valve, for safety or maintenance reasons, which may occur in a time scale of minutes. Thus, for the simulation of fast transients in the transport system (e.g. disruption in a compressor station, valve closure for safety reasons etc.) the inertia term is considered. In contrast to the slow transient case, the momentum equation for fast transients contains a time derivative which complicates the solution of the differential equation. Thus, we make an intermediate step to approximate the inertia term by performing an implicit time integration of the FTE between $\Delta t = t_{n+1} - t_n$. This approach yields the following finite difference equation.

$$\frac{dP^{n+1}}{dx} + \frac{2g \sin \alpha}{c^2} P^{n+1} = -\frac{2\rho_n p^{n+1}}{\Delta t A} (Q^{n+1} - Q^n) - \frac{\lambda \rho_n^2 c^2}{\eta_e^2 D A^2} |Q^{n+1}| Q^{n+1} \quad (2.19)$$

Similarly to the slow transient case, if we average the coefficients of the flow rate Q^{n+1} on the right hand side over the pipe segment $\Delta x = l$ we can obtain a pressure drop equation which includes an additional term reflecting the influence of inertia for rapid changes in the transport system.

$$\Delta P^{n+1} = R_f \cdot |Q^{n+1}| Q^{n+1} + R_i \cdot (Q^{n+1} - Q^n) \quad (2.20)$$

with

$$\Delta P^{n+1} = P_1^{n+1} - P_2^{n+1} e^s, \quad R_i = \frac{2\rho_n L_e p_m}{\Delta t A}, \quad p_m = \frac{2}{3} \frac{p_1^2 + p_1 p_2 + p_2^2}{p_1 + p_2}$$

As can be seen from the above equation, the pressure drop equation for fast transients turns into the equation for slow transient if the changes in flow rate between two time steps are marginal.

The mean pipeline pressure p_m can also be used to determine the linepack LP in the pipeline.

$$LP = \frac{A}{\rho_n \cdot c^2} \int_{x=0}^{x=l} p \, dx = \frac{p_m}{\rho_n \cdot c^2} V_{geo} \quad (2.21)$$

Linearisation of the Pipe Equation

Both derived pressure drop equations are non-linear, thus, in order to solve the set of equations for a pipeline network the equations have to be linearized and then solved iteratively for each time step t_{n+1} . We make use of the methods applied by van der Hoeven [69] for the linearisation of the steady state pressure drop equation for horizontal pipelines and extend his approach to the transient case taking into account the gravitational term. Linearisation basically means approximating the non-linear pressure drop curve with a tangent line that touches the curve at a specific point. The linearised pressure drop equation for a pipe (i, j) around a point $(\Delta P_{i,j}^{k,n+1}, Q_{i,j}^{k,n+1})$ can be expressed by

$$\Delta P_{i,j}^{k+1,n+1} - \Delta P_{i,j}^{k,n+1} = \left. \frac{d\Delta P_{i,j}^{k,n+1}}{dQ_{i,j}^{k,n+1}} \right|^k (Q_{i,j}^{k+1,n+1} - Q_{i,j}^{k,n+1}) \quad (2.22)$$

The FTE yields the following linear equation.

$$\Delta P_{i,j}^{k+1,n+1} - (2R_f|Q_{i,j}^{k,n+1}| + R_i) Q_{i,j}^{k+1,n+1} = -R_f|Q_{i,j}^{k,n+1}| Q_{i,j}^{k,n+1} - R_i Q_{i,j}^{k,n} \quad (2.23)$$

For the STE this expression yields

$$\Delta P_{i,j}^{k+1,n+1} - 2R_f|Q_{i,j}^k| Q_{i,j}^{k+1,n+1} = -\Delta P_{i,j}^{k,n+1} \quad (2.24)$$

The square pressure drop term ΔP may be converted to normal pressure drop Δp by dividing the pressure drop equation by $(p_i + p_j e^{s/2})$.

In the following subsection, we firstly give an overview of the different elements and node types comprising a gas network, secondly, we present a general graph theoretical representation of the gas network topology and finally, we use the integral form of the continuity equation to derive the equation system describing the gas flow dynamics in the integrated gas network system.

2.3.2. Modelling of Non-Pipe Facilities

Non-pipe facilities, such as compressor stations, regulator stations and valves play a key role in the operation and management of gas transport systems. These facilities enable the TSOs to supervise and control the gas stream, the pressure, the temperature and the line pack in the pipeline system.

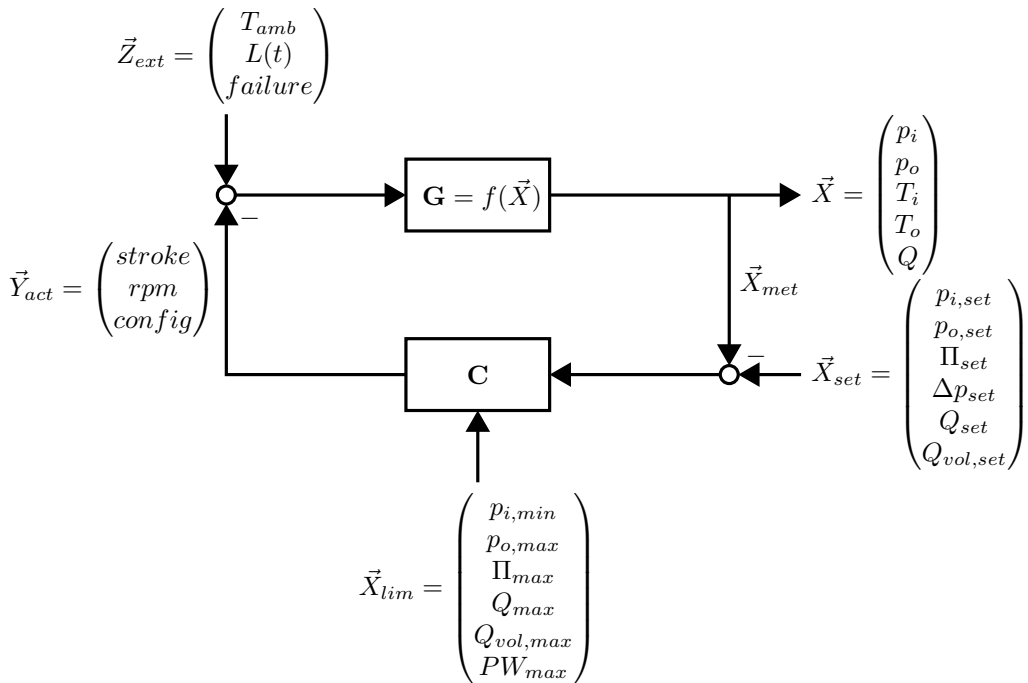


Fig. 2.3.: Functional diagram of a control system in compressor or regulator station

Compressor stations are usually installed at 100-200 kilometre intervals along the transport system. Their function is to increase the gas pressure to compensate for the pressure losses incurred during transportation. Regulator stations, in contrast, are primarily installed in combination with metering stations at all entry and exit stations (e.g. cross border stations, city gate stations, gas production fields, UGS, LNG terminals, stations at the interface to direct served customers such to Gas Power plants and large industrial customers) and at the interface of two connected pipeline subsystems with different MOP. The purpose of a regulator station is to reduce the inlet gas pressure to a lower outlet pressure and/or to regulate the quantity of gas flowing through the station. Valves in turn, are installed every 10-30 km along the pipeline system and serve the purpose of

routing the gas stream and shutting down sections of the network for maintenance or in case of a disruption.

Compressor stations and regulator stations are typically operated at a desired set point, which is controlled by a designated Automatic Control System (ACS). The purpose of such a system is to keep the station at the desired set point and to ensure that station constraints are not violated. Figure 2.3 shows a simplified functional diagram of an automatic control system, where \vec{X} marks the set of state variables at the station inlet and outlet (e.g. gas pressure p , temperature T and flow rate Q), \mathbf{G} the set of (differential) equations describing the physical processes in the station (e.g. adiabatic gas compression, isenthalpic gas expansion etc.), \vec{Z}_{ext} the set of external factors directly influencing the physical process (e.g. ambient temperature T_{amb} , fluctuations in demand and supply $L(t)$, technical failures etc.), \vec{X}_{met} the set of metered state variables, \vec{X}_{set} the set of control set points available to the dispatcher (e.g. flow rate set point Q_{set} , inlet and outlet pressure set point $p_{i,set}$ and $p_{o,set}$), \mathbf{C} the control algorithm of the controller, \vec{X}_{lim} the set of station constraints (e.g. maximum outlet pressure, maximum available compression power) and \vec{Y}_{act} the set of available actuators to act on the process (percent opening of the regulator flow area, shaft revolution etc.). The state variables \vec{X} are continuously metered by sensors and metering devices installed in the station (\vec{X}_{met}). The metered data is then compared to the desired operating set point \vec{X}_{set} requested by the dispatcher. The dispatcher can only assign one set point at a time, since the ACS typically permits the control of only one state variable at a time. Additional set points are then treated as constraints. The deviations between the metering data \vec{X}_{met} and the set point \vec{X}_{set} are forwarded to the controller \mathbf{C} . The controller then checks if the deviations are within acceptable margins and if the desired set point does not violate any station constraints (\vec{X}_{lim}). If a correction of the state variables is necessary to maintain the set point the controller makes use of the actuators \vec{Y}_{act} to act on the physical process \mathbf{G} . In case a requested set point is not permitted the controller will typically relax the set point to the next closest possible operating point.

In order to model the operation and control of non-pipe facilities, we need a mathematical description of the physical process (i.e. an equation describing the correlation between the state variables $\mathbf{G} = f(\vec{X})$), a list of control settings that can be assigned to each facility and a list of constraints limiting the operating region of each facility.

Modelling of Compressor Stations

Compressor stations are the most important and complex non-pipe facilities in the gas transport system. A compressor station usually consists of a number of compressor units made up of centrifugal or reciprocating compressors which are propelled by asynchronous electric motors or gas turbines. Centrifugal compressors are more common than recip-

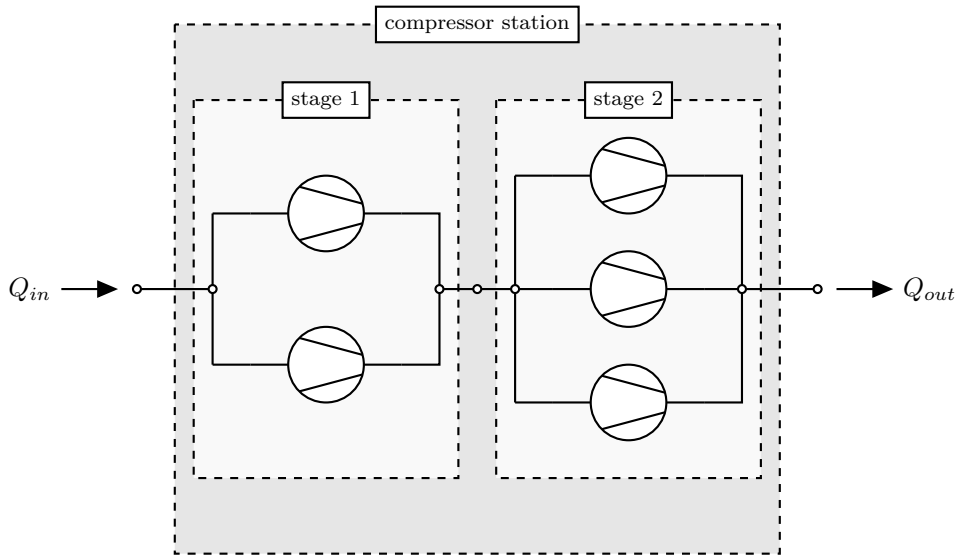


Fig. 2.4.: Compressor station with two stages and a parallel configuration of units

roating compressors, thus, the scope of this Section will be mainly on centrifugal compressors. The compressor units may be positioned in parallel and/or in multiple serial stages, in order to increase the compression capacity of the station and to enable a redundant, reliable and economical operation of the station. Figure 2.4 shows an example of a compressor station configuration, which consist of two stages, each stage with compressor units installed in parallel. A parallel configuration increases the compression capacity, i.e. the maximum quantity of gas that can be compressed per unit time, while a multistage configuration enables higher compression ratios Π , i.e. the ratio between outlet and inlet pressure. The compression process is a thermodynamic process that can be expressed by the following equation, derived from the first and second law of thermodynamics and the state equation for real gases under the assumption of adiabatic and isentropic conditions.

$$H_{ad} = \frac{\kappa}{\kappa - 1} Z_i T_i R \left[\Pi^{\frac{\kappa-1}{\kappa}} - 1 \right] \quad (2.25)$$

where H_{ad} is the adiabatic head, κ the isentropic exponent, R the specific gas constant, Z_i and T_i the gas compressibility factor and temperature at the inlet, respectively. The adiabatic head H_{ad} is the amount of specific energy (energy per mass) required to increase the inlet gas pressure p_i to a higher outlet pressure p_o assuming an ideal isentropic process (a reversible process without losses) with no heat transfer between the station and its surroundings. The actual compression process, which takes place in the centrifugal or piston compressor, is connected with losses which are accounted for by the adiabatic efficiency η_{ad} .

$$\eta_{ad} = \frac{H_{ad}}{H_{real}} \quad (2.26)$$

where H_{real} is the required specific energy for the actual process. A single centrifugal compressor typically has an adiabatic efficiency from $\eta_{ad} = 0.75 \dots 0.84$ [93], depending on its operating point ($f(\Pi, Q_{vol})$). The energy needed for the gas compression is provided by the driver through a single or multiple rotating shaft connected to the compressor. The required shaft power yields

$$PWS = \frac{H_{ad} \cdot \rho_n}{\eta_{ad}} \cdot Q \quad (2.27)$$

where ρ_n is the gas density at reference conditions. The driver can be either a gas turbine, which uses some of the transported gas from the pipelines as a fuel, or an electric motor, which requires a reliable electric power source close to the station. The power input PWD to the driver and the equivalent fuel consumption Q_f can be expressed by the following two equations.

$$PWD = \frac{PWS}{\eta_m} \quad (2.28)$$

$$Q_f = \frac{PWD}{GCV} \quad (2.29)$$

where η_m is the mechanical efficiency of the driver and GCV the upper calorific value of the transported gas. The losses of the driver are accounted for by the mechanical efficiency η_m . For gas turbines the mechanical efficiency typically ranges from $\eta_m = 0.28 \dots 0.38$ [93], while for electric drivers the efficiency is usually from $\eta_m = 0.7 \dots 0.92$. The extracted fuel from the network can be accounted for in the hydraulic model by applying the following

linearization for the fuel offtake, and assigning the resulting load to the inlet of the compressor station.

$$-\frac{K_i Q}{p_i} \Pi^{c_\kappa} \cdot p_i^{k+1} + \frac{K_i Q}{p_o} \Pi^{c_\kappa} \cdot p_o^{k+1} + \frac{K_i}{c_\kappa} [\Pi^{c_\kappa} - 1] \cdot Q^{k+1} + L_i^{k+1} = 0 \quad (2.30)$$

with

$$K_i = f \frac{Z_i T_i R \rho_n}{\eta_{ad} \eta_m GCV}, \quad \Pi = \frac{p_o}{p_i}, \quad c_\kappa = \frac{\kappa - 1}{\kappa}$$

where f is the fraction of driver power provided by gas turbines installed in the station. f is equal one if only electric driven turbines are installed in the station.

The operation of a centrifugal compressor is usually limited to an operating region referred to as the compressor envelope. The compressor envelope is usually depicted in a compressor wheel map, where the adiabatic head H_{ad} or the pressure ratio Π ($H_{ad} \sim \Pi$) is plotted against the volumetric flow rate (Q_{vol}). Figure 2.5 a) shows a schematic view of a compressor wheel map with the operating region restricted by the four solid red lines, which are referred to as surge line, choke line, line of maximum and minimum shaft revolution. The surge line determines the minimum volumetric flow rate ($Q_{vol,min}$) for a specific shaft revolution and is the most critical operating area. Operation beyond the left side of the surge line can cause great damage to the compressor. Usually, this area is prevented by a designated surge protection control system, which recycles a fraction of the compressed

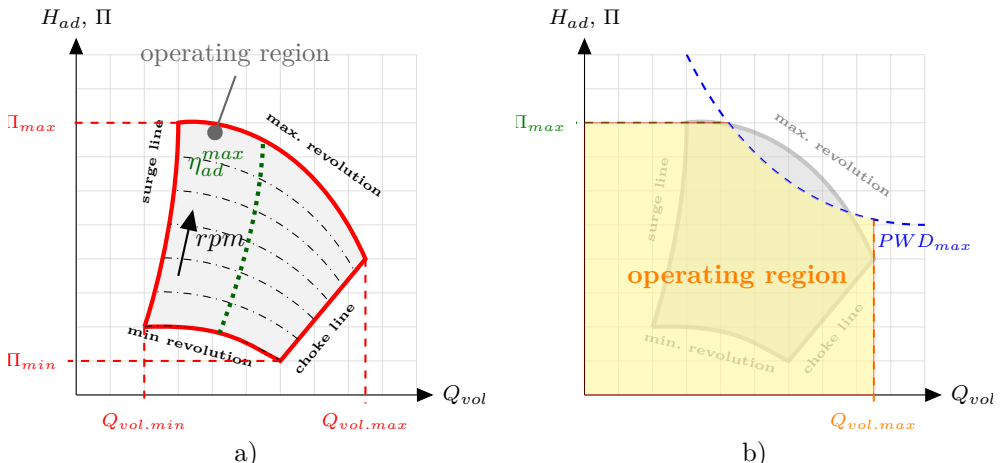
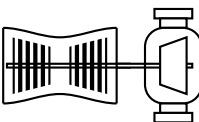
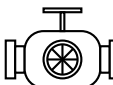
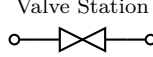


Fig. 2.5.: a) Typical operating envelope of a centrifugal compressor , b) Proposed aggregated operating region for the generic compressor station model

Facility	Control Modes	Constraints
Compressor Station 	inlet pressure ($p_{i,se}$) outlet pressure ($p_{o,se}$) pressure ratio (Π_{se}) pressure difference (Δp_{se}) flow rate (Q_{se}) volumetric flow ($Q_{vol,se}$) flow velocity (V_{se}) shaft power (PWS_{se}) driver power (PWD_{se}) driver fuel ($Q_{f,se}$) closed (OFF) bypass (BP)	<u>internal hard limits:</u> $p_o \geq p_i \& Q \geq 0$ <u>user defined limits:</u> max. outlet pressure ($p_{o,max}$, 80 bar-g) min. inlet pressure ($p_{i,min}$, 25 bar-g) max. volumetric flow ($Q_{vol,max}$, 100 m ³ /s) max. flow rate (Q_{max}) max. pressure ratio (Π_{max} , 2) max. driver power (PWd_{max} , 100 MW)
Regulator Station 	inlet pressure ($p_{i,se}$) outlet pressure ($p_{o,se}$) pressure difference (Δp_{se}) flow rate (Q_{se}) volumetric flow ($Q_{vol,se}$) flow velocity (V_{se}) closed (OFF) bypass (BP)	<u>internal hard limits:</u> $p_i \geq p_o \& Q \geq 0$ <u>user defined limits:</u> max. outlet pressure ($p_{o,max}$, 80 bar-g) min. inlet pressure ($p_{i,min}$, 25 bar-g) max. volumetric flow ($Q_{vol,max}$, 100 m ³ /s) max. flow rate (Q_{max})
Valve Station 	closed (OFF) opened (BP)	<u>internal hard limit:</u> $V \leq 60 \text{ m/s}$ <u>user defined limits:</u> max. flow velocity (V_{max} , 30 m/s)

Tab. 2.1.: Overview of available control modes and constraints settings for non-pipe facilities modeled as elements. Ad-hoc numeric values illustrated; values may differ in other networks. Numeric values for the different limits are typical values in a gas transport system, but may be different for different networks.

gas from the compressor outlet back to the inlet, in order to prevent an unstable operation of the compressor. Another important line, is the line of maximum adiabatic efficiency (η_{ad}^{max} , dotted green line in Fig. 2.5), which indicates the most economical working point for a specific shaft revolution. Starting from this line the adiabatic efficiency decreases left towards the surge and right towards the choke line. In contrast to the surge line, the choke line is a soft limit, to avoid an uneconomical operation of the station, since a working point allocated beyond this line is connected with a significant reduction of the adiabatic efficiency η_{ad} . The wheel map depicted in Fig. 2.5 a) describes the operation of

a single centrifugal compressor of a compressor unit installed in a compressor station. As explained in Fig. 2.4 a station may have a number of such units with different types of machines and configurations. A detailed model of the entire station would require a large pool of input data, such as the wheel maps of all compressors, the performance curves of all drivers, the control laws implemented in the ACS, the characteristics of the cooler and many more. From experience, these data are not completely available even to the TSOs and if available they are not easily accessible to the public. In many practical cases, a reduced model is sufficient to capture the basic characteristics of the entire station. Thus, it is reasonable to use a number of aggregated parameters describing the operation, control and constraints of the station. These parameters can be used to reduce the actual station to a generic model. The control of the station can be modelled by the control modes listed in Tab. 2.1. The aggregated operating region of the station can be captured by the area bounded by the generic constraints $Q_{vol,max}$, Π_{max} , PWD_{max} as depicted in Fig. 2.5 b). Additional generic constraints and their corresponding default values are listed in Tab. 2.1. The adiabatic efficiency η_{ad} of the compressors and the mechanical efficiency η_m of the drivers are aggregated to an average value for the entire station. If the station is operated (i.e. control mode is neither *OFF*, *BP*) the working point needs to be checked against the defined generic constraints.

Modelling of Entry & Exit Stations

Each entry and exit point in the transport system and each transition point between two different transmission networks is typically equipped with a regulator and metering station to control and monitor the quantity of gas entering or exiting the network, and the supply or delivery pressures at these crucial points of the network.

In the following, the structure and operation of gas stations are explained. Afterwards an overview of the different types of gas stations in the gas transport system is given.

Figure 2.6 shows a typical schematic structure of a two street regulator and metering station and the technical devices and components installed in such stations, such as valves, filtering devices, heaters, regulators and flow meters. The primary street contains the regulator which is typically controlled by a designated automatic control system as described in Fig. 2.3. The secondary street, in contrast is not controlled and is available for maintenance or in case of a disruption in the primary street. It contains a control valve that can be adjusted manually. A gas station typically consists of more than two streets, in order to increase the capacity of the station and to have a back up in case of a disruption in the station. Gas stations are installed at different types of exit and entry points

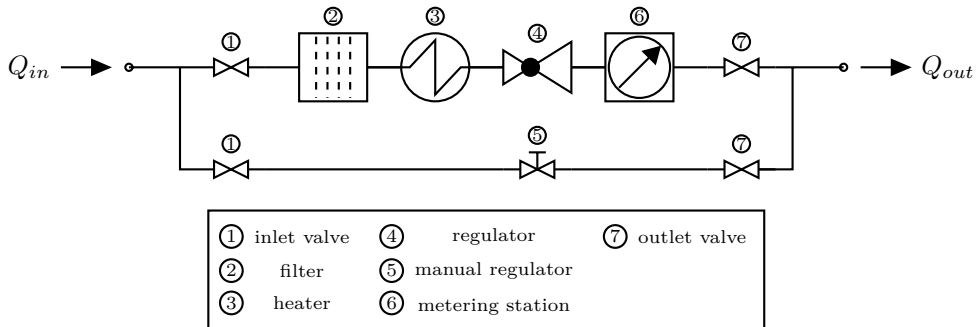


Fig. 2.6.: Typical schematic structure of a gas regulator and metering station

in the transport system, which can be subdivided into

- I. *Production Fields (PRO)*,
- II. *cross border import/export stations (CBI/CBE)*,
- III. *city gate stations (CGS, connection to local gas distribution system)*,
- IV. *stations of direct served customers (Gas Fired Power Plants (GFPP)), and*
- V. *transitional stations connecting the network systems of at least two independent entities*

Production fields connected to the transport system require a gas station in order to reduce the field pressure to pipeline pressure and to monitor the gas entering the transport system. The regulator stations in production fields are usually outlet pressure controlled. Cross border import and export stations are located at the national borders of two national transport systems operated by different entities. Transitional gas stations, in turn, are located at interconnection points between two transmission networks in one country owned by different TSOs and/or operated at different pressure levels. The quantity of gas imported or exported through cross border and transitional stations is typically characterized by relatively small daily and yearly fluctuations.

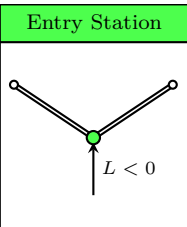
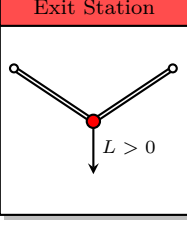
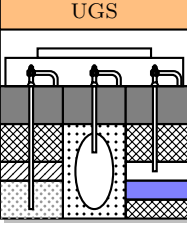
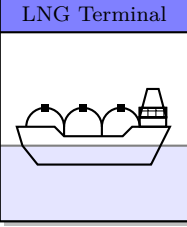
City gate stations, in contrast, are located at the interface to the local gas distribution system. The amount of gas leaving the transport system at these stations is normally connected with relatively large daily and seasonal fluctuations, since the majority of customers supplied are small customers, like households, commercial customers etc., who use gas mainly for heating and cooking. City gate stations play a crucial role in terms of security of gas supply, since protected customers receive gas from these stations. According

to Article 2 of the Regulation [12] protected customers include all household customers connected to a gas distribution network, social services, small and medium-sized enterprises that do not represent more than 20% of the final use of gas entering the distribution station and district heating installations with no fuel switching that provide heating to households. Stations of direct served customers, are at the interface to large consumers such as gas fired power generation plants and large industries, which are served directly from the transport pipeline. The quantity of gas delivered to these customers is usually constant throughout the year and may fluctuate during the day, for instance, if a gas power plant is used for peak load shaving.

At each of these presented stations, contractual agreements exist regarding gas quality, quantity and pressure, which have to be met by the different parties to avoid legal penalties. In a liberalized gas market, these contractual agreements are typically established by gas traders, also referred to as shippers, who have contracts with gas producers for buying a certain quantity of gas for a given market price, contracts with TSOs for booking entry, exit and transport capacities (nominations) and contracts with consumers for delivering the commodity [94]. Since most gas stations are typically controlled and are located at the boundary of the network, it is reasonable to model these stations by a single node, which can be used to reflect the pressure or flow control of the actual station. Table 2.2 shows the available control modes and constraint parameters for modelling an entry or exit station. The contractual constraints, can be modelled by the limits for the flow rate and pressure. In case a transitional gas station or a cross border station between two pipeline elements is present in the network model, a regulator element is used to model the operation of this station.

Modelling of Underground Gas Storage Facilities

The transport of natural gas from production sites to consumption areas may take a significant amount of time depending on the distance, the quantity of gas transported and the type of transportation chosen (e.g. LNG-vessels or solely pipeline transport). While the quantity of gas supplied to the transport system remain relatively constant throughout the year, demands may change depending on the season and the ambient temperature. During winter gas consumption is inherently greater than during summer. Thus, it may happen that gas arriving to the transport system from production fields or cross border points may not be needed right away. However, in order to keep the surplus of gas in the transport system and close to consumption areas for seasons of peak demand, natural gas is stored in UGS facilities and withdrawn when demanded. Gas

Facility	Control Modes	Constraints
	pressure (p_{set}) inflow (Q_{set})	<u>internal hard limits:</u> $L \leq 0$ <u>user defined limits:</u> min. supply flow (Q_{min}) max. supply flow (Q_{max}) min. supply pressure (p_{min}) max. supply pressure (p_{max})
	pressure (p_{set}) outflow (Q_{set})	<u>internal hard limits:</u> $L \geq 0$ <u>user defined limits:</u> min. delivery flow (Q_{min}) max. delivery flow (Q_{max}) min. delivery pressure (p_{min}) max. delivery pressure (p_{max})
	pressure (p_{set}) withdrawal/injection rate (Q_{set}) initial working inventory (INV) withdrawal state (WDR) injection state (INJ)	<u>internal hard limits:</u> $L^{wdr} \leq 0 \text{ & } L^{inj} \geq 0$ <u>user defined hard limits:</u> max. working inventory ($I_{w,max}$) max. withdrawal rate ($Q_{wdr,max}$) max. injection rate ($Q_{inj,max}$) <u>user defined limits:</u> max. supply pressure ($p_{wdr,max}$) min. offtake pressure ($p_{inj,min}$)
	pressure (p_{set}) regasification rate (Q_{set}) initial working inventory (INV) arriving vessel size ($VESSEL$)	<u>internal hard limits:</u> $L \leq 0$ <u>user defined hard limits:</u> max. working inventory ($I_{w,max}$) max. regasification rate ($Q_{reg,max}$) <u>user defined limits:</u> max. supply pressure ($p_{reg,max}$)

Tab. 2.2.: Overview of available control modes and constraints settings for non-pipe facilities modelled as nodes

storage facilities increase the flexibility and ability to react to long-term and short-term fluctuations and to disruptions in gas supply and demand.

The operation of UGS facilities can be characterized by different parameters. The most important ones are described below.

I. Storage Inventory I_s :

Quantity of natural gas currently stored in the storage reservoir.

II. Maximum Storage Inventory $I_{s,max}$:

Maximum quantity of gas that can be stored in the storage reservoir.

III. Base Gas Inventory I_b :

Minimum quantity of gas that remains in the storage reservoir to ensure an adequate reservoir pressure for the withdrawal process.

IV. Working Gas Inventory I_w :

Difference between storage inventory and base gas inventory.

V. Maximum Working Gas Inventory $I_{w,max}$:

Total amount of gas that can be withdrawn from the storage reservoir during normal operation.

VI. Withdrawal Rate Q_{wdr} :

Flow rate at which natural gas is withdrawn from the storage facility and injected into the transport system.

VII. Maximum Withdrawal Capacity Q_{wdr}^{max} :

Maximum possible withdrawal rate at which natural gas can be withdrawn from the storage facility and injected into the transport system. Maximum withdrawal capacity is at its peak when storage inventory reaches maximum storage inventory and decreases as gas is withdrawn from storage

VIII. Injection Rate Q_{inj} :

Flow rate at which natural gas is withdrawn from the transport system and injected into the storage reservoir.

IX. Maximum Injection Capacity Q_{inj}^{max} :

Maximum possible injection rate at which natural gas can be withdrawn from the transport system and injected into the storage reservoir. Maximum injection capacity is at peak when working gas is fully withdrawn and decreases while gas is injected into the reservoir.

X. Turn-Over Rate T_I :

Time required for a storage cycle, i.e to empty and refill the working inventory of the storage reservoir

In principle, two kinds of storage facilities can be classified, namely, base load and peak load facilities [95]. Base load storages can store large amounts of natural gas in their reservoirs, but have relatively low withdrawal and injection rates. They are suitable for covering long-term seasonal demands. In these facilities gas is injected during seasons of low demand, mostly in non-heating periods from April to October, and withdrawn during seasons of high demand, mostly in heating periods from November to February. The most common type of base load facility connected to gas transport systems are depleted gas fields, which are emptied gas production fields close to consumption areas that were converted to UGS facilities. Depleted gas fields have several advantages. They do not require further exploration and can take advantage of existing wells and technical devices of the former production field. Depleted gas fields are characterized by their reservoir depths that can be from 2,500-4,500 m, their enormous storage capacity which can amount to several billion cubic meters and their relatively low withdrawal and injection rates. They normally have a turn-over rate of one year. Moreover, they may require a base gas inventory of up to 50% of working gas inventory [96].

In contrast to base load facilities, peak load facilities have relatively high withdrawal rates, but smaller storage capacities compared to base load storages. These facilities have relatively short turn-over rates and are mostly used to cover short-term peak demands. Salt cavern facilities are the most common type of peak load storages. They are formed in underground salt deposits and are utilized for storing large volumes of natural gas close to consumption areas. The storage capacities of salt caverns is much lower than that of depleted fields, however, salt caverns have much higher withdrawal rates. Their turn over rates are between a day and a week [95]. Moreover, they require relatively small amounts of base gas inventory (usually 20-30% of working gas inventory) [96].

Another type of storage facility, which has characteristics of base load and peak load storages are formed in aquifers. Aquifer storages originated from natural aquifers which were converted to allow the storage of natural gas. Their geological structure is similar to depleted gas fields. The storage reservoir in aquifer storages is formed between an overlying impermeable cap rock and the underlying ground water, which contribute to maintaining reservoir pressure during withdrawal. Aquifer storages require a relatively large amount of base gas inventory which can be as high as 80% of working gas inventory. Due to their high development, maintenance and operating costs aquifers are the least attractive type of UGS.

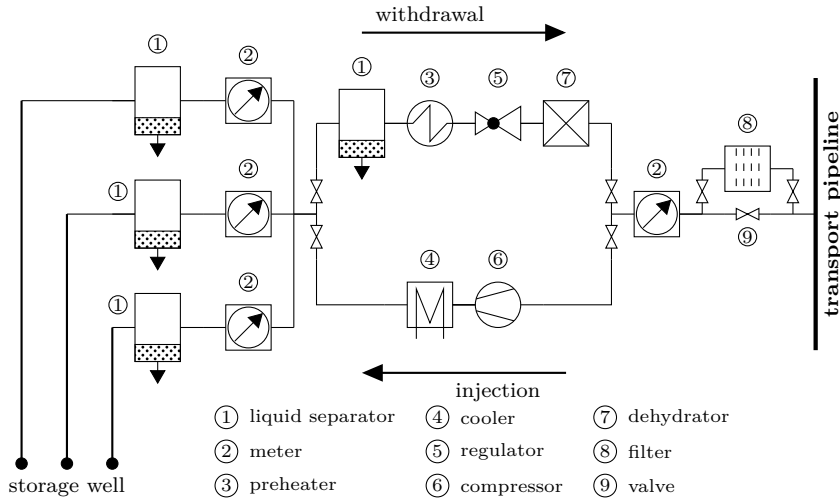


Fig. 2.7.: Typical schematic structure of the above ground components of an underground gas storage facility

The structure of the overground section of UGS facilities is very similar for all three types of storages and is illustrated schematically in Fig. 2.7. Some of the overground components are well heads, pipe gatherings, liquid separators, coolers, heaters, regulators, compressors, dryers, filters, valves and metering devices.

The operation of UGS facilities is divided into two processes, namely, the withdrawal process, where working gas is withdrawn from the reservoir and added to the pipeline, and the injection process, where gas is taken from the pipelines and injected into the reservoir. The withdrawal process is controlled by a regulator station, which reduces the pressure of the gas withdrawn from the reservoir (upto 350 bar-g depending on the storage type and stock level) to pipeline pressure, while the injection process is controlled by a compressor station, which increases the pressure of the gas taken from the pipeline to reservoir pressure. The pressure in the reservoir depends on the total gas inventory in the reservoir. The more gas is withdrawn from the reservoir, the lower the reservoir pressure and the lower the maximum withdrawal rate of the station. In order to reflect the injection and withdrawal process, UGS facilities are modelled as a single node (storage node), which is either a supply node, during the withdrawal process or a demand node during the injection process. During the withdrawal process the load of the node corresponds to the withdrawal rate, while during injection the load is equal to the injection rate. Furthermore, the characteristics of UGS facilities are modelled by the scenario parameters listed in the second column of Tab. 2.2. The control mode of the facility can be either

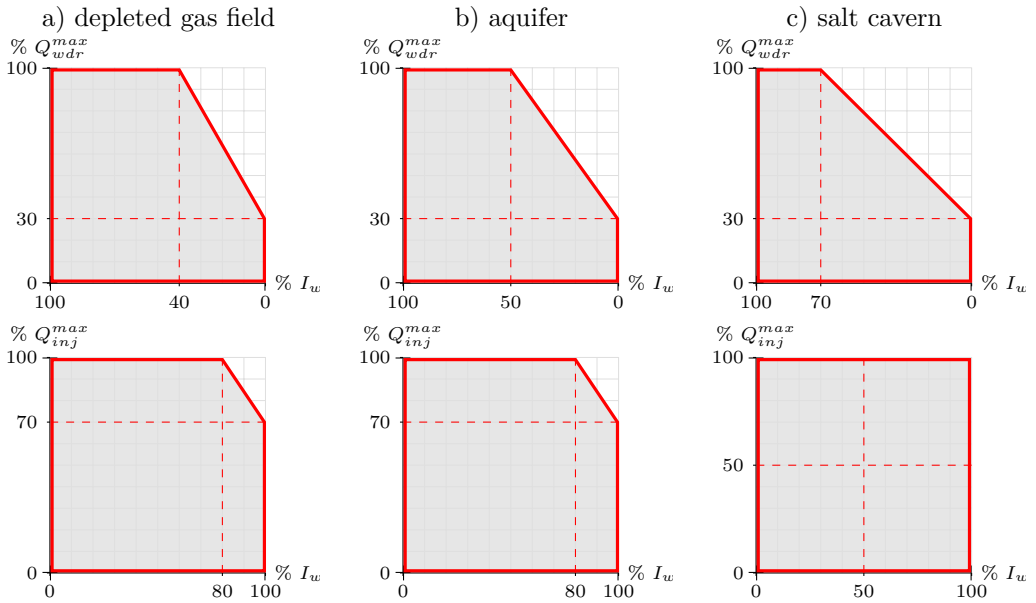


Fig. 2.8.: Typical UGS envelopes for depleted gas fields, aquifer and salt cavern storage for the withdrawal process (top) and the injection process (bottom) [97,98]

pressure control (p_{set}) or flow control (L_{set}). The current process at the station can be specified by the injection state INJ or withdrawal state WDR (default state), while the initial working gas inventory can be set by the parameter INV . The initial working gas inventory is important, since it determines the working point of the facility at the start of the simulation. In addition, the third column in Tab. 2.2 gives an overview of parameters describing the constraints of UGS facilities, in particular, their operating envelope.

The operating region of a storage facility is typically reflected by its storage envelope, which depicts the technically possible operating points of the facility in terms of withdrawal rate (Q_{wdr}), injection rate (Q_{inj}) and working gas inventory (I_w). The shape of the storage envelope depends on a number of properties, such as, the storage type, the maximum and minimum reservoir pressure, minimum gas inventory (cushion gas), the available compression power for injection and withdrawal etc. Figure 2.8 shows typical storage envelopes for the withdrawal and injection process of the three storage types.

The actual operating point of the storage facility will be considered by monitoring the withdrawal/injection rate and working gas inventory in each time step and ensuring this

point lies within the storage envelope. The working gas inventory in the storage reservoir at each time step can be obtained by

$$I_w(t) = I_w(t_0) + \int_{t_0}^t Q_{inj}(t) - Q_{wdr}(t) dt \quad (2.31)$$

where t_0 is the initial time point. Knowing the working gas inventory and the withdrawal or injection rate, the operating point can be determined and checked for each time step. If the operating point is outside the storage envelop, the time step will be recalculated using the boundary values.

Modelling of LNG Terminals

In cases where a direct pipeline connection between the gas producing region and the consumption area is unfeasible or inefficient due to the distances and the geographical conditions (e.g. production and consumption sites are separated by waters), natural gas may be liquefied and then transported with specially designed LNG vessels to consumption regions. Since the volume occupied by LNG is almost 600 times smaller than that occupied by gaseous natural gas at atmospheric condition a large quantity of gas can be transported with LNG vessels, which can accommodate upto 150,000 m³ of LNG [93]. The liquification of natural gas is conducted at temperatures of approximately -160 °C in liquification plants located close to shipping ports in the producing regions. During transportation this temperature has to be maintained in order to keep LNG in liquefied form. The vessels transporting LNG to the consumption regions are normally powered by steam turbines, which use a fraction of the transported LNG as a fuel. These vessels can reach velocities of upto 20 knots (approx. 37 km/h) [93]. The transported LNG arrives to the consumption regions at LNG regasification terminals which are located at shipping ports close to consumption areas.

Figure 2.9 shows a typical schematic structure of a LNG regasification terminal, which comprises of a number of technical components such us pipe gatherings, high pressure pumps, vaporizers and metering devices. When the LNG vessel arrives to the terminal the transported LNG is firstly withdrawn from the vessel and injected into a designated LNG storage tank from the top, where the LNG is kept at a temperature of approx. -160 °C and a pressure of 150-250 mbar-g. During the relocation process some of the LNG may vaporize in the piping system and in the LNG storage tank. Some of the vaporized LNG is returned to the LNG vessel through a designated vapor return system. The LNG

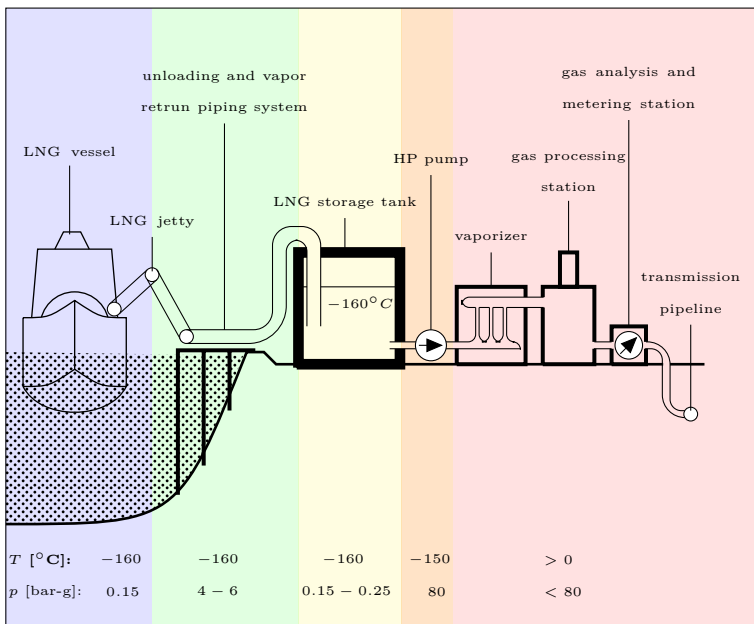


Fig. 2.9.: Typical schematic structure of a LNG regasification terminal

stored in the storage tank is withdrawn from the bottom of the tank and directed to a number of high pressure pumps where the pressure of the LNG is raised to pipeline pressure (in this case 80 bar-g). The actual regasification of the LNG is then conducted at vaporizing station, where the LNG is vaporized using air and/or the heat energy from the surrounding sea. After the regasification, the gas may be processed (filtering, water separation etc.) and then forwarded to the metering station before it is injected into the transport system.

LNG terminals can be used to increase the storage capacity, thus, the flexibility of the transport system to react to variations in demand and supply. Some LNG terminals can have storage capacities of upto 540,000 m³ of LNG, which is normally spread on a number of storage tanks.

The operation of LNG Terminals can be characterized by the following parameters:

I. **Gross Storage Capacity I_{LNG}^{\max} :**

Maximum amount of LNG that can be stored in the storage tanks.

II. **Maximum Working Inventory $I_{w,\text{LNG}}^{\max}$:**

Maximum amount of LNG that is available for regasification. The gross capacity is not completely available for regasification, since a small amount of LNG always remain

in the storage tank, to ensure a smooth operation of the facility. The maximum working inventory is the actual amount of LNG available for operation.

III. *LNG Inventory* I_{LNG} :

Amount of LNG currently stored in the LNG storage tanks.

IV. *LNG Working Inventory* $I_{w,LNG}$:

Amount of LNG currently stored in the LNG storage tanks that can be regasified and injected into the transport system.

V. *Regasification Rate* Q_{reg} :

Flow rate at which LNG is regasified and injected into the transport system.

VI. *Maximum Regasification Rate* Q_{reg}^{max} :

Maximum possible flow rate at which LNG can be regasified and injected into the transport system. Unlike UGS facilities the maximum regasification rate does not depend on the LNG inventory. Thus, the maximum regasification rate remains constant, when LNG is withdrawn from storage.

VII. *Vessel Discharge Rate* Q_{dis} :

Indicates how fast LNG transported in the vessel can be relocated from the vessel to the storage tanks

Similar to UGS facilities, LNG terminals can be regarded as supply nodes with an operating region limited by the LNG working inventory (the amount of LNG in the storage tanks available for regasification) and maximum regasification rate Q_{reg}^{max} . The working gas inventory decreases during withdrawal from storage and increases when LNG is discharged from an arriving LNG vessel and injected into storage, while the regasification capacity, remains constant, and is independent of the fluctuations in storage level.

The storage inventory in the tanks is monitored each time step in order to capture the operating point of the station correctly. Therefore, the LNG in storage will be transformed to an equivalent quantity of gaseous natural gas at standard conditions using the following relation for the relative density d_{lng} :

$$d_{lng} = \frac{\rho_{n,lng}}{\rho_{n,gas}} \quad (2.32)$$

which is the ratio between the density of LNG ($\rho_{n,LNG} \cong 421 \text{ kg/m}^3$) and gaseous natural gas $\rho_{n,gas}$ at standard condition. Using this relation the equivalent standard volume of working gas inventory in the LNG tank at any instant of time $I_w(t)$ yields

$$I_w(t) = d_{LNG} \cdot I_{LNG}(t_0) + \int_{t_0}^t d_{LNG} \cdot Q_{dis}(t) - Q_{reg}(t) dt \quad (2.33)$$

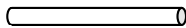
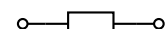
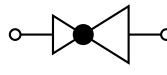
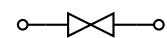
where $I_{LNG}(t_0)$ is the LNG in storage at the initial time point t_0 , $Q_{dis}(t)$ the vessel discharge rate and $Q_{reg}(t)$ the regasification rate. If I_w exceeds the equivalent maximum working gas capacity of the LNG terminal the load of the supply node will be set to zero.

Another constraint of LNG terminals is the maximum send-out pressure (p_{max}) which is restricted by the maximum compression power of the high pressure pumps. This constraint may restrict the regasification rate, since to inject gas into the transport system a pressure gradient between the terminal and the transport pipeline is needed. Thus, the send-out pressure constraint will be checked together with the other constraints after each time step. If any of the constraints is violated the boundary values will be applied and the time step will be recalculated. If no compatible set point can be found the load will be set to zero.

2.3.3. Network Description

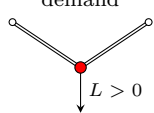
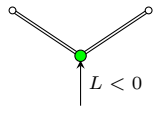
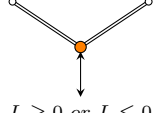
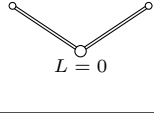
The components in a gas transport system can be described using basic elements of graph theory, namely, nodes and directed edges. A directed edge represents an element with an inlet, an outlet and a flow direction. The following elements listed in Tab. 2.1 are described by directed edges, namely, pipelines, compressors, regulators, valves and resistors. Pipelines and resistors are passive elements, since their behaviour is fully described by the physical equation, while compressors, regulators and valves are considered active elements, since their states can be controlled externally. Furthermore, for each element in Tab. 2.1 a description of the function and the basic equation describing their operation are listed. The operation of a compressor station for instance is generally an equation describing the required compression power from the driver, which can be either a gas turbine or electric driver.

The interconnection points between the individual network elements in Tab. 2.1 are referred to as nodes. Each element typically has at least one common inlet or outlet node with another element in the network. Moreover, nodes are the only location in the net-

Element Types	Description
Passive Elements	
pipe 	models a section of a pipeline, basic properties are length, diameter, roughness and pipe efficiency
resistor 	models passive devices that cause a local pressure drop (e.g. meters, inlet piping, coolers, heaters, scrubbers etc.)
Active Elements	
compressor 	models a compressor station with generic constraints, allows the specification of a control mode of the station (e.g. outlet pressure control, inlet pressure control, flow rate control etc.)
regulator 	models a pressure reduction and metering station located at the interface of two neighbouring networks with different maximum operating pressures, allows the specification of a control mode of the station (e.g. outlet pressure control, inlet pressure control, flow rate control etc.)
valve 	models a valve station, which is either opened or closed

Tab. 2.3.: Basic elements comprising gas transport networks

work where gas can be injected or extracted from the network. Similar to elements, we can distinguish the following type of nodes listed in Tab. 2.4, namely, demand, supply, storage and junction nodes. Demand nodes are points in the transport system, where gas is extracted from the network, such as city gate stations (CGS, connection to the local, low pressure distribution network), cross border export stations (CBE, transport of natural gas to neighbouring network systems) gas fired power plants and large industries (IND), which are directly served from the transport system. Supply nodes, in contrast, are entry points to the gas system from production fields (PRO), cross border import stations (CBI, gas import from neighbouring countries through pipelines) and LNG terminals, while storage nodes are locations of UGS facilities, where gas can either enter

Node Type	Description	Facilities
 demand $L > 0$	point, where gas is extracted from the network	CGS, CBE, GFPP, IND
 supply $L < 0$	point, where gas is injected into the network	PRO, CBI, LNG
 storage $L \geq 0 \text{ or } L \leq 0$	point, where gas is injected or extracted from the network	UGS
 junction $L = 0$	point, where a topological change or a change in pipe properties occurs (e.g. diameter, inclination)	-

Tab. 2.4.: Classification and characteristics of nodes in the network

or exit the network. The topology of the entire network is described by the following node-branch incidence matrix:

$$\mathbf{A} = [a_{i,j}]^{n \times m} \quad a_{i,j} = \begin{cases} +1, & \text{node } i \text{ is outlet of element } j \\ -1, & \text{node } i \text{ is inlet of element } j \\ 0, & \text{node } i \text{ and element } j \text{ are not connected} \end{cases} \quad (2.34)$$

where n is the number of nodes, m the number of elements and $a_{i,j}$ the elements of matrix \mathbf{A} . Matrix \mathbf{A} can be decomposed in a node-pipe incidence matrix \mathbf{A}_P describing only pipe connections and a node-non-pipe incidence matrix \mathbf{A}_N describing non-pipe connections.

$$\mathbf{A} = [\mathbf{A}_P | \mathbf{A}_N] \quad (2.35)$$

Each node in the network is characterized by its nodal pressure p_i and nodal load L_i , while each branch is characterized by its gas flow rate Q_j . The set of nodal pressures, nodal loads and element flow rates can be described by their corresponding vectors.

$$p = \begin{pmatrix} p_1 \\ p_2 \\ \vdots \\ p_n \end{pmatrix}, \quad P = \begin{pmatrix} p_1^2 \\ p_2^2 \\ \vdots \\ p_n^2 \end{pmatrix}, \quad L = \begin{pmatrix} L_1 \\ L_2 \\ \vdots \\ L_n \end{pmatrix}, \quad Q = \begin{pmatrix} Q_1 \\ Q_2 \\ \vdots \\ Q_m \end{pmatrix} \quad (2.36)$$

where

$$p_i \geq 0, \quad L_i : \begin{cases} > 0, & \text{demand} \\ < 0, & \text{supply} \end{cases}, \quad Q_j : \begin{cases} > 0, & \text{flow direction is from inlet to outlet} \\ < 0, & \text{flow direction is from outlet to inlet} \end{cases} \quad (2.37)$$

Similarly to the incidence matrix \mathbf{A} , the flow vector Q can be decomposed in a pipe and non-pipe component.

$$Q = [Q_P | Q_N]^T \quad (2.38)$$

2.3.4. System of Equations for the Total Network

The dynamic behaviour of a gas transport system is primarily determined by the pipeline elements. As discussed in Section 2.3.1, gas pipelines have four basic properties, namely, linepack, resistance, inertia and gravity. Linepack and resistance are the most dominant properties, while gravity and inertia play a secondary role. A pipeline network can be segmented into a number of pipeline sections, by distributing the aforementioned properties to the corresponding pipe segments. Figure 2.10 demonstrates how this can be done for a section of a pipe network. In this example, the volumes of the pipelines are equally distributed and assigned to the inlet and outlet nodes of each pipeline. The quantity of gas $Q_{i,j}$ transferred between two nodal volumes depends on the pressure difference p_i and p_j , the resistance, the inertia and the inclination of the pipeline segment between the two nodal volumes. This relation is described by the pressure drop equation (2.16) derived in Section 2.3.1. According to the continuity equation (2.15), the pressure in the nodal volume may change in time if there is an imbalance between inflows and outflows to the

nodal volume V_i . This can be expressed by the integral form of the continuity equation applied to node i .

$$\frac{V_i}{\rho_n c_{i,j}^2} \frac{dp_i}{dt} = \sum_{j=1}^k a_{i,j} Q_{i,j} - L_i \quad (2.39)$$

with

$$V_i = \frac{\pi}{8} \sum_{j=1}^k D_{i,j}^2 \Delta x_{i,j} \quad (2.40)$$

where L_i is the external load extracted/injected to node i with volume V_i and $D_{i,j}$ the diameter of pipe segment (i, j) .

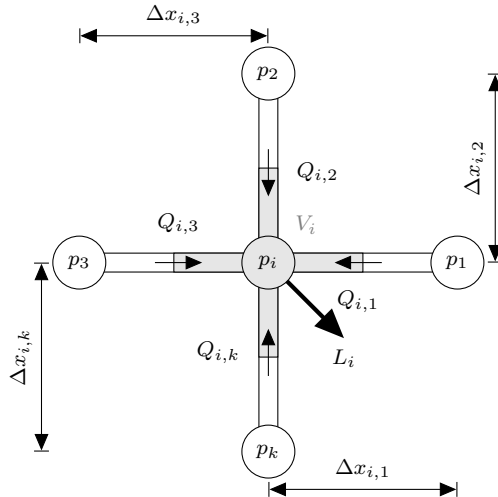


Fig. 2.10.: Law of mass conservation for a nodal control volume in a gas network

The continuity equation can be expressed for each node in the network, thus, we obtain a set of equations equal to the number of nodes defined for the network. If we perform an implicit time integration of the set of integral continuity equations for a time step $\Delta t = t_{n+1} - t_n$ and order the equation in terms of known variables and boundary conditions at time t_n and t_{n+1} (right hand side) and unknown variables at time t_{n+1} (left hand side) we obtain the following finite difference matrix equation for the integrated network:

$$\Phi p^{n+1} - \mathbf{A} Q^{n+1} = \Phi p^n - 0.5 (L^n + L^{n+1}) \quad (2.41)$$

where \mathbf{A} is the incidence matrix described in eq. (2.34), Q and L the vectors of element flows and nodal loads described in eq. (2.36) and Φ the following diagonal matrix describing the pressure coefficients ϕ_i :

$$\Phi = \text{diag}\{\phi_1, \phi_2, \dots, \phi_n\}, \quad \phi_i = \frac{V_i}{\rho_n c_{i,j}^2 \Delta t} \quad (2.42)$$

As can be seen from the right hand side of equation (2.41), to obtain the state of the network for a time in the future (t_{n+1}) we need information on the state in the past (t_n) and the boundary conditions in the future (L^{n+1}), thus, a transient simulation requires an initial state and boundary conditions. Typically, a steady state solution of the network is chosen as an initial condition to start the transient calculation. The equations for the steady state can be obtained if we set $p^n = p^{n+1}$ and $L^n = L^{n+1}$ or the nodal volume V_j to zero, which will result in an equation describing Kirchhoff's first law, which implies the sum of incoming and outgoing flows Q_j in a node i to be equal to the nodal load L_i .

$$\mathbf{A} Q = L \quad (2.43)$$

2.3.5. Boundary Conditions

The matrix equation derived in the previous section requires additional linear independent equations in order to close the entire problem, since the number of unknowns is greater than the number of equations. These equations are provided by the linearised pressure drop equations (2.22) and additional equations describing the control mode of non-pipe elements (e.g. compressors and regulators), and the control of facilities at entry and exit points of the network. The operation of compressor stations and regulator stations are typically controlled by a designated automated control system, which ensures the desired operating set point (e.g. outlet pressure, flow rate, inlet pressure etc.) is maintained and constraints are not violated. At each gas entry and exit point in the transport system there is typically a regulator station that controls the flow rate or pressure at a desired set point. Thus, we can reflect this control by assigning to each demand, supply and storage node the corresponding control of the connected facility. In the following the missing equations describing the control modes are elaborated.

Control Mode	Equation	Coefficients $c_1 \cdot p_1 + c_2 \cdot p_2 + c_3 \cdot Q = d$
inlet pressure ($p_{i,set}$)	$p_i = p_{i,set}$	$c_1 = 1, c_2 = 0, c_3 = 0, d = p_{i,set}$
outlet pressure ($p_{o,set}$)	$p_o = p_{o,set}$	$c_1 = 0, c_2 = 1, c_3 = 0, d = p_{o,set}$
pressure ratio (Π_{set})	$\frac{p_o}{p_i} = \Pi_{set}$	$c_1 = -\Pi_{set}, c_2 = 1,$ $c_3 = 0, d = 0$
pressure difference (Δp_{set})	$p_o - p_i = \Delta p_{set}$	$c_1 = -1, c_2 = 1,$ $c_3 = 0, d = \Delta p_{set}$
flow rate (Q_{set})	$Q = Q_{set}$	$c_1 = 0, c_2 = 0, c_3 = 1, d = Q_{set}$
volumetric flow ($Q_{vol,set}$)	$Q = \frac{p_i}{Z_i T_i R \rho_n} Q_{vol,set}$	$c_1 = -\frac{Q_{vol,set}}{Z_i T_i R \rho_n}, c_2 = 0,$ $c_3 = 1, d = 0$
shaft power (PW_{sset})	$PW_{sset} = \frac{K_i Q}{c_\kappa} [\Pi^{c_\kappa} - 1]$ $K_i = \frac{Z_i T_i R \rho_n}{\eta_{ad} \eta_m}, \Pi = \frac{p_o}{p_i},$ $c_\kappa = \frac{\kappa - 1}{\kappa}$	$c_1 = -\frac{K_i Q}{p_i} \Pi^{c_\kappa}, c_2 = \frac{K_i Q}{p_o} \Pi^{c_\kappa},$ $c_3 = \frac{K_i}{c_\kappa} [\Pi^{c_\kappa} - 1], d = PW_{sset}$
driver power (PW_{dset})	$PW_{dset} = \frac{K_i Q}{c_\kappa} [\Pi^{c_\kappa} - 1]$ $K_i = \frac{Z_i T_i R \rho_n}{\eta_{ad} \eta_m GCV}, \Pi = \frac{p_o}{p_i},$ $c_\kappa = \frac{\kappa - 1}{\kappa}$	$c_1 = -\frac{K_i Q}{p_i} \Pi^{c_\kappa}, c_2 = \frac{K_i Q}{p_o} \Pi^{c_\kappa},$ $c_3 = \frac{K_i}{c_\kappa} [\Pi^{c_\kappa} - 1], d = PW_{dset}$
driver fuel ($Q_{f,set}$)	$Q_{f,set} = \frac{K_i Q}{c_\kappa} [\Pi^{c_\kappa} - 1]$ $K_i = \frac{Z_i T_i R \rho_n}{\eta_{ad} \eta_m GCV}, \Pi = \frac{p_o}{p_i},$ $c_\kappa = \frac{\kappa - 1}{\kappa}$	$c_1 = -\frac{K_i Q}{p_i} \Pi^{c_\kappa}, c_2 = \frac{K_i Q}{p_o} \Pi^{c_\kappa},$ $c_3 = \frac{K_i}{c_\kappa} [\Pi^{c_\kappa} - 1], d = Q_{f,set}$
bypass (BP)	$p_i = p_o$	$c_1 = -1, c_2 = 1, c_3 = 0, d = 0$
off (OFF)	$Q = 0$	$c_1 = 0, c_2 = 0, c_3 = 1, d = 0$

Tab. 2.5.: Control modes for non-pipe facilities and their mathematical implementation

Non-Pipe Equations

The general equations for non-pipe elements are provided by the following linear equation:

$$c_{1,j} p_1^{n+1} + c_{2,j} p_2^{n+1} + c_{3,j} Q_j^{n+1} = d_j \quad (2.44)$$

where $c_{1,j}$, $c_{2,j}$ and $c_{3,j}$ are scalar coefficients of the inlet node pressure p_1 , the outlet node pressure p_2 and the flow rate Q_j of non-pipe element j , respectively. In addition d_j is a constant on the right hand side. The different control modes for each non-pipe element and their corresponding equations are summarized in Tab. 2.1 & 2.5. The set of control modes for compressor stations are similar to that for regulator stations, while for valves only the control mode bypass and inactive is possible. Moreover, compressor and regulator elements may have constraints, which will be checked during the time integration process.

Nodal Equations

For each node either the nodal pressure p_i or the nodal load L_i has to be known for a future time step t_{n+1} . If the node is pressure controlled the pressure p_i is set to a desired set point p_{set} , while the corresponding load L_i is calculated for the equivalent time step. In contrast, if the node is load controlled, the load L_i is assigned a desired set point L_{set} and the resulting nodal pressure p_i is calculated. For junction nodes the control mode is always inactive since these nodes are characterized by a zero nodal load, thus, for these nodes a resulting pressure is calculated. The control mode for each node i can be generally

Control Mode	Equation	Coefficients
pressure (p_{set})	$p_j = p_{set}$	$k_p = 1, k_L = 0, b = p_{set}$
supply/offtake flow (Q_{set})	$L_j = Q_{set}$	$k_p = 0, k_L = 1, b = Q_{set}$
off (OFF)	$L_j = 0$	$k_p = 0, k_L = 1, b = 0$

Tab. 2.6.: Overview of available scenario parameter (control modes) for facilities modelled as demand, supply or storage nodes and their mathematical implementation

described by the following linear scalar equation.

$$k_{p,i} \cdot p_i^{n+1} + k_{L,i} \cdot L_i^{n+1} = b_i \quad (2.45)$$

where $k_{p,i}$ and $k_{L,i}$ are scalar coefficients of the nodal pressure p_i and nodal load L_i , respectively, and b_i is the value of the desired load or pressure set point (see Tab. 2.6 for values for coefficients for different control modes). Moreover, for each demand, supply and storage node constraints on load and pressure can be defined, which are listed in the last column of Tab. 2.2.

2.3.6. Algorithm

The equations elaborated for the nodes, non-pipe and pipe elements can be combined with eq. (2.41) to the following linear matrix equation for computing the state of the network for a future time step t_{n+1} based on an initial time step t_n and prescribed boundary conditions at nodes and non-pipe elements:

$$\begin{pmatrix} \Phi & -\mathbf{A}_P & -\mathbf{A}_N & \mathbf{I} \\ \mathbf{A}_{DP} & -\mathbf{R} & \mathbf{0} & \mathbf{0} \\ \mathbf{C}_P & \mathbf{0} & \mathbf{C}_N & \mathbf{0} \\ \mathbf{K}_P & \mathbf{0} & \mathbf{0} & \mathbf{K}_L \end{pmatrix} \begin{pmatrix} p^{n+1} \\ Q_P^{n+1} \\ Q_N^{n+1} \\ L^{n+1} \end{pmatrix} = \begin{pmatrix} \Phi p^n \\ B \\ E \\ S \end{pmatrix} \quad (2.46)$$

The first row of the matrix equation describes the set of nodal continuity equations (2.41), while the second row describes the linearized pipe equation (2.24)-(2.23), where matrix \mathbf{R} is a diagonal matrix representing the slope of the linearized pressure drop equations, B the intersection with the y-axis and \mathbf{A}_{DP} the pipe-node incidence matrix describing the pressure drop term DP . Finally, the third and fourth row describes the control mode of non-pipe elements (eq. (2.44)) and node facilities (eq. (2.45)), respectively.

Figure 2.11 shows a flow chart of the algorithm for the transient simulation. After an initial steady state solution is obtained the network is discretized in space (Δx) and time (Δt). In addition, the initial steady state solution is projected on the generated simulation grid, i.e. pipe flows, pressure distribution of the original network are assigned to the corresponding grid pipes and grid nodes. After the simulation grid is generated the matrix equation eq. (2.46) is solved iteratively for each time step t_{n+1} . First an initial approximation is made for the pressure drop equation using the linearisation described in eq. (2.22) then the matrices and vectors in eq. (2.46) are assembled in order to solve the

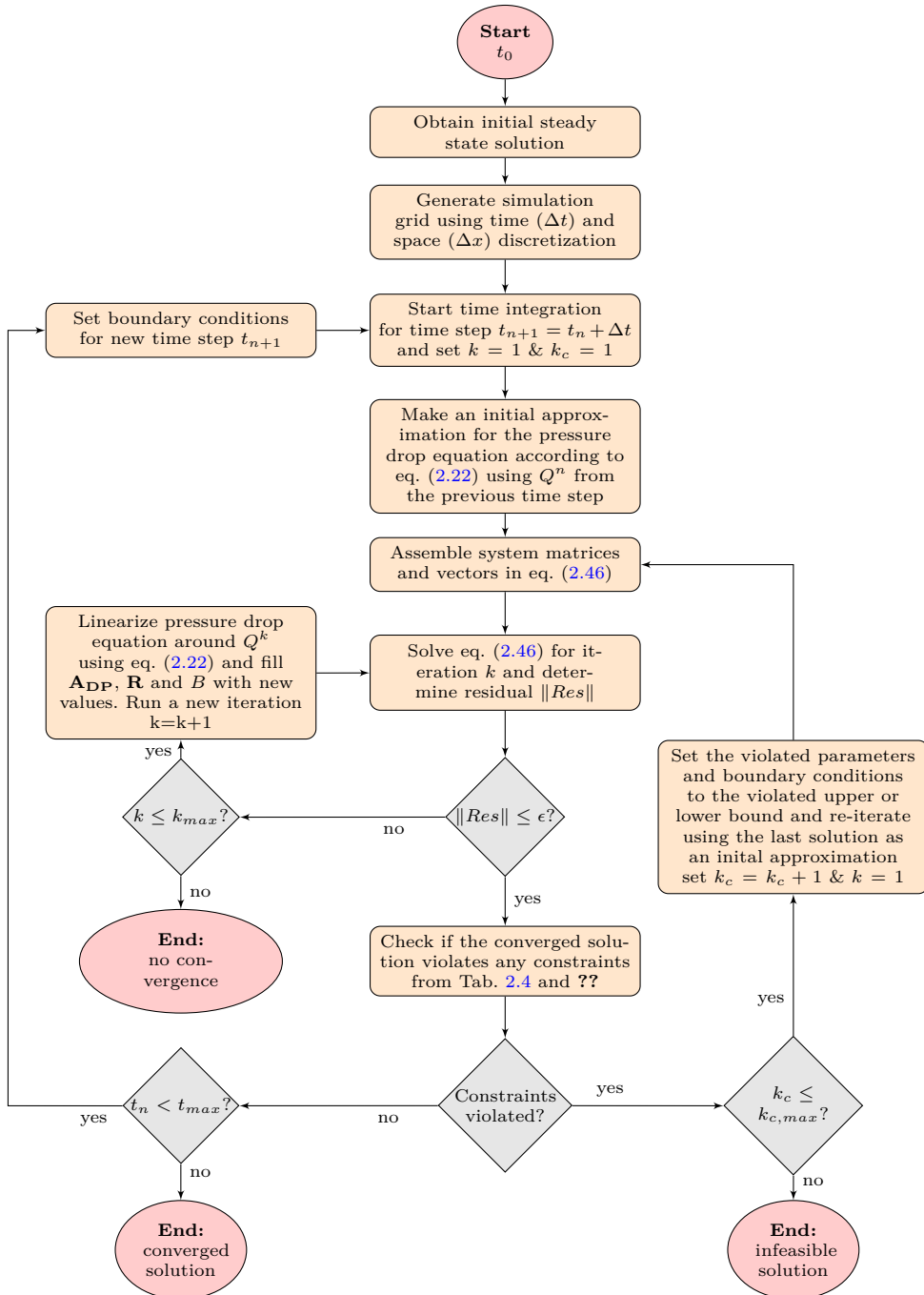


Fig. 2.11.: Flow chart for transient simulation

linearized matrix equation for the iteration step k . The obtained solution is then used to calculate the residual vector for the non-linear pressure drop equation.

$$Res = \Delta P^{n+1} - [R_f \cdot |Q^{n+1}|Q^{n+1} + R_i \cdot (Q^{n+1} - Q^n)] \quad (2.47)$$

The euclidean norm of the residual vector

$$\|Res\| = \sqrt{Res_1^2 + Res_2^2 + \dots + Res_{mp}^2}, \quad \|Res\| : \begin{cases} \leq \epsilon, & \text{converged solution} \\ > \epsilon, & \text{solution did not converge} \end{cases} \quad (2.48)$$

is then compared against a tolerance $\epsilon = [10^{-3}, \dots, 10^{-8}]$. The iteration continues if the residual is above the tolerance and if a maximum number of iterations (k_{max}) has not been exceeded. The residual will typically converge quadratically if the solution for an iteration step is relatively close to the final solution, which is the case if the boundary conditions between two time steps do not change rapidly. Depending on the magnitude of the changes between two time steps and the prescribed residual tolerance a converged solution is usually obtained within 1 to 5 iterations. In case a converge solution is not obtained for a time step one can adjust the residual tolerance ϵ and the maximum number of iterations k_{max} and then reiterate.

After a converged solution is obtained for a time step the solution is checked for constraints violation. If violations are found the iteration for the last time step will be repeated adapting the boundary conditions to the violated constraints. The algorithm continues with the next time step if a converged and feasible solution is found, otherwise the simulation is terminated. The entire simulation process ends successfully if for each time step a converged and feasible solution is obtained.

The algorithm is implemented into a numerical code using the programming language Visual Basic .NET.

2.4. Model Benchmarking

In this section, we benchmark the model proposed against the solutions obtained with other models available in the literature for a well-known triangular network and 30-Node sample network, in order to check the accuracy of the solutions obtained. Moreover, we make a specific study about the accuracy concerning the gravitational term in the momentum equation, and its importance in the solution for relatively small average slopes.

Proper validation is almost impossible given the scarcity of experimental data available for real networks.

2.4.1. Simulation of a triangular Network

The model is applied to solve the gas network depicted in Fig. 2.12 using the STE. The example network has been used in a number references [70, 73, 76, 77, 79, 86, 92] to benchmark the results with different transient methods. The results obtained with the model will be benchmarked against two of these references, namely, Osiadacz [92] and Ke and Ti [86] and the commercial software SIMONE. The network in Fig. 2.12 consists of three pipelines and two demand nodes (node 2 and node 3) that are supplied with gas by a single supply node (node 1). The network topology and pipe properties are

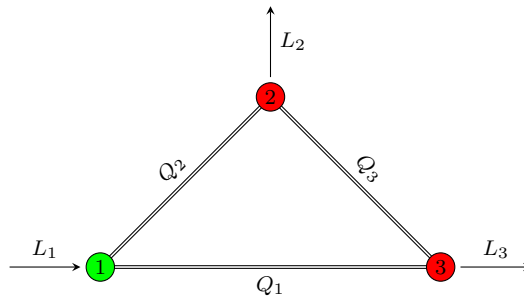


Fig. 2.12.: Topology of the 3 pipeline network

Pipe	Inlet	Outlet	Diameter [mm]	Length [km]	Roughness [mm]
1	1	3	600	80	0.012
2	1	2	600	90	0.012
3	2	3	600	100	0.012

Tab. 2.7.: Pipe data of the 3 pipeline network

listed in Tab. 2.7 while the simulation properties and gas properties are shown in Tab. 2.8. The properties are chosen according to those from the references in order to compare the results. To show the efficiency and the accuracy of the proposed model for low space resolutions the pipes are discretized by only one segment per pipeline ($\Delta x = l$)⁴. Unlike

⁴in [92] the pipelines are discretized in 10 segments while in [86] the pipelines are discretized in 5 segments

the pipe properties in the references [86, 92]⁵ the pipe roughness is taken into account for the computation of the friction factor. Thus, for each pipeline a roughness value typical for transport pipelines is assigned ($r = 0.012$ mm). Moreover, for the transient simulation a time step of 180 s and a total simulation time of one day is chosen. The boundary

parameter	symbol	value	unit
grid segments per pipe	J	1	[·]
time step	Δt	180	[s]
total simulation time	t_{max}	24	[h]
residual tolerance	ϵ	10^{-4}	[·]
gas temperature	T	278	[K]
dynamic viscosity	η	10^{-5}	[kg/m · s]
standard pressure	p_n	1.01325	[bar]
standard temperature	T_n	273.15	[K]
relative density	d	0.6	[·]

Tab. 2.8.: Input parameters for the transient simulation of the 3 pipeline network

conditions for the supply and demand nodes are shown in Fig. 2.13, where in a) the prescribed pressure profile of the supply node and in b) the load profile of the demand nodes are depicted. The supply node is pressure controlled with a constant pressure of 50 bar while the demand nodes are flow controlled with a fluctuating load profile according to Fig. 2.13 b). The required initial condition for the transient simulation is obtained through an initial steady state computation using the boundary conditions of the initial time step $t_0 = 0$ s ($p_1 = 50$ bar, $L_2 = 20 \text{ sm}^3/\text{s}$ and $L_3 = 40 \text{ sm}^3/\text{s}$). For both steady state and transient simulation a computation time of less than 1 s was needed to obtain a converged solution. The computations were run on an 2.4 GHz Intel Core i7 CPU with a 8GB RAM.

Figure 2.14 compares the computed pressure profile at the demand nodes with results from Osiadacz [92], Ke and Ti [86] and the SIMONE software. In general, the pressure at the demand nodes decreases with increasing nodal loads and increases as the nodal loads are decreasing. The results obtained with the integrated model is very similar to the results from the SIMONE software. In contrast, there are deviations between the model and the results from Osiadacz [92] and Ke and Ti [86], which could be caused by the different treatment of the friction and compressibility factor. However, the deviations are marginal (below 1%).

Figure 2.15 shows the evolution of a) the average pipeline flow and b) the total line pack and Fig. 2.16 a) the resulting load profile at supply node 1 and b) the total load balance

⁵in [92] the friction factor is assumed to be constant with a value of $\lambda = 0.012$ while in [86] the friction factor is computed without considering the pipe roughness

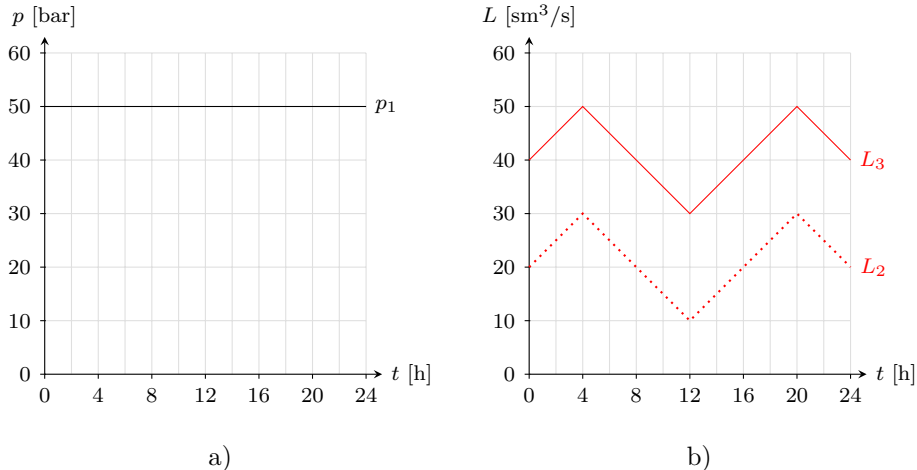


Fig. 2.13.: Initial conditions and boundary conditions for the transient simulation of the 3 pipeline network a) pressure condition at the supply node 1 and b) Load profile at the demand nodes 2 and 3

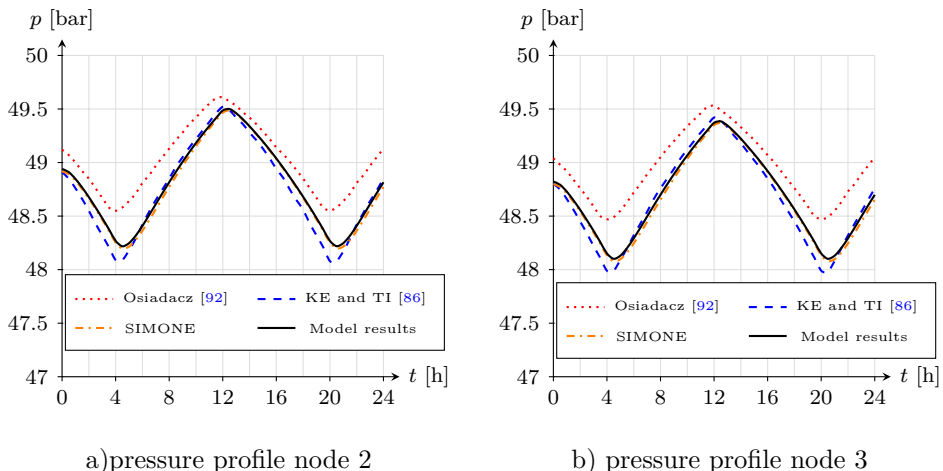


Fig. 2.14.: Computed pressure profiles at node 2 and node 3 compared to results from the literature and SIMONE

of the network. Since for these parameters no results are provided by Osiadacz [92] and Ke and Ti [86] the results obtained from the integrated model are only compared to SIMONE.

The evolution of the pipeline flow for pipe 1 and 2 fluctuates very similar to the corresponding nodal loads, while for pipe 3 the flow remains constant (see Fig. 2.15). The

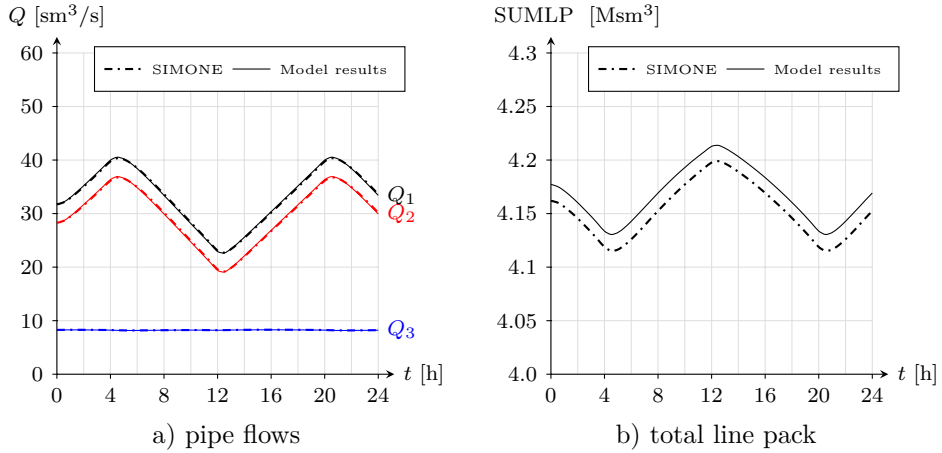


Fig. 2.15.: a) average pipe flow rate in pipelines b) total line pack in network

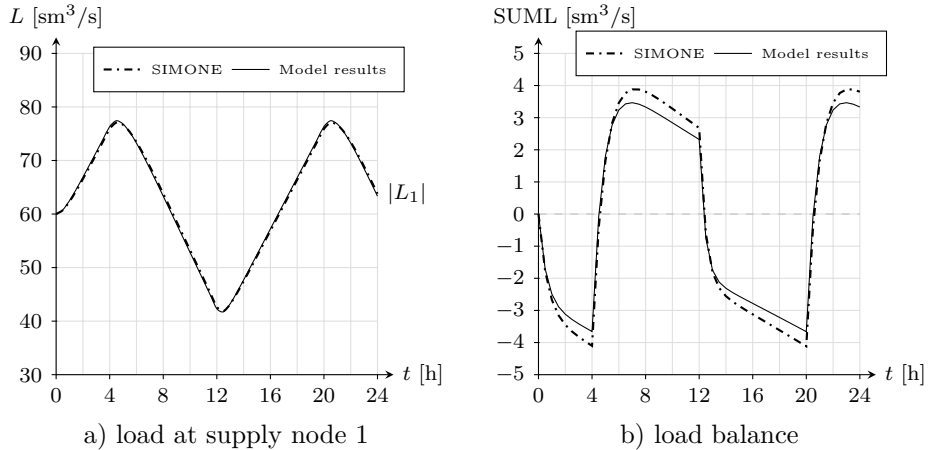


Fig. 2.16.: a) resulting load profile at supply node 1 b) load balance of the network

latter is due to the fact that the load difference between the inlet and outlet of pipe 3 (i.e. between node 2 and 3) is constant throughout the simulation even though both loads fluctuate. The results obtained for the pipe flows from the integrated model is again very similar to the SIMONE results.

The correlation between the total line pack of the network and the flow balance can be seen if we compare Fig. 2.15 b) to Fig. 2.16 b). The load balance is equal to the time derivative of the line pack, i.e. the slope of the line pack curve. Whenever the load balance is zero the line pack is at its local minimum/local maximum and whenever the load balance

is negative/positive the line pack decreases/increases, respectively. The linepack can be viewed as a buffer to balance short term load fluctuations until the supply node is able to react to the changes. The results obtained for the linepack and the flow balance from the integrated model and from SIMONE are similar. The deviation of the line pack is less than 0.5% and originates from the initial steady state calculation then remains constant throughout the transient simulation. The deviations of the load balance is less than 1% compared to the calculated load profile at the supply node shown in Fig. 2.16 a). These deviations observed for the load balance is actually the difference between the two curves in Fig. 2.16 a).

2.4.2. Influence of the inclination term

The majority of the hydraulic gas models in the literature do not consider the gravitational term in the momentum equation. In this section, we demonstrate the influence of the gravitational term for even small pipe inclinations and compare the results to SIMONE computation in order to verify the accuracy of the model. The computations are conducted on the three pipeline network from the previous section using the same data as in Tab. 2.7 and 2.8 and Fig. 2.13. The elevation h_1 of the supply node 1 is varied from (-1000 m, ... 1000 m) in 500 m intervals which corresponds to the following inclinations α_j for each pipe j in the network. The inclination angle of pipe 3 remains zero since it is

Elevation h_1 [m]	α_1 [°]	α_2 [°]	α_3 [°]
-1000	0.716	0.637	0
-500	0.358	0.318	0
500	-0.358	-0.318	0
1000	-0.716	-0.637	0

Tab. 2.9.: Inclination angles for different elevations of node 1

not connected to the supply node. The results are shown in Fig. 2.17, where the resulting pressure profile for node 2 and 3 are plotted for different elevations of the supply node h_1 . The results show pressure shifts of approx. 2 bar per every 500 m of elevation compared to the horizontal case. The pipe outlet pressure decreases if the pipe is ascending ($\alpha > 0$) and increases if the pipeline is descending ($\alpha < 0$). Moreover, a remarkable observation can be made if the inlet and outlet pressures for the descending pipes are compared. For the chosen inclination for this pipelines the pressure increases in flow direction, i.e. the outlet pressure is greater than the inlet pressure, since the potential energy of the gas at the inlet is transferred to static pressure. The elevation change does not influence the shape

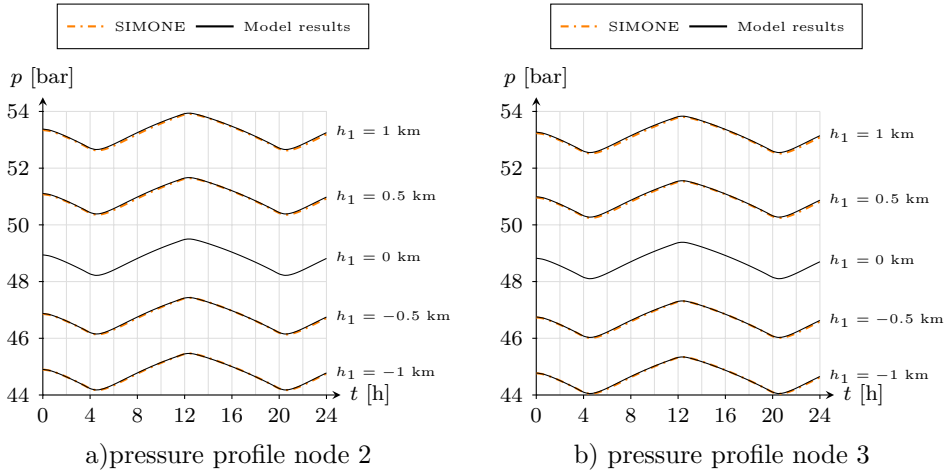


Fig. 2.17.: Computed pressure profiles at node 2 and node 3 for different elevations H_1 of node 1 compared to results from SIMONE

of the pressure profile since for each elevation the shape of the pressure profile remains unchanged and is just shifted by a certain amount along the vertical axis. The results obtained from the integrated model are very similar to those obtained from SIMONE, which confirms the accuracy of the integrated model. Moreover, the magnitude of the differences in pressure for the different inclinations indicate the importance of this term, which should not be neglected in large areas of the EU transmission networks, where easily these average slopes are exceeded.

2.4.3. Simulation of a 30-Nodes Gas Network Model

In the following, we benchmark the accuracy of the presented gas model against results from the commercial software SIMONE for a 30-Node sample network adapted from [92]. The data of the network topology, gas and pipe properties and steady state boundary conditions are given in Tab. A.1 and A.2. In the first step, we run a steady state simulation to obtain an initial state of the network, which we then use in a second step to compute a dynamic simulation over 24 hours, using the load profile shown in Fig. A.1, which we multiply with the steady state load for each demand node.

Figures 2.18 and 2.19 show the steady state solution, while Fig. 2.20 illustrates the results for the dynamic simulation. As can be seen, the results obtained with the developed gas model are very similar to the SIMONE results, which confirms the accuracy of the simulation model. The comparison of the steady state results obtained with the gas model

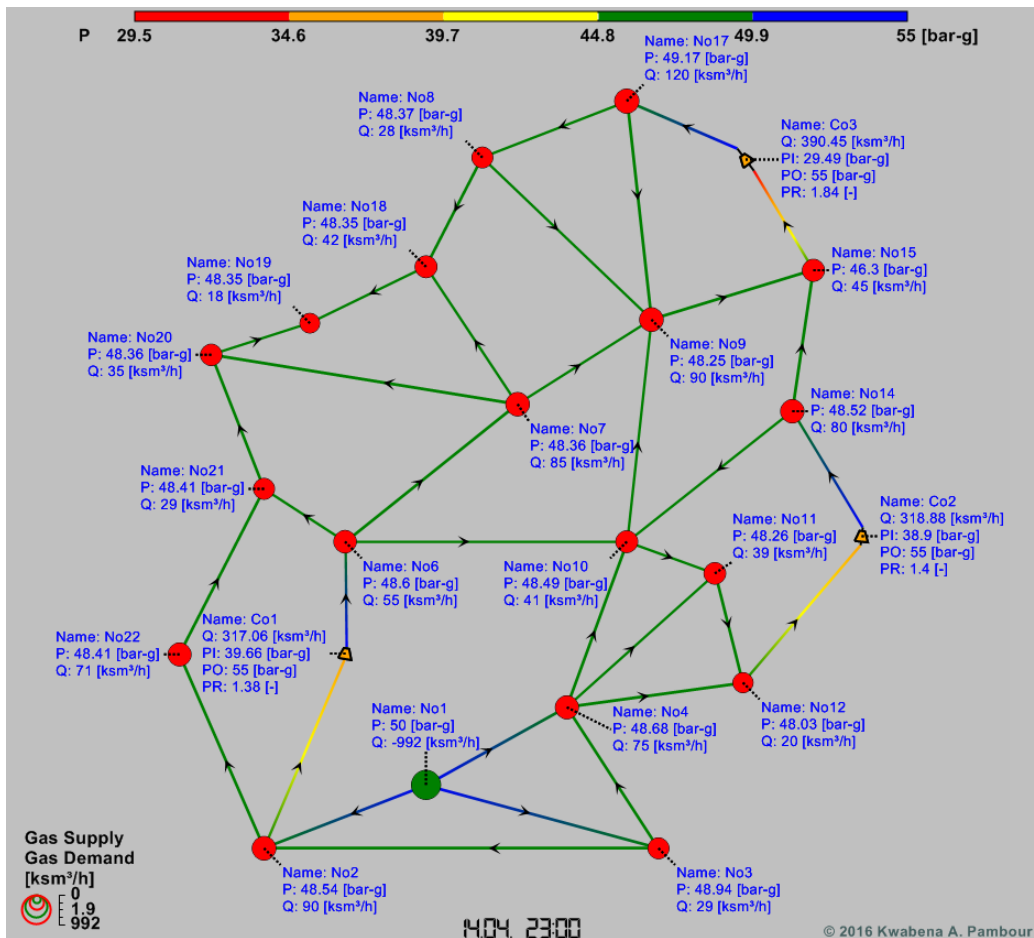


Fig. 2.18.: Steady state solution for the sample network obtained with the developed gas model

(see Fig. 2.18) and SIMONE (see Fig. 2.19) shows small deviations (< 0.2 bar) in the nodal pressure and compressor flow rate (< 2 ksm^3/h) in the area around compressor station Co3. Similar observations can be made for the time plots for the dynamic simulation (see Fig. 2.20). The shape of the time plots for the gas supply in the source node (see Fig. 2.20 a)) and the nodal pressure for three selected nodes (see Fig. 2.20 b) c) and d)) obtained with the gas model and SIMONE are very similar, however, small deviations (< 0.2 bar) can be observed for the last five simulation hours. Discrepancies for the transient model in other nodes are in the same range as the ones shown here. We consider these discrepancies (below 0.5%) as quite good results.

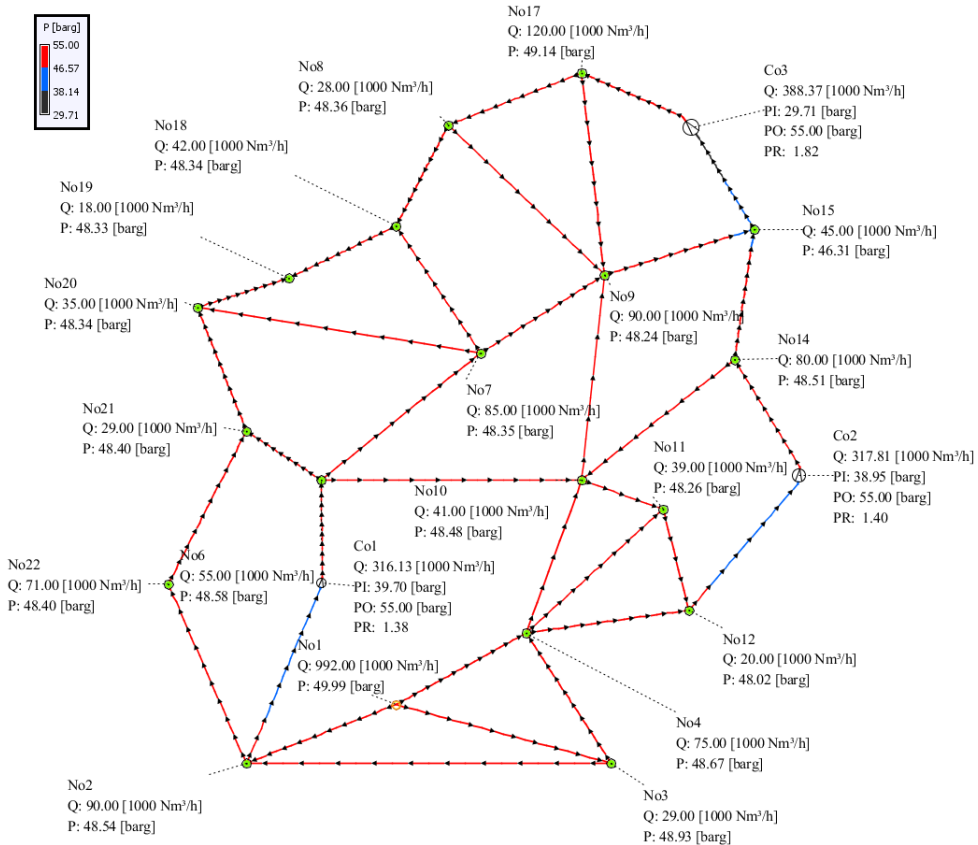


Fig. 2.19.: Steady state solution for the reference network obtained with SIMONE

2.5. Model Application: Bulgarian and Greek National Gas Transport System (NGTS)

The integrated model is applied to perform a transient simulation on a simplified model of the Bulgarian and Greek NGTS depicted in Fig. 2.21. The model comprises of 210 pipe elements (total pipe length of approx. 3600 km and total geometric pipe volume of approx. 1,600,000 m³, 11 compressor stations (10 located in Bulgaria and 1 in Greece) and 217 nodes (67 exit stations to the local distribution system (CGS) and to direct served customers (GFPP, IND), two Cross Border Export Stations (CBE), 2 Cross Border Import Stations, one LNG Terminal and one UGS facility). The Bulgarian-Greek NGTS is basically structured into two national transmission systems and a transit pipeline transporting a large quantity of gas from CBI Negru Voda to the CBEs at the border to Turkey (Mal-

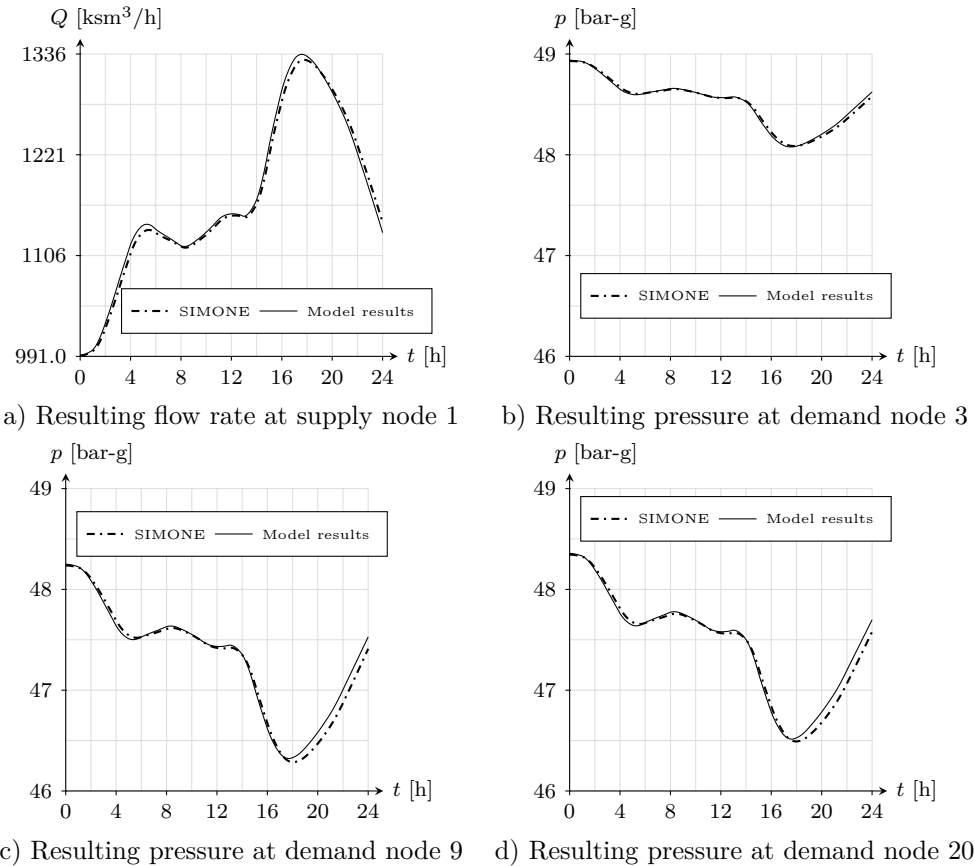


Fig. 2.20.: Comparison of simulation results for the sample network obtained with developed gas model and SIMONE

coclar), FYRO Macedonia (Zidilova) and Greece (Sidirokastron). Apart from the CBI in Negru Voda, there are three additional entry points to the transport system, namely, the UGS Chiren in Bulgaria (supply from storage during winter and injection during summer), the LNG Terminal Revythoussa in Greece, and the CBI-Kipi at the Greek-Turkish border.

Figure 2.21 shows the steady state pressure and load distribution and the flow direction for the network model computed with the integrated model. The input data for the loads are based on peak winter consumption in 2011. Moreover, each supply node in the model is pressure controlled while each compressor station (except the compressor station at UGS Chiren, which is typically used to increase the gas pressure for storage injection) is pressure ratio controlled with a pressure ratio set point ranging from 1.02 – 1.2. The diameter of

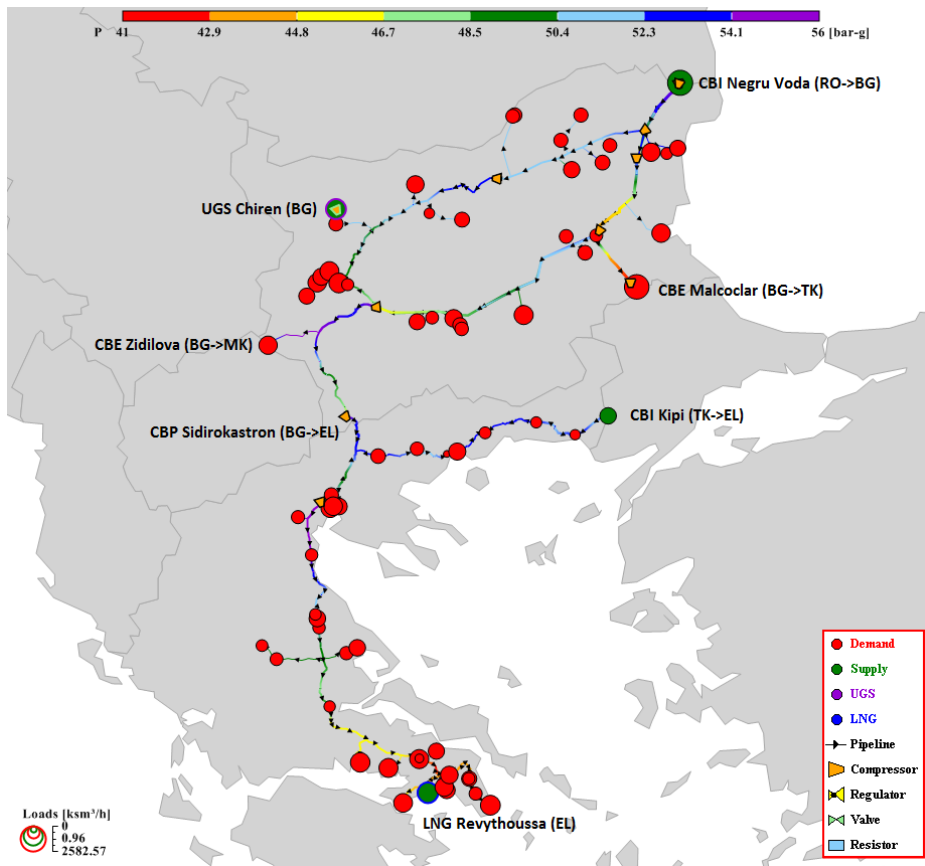


Fig. 2.21.: Steady state pressure and load distribution for the Bulgarian and Greek NGTS

the circles representing demand and supply nodes correspond to the magnitude of the steady state loads in logarithmic scale, as can be seen from the legend in the bottom left corner. Moreover, the colors of the pipe elements correspond to the pressure levels indicated in the color bar on top.

In the following, we use the steady state solution of the network depicted in Fig. 2.21 as an initial state to simulate and compare two different transient scenarios. In the first scenario (case 1) we simulate the normal operation of the Bulgarian-Greek NGTS by assigning the characteristic (relative) load profile depicted in Fig. 2.22 to all exit stations to the local distribution system (CGS), while for all other exit stations we assume a constant load profile corresponding to the steady state load. The absolute values of the load profile for the CGS nodes is obtained by multiplying the steady state load with the relative values in Fig. 2.22. Moreover, we change the control of CBI Negru Voda and CBI Kipi to

flow control with a flow rate set point corresponding to the steady state load, while the pressure set point for UGS Chiren and LNG Revythoussa as well as the pressure ratio set points for the compressor stations remain unchanged. Furthermore, we set a minimum pressure constraint for both CBE nodes to 30 bar-g and a minimum delivery pressure for all CGS nodes to 20 bar-g. In addition, we consider the constraints on the maximum withdrawal rate from UGS Chiren (175 ksm³/h) and the maximum regasification rate from LNG Terminal Revythoussa (570 ksm³/h).

In the second scenario (case 2) we simulate a supply shortage of 25% at the largest entry point to the NGTS, namely, CBI Negru Voda by successively reducing the steady state load from the initial time to 18:00 and then maintaining the value till the end of the simulation, as shown in Fig. 2.24. All other settings remain the same as in case 1. Both scenarios are computed for two gas days using the fast transient equation (FTE) derived in eq. (2.23). Table 3.7 lists additional settings for the simulation parameters.

The simulation grid is generated with a time resolution of 300 s and a space discretization based on the following criterion proposed by Kralik [99] :

$$J = \text{ceiling} \left\{ \max \left\{ \frac{|h_2 - h_1|}{200 \text{ [m]}}, \frac{l}{30000 \cdot D} \right\} \right\} \quad (2.49)$$

which basically means each pipe element is segmented in such a way that the elevation change between the inlet and outlet node is not greater than 200 m and the ratio between the pipe length l and pipe diameter D is not greater than 30,000. Applying this criteria to the network model yields a total grid size of 345 pipe segments and 352 nodes. Simulation results are shown in Fig. 2.23-2.29 and are discussed in the following.

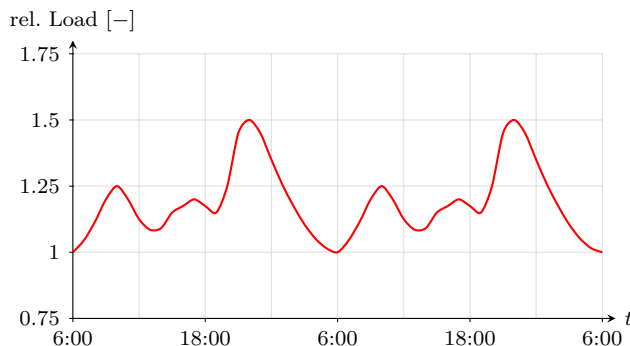


Fig. 2.22.: Load profile assigned to city gate stations

parameter	symbol	value	unit
time step	Δt	300	[s]
total simulation time	t_{max}	48	[h]
residual tolerance	ϵ	10^{-4}	[\cdot]
gas temperature	T	288.15	[K]
dynamic viscosity	η	10^{-5}	[kg/m·s]
standard pressure	p_n	1.01325	[bar]
standard temperature	T_n	273.15	[K]
relative density	d	0.6	[\cdot]

Tab. 2.10.: Input parameter for transient simulation of the Bulgarian-Greek network model

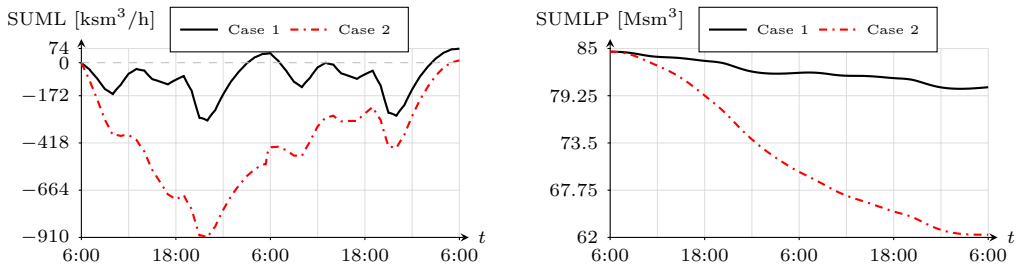


Fig. 2.23.: Load balance and line pack evolution of the network

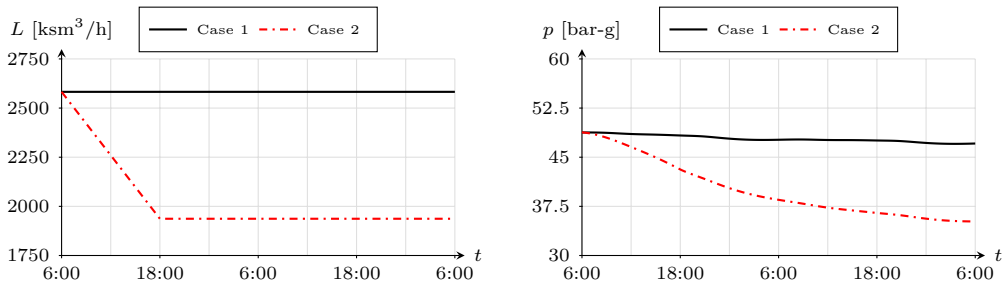


Fig. 2.24.: Load & pressure evolution at CBI Negru Voda

The results show how the supply reduction from the main entry point in CBI Negru Voda propagates through the network and affects the pressures and loads at downstream exit and entry points. Figure 2.23 illustrates the time evolution of the load balance (i.e. sum of inflow minus sum of outflow) and the total line pack in the combined NGTS for the examined cases. In both cases the initial line pack in the network decreases, however, the decrease in line pack is much greater for case 2 than for case 1, which can be explained by the difference in load balance for both cases. In case 2, the amount of gas extracted from

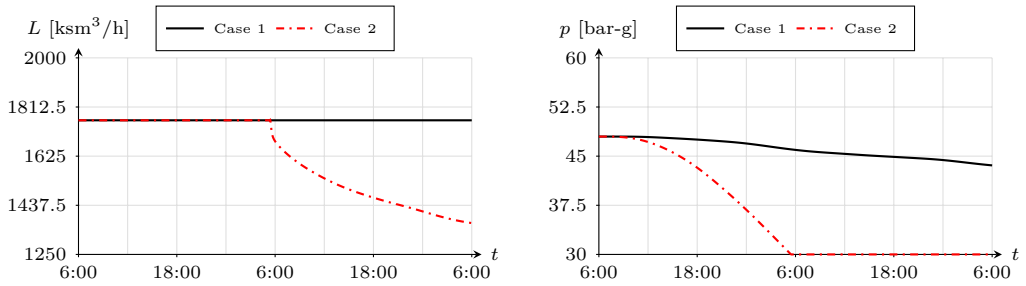


Fig. 2.25.: Load & pressure evolution at CBE Malcoclar

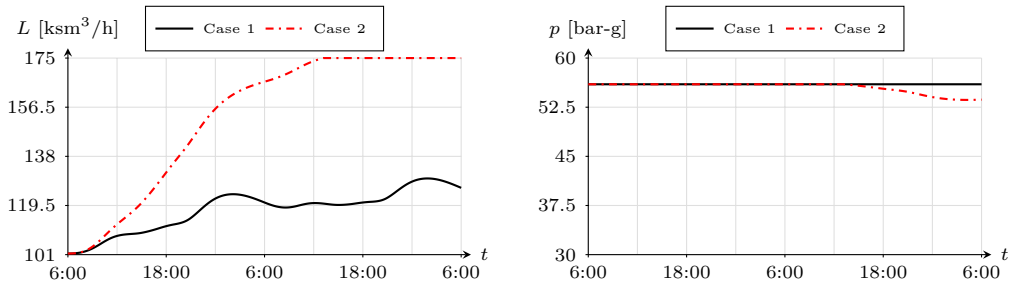


Fig. 2.26.: Load & pressure evolution at UGS Chiren

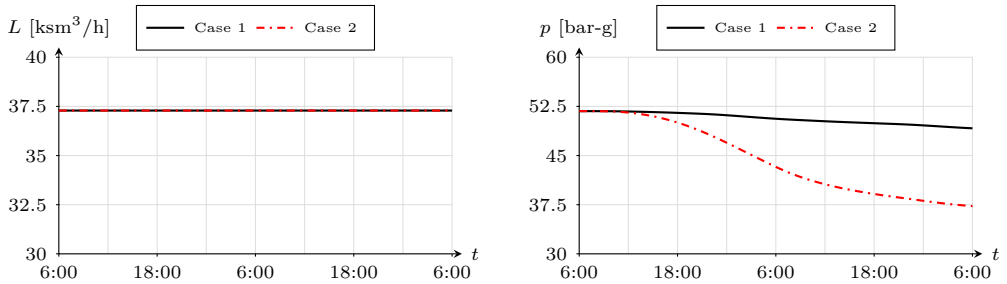


Fig. 2.27.: Load & pressure evolution at CBE Zidilova

the network is significantly higher than the amount injected due to the supply reduction in CBI Negru Voda, thus, the line pack in the pipelines is used as a buffer to satisfy demands until the system catches up. The observation for the total line pack are in line with the pressure profiles at the downstream entry and exit points. The nodal pressures for case 2 are either lower or equal to those for case 1 (see pressure profiles in Fig. 2.24-2.29).

In addition, the results show the capability of the model to consider constraints imposed on the network. For example, the load set point at CBE Malcoclar (Fig. 2.25) is not attained

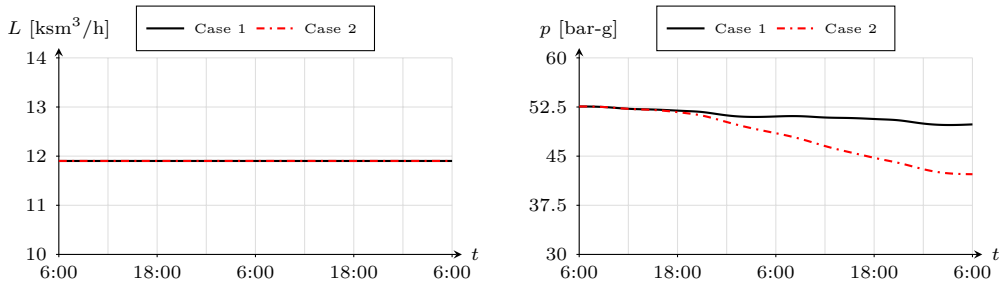


Fig. 2.28.: Load & pressure evolution at CBI Kipi

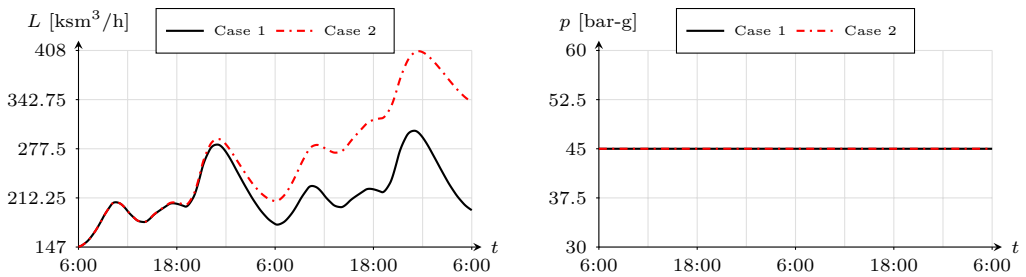


Fig. 2.29.: Load & pressure evolution at LNG Terminal Revythoussa

due to the delivery pressure constraint (30 bar-g) imposed on the CBE stations. After a simulation time of approx. 24 h the pressure reaches minimum delivery pressure. In order, to maintain the minimum pressure the load is reduced continuously. Another example of constraints consideration can be observed in Fig. 2.26, where the load and pressure evolution for UGS Chiren is depicted. Due to the supply reduction at CBI Negru Voda (case 2) the storage withdrawal increases rapidly in order to feed the gas customers in the consumption area around Sofia with gas. Around 12:00 on simulation day 2 the withdrawal rate reaches its maximum value ($175 \text{ ksm}^3/\text{h}$), thus, the pressure set point cannot be maintained and reduces slightly, while the withdrawal rate is kept at its maximum value.

Moreover, looking at the pressure and load evolutions for the exit and entry points downstream CBI Negru Voda, we can notice that the farther an entry or exit point is located from CBI - Negru Voda the later its loads and pressures are affected by the supply reduction. For instance, the resulting load profile for the LNG Terminal in Revythoussa is indifferent for both examined cases up until 12 hours after the beginning of the supply reduction at CBI Negru Voda, while for UGS Chiren and CBE Malcoclar an impact can be noticed a few hours after the start of the supply reduction. The magnitude of the reaction time roughly corresponds to the gas travel time, i.e. the ratio of total pipe length to

mean velocity from point A to B which corresponds to the amount of time a gas particle will need to travel between two points.

In conclusion, the results demonstrate the capability of the developed model to simulate the dynamic behaviour of a real gas transport system and the reaction of the system to supply disruptions.

2.6. Conclusion

In this chapter, we developed a transient hydraulic gas model for simulating the operation of real world natural gas transport systems in the context of security of gas supply. The model considers the physical laws governing the gas flow in pipelines, the most important facilities (e.g. compressor stations, entry and exit stations, storage facilities and LNG terminals) and their technical constraints. The set of equations describing the dynamics of the transport system were obtained by simplifying and adapting the full equations to the prevailing conditions in gas transport systems. Next, the equation system was discretised and linearised using an implicit time integration and a linearisation technique for the non-linear pipe equations.

Furthermore, the model was benchmarked against results from the literature and the commercial software SIMONE. The comparison of the results confirmed the capability of the model to reflect the dynamic behaviour of gas transport networks in an adequate and accurate manner.

In addition, the model was applied to a real world instance, namely, the operation of the Bulgarian-Greek national gas transport system under normal conditions and in the instance of a supply reduction from a main entry point. Again, the results obtained demonstrate the ability of the model to capture appropriately, the propagation of load and pressure fluctuations at entry and exit points and the flexibility to adapt accordingly the boundary conditions of the network in case of a constraints violation.

In this chapter, we addressed the gas system part of the following sub-research questions:

- *What are the most important facilities in the gas and electricity transmission networks in terms of security of supply?*
- *How can we develop a mathematical model that reflects appropriately their physical behaviour and their technical and contractual constraints?*

The developed gas model is suitable for scenarios with no control mode changes at controlled facilities such as compressor stations and valve stations during the simulation. In real time operation, TSOs may change the control mode and set points of facilities to mitigate the consequences of disruptions. These control changes will depend on the conditions in the gas network at the time of the disruption and the technical limits of the gas transport system. To address these aspects, the gas model needs to be extended by additional models. Furthermore, to ease the set up and analysis of different security of supply scenarios, a simulation platform is needed, where the such similation models can be implemented and executed. In the next chapter, we extend the gas system model by additional features and implement them into a simulation tool with a graphical user interface.

3. Model Extension and Implementation into a Simulation Software

This chapter is based on the following published conference paper:

- K. A. Pambour, R. Bolado-Lavin, and G. P. Dijkema, “[SAInt – A simulation tool for analysing the consequences of natural gas supply disruptions](#),” in *Pipeline Technology Conference (PTC) 2016*.

3.1. Introduction

The interruption of the gas flows to the EU through Ukraine in January 2009 has been the largest gas crises in the EU ever. Russian gas exports through Ukraine were drastically reduced on January 6th, 2009, and completely interrupted the day after. Gas flows resumed on January 20th and were completely restored only on January 22nd. This event triggered a deep analysis, led by the European Commission, of EU vulnerability to gas disruptions. The final result of this effort was the enactment of Regulation 994/2010 [12] on security of gas supply. According to this Regulation, MS have to develop a Risk Assessment (RA), a Preventive Action Plan (PAP) and an Emergency Plan (EP), among other obligations. The target of the RA is to identify the scenarios that introduce most risk into the system (more likely to happen and more severe in consequences). Results of the RA are input to the PAP and the EP. The target of the PAP is to deploy measures to prevent the occurrence of scenarios that contribute most to the risk, or at least to make them less likely to happen. The target of the EP is to design strategies to mitigate the consequences of severe scenarios, should they happen.

The development of a RA needs the identification of a number of scenarios, and the estimation of their probabilities and consequences. Normally, consequences are given in terms of non-supplied gas per off-take point of the gas transport network, and eventually integrated for the entire network. In this chapter, we focus our effort on the correct estimation of consequences of potential scenarios. Given the complex and dynamic behaviour

of a national or regional gas transport system, this estimation can only be done with adequate gas transport network simulation models. In the previous chapter, a mathematical model for gas transport networks was developed for simulating hydraulic transients in gas transport networks under isothermal conditions. The use of a transient hydraulic model is inevitable, due to the dynamic nature of the prevailing processes in gas systems. Nevertheless, the actual resolution of transport equations is not sufficient to simulate the degrees of freedom of a network to react to a transient or, more severe, to a gas disruption. In normal operation TSOs, following market decisions, network codes and network good practice management, have the capability to make decisions concerning the use of different network facilities (production sites - PS, underground gas storage facilities - UGS, liquefied natural gas regasification terminals - LNG, compressor stations – CS, cross border import stations - CBI, cross border export points – CBE, etc.) in order to optimize its use. When a gas disruption takes place, according to the EP other actors may intervene, as for example the Competent Authority (CA), obliging the TSO to adopt specific actions to mitigate the impact of the crises on gas customers.

In this chapter, the different actions that the operator, market actors and authorities may adopt in the event of a gas crisis as well as the infrastructural elements used to implement them are identified. Furthermore, the different possible control modes and constraints of each infrastructure element are identified and implemented into an integrated simulation software to analyse gas supply disruptions. The chapter is structured as follows: In Section 3.2 a formal definition of risk is provided, where we focus on the 'consequence' element of the term 'Risk'. Section 3.3 addresses the identification of the different measures that TSOs, authorities and market actors may adopt in the different steps of a gas crisis, and the types of facilities that may be affected by such decisions. Section 3.4 extends the gas network model developed in Chapter 2 by additional features that are needed to implement the potential countermeasures taken by TSOs during a gas crises. Finally, in Section 3.6 we demonstrate the actual implementation of the developed models in the previous sections by means of a real world instance.

3.2. Definition of Risk

The word 'risk' is frequently used in a very informal manner. Quite often, risk is defined as probability times consequence (or impact, or damage). Essentially, this means that a measure of risk has to account for potential consequences and weigh them with their corresponding probabilities (likelihoods). A more operational definition of risk is illustrated

in the following paragraphs. Standard ISO 31010 indicates that Risk Assessment attempts to answer the following fundamental questions:

- What could happen and why?
- What are the consequences?
- What is the probability of its future occurrence?

Kaplan and Garrick [100] showed that a formal answer to these three questions requires describing risk through the use of a set of triplets

$$R = \{< s_i, \phi_i, y_i >\} \quad i = 1, 2, \dots, N \quad (3.1)$$

where

1. s_i represents scenario i in the set of N scenarios considered.
2. ϕ_i is the probability of scenario i .
3. y_i is the potential consequence under the conditions of scenario i .

This constitutes a formal mathematical definition of risk, although it does not account for all sources of uncertainty. Under this definition each scenario is characterized by its probability and its consequence(s) (one or several consequence variables may be considered, but only one possible value of each consequence variable is considered). Adopting this definition of Risk means that all possible scenarios must be identified and the probability of each must be estimated. Moreover, for each scenario, the consequence(s) for the system must be assessed.

An RA, in order to be useful, has to be as accurate as possible, and certainly free of bias. The introduction of bias is a pervasive problem in RA. The most frequent reason to introduce bias in a RA is a poor identification of sources of risk (typically classified as hazards, equivalent to non-intentional events, and threats or intentional actions leading to undesired events). This problem produces in most occasions a severe underestimation of risk. This is the reason why many techniques have been developed in order to avoid this problem, from the simple brainstorming to the much more elaborate Failure Mode and Effect Analysis (FMEA) or the Hazard and Operability Analysis (HAZOP).

Nevertheless, the incorrect assessment of consequences of different scenarios leads certainly to biases in the estimation of risk, probably not as severe as the ones derived from a poor identification of sources of risk, but certainly undesired. This is a problem that has been

systematically ignored in the literature. Typically, problems of gas disruptions have been addressed at a very coarse level of granularity, as much in space as in time [101–106].

3.3. Measures to Mitigate the Impact of Gas Disruptions

Regulation 994/2010 [12] on security of gas supply has as one of its key elements the EP. According to the Regulation, the EP has to be designed taking into account the results of the RA. The target of the EP is to mitigate as much as possible the effects of risky scenarios, in order to contribute to decreasing the risk level associated to the studied gas system. This means it has to be designed to react to the scenarios that introduce more risk into the system, decreasing their consequences as much as possible.

Regulation 994/2010 [12] builds the EP upon three crisis levels:

1. 'Early warning': when there is concrete, serious and reliable information that an event may occur which is likely to result insignificant deterioration of the supply situation.
2. 'Alert': when a supply disruption or exceptionally high gas demand occurs which results in significant deterioration of the supply situation, but the market is still able to manage the situation.
3. 'Emergency': in the event of exceptionally high gas demand, significant supply disruption or other significant deterioration of the supply situation and in the event that all relevant market measures have been implemented but the supply of gas is insufficient to meet the remaining gas demand so that non-market measures have to be additionally introduced.

As it can be seen in the definition of the three crisis levels, security of gas supply market measures and non-market measures are listed. The Regulation [12] considers in its annexes II and III the main market and non-market measures that may be adopted, and these are further classified as either supply side or demand side measures. This classification is provided in Tab. 3.1. Some of these measures have more to do with the PAP than with the EP, as for example diversification of gas supply routes, the deployment of new LNG regasification facilities or of new gas storage facilities, investments in infrastructure, including bi-directional capacity, among others. These are options that, if adopted, lead to decreased probabilities of some potential events / crises, but cannot be adopted when the crisis has already started. Measures that have to do with the EP are, for example, increased production flexibility, increased import flexibility, and reverse flows, among

others. The security of supply measures considered in the Regulation [12] related to the

	Market measures	Non-market measures
Supply side measures	<ul style="list-style-type: none"> • increased production flexibility, • increased import flexibility, • facilitating the integration of gas from renewable energy sources into the gas network infrastructure (power to gas), • commercial gas storage-withdrawal capacity and volume of gas in storage, • LNG terminal capacity and maximal send-out capacity, • diversification of gas supplies and gas routes, • reverse flows, • coordinated dispatching by transmission system operators, • use of long-term and short-term contracts, • investments in infrastructure, including bi-directional capacity, • contractual arrangements to ensure security of gas supply. 	<ul style="list-style-type: none"> • use of strategic gas storage, • enforced use of stocks of alternative fuels (e.g. in accordance with Council Directive 2009/119/EC of 14 September 2009 imposing an obligation on Member States to maintain minimum stocks of crude oil and/or petroleum products (1)), • enforced use of electricity generated from sources other than gas, • enforced increase of gas production levels, • enforced storage withdrawal.
Demand side measures	<ul style="list-style-type: none"> • use of interruptible contracts, • fuel switch possibilities including use of alternative back-up fuels in industrial and power generation plants, • voluntary firm load shedding, • increased efficiency, • increased use of renewable energy sources. 	<ul style="list-style-type: none"> • enforced fuel switching, • enforced utilisation of interruptible contracts, where not fully utilised as part of market measures, • enforced firm load shedding.

Tab. 3.1.: Security of gas supply measures. Adapted from Regulation 994/2010 [12] on security of gas supply.

EP, when implemented in case of crisis, involve necessarily the use of some network facilities. Normally, the operator will have to react to the event triggering the crisis by changing the operational mode of some of the facilities. For example, to react to a sudden drop in imports through an entry point, the operator could change the control mode of some other entry points from flow control to pressure control in order to keep the

pressure at the normal operational level in the network, allowing the transport of gas to the areas close to the entry point affected by the gas disruption. This can be combined with a change in the control mode of other facilities to enhance the transport of gas in the desired direction, as for example CS. Table 3.2 shows the correspondence between the EP

Measure adopted	Facility used
<ul style="list-style-type: none"> • increased production flexibility, • increased import flexibility, • use of long-term and short-term contracts, contractual arrangements to ensure security of gas supply. • enforced increase of gas production levels, • use of long-term and short-term contracts, contractual arrangements to ensure security of gas supply. 	<u>Entry Stations:</u> CBI - Cross Border Entry Stations, PRO - Gas Production Fields
<ul style="list-style-type: none"> • use of interruptible contracts, • fuel switch possibilities including use of alternative back-up fuels in industrial and power generation plants • voluntary firm load shedding • enforced use of stocks of alternative fuels (e.g. in accordance with Council Directive 2009/119/EC of 14 September 2009 imposing an obligation on Member States to maintain minimum stocks of crude oil and/or petroleum products (1)) • enforced use of electricity generated from sources other than gas, • enforced fuel switching • enforced utilisation of interruptible contracts, where not fully utilised as part of market measures • enforced firm load shedding 	<u>Exit Stations:</u> CGS - City Gate Stations, GFPP - Gas Fired Power Plant Stations, IND Stations of Large Industrial Customers, CBE - Cross Border Export Stations
<ul style="list-style-type: none"> • commercial gas storage, • use of strategic gas storage, • enforced storage withdrawal. 	UGS - Underground Gas Storage Facility
<ul style="list-style-type: none"> • LNG terminal capacity and maximal send-out capacity, • increased import flexibility, • use of long-term and short-term contracts, contractual arrangements to ensure security of gas supply. 	LNG - Liquefied Natural Gas Regasification Terminals
<ul style="list-style-type: none"> • coordinated dispatching by transmission system operators 	All

Tab. 3.2.: Correspondence between EP measures and network facilities needed to implement them.

measures considered in the Regulation [12] and the network facilities needed to implement

them. For example, increased import flexibility means having in place the right contracts that allow increase flows with relatively short notice to react to problems. The way to implement this measure in the model is acting on the control mode of the entry stations across which the shipper that provides that flexibility can put gas into the system. The same would apply to contractual arrangements signed to ensure security of gas supply.

The facilities modelled in gas network model to simulate the flexibility of a gas transport network under normal operation and under gas crisis situations are: entry stations (CBIs, PROs), exit stations (CGS, GFPP, IND), UGS, LNG, and CS. In fact, entry and exit stations are modelled as nodes with flow or pressure control similar to the regulator and metering station installed in the actual station.

All measures that have to do with reduction of demand are simulated via exit stations. At the bottom of the table we can see coordinated dispatching by TSOs. This necessarily demands the use of all facilities available in the network.

3.4. Extended Model for Gas Infrastructures

The gas network model derived in the previous Chapter requires additional considerations in order to be suitable for examining security of supply scenarios, where the control modes of non-pipe facilities like compressor stations and UGS facilities may change in time due to an action of the TSO or a condition in the network. Thus, in this section we extend the algorithm for the gas network model presented in Chapter 2 by a Dynamic Event Feasibility Checking Algorithm (DFC), a Simulation Control Evaluation Algorithm (SCE) a Constraints and Control Handling Algorithm (CCH) for non-pipe facilities and a Dynamic Time Step Adaptation Method (DTA), which adapts the simulation time step Δt according to the changes in boundary conditions (e.g. changing the control mode in a compressor station, UGS, LNG terminals etc.) in order to capture rapid changes with a higher time resolution. The extended algorithm has been implemented into a software tool named **SAInt** (Scenario Analysis Interface for Energy Systems), which contains a graphical user interface and is developed in MS Visual Studio .NET with the object oriented programming language VB.NET. The algorithm implemented in **SAInt** is depicted in Fig. 3.1 and discussed further in this section.

Each case study in **SAInt** is modelled as a scenario which includes a time window, a global time step Δt_g , an initial state for the studied network and a list of scenario definition objects, defined by the user prior to the actual solution process. A scenario definition object, in turn, consist of a number of properties, which are specified in Tab. 3.3. Among

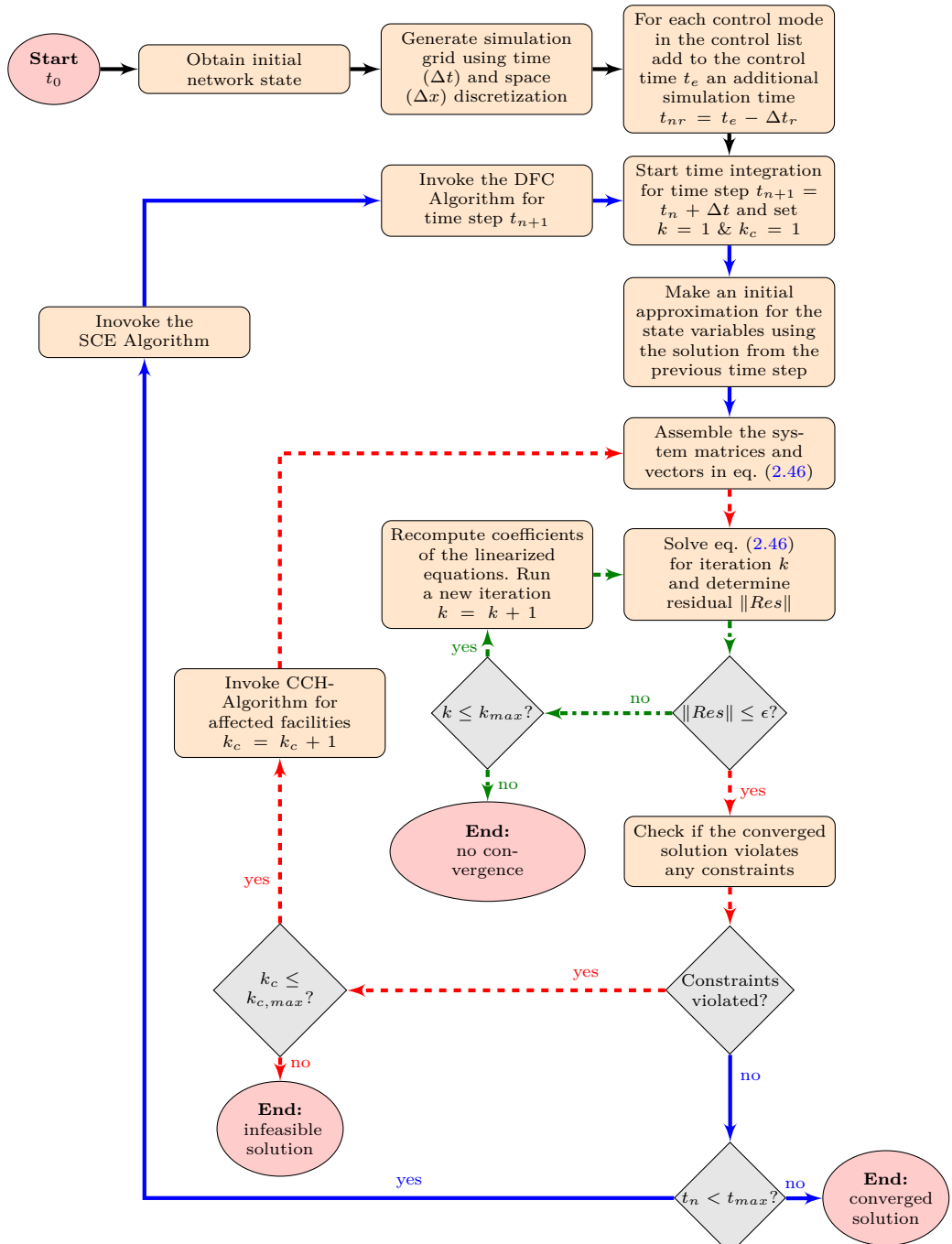


Fig. 3.1.: Flow diagram of the transient hydraulic solver implemented in the simulation tool SAInt

	Scenario Definition Object (user defined)	Simulation Control Object (internal)
Object Properties	<ul style="list-style-type: none"> • Active (Boolean) • Processed (Boolean) • Time (Date) • Object (NetObject) • Parameter (Enum) • Value (Double, ExpressionObject) • Profile (ProfileObject) • Condition (ExpressionObject) • Evaluation (Enum) 	<ul style="list-style-type: none"> • InterControl (ControlType) • InterControlValue (Double) • InitialControlValue (Double) • Condition (Delegate) • AddSimulationTime (Integer) • DoUntil (Date) • DoNext (SimulationControlObject) • DoNextAfter (Integer)

Tab. 3.3.: Overview of the properties of the scenario definition object and the simulation control object and their corresponding data types

	Profile Object
Object Properties	<ul style="list-style-type: none"> • Name (String) • ProfileType (Enum) • TimeStep (Integer) • InterpolationType (Enum) • DistributionType (Enum) • MeanValues (DoubleArray) • Deviations (DoubleArray)

Tab. 3.4.: Overview of the properties of the profile object and their corresponding data types

these properties are the *EventParameter* with its corresponding *Value*, i.e. the requested change in boundary condition (e.g. change in control set point, initial storage level, arrival of LNG vessel etc.) and the *EventTime*, i.e. the time at which the requested change should take place. In order to model the load fluctuations at these stations, the scenario event object contains a *Profile* property (s. Table 3.3) which can be used to assign a profile object to a flow controlled gas station. As shown in Fig. 3.1 before the actual time integration

process the program iterates through the list of scenario definitions and adds for each requested control change an additional simulation time point

$$t_{nr} = t_e - \min(\Delta t_g, \Delta t_r) \quad (3.2)$$

before the actual specified event time t_e . The default value for the reaction time Δt_r is set to three minutes (Δt_r). This enables a higher resolution for changes in control set points, if the global time step is chosen relatively high ($\Delta t_g \gg \Delta t_r$). The algorithm for the remaining solution process contains three major loops, namely, the time integration loop, marked by the solid blue flow arrows, the constraints and control handling loop, illustrated by the dashed red flow arrows and the iterative loop, indicated by the dashdotted green flow arrows in Fig. 3.1.

Time Integration Loop

The time integration loop is the outer loop of the transient solver. It has been extended by a dynamic event feasibility checking algorithm (DFC), which checks if a requested control set point for a future time point t_{n+1} is feasible, considering the present control of the station at time point t_n . If a requested set point is not feasible, the DFC will change the station control to the next closest feasible working point. In addition, for some requested control changes, like for instance, turning an operating compressor station into bypass, the DFC makes use of a simulation control object (SCO), which is an extension of a scenario definition object. The SCO inherits all properties of the scenario definition object and has, in addition, the properties listed in the third column of Tab. 3.3, which enable the control of the station until a specified simulation time (property *DoUntil*) and/or until a specified *Condition* is fulfilled. Moreover, the SCO has two properties named *InterControl* and *InterControlValue* which can be used to instruct the solver to apply a specific control of the station before the final control (*EventParameter*) is set. This property, for instance, can be used to model the transition of the control mode of a compressor station from operating ($p_o > p_i$ and $Q > 0$) to bypass ($p_o = p_i$) more realistically. In reality, the station will not go directly from operating into bypass, since this would cause an undesired backflow ($Q < 0$) due to the higher pressure at the station outlet compared to the inlet. To prevent this, the flow through the station is typically interrupted by a valve until the inlet pressure is slightly greater or equal to the outlet pressure. In this case, the bypass valve is opened to allow the flow to bypass the station. This situation can be modelled by the definition of a SCO as shown in listing 3.1 & 3.2. Listing 3.1 shows how the SCO is instantiated, while listing 3.2 illustrates how the instantiated SCO is evaluated in the

SCE algorithm. For this example, the *InterControl* property is set to the control mode *OFF* (Listing 3.1, l. 9) until the *Condition* property (Listing 3.1, l. 11), which verifies if the inlet pressure is greater outlet pressure, is *True*. If the condition is *False*, then the SCO requests a higher time resolution for future simulation time steps, depending on the difference between the inlet and outlet pressure (Listing 3.1,l. 19). The reason for increasing the time resolution is to capture the simulation time at which the condition function is fulfilled ($p_i \geq p_o$). Finally, the instantiated SCO is added to the simulation control list (listing 3.1, l. 25), in order to enable its evaluation by the SCE algorithm.

The SCE algorithm iterates through the SCOs in the simulation control list and evaluates all unprocessed SCOs. Listing 3.2 demonstrates how the SCO instantiated in Listing 3.1 would be processed by the SCE. The SCE, firstly, evaluates the condition function of the SCO (Listing 3.2, l. 2-3). If the condition function is *True*, the control of the station is set to the final control specified by the *EventParameter* and the *Value* property of the SCO (Listing 3.2, l. 7-8). Otherwise, the control of the station is set to the *Intercontrol* property of the SCO (Listing 3.2, l. 35-36) and an additional simulation time step is added (Listing 3.2, l. 38).

```

1  'instantiate the simulation control object
2  Dim SimCtrl = New SimulationControlObject With
3  {
4      .Active = True,
5      .Processed = False,
6      .EventTime = Solver.Time(n + 1),
7      .Object = Compressor(1),
8      .EventParameter = ScenarioParameter.BP,
9      .InterControl = ControlType.OFF,
10     .DoUntil = Solver.EndTime
11     .Condition =
12         Function(obj As NetObject, t As Integer, smc As ▶
13             →SimulationControlObject)
14             'check if compressor inlet pressure is greater outlet pressure
15             If (obj.FromNode.P(t) - obj.ToNode.P(t)) > 0 Then
16                 Return True
17             Else
18                 'compute the time step to be added to the
19                 'simulation time to increase the time resolution
20                 smc.AddSimulationTime = Math.Min(15, Math.Ceiling(3 * Math.Abs(↘
21                     →obj.FromNode.P(t) - obj.ToNode.P(t)) / 100000.0))
22                 Return False
23             End If
24         End Function
25     }
26     'add simulation control object to simulation control list
27     Scenario.SimCtrlList.Add(SimCtrl)

```

Listing 3.1: Instantiating a simulation control object for modeling the transition of a compressor station from operating into bypass in SAInt using the objectoriented programming language VB.NET

Iterative Loop

The iterative loop, in contrast, is the inner loop of the transient solver and serves the purpose of solving the linearised non-linear system of equations (eq. (2.46)) iteratively. The solution of the system of equations requires an efficient linear equation solver for each iteration step. We have extended the linear solver used in Chapter 2, by a direct sparse solver specifically designed for solving large scale unsymmetric sparse linear systems such as the system of equations expressed in eq. (2.46). The new solver enhances the capability of the simulation tool for solving large scale gas systems with thousands of elements with reasonable computation time and storage demand. Explaining the details of the sparse solver would go beyond the scope of this chapter. Thus, for more details we refer to [107–109].

```

1  'Evaluate the condition function of the SCO
2  If SimCtrl.Condition.EndInvoke( _
3      SimCtrl.Condition.BeginInvoke(Compressor(1), n, SimCtrl, Nothing, ↴
4          →Nothing)) Then
5      'add an additional simulation time for processing the new control ↴
6          →setting
7      Solver.AddTimeStep(Solver.Time(n).AddMinutes(3))
8      'assign the final control setting for the station
9      Compressor(1).Ctrl(n+1) = SimCtrl.EventParameter
10     Compressor(1).CtrlVal(n+1) = SimCtrl.Value
11     'check if a subsequent SCO is defined
12     If SimCtrl.DoNext IsNot Nothing Then
13         'assign the event time for processing the proceeding SCO
14         SimCtrl.DoNext.EventTime = Solver.Time(n).AddMinutes(SimCtrl.↘
15             →DoNextAfter)
16         'add the event time to the simulation time
17         Solver.AddTimeStep(Solver.Time(n).AddMinutes(SimCtrl.DoNextAfter))
18         'add the subsequent SCO to the simulation control list
19         Scenario.SimCtrlList.Add(SimCtrl.DoNext)
20     End If
21     'mark the SCO as processed to avoid future evaluation
22     SimCtrl.Processed = True
23     'check if the termination time for the SCO has been reached
24     ElseIf Solver.Time(n + 1) > SimCtrl.DoUntil Then
25         'check if a subsequent SCO was defined
26         If SimCtrl.DoNext IsNot Nothing Then

```

```

24     'assign the event time for processing the subsequent SCO
25     SimCtrl.DoNext.EventTime = Solver.Time(n).AddMinutes(SimCtrl.→
26     →DoNextAfter)
27     'add the event time to the simulation time
28     Solver.AddTimeStep(Solver.Time(n).AddMinutes(SimCtrl.DoNextAfter))
29     'add the subsequent SCO to the simulation control list
30     Scenario.SimCtrlList.Add(SimCtrl.DoNext)
31     End If
32     'mark the SCO as processed to avoid future evaluation
33     SimCtrl.Processed = True
34 Else
35     'assign the intermediate control setting for the station
36     Compressor(1).Ctrl(n+1) = SimCtrl.InterControl
37     Compressor(1).CtrlVal(n+1) = SimCtrl.InterControlValue
38     'add the additional simulation time computed in the condition function
39     Solver.AddTimeStep(Solver.Time(n).AddMinutes(SimCtrl.AddSimulationTime))
End If

```

Listing 3.2: Excerpt of the Simulation Control Evaluation Algorithm (SCE) for a compressor station implemented in SAInt using the objectoriented programming language VB.NET

Constraints and Control Handling Loop

The constraints and control handling loop is entered when a station constraint has been violated. In this case, the CCH algorithm for the station is invoked. The idea behind the CCH loop is to repeat the iterative loop for the last time point t_n using new control settings for the affected station. The new settings are generated by the CCH algorithm implemented for the specific station. The solver delivers a list of constraint violation objects(which contain information on the violated parameters and their corresponding constraint levels) to the CCH algorithm . The constraint level is an indicator of the significance of each constraint and how it should be treated by the solver. It is subdivided into the following four levels:

1. Warning:

The solver issues a warning of a constraint violation without invoking the CCH algorithm.

2. Soft limit:

The solver invokes the CCH algorithm, which tries to find a feasible working point for a limited number of iterations. If no feasible working point is found the solver ignores the violated constraint and proceeds with the next time step (t_{n+1}).

3. Hard limit:

The solver invokes the CCH algorithm, which tries to find a feasible working point for a limited number of iterations. If no feasible working point is found the simulation is aborted.

4. Stop limit:

The solver aborts the simulation without invoking the CCH algorithm.

The CCH algorithm tries to find a compromise between the violated parameter and the existing control set point by generating a new control setting for the station. If necessary, the CCH algorithm can issue an SCO for the affected station, which is then added to the simulation control list and evaluated in the SCE for the specified event time.

The design of the facility specific CCH algorithm requires a good understanding of the operation, the control and the technical limits of the key facilities in the gas system, which has been elaborated Chapter 2.

In the next section, we use these information to develop the CCH algorithm for compressor stations, UGS facilities, LNG terminals and exit/entry stations.

CCH Algorithm for Compressor Stations

The CCH algorithm for a compressor station is invoked whenever the solver detects a constraint violation after exiting a converged iterative loop for a simulation time (t_n). The algorithm is visualized in the flow diagram shown in Fig. 3.2. In the first CCH iteration ($k_c = 1$) for each affected simulation time t_n the saved constraint control for the station, which will be explained below, is cleared. In the first step of the CCH algorithm we check if internal constraints of the station are violated, thus, if the outlet pressure is greater or equal to the inlet pressure ($p_o \geq p_i$) and if the flow direction is from the inlet to the outlet ($Q \geq 0$). If internal constraints are violated the algorithm will change the control of the station to *OFF* for the subsequent repetition of the iterative loop and, in addition, instantiate a simulation control object (SCO) for turning the station into bypass, similar to the example discussed in listing 3.1 & 3.2. Moreover, a subsequent SCO is assigned to the *DoNext* property of the instantiated SCO, which enables the station to attempt to return to its original control before the violation of the internal constraint (s. listing 3.2, l. 10-17). With the property *DoNextAfter* we can also specify how many minutes after fulfilling the condition function or after the specified *DoUntil* time the subsequent SCO should be processed by the SCE. The default value for the *DoNextAfter* property is the global time step Δt_g .

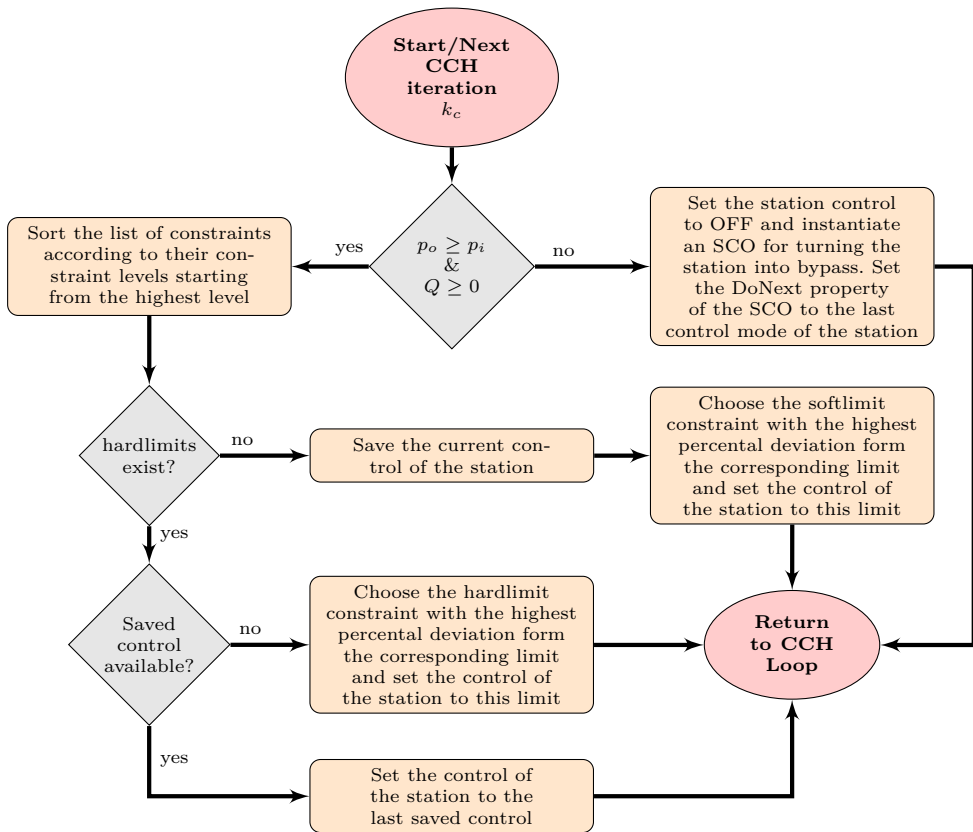


Fig. 3.2.: Constraints and Control Handling Algorithm for compressor stations implemented in the simulation tool SAInt

If no internal constraints exist, the algorithm sorts the list of violated constraints according to their constraint level starting from the highest level (hard limit). If the list of violated constraints contains only soft limits then the current control of the station is saved for subsequent iterations for the current simulation time t_n . Next, we set the control of the station to the soft limit with the highest percental deviation from its corresponding constraint value and return to the CCH loop.

In contrast if the violated constraints include any hard limits the algorithm firstly verifies if a saved control exist. This is to ensure that the processing of a soft limit does not trigger another hard limit. The saved control is always a control that allows the continuation of the simulation, even if not all soft limits could be removed after the maximum number of CCH iterations ($k_{c,max}$). If no saved control is available, thus, no acceptable working point has been found, then similar to the soft limits case the control of the station is set

to the hard limit with the highest percental deviation from its corresponding constraint. Finally the CCH algorithm is exited and returned to the CCH loop.

CCH Algorithm for Entry and Exit Stations

The CCH algorithm for entry and exit stations is illustrated in the flow diagram shown in Fig. 3.3. The first step of the algorithm is to check if the station is a demand or supply station and then to check if the internal constraints regarding the sign of the nodal load is violated. In this case the station is turned off by setting the nodal load to zero. Otherwise, the algorithm sorts the list of constraints and follows the same procedure as explained for compressor stations.

CCH Algorithm for UGS

Figure 3.4 shows the CCH algorithm for UGS facilities. The first step of the algorithm is to verify which storage process is currently running at the facility, i.e withdrawal (*WDR*) or injection (*INJ*) process. Depending on the running process the algorithm checks if internal constraints are violated. If the nodal load is positive and the working inventory is smaller zero for the withdrawal process, the station is turned off by assigning a zero load to the node. The same setting is applied, if the nodal load is negative or the working inventory is greater maximum working inventory in an injection process. In case none of these internal constraints are violated, the algorithm checks if the current load exceeds the maximum withdrawal/injection rate respectively and changes the control of the station accordingly. If no internal constraints are violated, the constraint violation is then either the maximum gas withdrawal pressure (restricted by the maximum operating pressure of the pipeline system) or the minimum gas injection pressure (restricted by the minimum line pack for operating the network and the minimum inlet pressure to the compressor station in the UGS facility). In this case, the control of the station is set to pressure control with a pressure value equal to the limiting pressure.

CCH Algorithm for LNG Terminals

Figure 3.5 shows a flow diagram of the CCH algorithm for LNG terminals. The algorithm firstly checks if the nodal load is negative and if the working gas inventory is depleted and then shuts down the station if one of these conditions is fulfilled. If none of these internal constraints are violated the algorithm then checks if the nodal load is greater

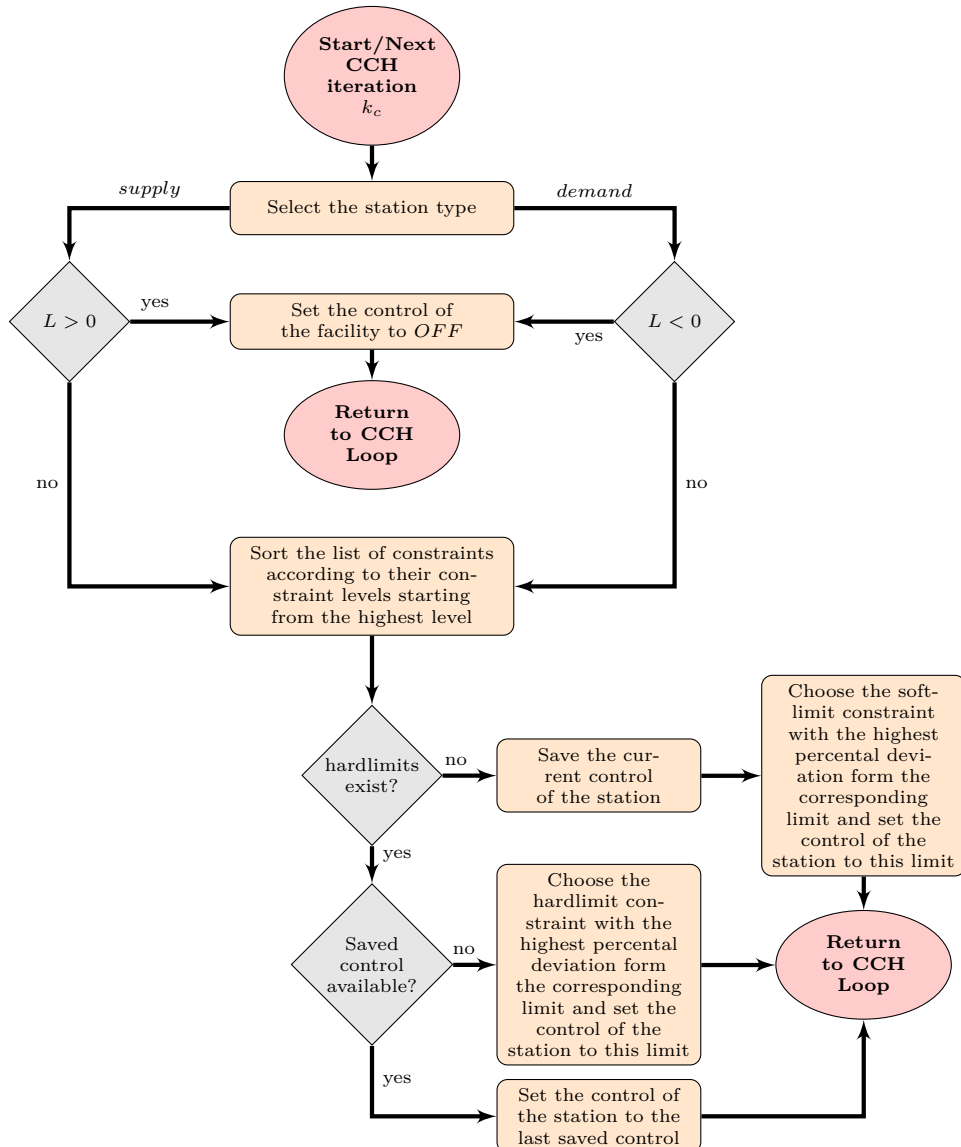


Fig. 3.3.: Constraints and Control Handling Algorithm for entry and exit stations implemented in the simulation tool SAInt

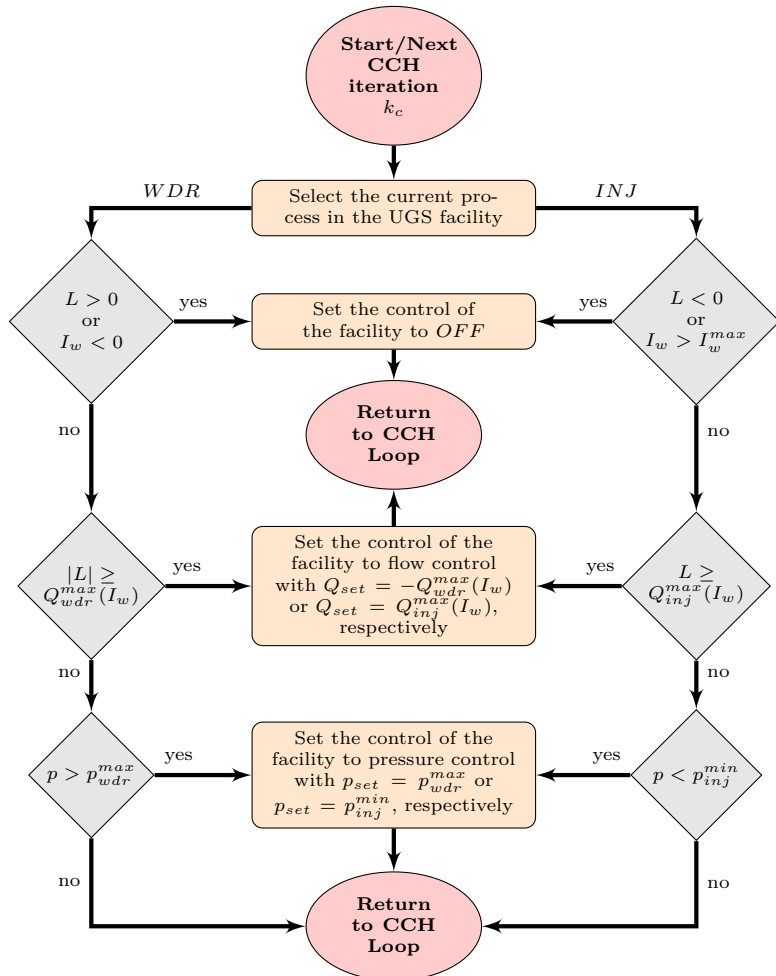


Fig. 3.4.: Constraints and Control Handling Algorithm for UGS facilities implemented in the simulation tool SAInt

than the maximum regasification rate and sets the control of the station to the limiting flow rate in case of a violation. If also the maximum regasification rate is not violated, then the algorithm checks if the maximum gas injection pressure is exceeded and changes the control of the station to the limiting pressure, in case of a violation. After as new control is set for the terminal the CCH algorithm returns to the CCH loop.

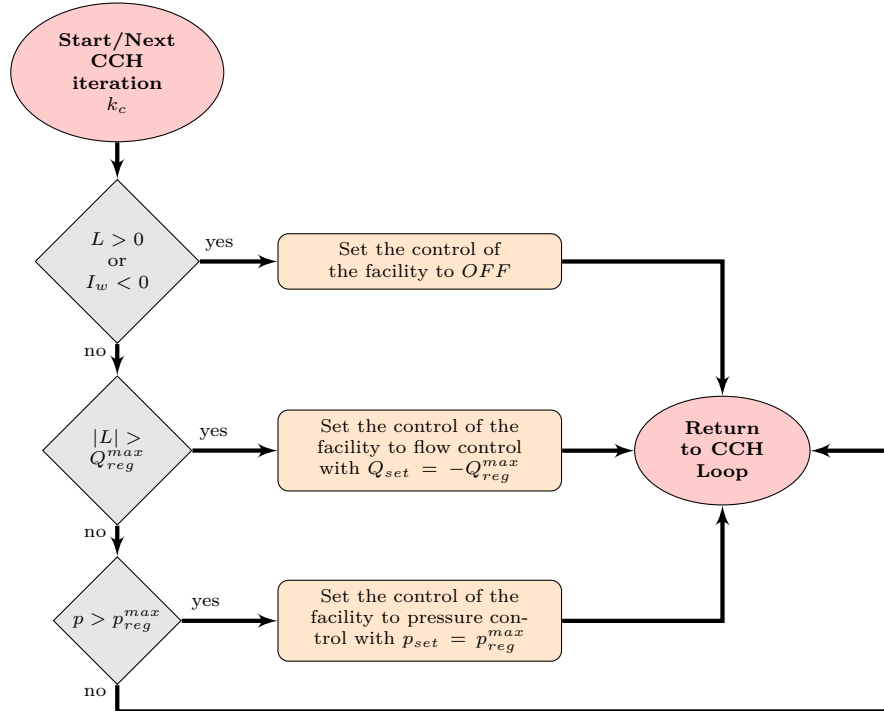


Fig. 3.5.: Constraints and Control Handling Algorithm for LNG Terminals implemented in the simulation tool SAInt

3.5. Modelling of Measures to Mitigate the Impact of Disruptions

The different generic control modes for non-pipe facilities presented in Chapter 2 are similar to those available to TSOs to manage their actual systems and to react to disruptions in the GTS. A TSO can typically change the settings of each facility dynamically depending on the current state of the system and the forecasts for gas supply and demand. In case of a disruption, the TSO will typically follow a strict sequence of actions and measures

(protocol) to mitigate the impact of the disruption. The degrees of freedom available to the TSO to apply these measures, which are included in the Emergency Plan and are based on the events identified in the Risk Assessment, depend on the legal commitments with other stakeholders (gas customers, shippers, producers, competent authorities etc.) and the technical restrictions imposed by the gas infrastructure (pressure, flow and power limits etc.). To model these actions together with the available control modes listed in Tab. 2.1 & 2.2, we introduce a conditional expression for the execution of a requested control change of a non-pipe facility. The conditional expression may depend on a number of different network parameters, such as the line pack, the available supply capacities and gas demands. By doing this, we enable the simulation model to react dynamically to a disruption, similar to how a TSO would react in reality, allowing by these means a more realistic simulation of the gas network behaviour and a better estimation of gas crises consequences.

Furthermore, to model the different entities and their responsibilities in the simulation model of interconnected multinational gas transport systems, we introduce the possibility to subdivide the network model into different subsystems, which are then assigned to the different entities responsible for their operation. Each subsystem inherits the properties from total network model. This way, the parameters of the subsystems can be used in the conditional expressions to request a change in control mode for a specific facility. For instance, an increase in gas supply to a subsystem can be initiated in case of a drop in line pack below a certain threshold. In the next section, we give a brief description of the developed simulation software **SAInt**. Finally, we demonstrate the capabilities of the software by applying it to a real world instance.

3.6. Model Application

The models presented in this chapter are implemented into a simulation software - **SAInt** (Scenario Analysis Interface for Energy Systems). **SAInt** is divided into two separate modules, namely, **SAInt-API** (Application Programming Interface) and **SAInt-GUI** (Graphical User Interface). The API is the main library of the software and contains all solvers and classes for instantiating the different objects comprising the gas system model (nodes, pipes, compressors etc.). The API is independent of the GUI and can be used separately in other environments supporting .NET libraries (e.g. MS Excel, Visual Studio etc., IronPython). **SAInt-GUI** is the graphical interface, which enables a visual communication between the API and the user. The GUI uses the classes and solvers provided by the API to perform the simulation tasks requested by the user.

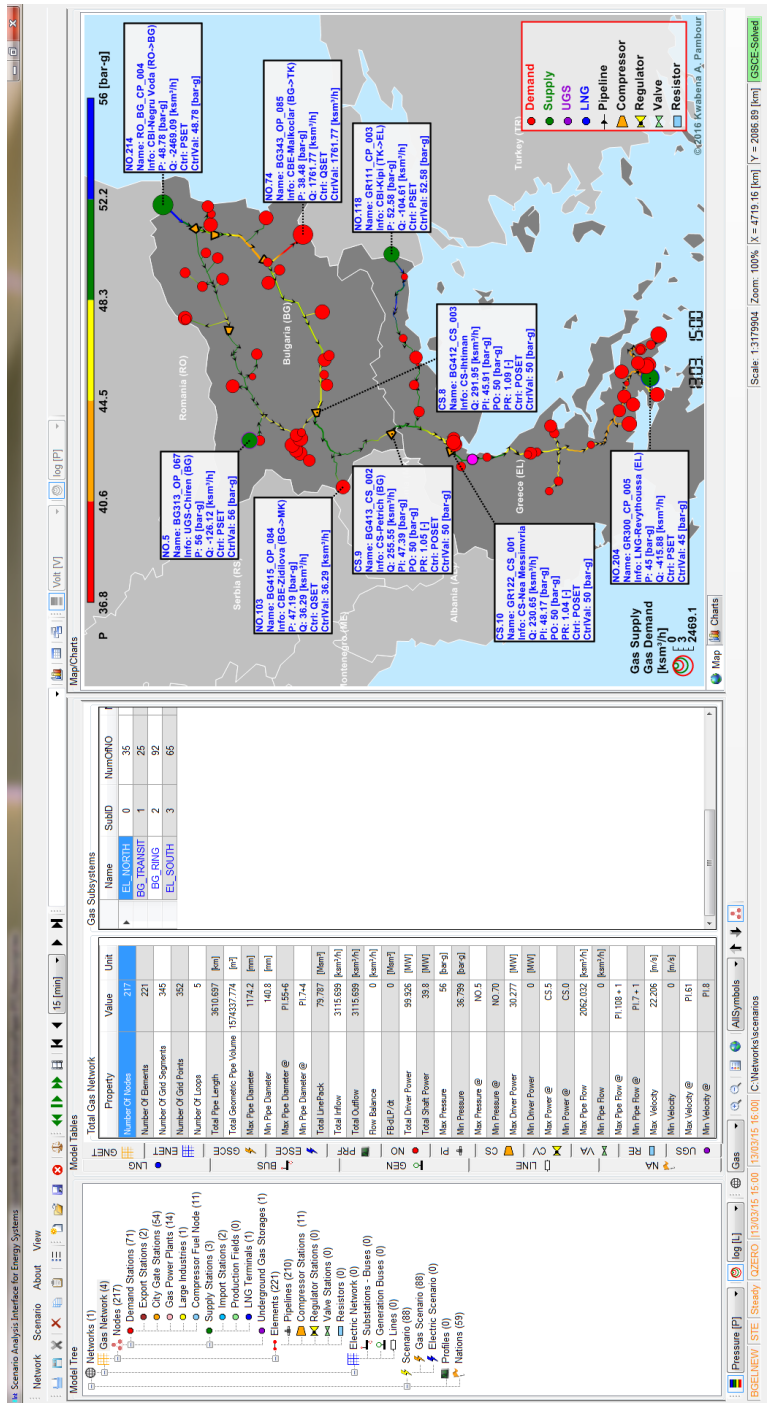


Fig. 3.6.: Snapshot of the network model of the Bulgarian-Greek NGTS in the graphical user interface of the simulation tool SAInt

In this section, we apply **SAInt** to perform a case study on one of the regions affected by the gas crisis in January 2009, namely, the Bulgarian and Greek NGTS. In the case study,

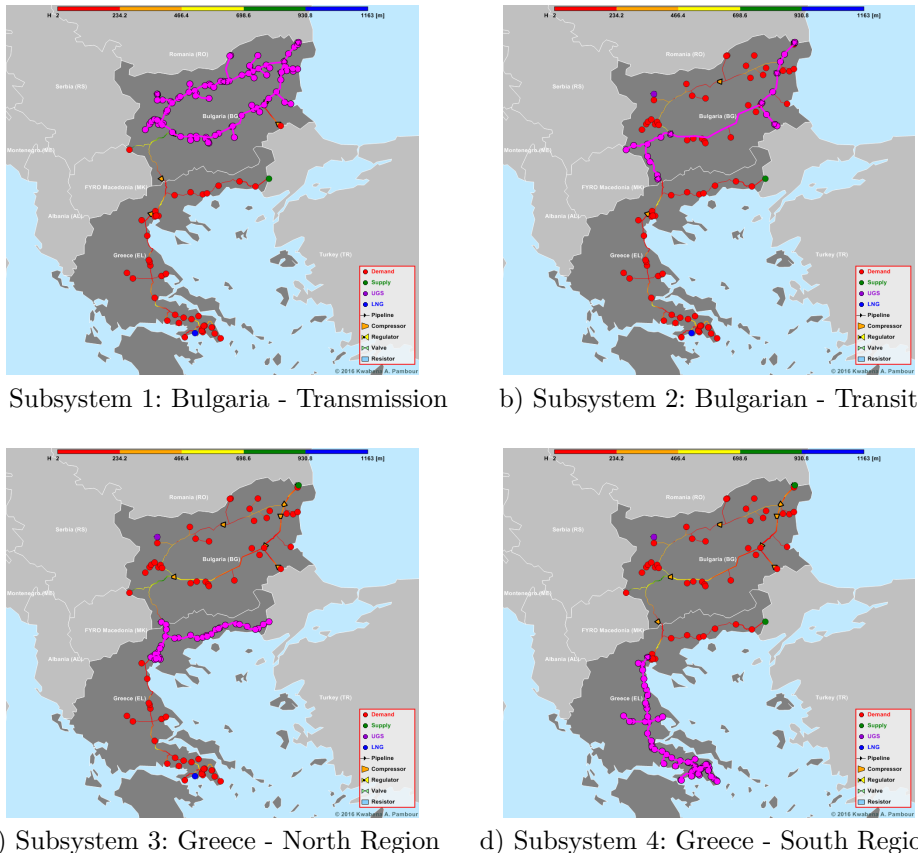


Fig. 3.7.: Assigned subsystems in the Bulgarian-Greek simulation model

we assess the resilience of the network in case of a disruption in a compressor station. We apply mitigation measures to reduce the impact of the disruption by changing the settings of specific facilities using conditional control settings. Figure 3.6 shows a snapshot of the network model in the graphical user interface of **SAInt**.

For the case study, we divide the network model into four subsystems, as shown in Fig. 3.7 and Tab. 3.6. We will use the parameters of the subsystems to define conditional expressions for the control of surrounding non-pipe facilities.

In order to start the dynamic simulation, an initial state of the network model (obtainable from a steady state computation), is required. The results of the steady state computation

Property	Value	Unit
Number Of Nodes	217	
Number Of Elements	221	
Number Of Grid Segments	345	
Number Of Grid Points	352	
Number Of Loops	5	
Total Pipe Length	3610.697	[km]
Total Geometric Pipe Volume	1574337.774	[m ³]
Max Pipe Diameter	1174.2	[mm]
Min Pipe Diameter	140.8	[mm]

Tab. 3.5.: Properties of the Bulgarian-Greek NGTS

Subsystem	Nodes	Elements	Supply	Demand	Compressor
BG_RING	92	95	0	32	4
BG_TRANSIT	25	27	1	2	6
EL_NORTH	35	34	1	11	0
EL_SOUTH	65	65	1	26	1

Tab. 3.6.: Properties of the assigned subsystems

Parameter	Symbol	Value	Unit
time step	Δt	900	[s]
total simulation time	t_{max}	48	[h]
gas temperature	T	288.15	[K]
dynamic viscosity	η	10^{-5}	[kg/m · s]
standard pressure	p_n	1.01325	[bar]
standard temperature	T_n	273.15	[K]
relative density	d	0.6	[−]

Tab. 3.7.: Input parameter for transient simulation of the Bulgarian-Greek network model

are shown in the map in Fig. 3.6, where the pressure and load distribution and the gas flow direction in the pipelines are depicted. The input data for the loads are based on peak winter consumption in 2011. Furthermore, each supply node in the model is pressure controlled, while each compressor station (except the compressor station at UGS-Chiren, which is typically used for storage injection) is outlet pressure controlled with pressure set points ranging from 40-54 bar-g. For the cross border import stations Negru Voda and Kipi, we define constraints for the maximum pressure and maximum supply quantity, as shown in the snapshot of the node dialogues in Fig. 3.8 & 3.9. For the dynamic simulation, we assign to the demand nodes representing city gate stations the characteristic relative load profile depicted in Fig. 3.11, which we multiply with the corresponding steady state loads. For the other demand nodes, we assume a constant profile equal to the steady state

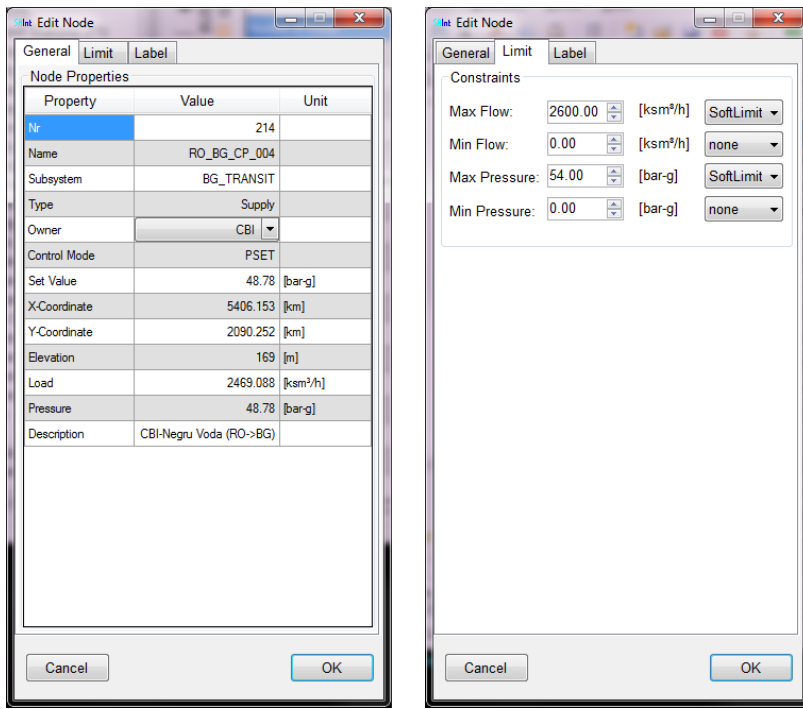


Fig. 3.8.: Snapshot of the SAInt-Node-Editor showing the assigned constraints to CBI-Negru Voda

load. Moreover, for each city gate station, we define a minimum delivery pressure limit of 20 bar-g and for the two cross border export stations a minimum delivery pressure of 30 bar-g. Furthermore, for UGS-Chiren and LNG-Revythoussa, we use the storage envelope and facility limits shown in the snapshot of the storage and LNG-Terminal dialogue in Fig. 3.10. Additional simulation settings and gas properties are listed in Tab. 3.7.

To assess the resilience of the network and to show the capability of the simulation tool to model the reaction of the gas system to supply disruptions, we introduce a disruption in compressor station CS-Petrich located at the Bulgarian-Greek border. Figure 3.12 shows a snapshot of the SAInt- Scenario Definition Table, where the different control mode definitions are listed. After the start of the simulation (6:00), we interrupt the gas flow from the Bulgarian transit pipeline to Greece by shutting down the compressor station CS-Petrich at 12:00. The flow interruption is relaxed 12 hours later at midnight 00:00 by changing the control mode of the station to bypass. To mitigate the supply disruption, we define conditional control settings to the surrounding compressor stations, namely,

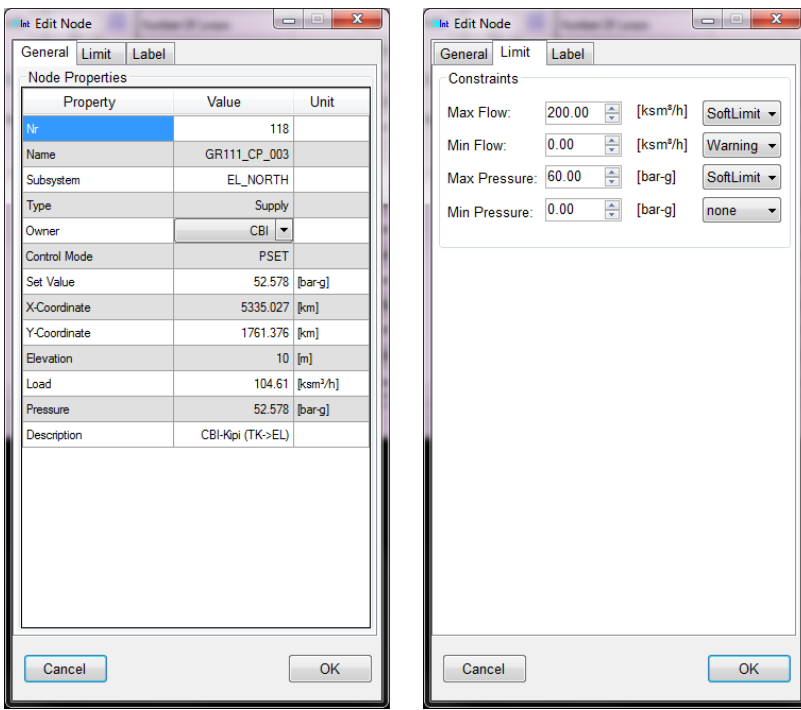


Fig. 3.9.: Snapshot of the SAInt-Node-Editor showing the assigned constraints to CBI-Kipi

CS-Ihtiman and CS-Nea Messimvria. We request a change in control mode for CS-Nea Messimvria from outlet pressure to inlet pressure control with a control set point of 35 bar-g, if the minimum pressure in the subsystem EL_North is below 30 bar-g, in order to stabilize the pressure in EL_North.

In addition, we request a change in control mode for CS-Ihtiman from outlet pressure control to maximum driver power control, whenever the line pack in the subsystem EL_South goes below 12.5 Msm³. If the line pack is above this threshold, we request the station to return to its original outlet pressure control. In reality such a control change would require the coordination of the two TSOs as indicated in the list of mitigation measures in Tab. 3.2. The results of the computation are shown in Fig. 3.16 - 3.20 and are discussed in the following.

Figures 3.16 - 3.18 show the time series of the station control, inlet and outlet pressure and flow rate for the compressor stations CS-Ihtiman (top plot, CS.8), CS-Petrich (middle plot, CS.9) and CS-Nea Messimvria (bottom plot, CS.10). As can be seen in the middle time plots, the flow through CS-Petrich is interrupted at 12:00, causing the inlet pressure

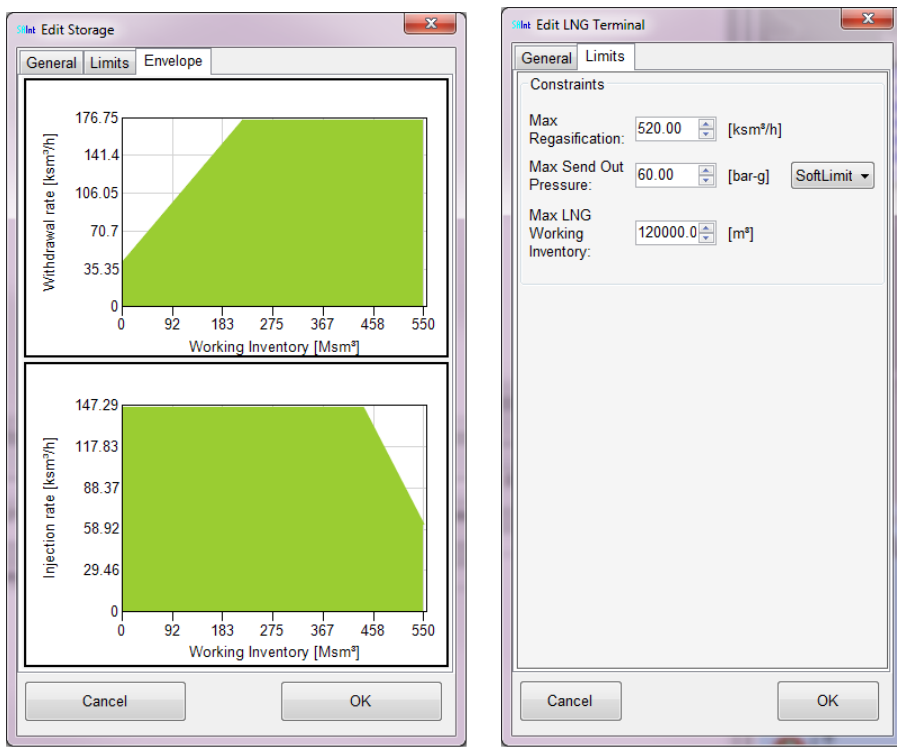


Fig. 3.10.: Snapshot of SAIInt-Storage Editor (left) and LNG-Terminal-Editor (right) showing the assigned properties for UGS-Chiren (left) and LNG-Terminal-Revythoussa (right)

to increase and the outlet pressure of the station to decrease. The disruption also affects the pressure level and total line pack in the subsystem EL_North as depicted in figure 3.13, where the total line pack and the minimum pressure in the subsystems EL_North (GSUB.0) and EL_South (GSUB.3) are depicted. At approximately 15:00 the minimum pressure in subsystem EL_North drops below 30 bar-g, which is the threshold for changing the control of CS-Nea Messimvria to inlet pressure control. At the time where this condition is fulfilled, the inlet pressure of CS-Nea Messimvria is above the requested set point of 35 bar-g, thus, to achieve the requested set point the station compresses more gas from the suction to the discharge side, causing the flow rate to increase (see bottom plot of Fig. 3.18) and the driver power to reach its maximum value (s. bottom plot of Fig. 3.16). The requested inlet pressure set point is finally reached at approx 18:00 (see bottom plot of Fig. 3.17).

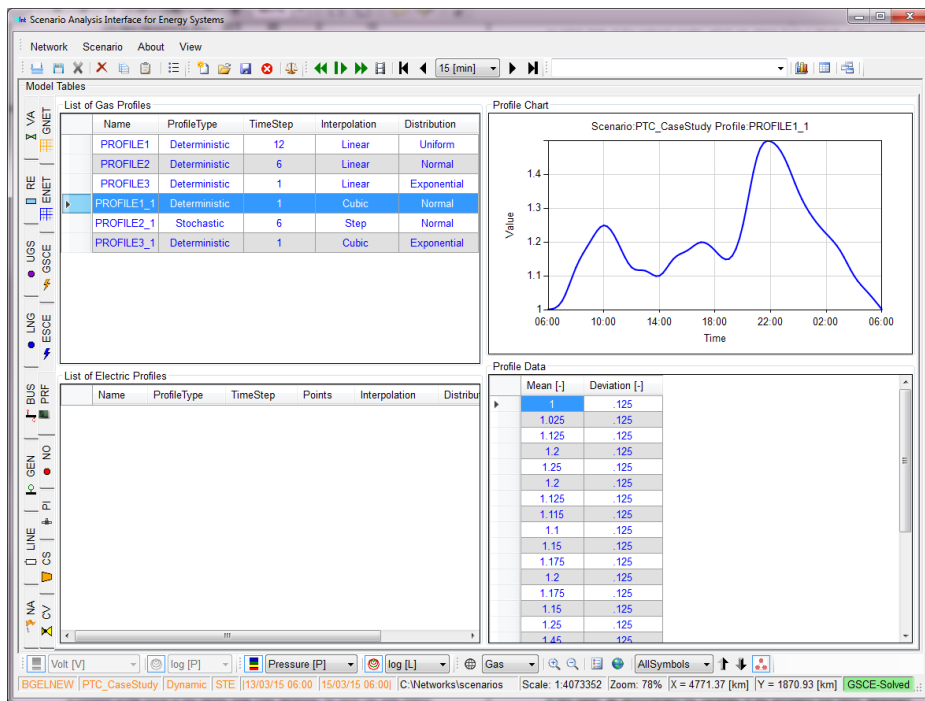


Fig. 3.11.: SAInt-Profile-Editor showing the relative 24 h load profile assigned to demand nodes representing city gate stations

The effect of the second mitigation measure can be seen if we compare the time series of the line pack in subsystem EL_South (Fig. 3.13) and the time series for the compressor station CS-Ihtiman. At approx. 21:00 the line pack in subsystem EL_South drops below 12.5 Msm³, causing the compressor station to change its original pressure outlet set point from 50 bar-g to the maximum outlet pressure 54 bar-g. This set point differs from the requested maximum driver power control (see Fig. 3.12). The reason for this is that operating the compressor station at maximum driver power would violate the maximum outlet pressure constraint, thus the constraint and control handling algorithm considers the next feasible working point, which in this case is the maximum outlet pressure.

The maximum outlet pressure control is relaxed at approx. 4:00, when the line pack in subsystem EL_South rises above 12.5 Msm³. In this case the station is set back to its original outlet pressure control of 50 bar-g. Since the original pressure set point is below the outlet pressure at 4:00 (54 bar-g), the flow through the station is firstly interrupted until the outlet pressure drops back to 50 bar-g.

The screenshot shows a software interface titled "Scenario Analysis Interface for Energy Systems". The main window contains a table titled "Model Tables" with the following columns:

	Active	Time	Evaluation	Condition	Object	Nr	Parameter	Profile	Value	Unit
	<input checked="" type="checkbox"/>	13/03 06:00	NONE		NO	50	QSET	PROFILE1_1	1.494	[ksm³/h]
	<input checked="" type="checkbox"/>	13/03 06:00	NONE		NO	28	QSET	PROFILE1_1	2.86	[ksm³/h]
	<input checked="" type="checkbox"/>	13/03 06:00	NONE		NO	30	QSET	PROFILE1_1	2.759	[ksm³/h]
	<input checked="" type="checkbox"/>	13/03 06:00	NONE		NO	166	QSET	PROFILE1_1	1.662	[ksm³/h]
	<input checked="" type="checkbox"/>	13/03 06:00	NONE		NO	167	QSET	PROFILE1_1	12.913	[ksm³/h]
	<input checked="" type="checkbox"/>	13/03 06:00	NONE		NO	164	QSET	PROFILE1_1	12.827	[ksm³/h]
	<input checked="" type="checkbox"/>	13/03 06:00	NONE		NO	145	QSET	PROFILE1_1	47.296	[ksm³/h]
	<input checked="" type="checkbox"/>	13/03 06:00	NONE		NO	157	QSET	PROFILE1_1	1.234	[ksm³/h]
	<input checked="" type="checkbox"/>	13/03 06:00	NONE		NO	163	QSET	PROFILE1_1	1.025	[ksm³/h]
	<input checked="" type="checkbox"/>	13/03 06:00	NONE		NO	168	QSET	PROFILE1_1	.605	[ksm³/h]
	<input checked="" type="checkbox"/>	13/03 06:00	NONE		NO	175	QSET	PROFILE1_1	73.891	[ksm³/h]
	<input checked="" type="checkbox"/>	13/03 06:00	NONE		NO	210	QSET	PROFILE1_1	5.529	[ksm³/h]
	<input checked="" type="checkbox"/>	13/03 06:00	NONE		NO	212	QSET	PROFILE1_1	24.439	[ksm³/h]
	<input checked="" type="checkbox"/>	13/03 06:00	NONE		NO	213	QSET	PROFILE1_1	.837	[ksm³/h]
	<input checked="" type="checkbox"/>	13/03 06:00	NONE		NO	209	QSET	PROFILE1_1	1.444	[ksm³/h]
	<input checked="" type="checkbox"/>	13/03 06:00	NONE		NO	179	QSET	PROFILE1_1	.093	[ksm³/h]
	<input checked="" type="checkbox"/>	13/03 06:00	NONE		NO	186	QSET	PROFILE1_1	.51	[ksm³/h]
	<input checked="" type="checkbox"/>	13/03 06:00	NONE		NO	122	QSET	PROFILE1_1	.684	[ksm³/h]
	<input checked="" type="checkbox"/>	13/03 06:00	NONE		NO	112	QSET	PROFILE1_1	56.237	[ksm³/h]
	<input checked="" type="checkbox"/>	13/03 06:00	NONE		NO	146	QSET	PROFILE1_1	42.622	[ksm³/h]
	<input checked="" type="checkbox"/>	13/03 06:00	NONE		NO	119	QSET	PROFILE1_1	.249	[ksm³/h]
	<input checked="" type="checkbox"/>	13/03 06:00	NONE		NO	111	QSET	PROFILE1_1	1.219	[ksm³/h]
	<input checked="" type="checkbox"/>	13/03 06:00	NONE		NO	130	QSET	PROFILE1_1	.026	[ksm³/h]
	<input checked="" type="checkbox"/>	13/03 06:00	NONE		NO	208	QSET	PROFILE1_1	.96	[ksm³/h]
	<input checked="" type="checkbox"/>	13/03 06:00	NONE		NO	150	QSET	PROFILE1_1	.952	[ksm³/h]
	<input checked="" type="checkbox"/>	13/03 06:00	NONE		NO	154	QSET	PROFILE1_1	3.977	[ksm³/h]
	<input checked="" type="checkbox"/>	13/03 06:00	NONE		NO	165	QSET	PROFILE1_1	.561	[ksm³/h]
	<input checked="" type="checkbox"/>	13/03 06:00	NONE		NO	131	QSET	PROFILE1_1	18.403	[ksm³/h]
	<input checked="" type="checkbox"/>	13/03 06:00	NONE		NO	133	QSET	PROFILE1_1	1.495	[ksm³/h]
	<input checked="" type="checkbox"/>	13/03 06:00	NONE		NO	143	QSET	PROFILE1_1	14.154	[ksm³/h]
	<input checked="" type="checkbox"/>	13/03 06:00	NONE		NO	155	QSET	PROFILE1_1	2.024	[ksm³/h]
	<input checked="" type="checkbox"/>	13/03 12:00	DolTRUE	gsub_EL_SOUTH.ip.[Msm3]>12.5	CS	8	POSET	-	.50	[bar-g]
	<input checked="" type="checkbox"/>	13/03 12:00	DoUntiTRUE	gsub_EL_SOUTH.ip.[Msm3]<12.5	CS	8	POWMAX	-	-	-
	<input checked="" type="checkbox"/>	13/03 12:00	NONE		CS	9	OFF	-	-	-
	<input checked="" type="checkbox"/>	13/03 12:00	DolTRUE	gsub_EL_NORTH.PMIN.[barg]<30	CS	10	PISET	-	.35	[bar-g]
	<input checked="" type="checkbox"/>	14/03 00:00	NONE		CS	9	BP	-	-	-

Below the table, there is a toolbar with various icons for file operations, zoom, and simulation controls. At the bottom, there is a status bar displaying "BGELNEW | PTC_CaseStudy | Dynamic | STE | 13/03/15 06:00 | 15/03/15 06:00 | C:\Scale: 1:3036665 | Zoom: 105% | X = 5039.09 [km] | Y = 1834.96 [km] | GSCE-Solved ::".

Fig. 3.12.: Snapshot of the SAInt scenario definition table showing the defined boundary conditions disruption events and mitigation strategy for the case study

Figures 3.14-3.20 show the time series of the station control, pressure and load for the four entry points CBI-Negru Voda, CBI-Kipi, UGS-Chiren and LNG-Revythoussa. In these plots, we see the effect of the station constraints on the control set point of the station and also how the disruption in CS-Petrich affected the entry points. The most affected facilities are CBI-Kippi and LNG-Revythoussa, where the gas supply rises to its maximum, in order to balance the demand in the northern and southern Greek region.

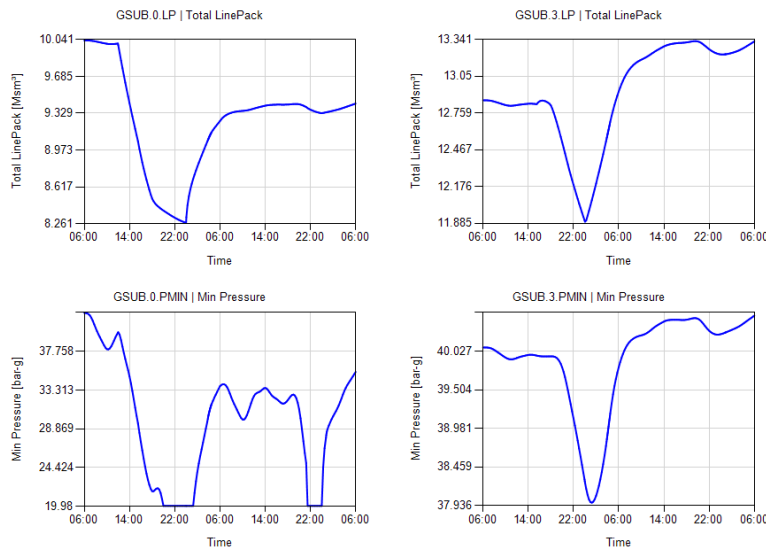


Fig. 3.13.: Time series of Line Pack (LP) and Minimum Pressure (PMIN) in the subsystems EL_NORTH (GSUB.0) and EL_SOUTH (GSUB.3)

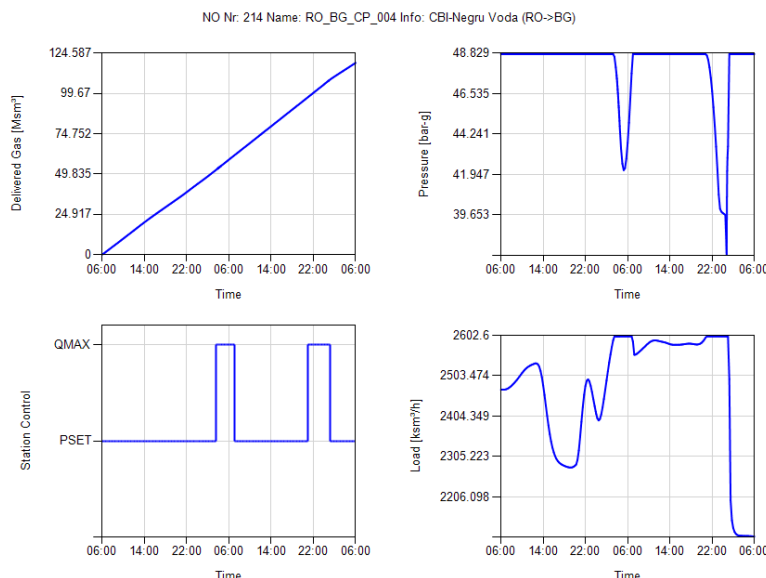


Fig. 3.14.: Time series of delivered gas quantity, station control, load and pressure for the Cross Border Import Negru Voda

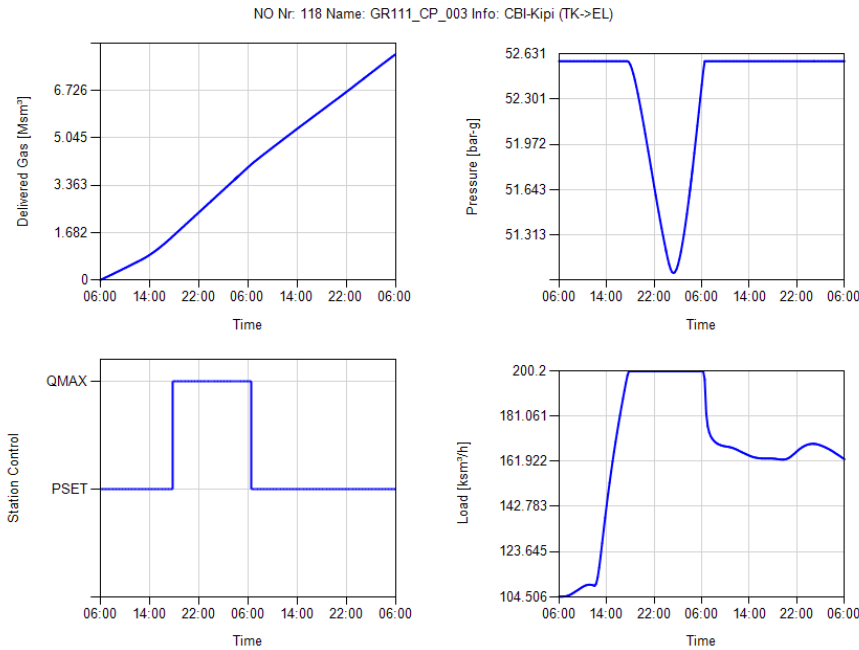


Fig. 3.15.: Time series of delivered gas quantity, station control, load and pressure for the Cross Border Import Kipi

3.7. Conclusion

In this chapter, the gas network model from Chapter 2 was extended and implemented into a simulation software with a graphical user interface named **SAInt**. The software is designed for analysing the consequences of natural gas supply disruptions. In the first part, a formal definition of the term Risk was given and the different elements comprising a Risk Assessment, namely, the identification of potential scenarios and the estimation of their probability and consequences, were discussed. We pointed out the importance of estimating the consequences of potential scenarios in an adequate manner, using hydraulic models that reflect the dynamic behaviour of gas transport systems appropriately. Furthermore, we gave an overview of the different mitigation measures that can be adopted to reduce the impact of gas supply disruptions and the facilities in the gas infrastructure to apply these measures. Next, we presented an algorithm for solving the physical equations describing the dynamic behaviour of gas transport systems. In addition, we elaborated how to model the control settings of non-pipe facilities such as compressor stations and regulator stations and how these control modes are implemented in the simulation tool

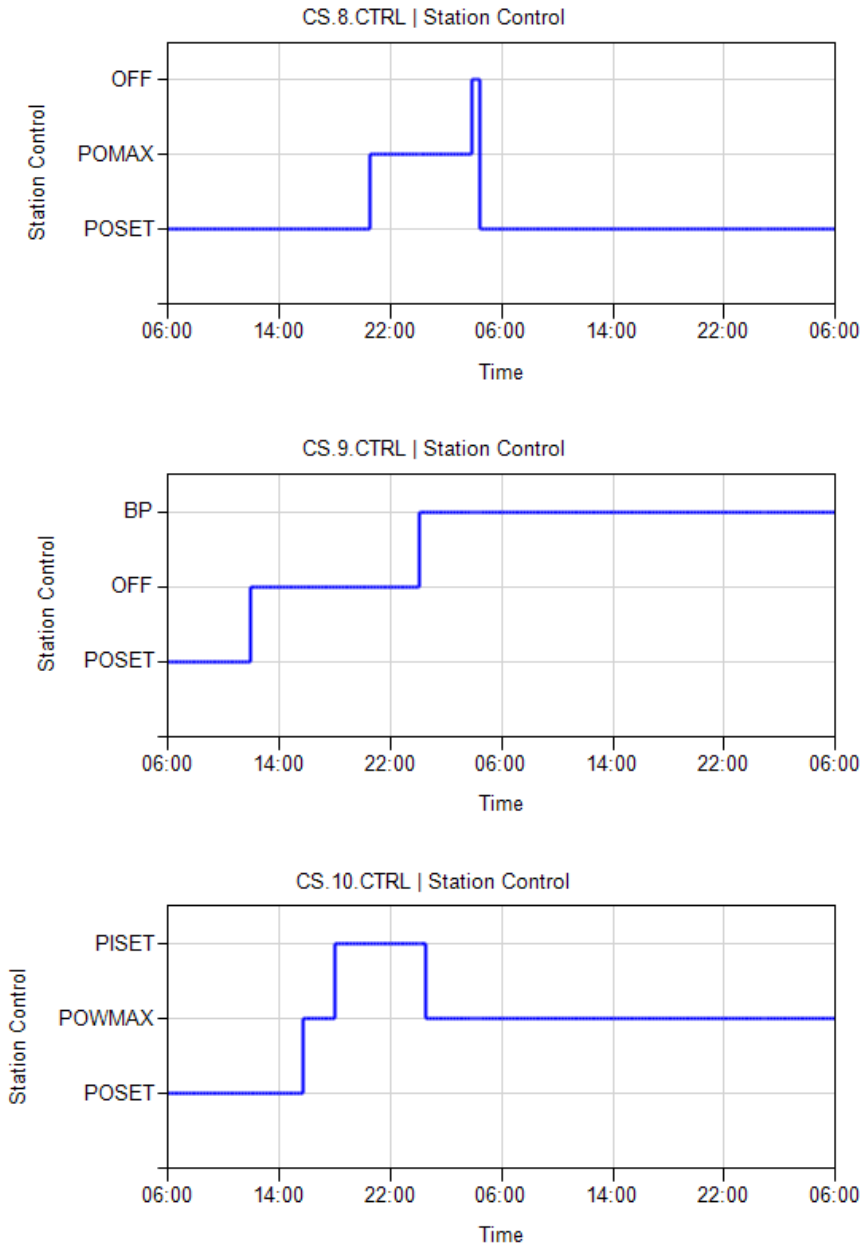


Fig. 3.16.: Time series of station controls for compressor stations CS-Ihtiman (CS.8), CS-Petrich (CS.9) & CS-Nea Messimvria (CS.10)

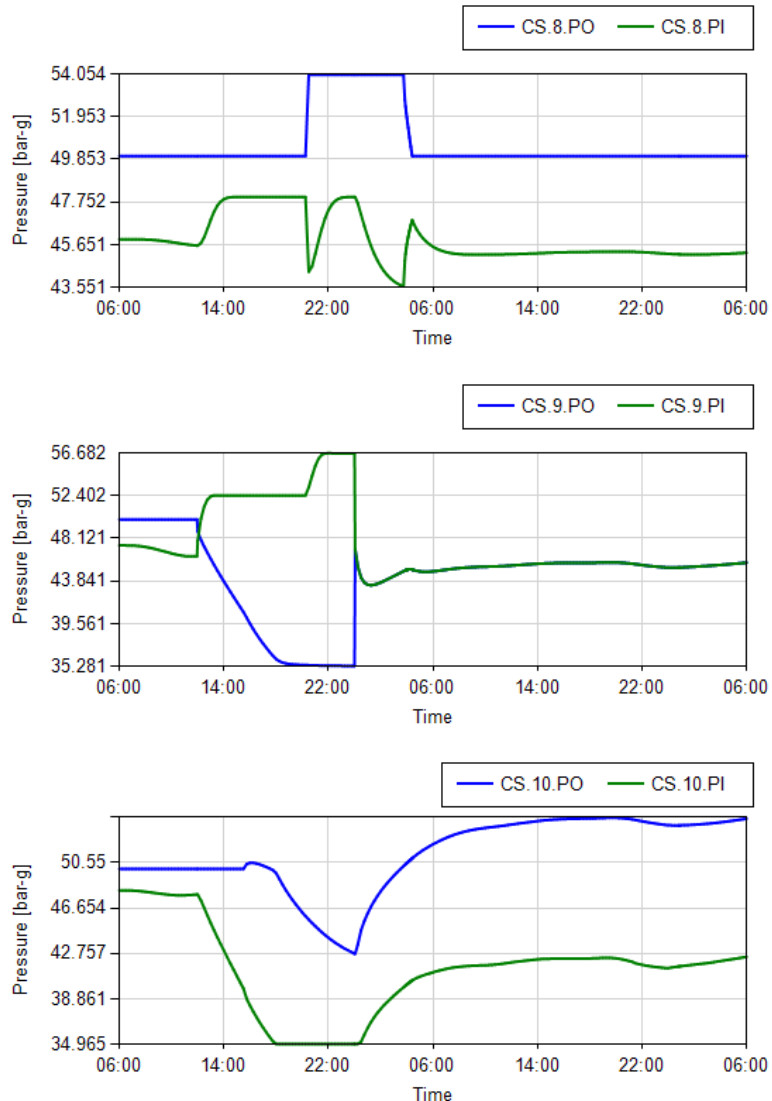


Fig. 3.17.: Time series of inlet pressure (PI) and outlet pressure (PO) for compressor stations CS-Ihtiman (CS.8), CS-Petrich (CS.9) & CS-Nea Messimvria (CS.10)

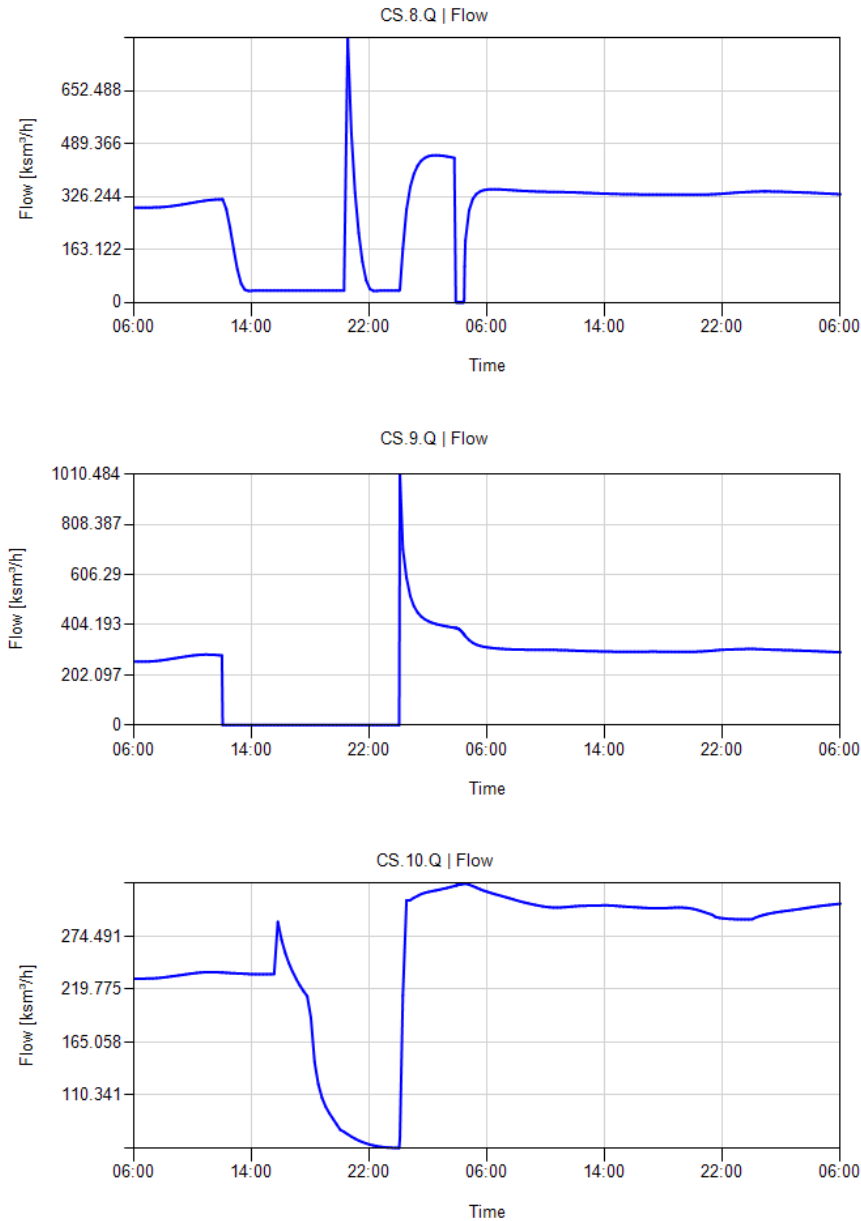


Fig. 3.18.: Time series of flow rate (Q) for compressor stations CS-Ihtiman (CS.8), CS-Petrich (CS.9) & CS-Nea Messimvria (CS.10)

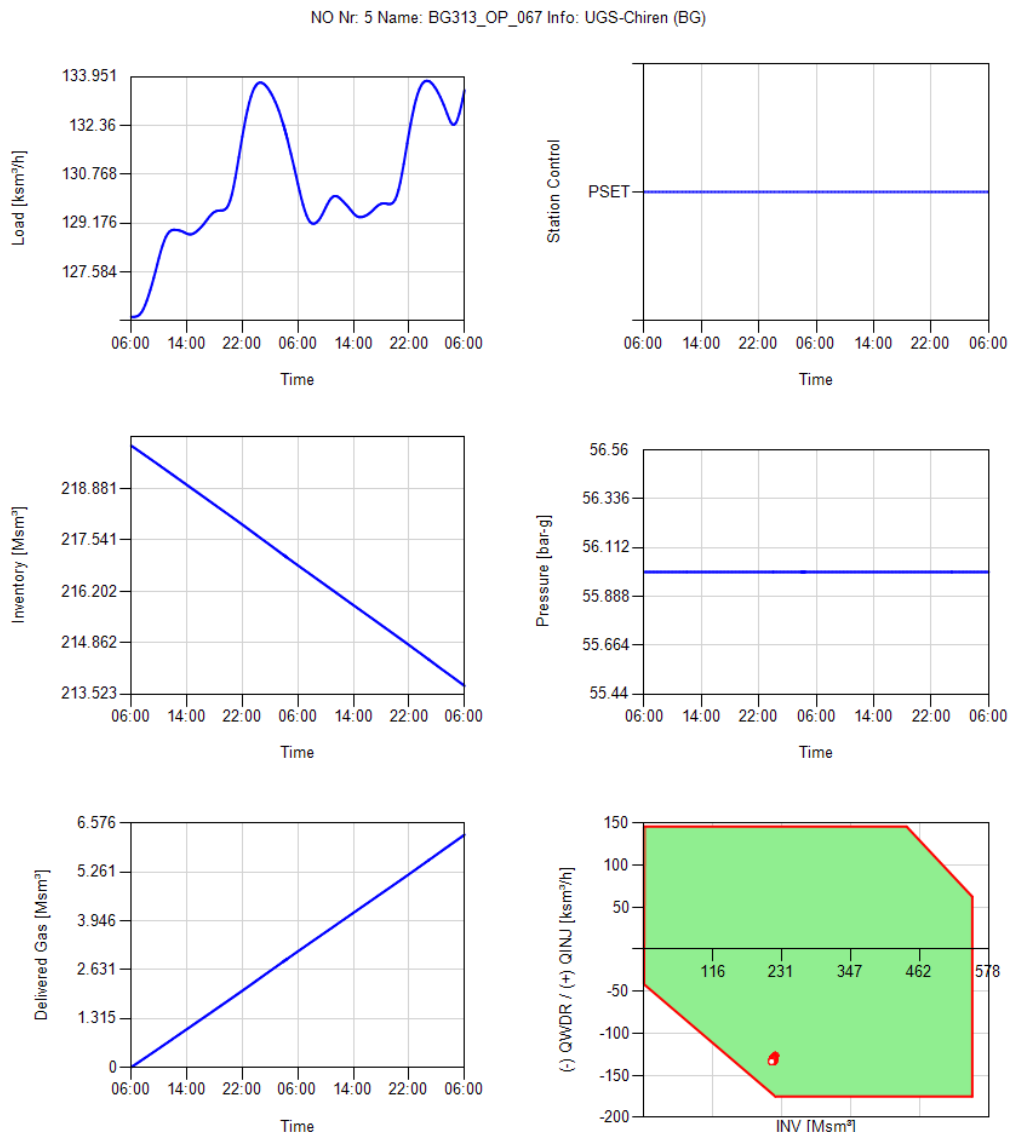


Fig. 3.19.: Time series of the supply, storage inventory, delivered gas quantity, station control, pressure and storage envelope for the Underground Gas Storage Facility Chiren

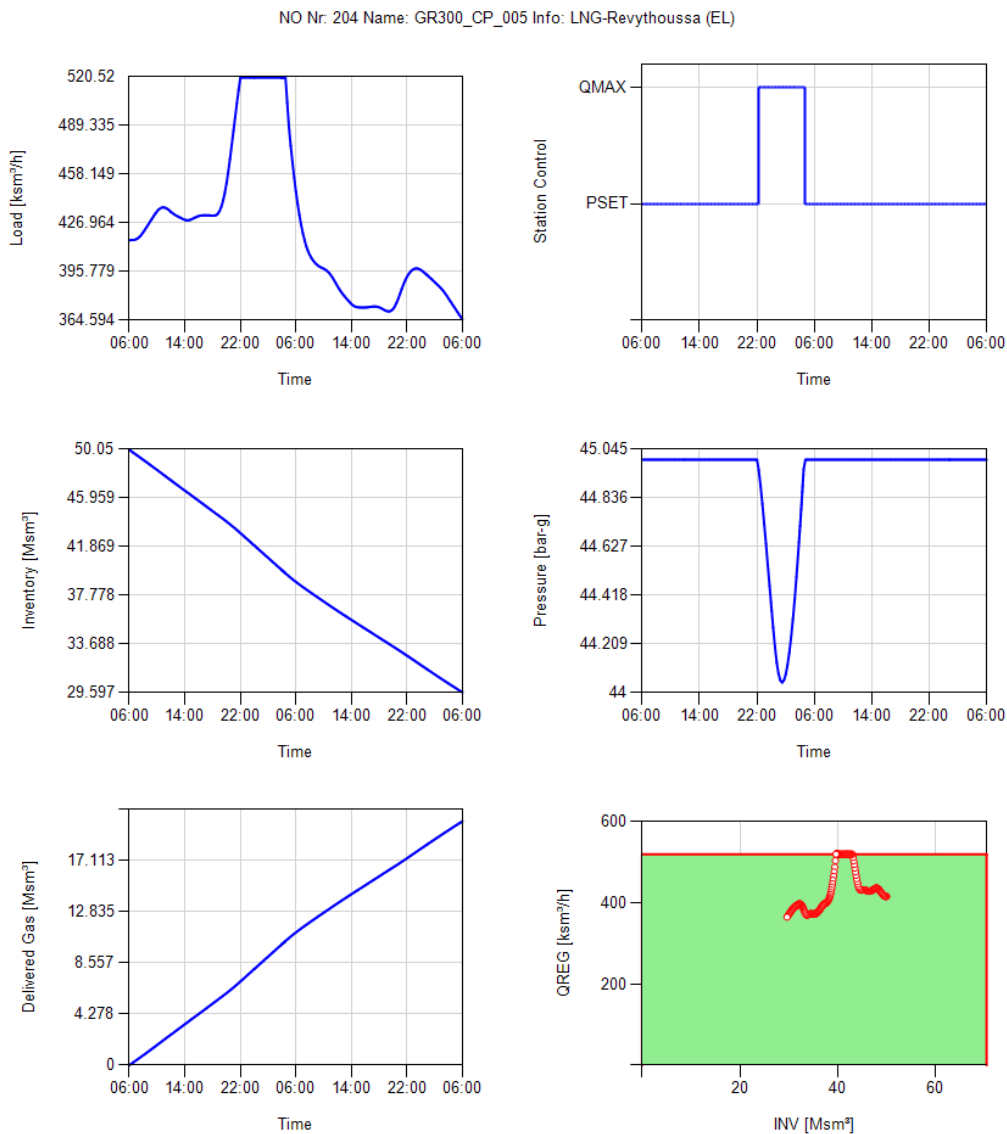


Fig. 3.20.: Time series of the supply, storage inventory, delivered gas quantity, station control, pressure and storage envelope for the LNG-Terminal Revythoussa

SAInt. Finally, we applied the methods developed in this chapter to a real world instance, where we demonstrated the capability of the developed tool to simulate gas supply disruptions and to model and asses demand and supply side measures to mitigate the impact of gas supply disruptions.

This chapter focused on addressing the following sub-research questions, which have been partly addressed in Chapter 2:

- *How can we develop a mathematical model that reflects appropriately their physical behaviour and their technical and contractual constraints?*
- *What countermeasures can be deployed to mitigate the impact of disruptions and how can these countermeasures be integrated into the combined model?*

The features added to the gas model enable the modelling of different kinds of disruption scenarios and the implementation of countermeasures to mitigate these disruptions. In the next chapter, we develop the models for the electric power system and identify the most important interconnections between the gas and electricity system. Furthermore we use the developed gas model to develop a co-simulation framework between **SAInt** and the Matlab-based open source power system library MATPOWER [116].

4. Co-Simulation Framework for interdependent Gas and Electricity Transmission Networks

This chapter is based on the following peer reviewed journal article and conference paper:

- K. A. Pambour, B. Cakir Erdener, R. Bolado-Lavin, and G. P. Dijkema, “[Development of a simulation framework for analysing Security of Supply in integrated gas and electricity systems](#),” *Applied Sciences*, vol. 7, no. 1, pp. 47, 2017.
- K. A. Pambour, B. Cakir Erdener, R. Bolado-Lavin, and G. P. J. Dijkema, “[An integrated simulation tool for analysing the operation and interdependency of natural gas and electric power systems](#),” in *Pipeline Simulation Interest Group (PSIG) Conference 2016*.

4.1. Introduction

Large scale energy infrastructures for natural gas and power play a crucial role for any well-functioning society. These infrastructures are systematically analysed and controlled in order to understand their operational characteristics and to provide an energy efficient operation and a sufficient level of security of supply. However, ensuring the required level of security of supply is becoming more challenging, especially because of increasing interconnection among the facilities in both systems.

The dependence of power generation on natural gas has increased the vulnerability of electric power systems to interruptions in gas supply, transmission, and distribution. Since the storage of gas on-site is not an option, as it is for coal and fuel oil, the direct gas delivery through pipelines becomes more critical during unexpected events in electricity systems like peak periods or disruptions. Particularly, short-term problems caused by pipeline constraints that cause an inability of a generator to receive fuel gas can seriously affect security of power supply [13].

Another issue is the lack of predictability of renewable generation, which might increase the magnitude of imbalances in the gas system. Although the increasing share of renewables will cause a reduction of the power system dependency on natural gas, forecasting the amount of gas needed to serve GFPPs will become more challenging due to growing penetration of variable resources. Additionally, shale gas production already had a significant impact on the deployment of new infrastructures, especially in the USA, where the installed capacity of GFPPs has increased enormously during the last years and is expected to continue increasing in the coming years [110]. This increase has obviously tightened the dependency of the electricity system on the gas system. This could also be the case in other regions of the world, including Europe, especially under scenarios of abundant shale gas and low carbon policies.

Not only is the power system dependent on gas, but also the gas system is dependent on power. A gas network consists of different facilities that depend on electrical power in order to maintain normal operation (e.g., electric driven compressors, LNG facilities, UGS facilities, valves, regulators, gas meters). The usage of electric drivers in gas facilities is increasing due to advantages regarding environmental impacts and flexibility compared to gas turbines [10]. Moreover, increased availability, better control, improved energy efficiency, and shorter delivery times are other important and attractive advantages of electric drivers. Since the proper functioning of electric drivers requires a reliable power supply, gas system dependency on the power system can be considered critical. Additionally, the present advancement in the P2G technology, where excess power generation from renewable sources is used to produce hydrogen or synthetic natural gas will significantly contribute to the coupling of both systems [48], since the power system will depend on the gas system as an energy storage provider.

Summarizing these aspects, it appears that interconnections between gas and electricity systems make the entire energy system vulnerable, since a disruption occurring in one system (e.g., an unexpected failure) may propagate to the other system and may possibly feed back to the system, where the disruption started. Tight relations are increasing the potential risk for catastrophic events, triggered by either intentional or unintentional disruptions of gas or electricity supply and possibly magnified by cascading effects. Analysing the two systems in an integrated manner and developing a combined assessment methodology is needed in order to know whether and how such interdependencies may contribute to the occurrence of large outages and to ensure the proper functioning of the energy supply system.

In this chapter, we propose a co-simulation framework for assessing the interdependency of integrated gas and power systems in terms of security of supply. The framework combines

a steady state AC-flow model with the transient hydraulic gas network model developed in Chapters 2 and 3. The data exchange between the two models is established through the developed software application **SAInt**, which contains a graphical user interface for creating the network models and scenarios for evaluating the simulation results. The proposed framework implemented into **SAInt** is intended to be used by system operators, researchers, operational planners interested in analysing the operation and interdependency of gas and electricity systems in terms of security of energy supply; i.e., to analyse the cascading impacts of contingencies on the operation of integrated gas and power systems and to assess system flexibilities by providing information on system abilities to react to changes.

To achieve these goals, the chapter follows the following pattern. In Section 4.2, an introduction to electric power systems is given and the physical equations and simulation models are elaborated followed by Section 4.3, where the the most important interconnections between gas and electric transmission networks and the coupling equations reflecting these interconnections are presented. Section 4.4 is dedicated to explaining the development of the co-simulation framework which is finally applied to perform a contingency analysis on a real life-sized test network.

4.2. Electric Power System Models

An electric power system can be divided into three subsystems operating at different voltage levels, namely, the generation (11-35 kV), transmission (usually above 110 kV) and distribution system (11 kV- 400 V or 230 V)⁶. The generation system produces electricity by converting primary energy sources (e.g. fossil fuels, wind, hydro etc.) to electric energy, using synchronous turbo generators, which are driven by gas, steam, water or wind turbines. The generating units inject Alternating Currents (AC) to a 3-phase transmission system at a constant voltage magnitude ($|V|$) and frequency (f) (usually 50 Hz). Voltage magnitude and frequency are typically controlled by a designated Automatic Generation Control System (AGC) [111].

In order to reduce the power losses incurred during transportation ($\cong I^2 \cdot R$), the output voltages of generation units are usually increased to transmission system level using step up transformers. The transmission system provides a network of interconnected lines and substations to enable a safe and reliable transport of electric power to large customers

⁶the primary distribution system typically starts at 6.6 kV, 3.3 kV or 11 kV and the secondary distribution system is 230 V or 400 V

directly served from the transmission grid and to smaller customers supplied through the local distribution system. The distribution system is typically operated at lower voltage levels, thus, the voltage level of the transmission system is reduced by step down transformers installed at substations connected to the distribution system. In this thesis, we focus primarily on the high voltage electric transmission system, which is the most crucial subsystem in the power supply chain.

A power transmission system is described by a directed graph $G = (V, E)$ consisting of a set of nodes V and a set of branches E , where each branch $e \in E$ represent a transmission line or a transformer and each node $i \in V$ a connection point between two or more electrical components, also referred to as bus. At some of the buses power is injected into the network, while at others power is consumed by system loads.

In contrast to gas transmission systems, electric power systems are predominantly in steady state operation or in a state that could with sufficient accuracy be regarded as steady state [112]. Thus, the 3-phase transmission system is typically modelled as a balanced per phase equivalent system using linear models for the elements involved in the transport process.

Transmission lines and transformers can be described by a generic per-phase equivalent π -circuit model depicted in Fig. 4.1, which reflects the basic properties of both components, such as resistance R_{ft} , reactance X_{ft} , line charging susceptance b_{ft} , transformer tap ratio t_{ft} and phase shift angle ϕ_{ft} . From the π -circuit model, we can derive for each branch

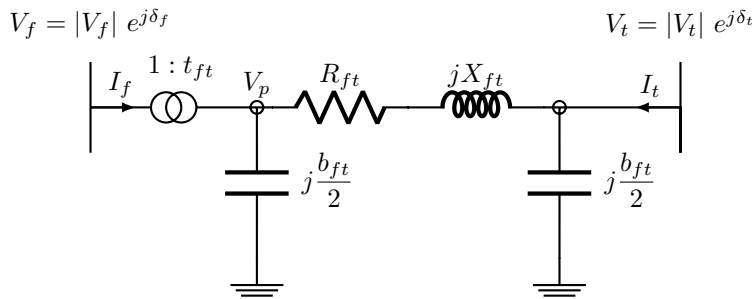


Fig. 4.1.: Generic branch model (π -circuit) for modelling transmission lines ($t_{ft} = 1$ & $\phi_{ft} = 0$), in-phase transformers ($\phi_{ft} = 0$) and phase-shifting transformers ($\phi_{ft} \neq 0$). The transformer tap ratio is modelled only on the from-Bus side of the branch model.

$e \in E$ a branch admittance matrix \mathbf{Y}_{br} , which relates the complex from-bus and to-bus

current injections I_f & I_t , respectively, to the complex from-bus and to-bus voltages V_f & V_t , respectively, as follows:

$$\begin{bmatrix} I_f \\ I_t \end{bmatrix} = \begin{bmatrix} a_{ft}^2(y_{ft} + \frac{b_{ft}}{2}) & -t_{ft}^* \cdot y_{ft} \\ -t_{ft} \cdot y_{ft} & a_{tf}^2(y_{ft} + \frac{b_{ft}}{2}) \end{bmatrix} \begin{bmatrix} V_f \\ V_t \end{bmatrix} \quad (4.1)$$

with

$$t_{ft} = \frac{V_p}{V_f} = a_{ft} e^{j\phi_{ft}}, \quad a_{ft} = \frac{|V_p|}{|V_f|}, \quad y_{ft} = \frac{1}{R_{ft} + jX_{ft}} = \frac{1}{Z_{ft}} \quad (4.2)$$

The elements of the branch admittance matrices can be used to assemble the bus admittance matrix \mathbf{Y}_{bus} which describes the relation between the vector of complex bus current injections \mathbf{I} to the vector of complex bus voltages \mathbf{V} for the entire power network.

$$\mathbf{I} = \mathbf{Y}_{\text{bus}} \cdot \mathbf{V}, \quad \mathbf{Y}_{\text{bus}} = [Y_{ij}]^{N_b \times N_b} \quad (4.3)$$

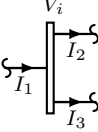
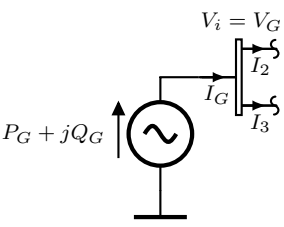
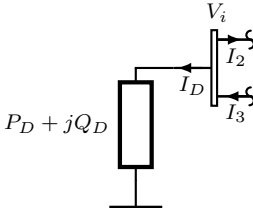
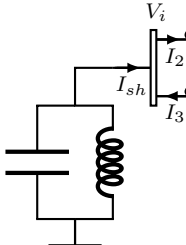
The in- and outflow of electric power to the power system is modelled by generation units, loads, shunt capacitors and reactors connected to the buses of the power system. Table 4.1 shows a list of these components, their function and constraints.

4.2.1. AC-Power Flow Model

The steady state analysis of a power system involves the determination of the voltage magnitudes $|V_i|$, voltage angles $|\delta_i|$, active power P_i and reactive power Q_i supply at each bus i , considering the constraints imposed by the different facilities and components in the power system. These state variables are computed from the power flow balance equation, derived from Kirchhoff's Current Law (KCL) applied to each bus. The power balance equation for a bus i yields the following two non-linear equations for the active and reactive power balance:

$$P_i(\delta, |V|) = \sum_{j=1}^n |V_i||V_j||Y_{ij}| \cos(\delta_i - \delta_j - \theta_{ij}) \quad (4.4)$$

$$Q_i(\delta, |V|) = \sum_{j=1}^n |V_i||V_j||Y_{ij}| \sin(\delta_i - \delta_j - \theta_{ij}) \quad (4.5)$$

Facility	Function	Constraints
 <p>Bus</p>	connection point between transmission lines, transformers, loads, capacitors, reactors,	
 <p>Generation</p>	<p>injects electric power into the power system, by converting primary energy sources (oil, gas, coal, wind, hydro etc.) to electric energy; bus voltage V_i and frequency f_i at buses connected to generation units are typically controlled at a specific set point V_G, f_G</p>	upper and lower limit on reactive power Q_G and active power P_G injection restricted by reactive power capability curve of the generation unit $P_{G,min} \leq P_G \leq P_{G,max}$ & $Q_{G,min} \leq Q_G \leq Q_{G,max}$ (i.e. operating region is restricted by field current heating limit, stator current heating limit, end region heating limit)
 <p>Load</p>	represents consumption of electric power by large customers directly served from the transmission grid or the total power consumption from the local distribution grid connected to the transmission system at the respective substation	upper and lower limits on voltage magnitude $ V_{min} \leq V \leq V_{max} $
 <p>Shunt Capacitor/Reactor</p>	shunt reactors are placed locally to control the steady state over-voltages at buses under light load conditions, while shunt capacitors are used to boost a bus voltage in a stressed system	

Tab. 4.1.: Basic components in an electric network model

$$P_{G,i} - P_{D,i} - P_i(\delta, |V|) = 0 \quad (4.6)$$

$$Q_{G,i} - Q_{D,i} - Q_i(\delta, |V|) = 0 \quad (4.7)$$

where $P_{G,i}$, $Q_{G,i}$ are active and reactive power generation at bus i , respectively, $P_{D,i}$, $Q_{D,i}$ active and reactive power demanded at bus i , respectively, and $Y_{ij} = |Y_{ij}|(\cos(\theta_{ij}) + j \sin(\theta_{ij}))$ the elements of the bus admittance matrix describing the branch connection between bus i and any connected bus j . The solution of the power flow equations (4.6) - (4.7) requires additional boundary conditions in order to close the problem, which are provided by the set points for generation units and loads. In the traditional power flow analysis, each bus is classified depending on the prescribed boundary conditions into the following three bus types:

1. Slack-Bus (Reference Bus):

Voltage magnitude $|V|$ and voltage angle δ are specified and active power P and reactive power Q are computed. A slack bus is usually connected to a generation unit with terminal voltage control. At least one slack bus is needed as a voltage angle reference and also for balancing the active power losses not covered by other generation units.

2. PV-Bus (Generation Bus):

Active power P and voltage magnitude $|V|$ are prescribed and voltage angle δ and reactive power Q are computed. Buses connected to generation units with terminal voltage control are specified as PV-Buses. If the reactive power limit of a PV-Bus is violated during computation the PV bus is changed to a PQ-Bus and the reactive power is set to the next closest feasible working point.

3. PQ-Bus (Load Bus):

Active power P and reactive power Q are prescribed and voltage magnitude $|V|$ and voltage angle δ are computed. Buses with purely load connections are usually classified as PQ-Buses.

4.2.2. Distributed Slack Bus Model

In a real power system a single slack bus, that balances the active power of the total system does not exist. Thus, to model the power generation and the balancing of the power system more realistically, the concept of distributed slack bus generation is typically used [113–115], which enables the balancing of the power system by regulating the active power output of a selected number of generation units. For each generation unit, we specify

an active power generation set point $P_{G,i}^{set}$ and a participation factor K_i , describing the flexibility of the generation unit to regulate a fraction of the required additional generation ΔP for balancing the power system. The additional generation can be expressed as follows:

$$\Delta P = \sum_{i=1}^n P_{G,i}^{set} - P_{D,i} - P_{Loss} \quad (4.8)$$

where P_{Loss} is the total power loss of the power system. The active power balance equation (4.6) can be modified as follows, while the reactive power balance equation (4.7) remain unchanged:

$$P_{G,i}^{set} + K_i \cdot \Delta P - P_{D,i} - P_i(\delta, |V|) = 0 \quad (4.9)$$

$$\sum_{i=1}^n K_i = 1 \quad (4.10)$$

The resulting system of non-linear power flow equations is solved iteratively using a Netwon-Raphson approach:

$$\mathbf{J}(\mathbf{x}^k) \cdot \Delta \mathbf{x}^k = -\mathbf{F}(\mathbf{x}^k) \quad (4.11)$$

$$\mathbf{x}^{k+1} = \mathbf{x}^k + \Delta \mathbf{x}^k \quad (4.12)$$

where \mathbf{J} is the Jacobi matrix, \mathbf{F} residual vector and $\mathbf{x} = [\delta, |V|, \Delta P]^T$ the solution vector.

4.2.3. AC-Optimal Power Flow Model

The operation of a power system is restricted by a number of constraints imposed by technical components and stakeholders (producers, consumers, regulators etc.) involved in the power supply chain. Transmission lines, for instance, can only transport a limited amount of power due to thermal restrictions, while the operation of power plants is limited by the capability curves of the installed generators. The power TSO is responsible for respecting these constraints, while operating the system in an economic and secure manner.

The AC-power flow model presented in Section 4.2.1 gives a solution for the power system without respecting the constraints mentioned above. Thus, after a power flow solution is obtained the feasibility of the solution has to checked against the limits of the power

system and the boundary conditions have to be adapted iteratively in order to obtain a feasible solution (e.g. changing the control settings of generators, load buses and lines).

To avoid this iterative process, an AC-optimal power flow (AC-OPF) model can be used, which gives a solution to the power flow problem that satisfies a given set of constraints. The AC-OPF model is expressed by the following non-linear inequality constrained optimization problem:

$$\min_{\mathbf{X}} \quad f(\mathbf{X}) = \sum_{i=1}^{N_g} c_{0,i} + c_{1,i} P_{G,i} + c_{2,i} P_{G,i}^2 \quad (4.13)$$

$$s. t. \quad G_{P,i}(\mathbf{X}) = P_i(\mathbf{V}) - P_{G,i} + P_{D,i} = 0, \quad i = 1 \dots N_b \quad (4.14)$$

$$G_{Q,i}(\mathbf{X}) = Q_i(\mathbf{V}) - Q_{G,i} + Q_{D,i} = 0, \quad i = 1 \dots N_b \quad (4.15)$$

$$P_i(\mathbf{V}) = \sum_{j=1}^{N_b} |V_i| |V_j| |Y_{ij}| \cos(\delta_i - \delta_j - \theta_{ij}), \quad i = 1 \dots N_b \quad (4.16)$$

$$Q_i(\mathbf{V}) = \sum_{j=1}^{N_b} |V_i| |V_j| |Y_{ij}| \sin(\delta_i - \delta_j - \theta_{ij}), \quad i = 1 \dots N_b \quad (4.17)$$

$$H_k^f(\mathbf{X}) = S_k^f * S_k^f - S_k^{max 2} \leq 0, \quad k = 1 \dots N_l \quad (4.18)$$

$$H_k^t(\mathbf{X}) = S_k^t * S_k^t - S_k^{max 2} \leq 0, \quad k = 1 \dots N_l \quad (4.19)$$

$$\delta_i = \delta_i^{ref}, \quad i = i_{ref} \quad (4.20)$$

$$|V_i^{min}| \leq |V_i| \leq |V_i^{max}|, \quad i = 1 \dots N_b \quad (4.21)$$

$$P_{G,i}^{min} \leq P_{G,i} \leq P_{G,i}^{max}, \quad i = 1 \dots N_g \quad (4.22)$$

$$Q_{G,i}^{min} \leq Q_{G,i} \leq Q_{G,i}^{max}, \quad i = 1 \dots N_g \quad (4.23)$$

where the decision variables expressed by vector \mathbf{X}

$$\mathbf{X} = \begin{bmatrix} \Delta & \mathbf{V}_m & \mathbf{P}_G & \mathbf{Q}_G \end{bmatrix}^T \quad (4.24)$$

are the set of bus voltage angles Δ , bus voltage magnitudes \mathbf{V}_m and active and reactive power generation \mathbf{P}_G and \mathbf{Q}_G , respectively. f in eq. (4.13) is a scalar quadratic objective function, which describes the total operating costs for each committed generation unit in terms of its active power generation, while the non-linear equality constraints expressed by eq. (4.14)–(4.17) describe the set of active and reactive power balance equations derived in Section 4.2.1 (see eq. (4.6) - (4.7)). Equations (4.18) and (4.19) are non-linear inequality constraints, which describe the transmission capacity limits S_k^{max} for each line, while the upper and lower limits of the decision variables are described by eq. (4.21)–(4.23). For

each isolated sub network one bus is chosen as the voltage angle reference (see eq. (4.20)), i.e., the voltage angle of the reference bus is set to zero.

The described AC-OPF model is implemented into the open source power flow library MATPOWER [116], which is utilized as the power system simulator in the context of the proposed co-simulation framework.

4.3. Interconnection between Gas and Power Systems

Gas and electric power systems are physically interconnected at different facilities. The most important connections between the two systems are as follows:

1. *Power supply to electric drivers installed in gas compressor stations:*

The electric power consumed by the compressor station can be described by the following expression (derived from the first and second law of thermodynamics for an isentropic compression process) describing the required driver power $P_{D,i}^{CS}$ for compressing the gas flow Q from inlet pressure p_1 to outlet pressure p_2 [92, 93]:

$$P_{D,i}^{CS} = f \frac{\kappa}{\kappa - 1} \frac{Z_1 T_1 R \rho_n Q}{\eta_{ad} \eta_m} \left[\frac{p_2}{p_1}^{\frac{\kappa - 1}{\kappa}} - 1 \right], \quad i = 1 \dots N_{CS} \quad (4.25)$$

where f is a factor describing the fraction of total driver power provided by electric drivers, η_{ad} the average adiabatic efficiency of the compressors, η_m the average mechanical efficiency of the installed drivers, p_2 the outlet pressure, p_1 , Z_1 , T_1 the inlet pressure, compressibility factor, temperature, respectively, R the gas constant, and κ the isentropic exponent.

The power supply to the gas network is added to the active power demand in the electric model.

2. *Electric power supply to LNG terminals and UGS facilities:*

We capture this interaction by assuming a linear function in terms of the regassification or withdrawal rate L_{rw} , respectively:

$$P_{D,i}^{rw} = k_{i,0} + k_{i,1} \cdot L_{rw,i} \quad (4.26)$$

3. *Fuel gas offtake from gas pipelines for power generation in GFPPs:*

The required fuel gas $L_{GFPP,i}$ for active power generation $P_{G,i}$ at plant i can be

expressed in terms of the thermal efficiency η_T of the GFPP and the gross calorific value GCV of the fuel gas, as follows:

$$L_{GFPP,i} = \frac{P_{G,i}}{\eta_T \cdot GCV}, \quad i = 1 \dots N_{GFPP} \quad (4.27)$$

4.4. Integrated Co-Simulation Framework for Security of Supply Analysis

The modelling framework carried out within **SAInt** considers the integrated gas and electricity transmission network under cascading outage contingency analysis. The cascading outages are investigated when the gas or electricity system has just experienced a disruption, like a shortage in supply or transmission capacity. The framework comprises of

- (i) a simulator (MATPOWER) for solving an AC-OPF for the power system,
- (ii) a transient hydraulic gas simulator (**SAInt**) for the gas system which includes sub-models of all relevant pipe and non-pipe facilities
- (iii) and an interface (**SAInt**) which handles the communication and data exchange between the two isolated simulators.

In order to perform power flow calculations and to extend the functionality of **SAInt**, **SAInt-API** is linked to MATLAB using the Matlab COM Automation Server. This link is used to establish a communication between the Matlab-based open source power flow library MATPOWER [116] and **SAInt**. This allows the execution of AC-PF and AC-OPF with MATPOWER and the data exchange, evaluation and visualization of the obtained results using **SAInt-GUI**.

The proposed co-simulation framework is illustrated in the flow diagram depicted in Fig. 4.2, which is explained further below.

The power system model is designed to provide a realistic representation of the behaviour of an actual power system, when subjected to contingencies. Cascading effects of contingencies in the power grid are very complex phenomena, and identifying the typical mechanisms of cascading failures and understanding how these mechanisms interact during blackouts is an important research area [117–122]. Potential mechanisms that might be modelled include overloaded line tripping by impedance relays due to the low voltage and high current operating conditions, line tripping due to loss of synchronism, the undesirable generator tripping events by over-excitation protection, generator tripping due to

abnormal voltage and frequency system condition, and under-frequency or under-voltage load shedding. For each additional mechanism of cascading failure included in a model, assumptions must be made about how the system will react to these rarely observed operating conditions. This chapter introduces a steady state AC-flow model which is adapted to reflect a set of corrective actions performed by TSOs when trying to return the system to a stable operating condition after a contingency.

While the initial contingency can usually be considered as being a random event, an interaction of cascading failure mechanisms exists in the subsequent events. For example, the loss of critical components such as tripping of transmission lines creates load redistribution to other components, which might become overloaded. The overall network is then weakened due to the stress on remaining elements, possibly leading to an instability. If corrective action plans are not applied quickly further failures might be created as a consequence leading to a blackout. In this chapter, this cascading failure phase, starting with the initiating event is modelled, where the cascading contingencies occurrence are affected by operator actions and the times between subsequent events are considered in a range of tens of seconds to 1 hour. Various system adjustments that are considered include the post-contingency redispatch of active and reactive resources, cascade tripping of an overloaded transmission line, tripping or re-dispatching of generators due to load-/generation imbalance, and load shedding at load buses to prevent a complete system blackout when insufficient voltage magnitudes are observed.

The initial state of the model is obtained by solving the standard AC optimal power-flow problem as described in eq. (4.13)–(4.23), which yields the optimum hourly generator dispatch for given hourly loads for given cost functions for each generator and bus voltage and line loading constraints. To execute this task MATPOWER 6.01b AC-OPF algorithm is utilised [116].

Any change from the initial state caused by a contingency event, such as a (simultaneous) failure of one or more transmission lines, failure of a generation unit or decreased amount of generation capacity due to lack of gas supply, can be introduced in the model by defining a scenario parameter for the corresponding facility as described in Chapter 3.

Whenever a contingency is observed in the system, an imbalance between total generation and total load may occur. In order to re-balance the system, the model redistributes the missing or excess power to the remaining facilities in the power grid. The power re-dispatch is obtained by running the AC-OPF model, while considering the new topology triggered by a previous disruption (e.g., lines and generation units may be disconnected). However, since the system is under a stressed state, the AC-OPF algorithm may deliver an

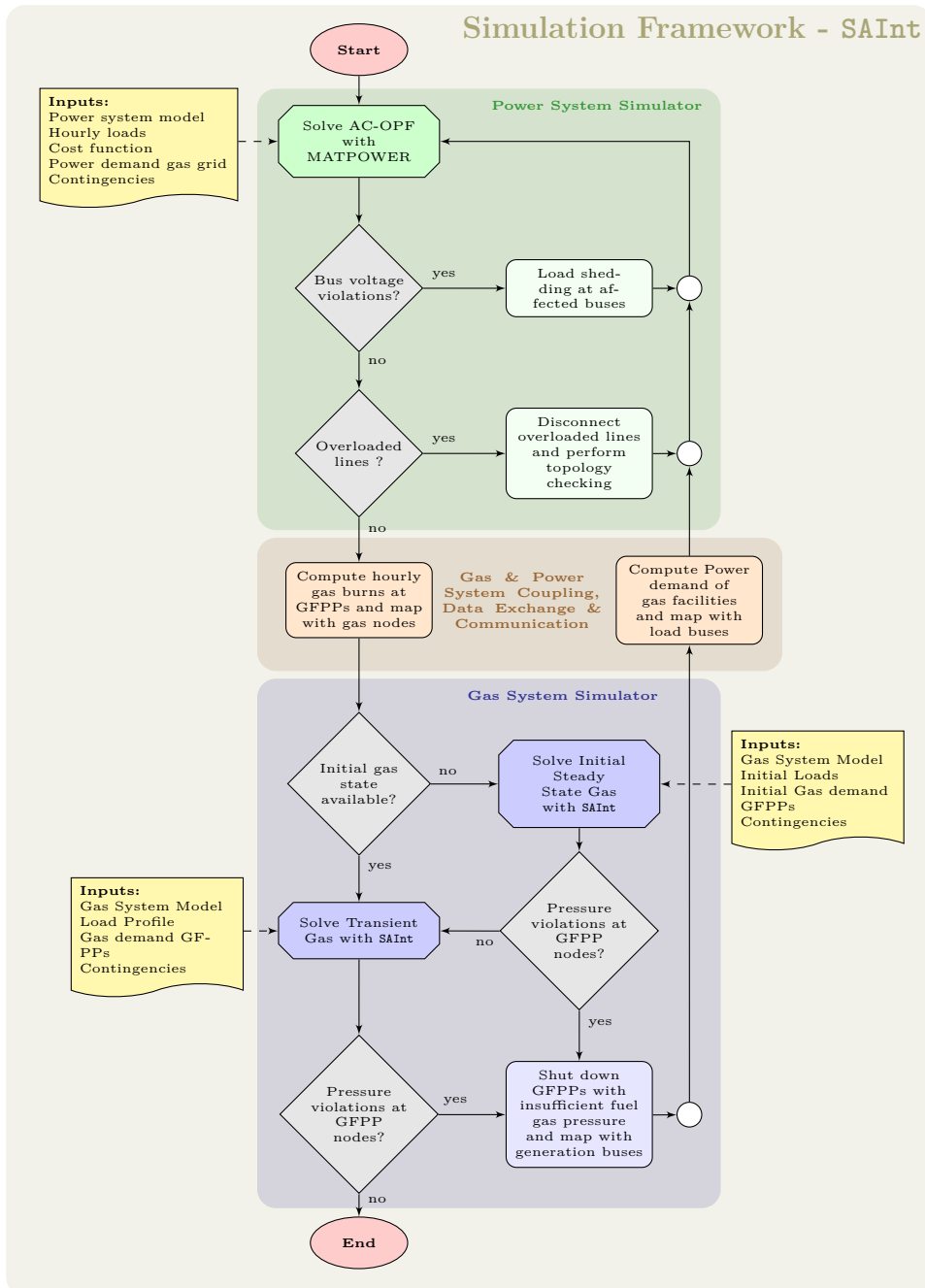


Fig. 4.2.: Flow chart of the proposed Simulation Framework **SAInt**, showing the implemented algorithm.

infeasible solution that does not satisfy the convergence criteria, since system constraints such as line overloading or voltage limits cannot sustain the desired system loads. In order to allow the system to find a converged solution, the bus voltage ($|V| \geq |V^{min}|$) and line capacity constraints ($S_f \cdot S_f^* \leq S^{max2}$ & $S_t \cdot S_t^* \leq S^{max2}$) in the standard AC-OPF formulation are relaxed for the re-dispatching process. The re-dispatching process is followed by a two step feasibility checking procedure. In step one, bus voltage violations are mitigated by performing load shedding at the affected buses and recomputing the relaxed AC-OPF until no voltage violations are detected, so called under-voltage load shedding. The model assumes that there is enough time for the operator to implement under voltage load shedding to prevent a voltage collapse, which is the root cause of most of the major power system disturbances [123–125]. The model sheds load in blocks of 2% for the corresponding bus until the relaxed bus voltage constraint is satisfied. If a violation is not eliminated although the load sheds more than 50% of its original load, we assume complete failure of the affected bus and set the load value to zero [15]. The second step of the feasibility checking procedure follows after all bus voltage violations have been remedied in the first step. During the re-dispatching process new failures may occur at certain components as they become overloaded. In this chapter the overloads are aimed to be strictly avoided for all component contingencies. This means that it is assumed that the probability for line trip is 1 when line flow exceeds its thermal capacity with a tolerance parameter. The second step involves disconnecting overloaded transmission lines from the power grid and recomputing the relaxed AC-OPF until a feasible solution is obtained. It should be noted that, the connectivity of the network is checked in every simulation step prior to the AC-OPF computation in order to detect isolated facilities. The algorithm used for checking the connectivity is based on the well-known minimum spanning tree algorithm and is described in detail in [15].

After obtaining a feasible solution for the power system, the resulting hourly power generation of GFPPs is converted into a hourly gas demand profiles and provided as input to the gas model. The gas model needs an initial state for running the transient simulation. This state can either be a solution of a steady state simulation or the terminal state of a transient simulation. If an initial state is not available the algorithm uses the initial loads of the generated gas demand profiles for GFPPs to compute a steady state solution. This solution is then used as an initial state for the transient simulation. After each transient or steady state simulation the algorithm checks if the fuel gas pressures at GFPP nodes are sufficient to operate the facilities. If an insufficient fuel gas pressure is detected, the affected GFPP is shut-down and the power system model is recomputed. The algorithm is terminated if no pressure violations are detected after the transient gas simulation.

Finally, the amount of energy not supplied is calculated as an indicator of the impact of the disruption event.

The gas and electric model described above are connected through an interface which enables the communication and data exchange between the two simulators (i.e., MAT-POWER as power system simulator and **SAInt** as transient gas simulator, see Fig. 4.2). The time integration of the combined model is performed separately for the two systems and the interconnection between them is established through data exchange at discrete time and space points.

The timing of the power model is based on the discrete event simulation concept. It is assumed that the configuration of the power system (e.g., the state of generation units and lines) remains unchanged between events and changes only at the time of the specific event. If no events are scheduled or triggered in the course of the simulation the time step of the power system corresponds to a reference time step of 1 hour.

In contrast to the power system, the time integration of the transient gas model, is based on a dynamic time step adaptation method, which adapts the time resolution with respect to the control changes of controlled gas facilities during the solution process. The DTA allows capturing rapid changes in the gas system (shut-down of a power plant or compressor station etc.) with a higher time resolution. In this context, the gas model can be viewed as a quasi-continuous system, where the values of the state variables (i.e., nodal pressure p , element flows Q and nodal loads L) between two discrete time points are approximated by linear interpolation. If no events are scheduled or triggered in the course of the simulation the time step of the gas system corresponds to a reference time step of 15 min.

In the following section, the proposed framework is applied to perform a contingency analysis for an integrated gas and power system network.

4.5. Model Application

In this section, an integrated gas and power network is constructed to demonstrate the previously discussed simulation framework implemented in **SAInt**. Three supply side scenarios (one non-disrupted scenario (base case) and two supply disruption scenarios) are presented in order to demonstrate the value of the proposed framework and to stress the importance of modelling the interdependence between gas and power systems with respect to security of supply.

The proposed scenarios are performed on the test network depicted in Fig. 4.3. The test network applied in this chapter is a model of a real gas and electric power network of a European region. Due to confidentiality reasons and the sensitivity of the presented results, the topology and facility names of the real network have been disguised. The network topology and properties used for the computations, however, are realistic data for the combined network). The scenarios are composed of a number of extreme events causing more than two network facilities to be deactivated or to cascade out of service. The sample network includes a power grid with 158 buses, 62 generating units with

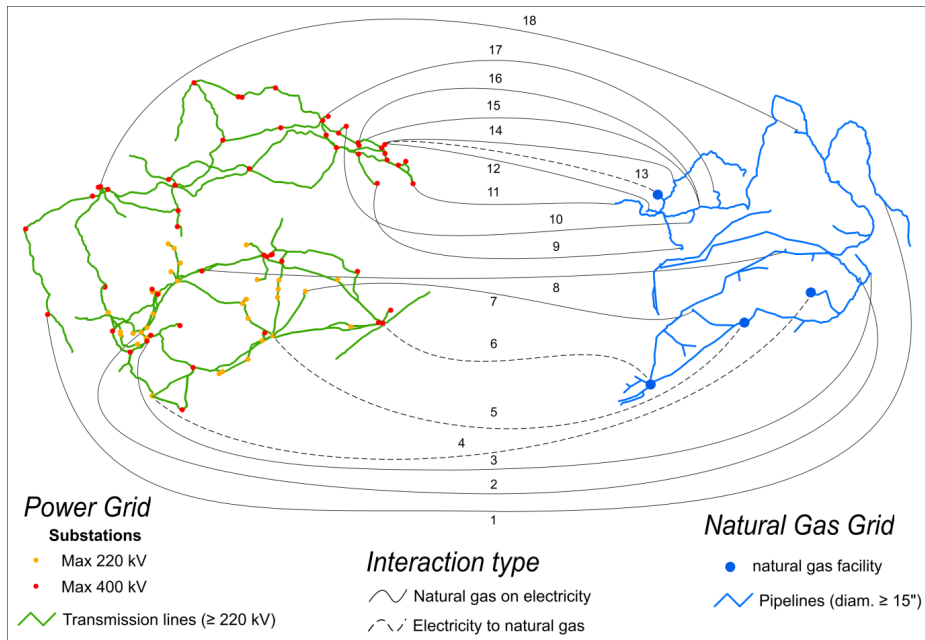


Fig. 4.3.: Integrated gas and power network applied in the case study. Map shows a real network of an European region, which has been disguised due to confidentiality reasons. The network data and properties used for the case studies, however, are original input data for the actual network. The solid black lines (lines 1–3, 7–12, 14–18) represent interconnections between Gas Fired Power Plants (GFPPs) in the power grid (**left**) and their fuel gas offtake points in the gas grid (**right**), while the dashed black lines (4–6, 13) represent interconnections between electric buses in the power grid (**left**) supplying electric power to connected facilities in the gas grid.

22,076 MW installed capacity based on different generation mix that mainly consists of lignite (33%), natural gas (28%), coal (20%), wind power (7%) and others (12%). The transmission system consists of 194 high voltage transmission lines with total line length

of approx. 8,000 km. The base voltage levels for the transmission lines are distinguished between 200 kV and 400 kV.

The solution of the AC-OPF equations requires the knowledge of the voltage levels, admittances as well as the maximum thermal capacities of the transmission lines. The reactance of a line depends mainly on its physical properties. It increases proportionally to the geometric length of the line. Therefore, in the scope of this work, we assume equal physical properties for all lines and use the length to determine the reactance. A typical value for the reactance of a transmission line per unit length is 0.2 [Ω/km]. Regarding the thermal capacities of the transmission lines, we assume a transmission capacity of 800 MW for 400 kV lines and 530 MW for 200 kV lines. In AC-OPF analysis the reactive power has strong influence on voltage drop thresholds. Thus, during AC OPF analysis, the maximum and minimum voltage levels for buses are considered and a value between 1.12 and 0.96 p.u. is assigned, respectively.

The gas network comprises of 345 pipe segments with a total pipe length of roughly 4,000 km, 10 compressor stations and 352 nodes (54 CGSs), 15 stations to direct served customers (14 GFPPs and one IND), two CBEs (CBE_1 & CBE_2), one CBI, one LNG terminal, one production field and one UGS facility. The CBI, PRO, LNG terminal and UGS facility are pressure controlled, while each compressor station is pressure ratio controlled with a pressure ratio set point ranging between 1.02 and 1.2. The input data for the compressor stations are listed in Tab. 4.2. The data used for the facilities supplying gas to the gas system are given in Tab. 4.3, while the data for the GFPPs are listed in Tab. B.7. The minimum delivery pressure for the 14 GFPPs is set to 30 bar-g while the time needed to reach complete shut-down of a GFPP is set to 45 min.

The transient scenarios for the integrated gas and power network are simulated by assigning the relative load profile depicted in Fig. 5.8 to the relevant exit stations (left plot represents the gas load profile and right plot the power load profile). It should be noted that the relative load profile for the gas system is only assigned to CGSs, which are the connection points between the gas transmission and local distribution system. For all other exit stations (CBE_1, CBE_2, IND) a constant load profile corresponding to the steady state load is assumed. The absolute values of the load profile for CGS nodes are obtained by multiplying the steady state load with the relative values in Fig. 5.8 (left plot). The load profiles of the 14 GFPPs in the gas model are provided by the power model based on allocating the results obtained from the AC-OPF analysis to the corresponding nodes in the gas model. For the power network, the resulting loads for a time window of 24 h are obtained by multiplying the initial loads by the relative profile depicted in Fig. 5.8 (right plot). All 14 GFPPs in the power grid are physically interconnected to the gas

Compressor Station	PRSET [-]	PRMAX [-]	PWMAX [MW]	POMAX [bar-g]	PIMIN [bar-g]
CS_1	1.05	1.6	10	54	34
CS_2	1.02	1.45	44	54	25
CS_3	1.01	1.6	60	54	25
CS_4	1.2	1.45	25	54	25
CS_5	1.2	1.45	80	54	25
CS_6	1.2	1.3	35	54	25
CS_7	1.2	1.45	50	54	25
CS_8	1.2	1.7	20	54	25
CS_9	1.2	1.7	20	54	25
CS_10	1.05	2	10	65	25

Tab. 4.2.: Compressor station control (PRSET—Pressure Ratio Set Point) and constraints (PRMAX—Maximum Pressure Ratio, PWMAX—Maximum Available Driver Power, POMAX—Maximum Discharge Pressure, PIMIN—Minimum Suction Pressure).

Gas Supply	k_0 [MW]	k_1 $\left[\frac{\text{MW}}{\text{sm}^3/\text{s}} \right]$	PSET [bar-g]
CBI	-	-	50
PRO	-	-	52.6
UGS	3.5	0.01	56
LNG	5	0.03	50

Tab. 4.3.: Input data for facilities supplying the gas system with gas.

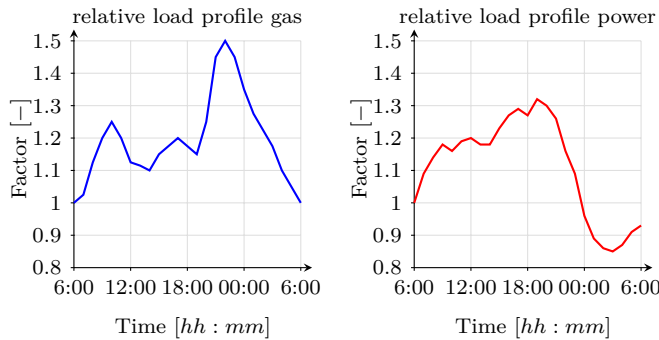


Fig. 4.4.: Load profiles gas (left side) and power (right side) networks.

network. Furthermore, we assume additional interconnections between the gas and power network at two compressor stations, at the LNG terminal and at the UGS facility, which are supplied with power from the electric grid. The integrated gas and power network

Name	c_0 [€]	c_1 $\left[\frac{\text{€}}{\text{MW}}\right]$	c_2 $\left[\frac{\text{€}}{\text{MW}^2}\right]$	η_T [%]	P_G^{\max} [MW]	P_G^{\min} [MW]	Q_G^{\max} [MVAr]	Q_G^{\min} [MVAr]	p^{\min} [bar·g]
GFPP_1	0	220.86	0	60	475	0	332.5	-285	30
GFPP_2	0	220.86	0	41	130	0	91	-78	30
GFPP_3	0	220.86	0	57	101	0	70.7	-61	30
GFPP_7	0	220.86	0	45	180	0	126	-108	30
GFPP_8	0	220.86	0	44.5	105	0	73.5	-63	30
GFPP_9	0	220.86	0	51	420	0	294	-252	30
GFPP_10	0	220.86	0	30	1,127	0	788.9	-676	30
GFPP_11	0	220.86	0	40	360	0	252	-216	30
GFPP_12	0	220.86	0	48	420	0	294	-252	30
GFPP_14	0	220.86	0	30	766.7	0	536.7	-460	30
GFPP_15	0	220.86	0	45	147.8	0	103.5	-89	30
GFPP_16	0	220.86	0	61	435	0	304.5	-261	30
GFPP_17	0	220.86	0	67	390	0	273	-234	30
GFPP_18	0	220.86	0	55	410	0	287	-246	30

Tab. 4.4.: Input data for GFPPs connected to the gas and electric power system. Numbering of GFPPs corresponds to the numbering of the solid interconnection lines in Fig. 4.3

with 18 physically interconnected facilities is illustrated in Fig. 4.3. Additional input parameters for the gas simulator are given in Tab. 5.1. Applying the simulation tool **SAInt**

Parameter	Symbol	Value	Unit
time step	Δt	900	[s]
total simulation time	t_{\max}	24	[h]
gas temperature	T	288.15	[K]
dynamic viscosity	η	1.1×10^{-5}	[kg/m·s]
pipe roughness	k	0.012	[mm]
reference pressure	p_n	1.01325	[bar]
reference temperature	T_n	273.15	[K]
relative density	d	0.6	[–]
gross calorific value	GCV	41.215	[MJ/sm ³]

Tab. 4.5.: Input data for the gas simulator.

on the presented sample network, some preliminary observations on cascading outage contingency analysis can be made. Initially, a base case scenario (scenario 0) with no supply disruption in any of the two interlinked networks is introduced. In the base case scenario, we capture the behaviour of the networks at normal operation. Then, we compare the base case scenario with two scenarios, where we introduce a number of disruption events and simulate the reaction of the system to these events. The simulated grid is generated with a time resolution of 900 s and all scenarios are simulated for one gas day from 06:00

to 06:00 (For the case study, we chose a simulation time of one operating day (24 h) with a time resolution of 15 min for the gas model and a time resolution of one hour for the power model, in order to keep the size of input data and information at a moderate level for the results discussion. However, the framework is designed to allow an extension and adaptation of the time window and resolution depending on if a short or long term study of a contingency scenario is of interest. It should be noted that although it is possible to change the status of the failed components (repairing and restoration can be modelled) within the simulation, the scenarios that are presented in this study do not take into account the repairing activity in order to analyse system capabilities in worst-cases.

While the first scenario involves a disruption of several supply points in the gas network, the second scenario includes supply disruptions triggered by the power network. In scenario 1, we assume a reduced regasification rate for the LNG terminal from maximum via a ramp-down between 06:00 and 07:00 (see Fig. 4.5), which corresponds to an expected 7-day delay in cargo. In addition, we assume a supply disruption at the production field causing a ramp down of the supply between 08:00 and 09:00 (see Fig. 4.5). Furthermore, a 30% supply reduction at CBI station at time 14:00 is implemented via a ramp-down between 14:00 and 15:00 (see Fig. 4.5). Scenario 2 is related to power network contingencies and initial contingency set consist of the loss of major lignite power plant with 1157 MW operational capacity at 07:00 and 70% lack of power generation from wind turbines at 06:00 (see Fig. 4.5).

In the following, we discuss the simulation results for the three scenarios ⁷.

The sequence of initial events (shown in black) and their consequences (shown in orange and red) are summarized in Fig. 4.5 and 4.6 for scenario 1 and scenario 2, respectively. It can be seen from the figures that when a minimum pressure violation for a GFPP is detected in the gas model, the failure of the corresponding power plant is applied after 45 min due to the required shut-down time. Figures 4.7–4.9 show the difference in gas supply to the system through the CBI station, the production field and the LNG terminal. There is a big difference in inflows to the system through these supply points in scenario 0 and scenario 1, where the difference is more than 20 Msm³/d (Million standard cubic meter per day), where the reference pressure is 1.0135 bar and the reference temperature is 0 °C. The impact of this observation can be seen in Figures 4.7–4.11. Figure 4.10 shows that the disruptions introduced in scenario 1 have the highest impact on the gas network, since the flow balance, which is the sum of inflow minus sum of outflow, is always negative; the

⁷The simulation results and conclusions are based on the input data chosen for the sample network. While some data were provided by the TSOs, others were not available (e.g., pipe roughness, gas temperature, line properties etc.) and were therefore estimated using typical values. Thus, these input data are connected with uncertainties

system is not able to supply enough gas to balance the demand. In fact, the flow balance is quite negative throughout the time, peaking down to a value of $-32 \text{ Msm}^3/\text{d}$. As a result, the quantity of gas stored in the pipeline (i.e., the linepack) reduces significantly as time passes. The flow balance can be viewed as the time derivative of the linepack, thus, if the flow balance is negative the linepack decreases and if positive the linepack increases. A zero flow balance corresponds to no change in linepack. Latter is the assumption made in steady state gas models, which cannot capture the changes in linepack, and therefore, the real behavior of the gas system appropriately. Moreover, Fig. 4.10 shows a decrease in linepack from ca. 85 to 67 Msm^3 for scenario 1 (approx. 18 Msm^3 lost along the day in the pipelines). In contrast, in scenario 0 only approx. 1.5 Msm^3 of linepack is extracted. This produces a steady decrease of pressure in the CBI station, the production field and the LNG facility causing the pressure to reduce to approx. 39 , 42 and 31 bar-g , respectively (see Fig. 4.7–4.9).

An important observation is the pressure drop to approximately 31 bar-g at the LNG terminal, which is the main gas supplier for some of the GFPPs in the hydraulic region. This value is slightly above the 30 bar-g minimum delivery pressure threshold required by the GFPPs. When gas supplies are scarce, the only way to maintain sufficient pressure and to allow the network to continue operating is to reduce consumption, either through curtailment or fuel switching, if there is the chance to do this with some power plants. In scenario 1, gas curtailment at GFPPs is implemented, presuming that replacement fuel is not available in any of the investigated GFPPs.

Figure 4.11 shows the behavior of the UGS facility, the only supply node able to increase gas supply to satisfy the increased demand in scenario 1. The UGS facility is able to maintain its pressure set point till the end of the simulation (see Fig. 4.11). The disconnection of four GFPPs from the gas network at $14:15$, $15:45$ and $16:30$, respectively, allows the gas system to continue running (see Fig. 4.5 and 4.12). The pressure and load profiles for failed GFPPs are given in Fig. 4.12 and 4.13. This curtailment was sufficient to cope with the pressure drop in the network. Therefore, there was no need of gas curtailment at CGSs, where protected customers (e.g., households, public services) are supplied with gas. Figure 4.14 and 4.15 depict the voltage profiles for a selected number of buses, where minimum voltage violation is detected for scenario 1 and 2, respectively. In order to keep the bus voltage above the minimum voltage level, load shedding is implemented at the affected buses. The left plots in Fig. 4.14 and 4.15 show the voltage profiles of the affected buses for the computation where voltage violations were detected and no countermeasures were employed to avoid this violation, while the right plots show the voltage profiles after implementing load shedding at the affected buses. As can be seen

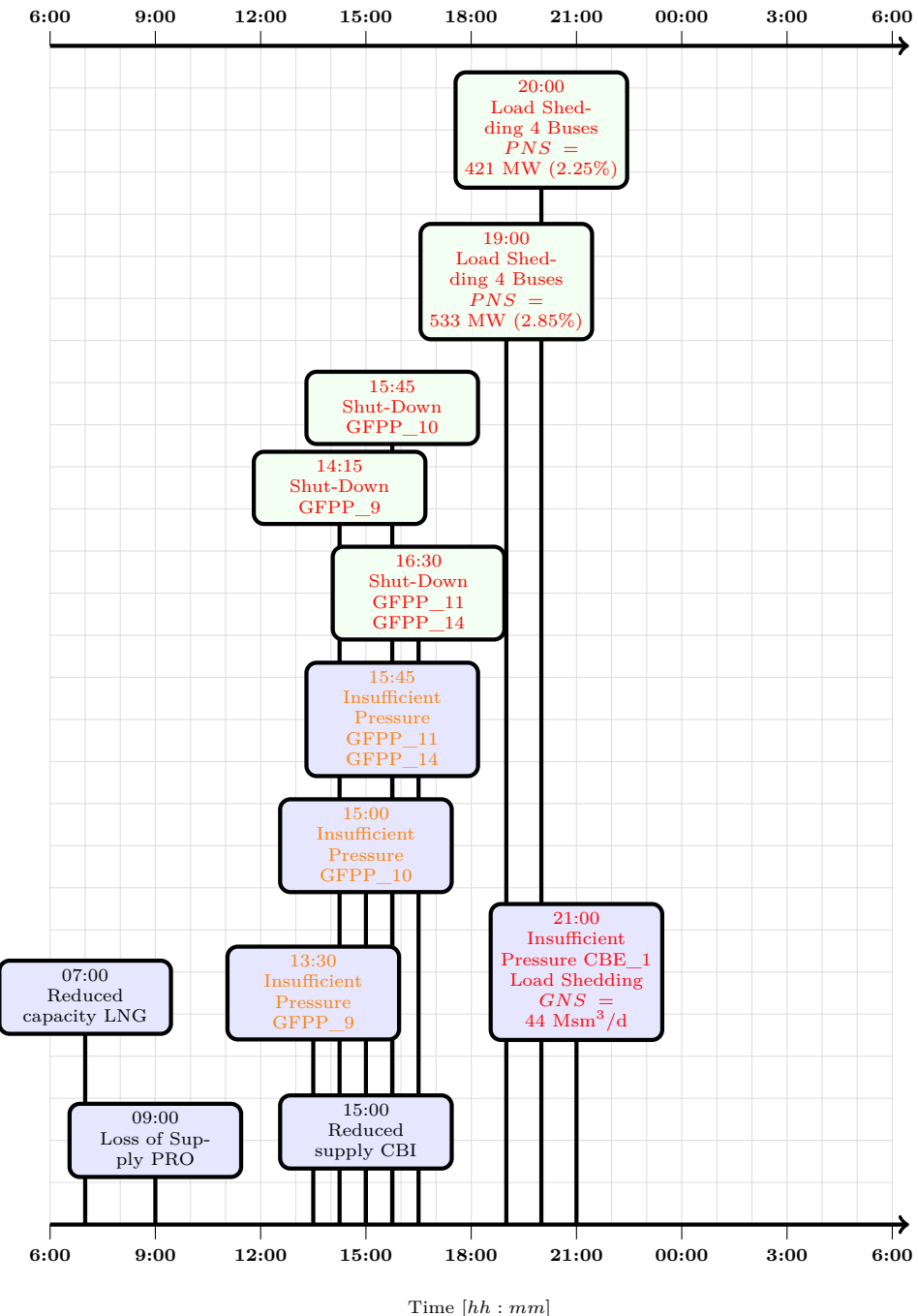


Fig. 4.5.: Timing of initial (**black**) and cascading (**orange**, **red**) events for Scenario 1. Abbreviation PNS stands for power not supplied, while GNS stands for gas not supplied, value in brackets refers to the fraction of not supplied power/gas with respect to total power/gas loads.

in the right plots of Fig. 4.14 and 4.15, the bus voltages recover to a value above the minimum voltage threshold after load shedding is implemented. However, due to load shedding some customers connected to the affected buses are not supplied with enough electricity (see Figs. 4.5 and 4.6).

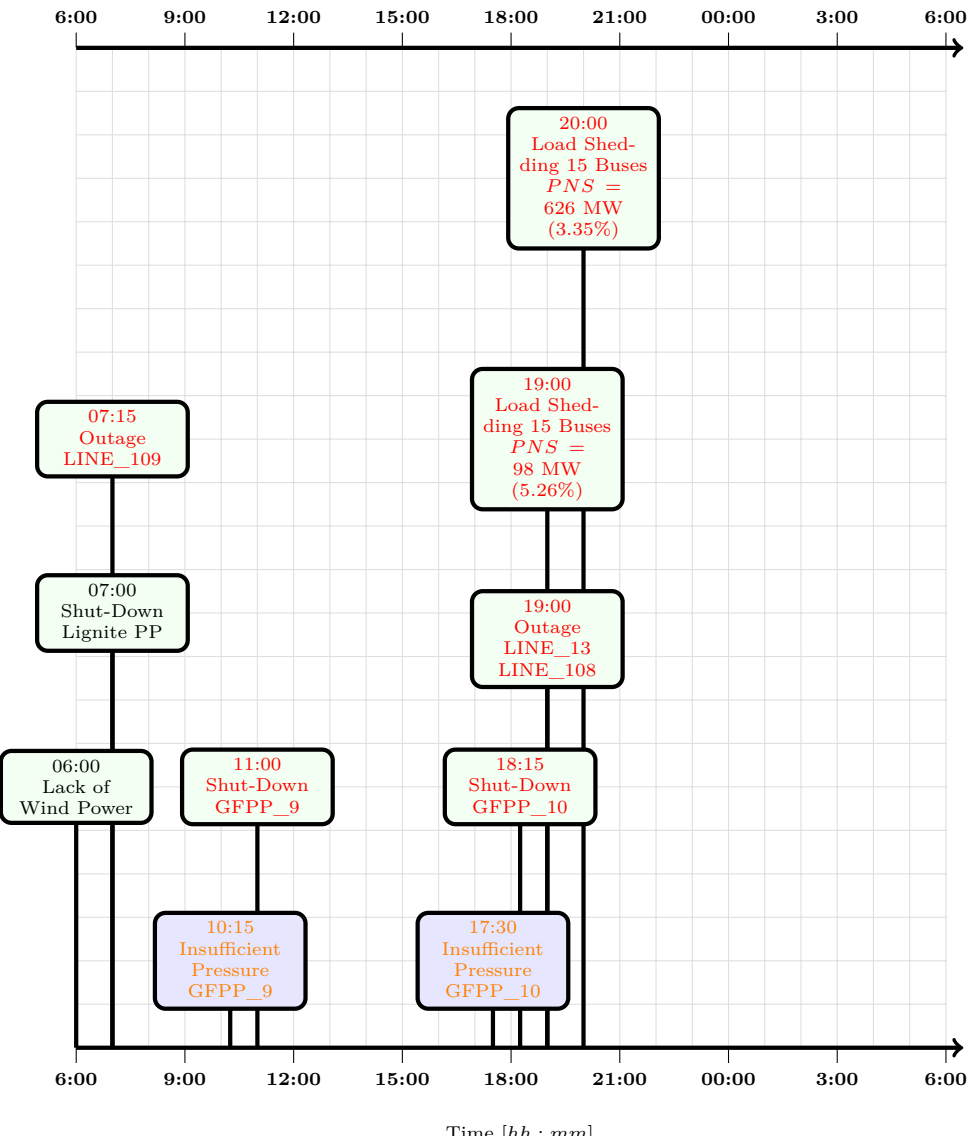


Fig. 4.6.: Timing of initial (**black**) and cascading (**orange**, **red**) events for Scenario 2. Abbreviation PNS stands for power not supplied, value in brackets refers to the fraction of not supplied power with respect to total loads.

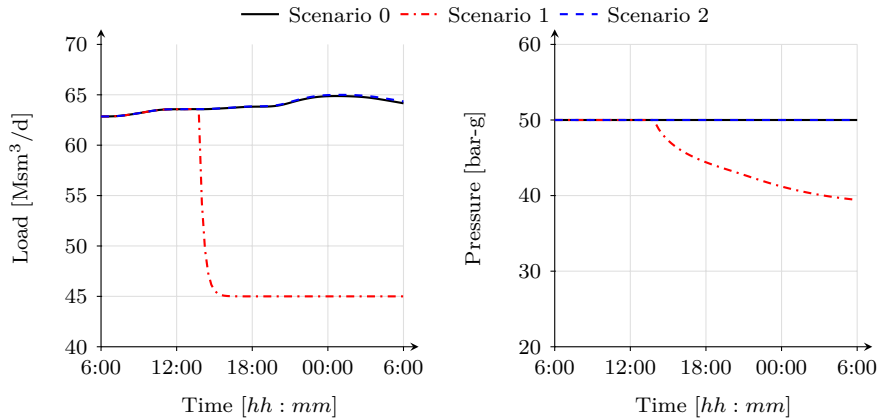


Fig. 4.7.: Time evolution of gas supply and pressure at the cross border import (CBI) node for the computed scenarios

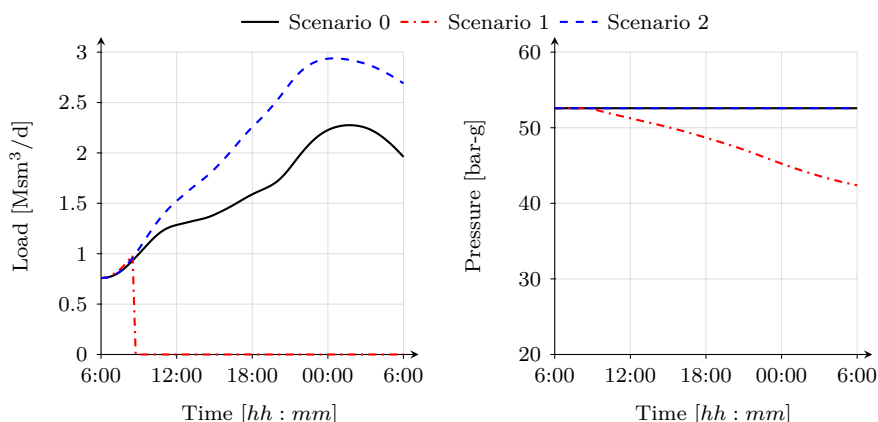


Fig. 4.8.: Time evolution of gas supply and pressure at the production field for the computed scenarios.

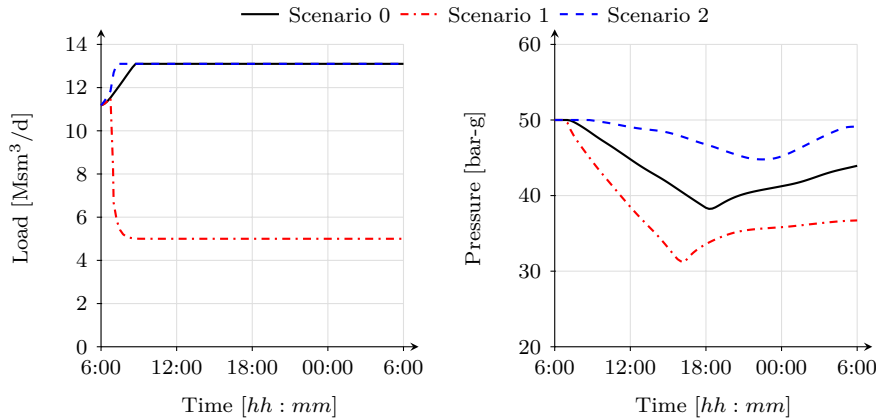


Fig. 4.9.: Time evolution of regasification rate and pressure at the liquefied natural gas (LNG) terminal for the computed scenarios.

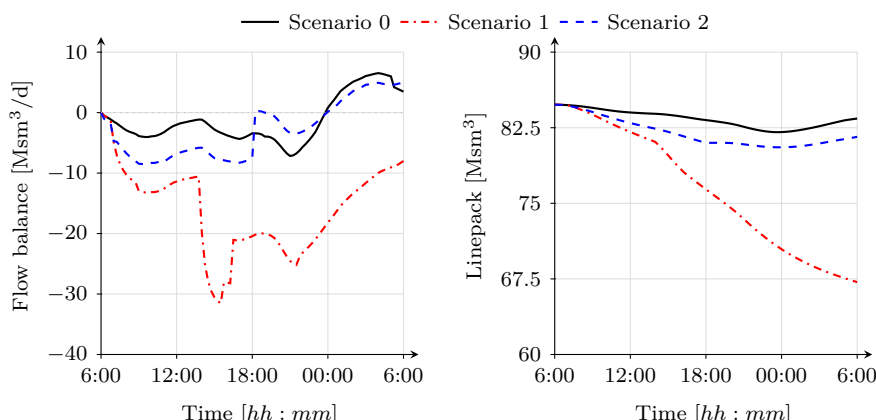


Fig. 4.10.: Time evolution of flow balance (sum of inflow minus sum of outflow) and linepack for the computed scenarios.

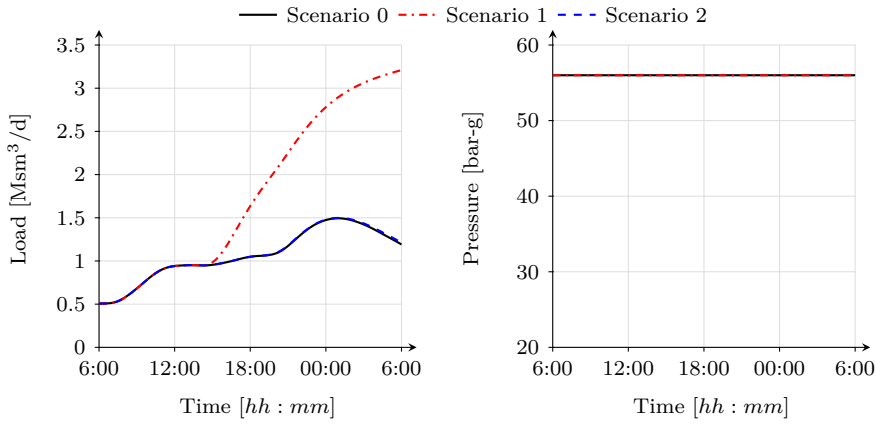


Fig. 4.11.: Time evolution of withdrawal rate and pressure at underground gas storage (UGS) facility for the computed scenarios.

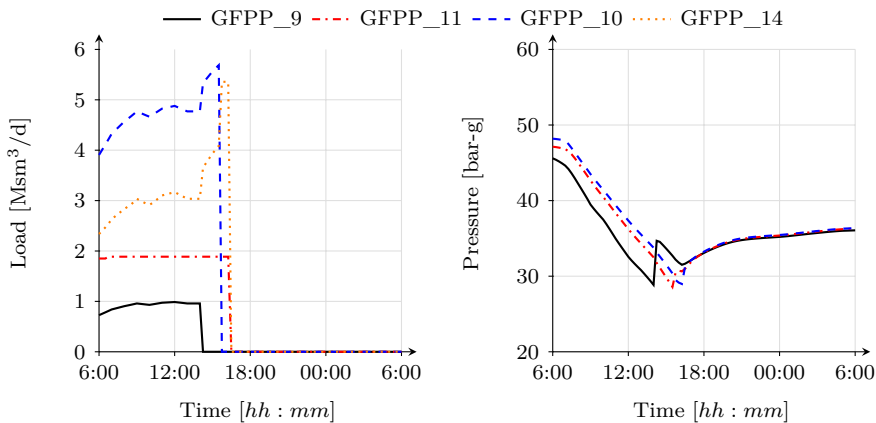


Fig. 4.12.: Time evolution of load and pressure of failed GFPPs in scenario 1.

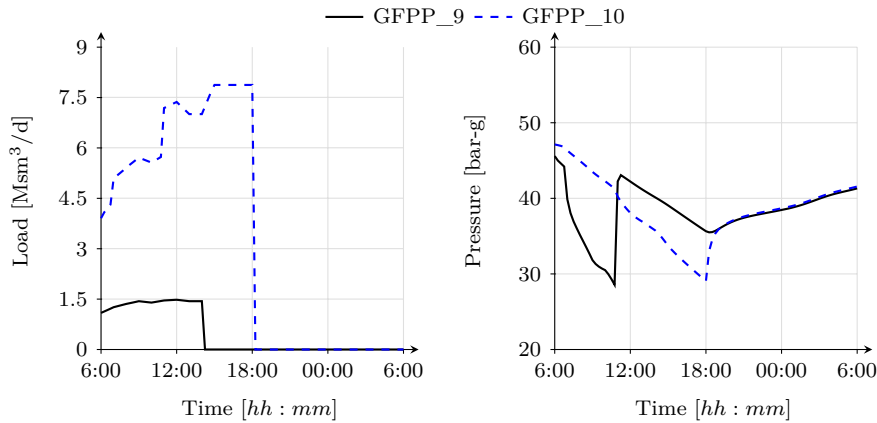


Fig. 4.13.: Time evolution of load and pressure of failed GFPPs in scenario 2.

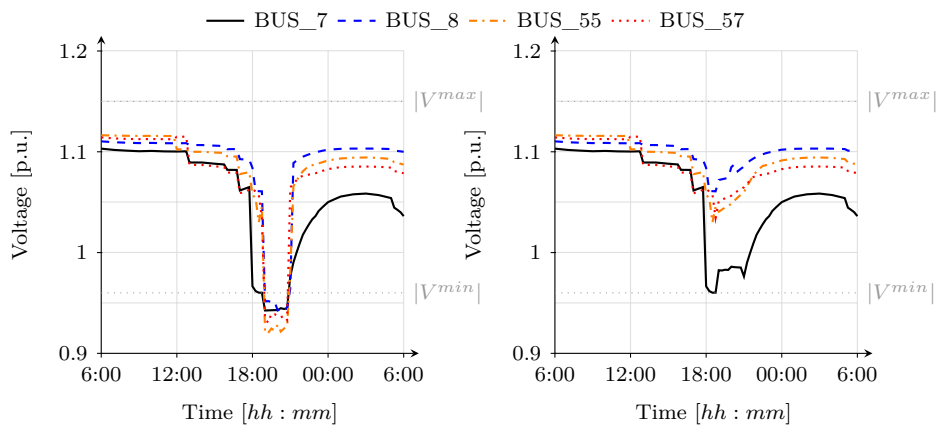


Fig. 4.14.: Time evolution of bus voltage before load shedding (**left**) and after (**right**) for scenario 1. All four buses where load shedding was applied are shown in this figure.

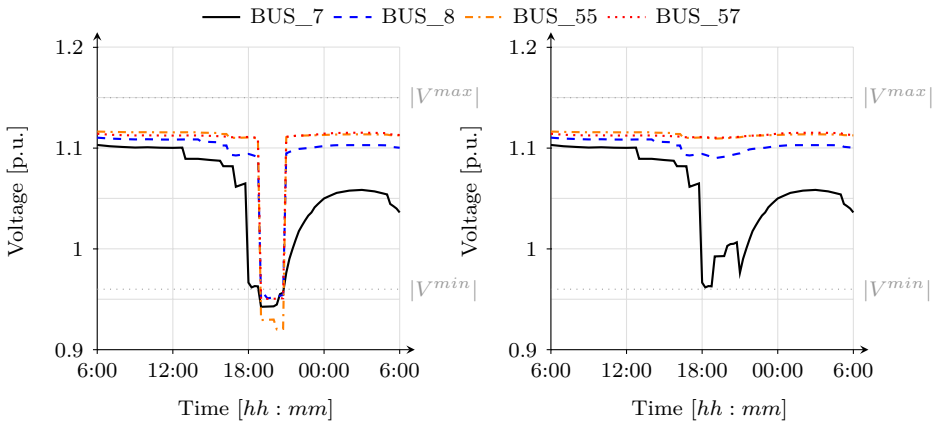


Fig. 4.15.: Time evolution of bus voltages before load shedding (**left**) and after (**right**) for scenario 2. Load shedding was applied at 15 buses. Among these buses are the 4 buses from scenario 1, which are shown in this figure.

Regarding the CBE_1 station, due to the pressure drop at the station (see Fig. 4.16), the flow is restricted around 21:00 because the threshold pressure of 30 bar-g is reached. This is the only way to keep minimum delivery pressure at that exit point; otherwise problems would arise downstream due to too low pressure. Figure 4.16 shows the drop in flow (around 8 Msm³/d) at CBE_1 station due to the pressure restriction. Moreover, the

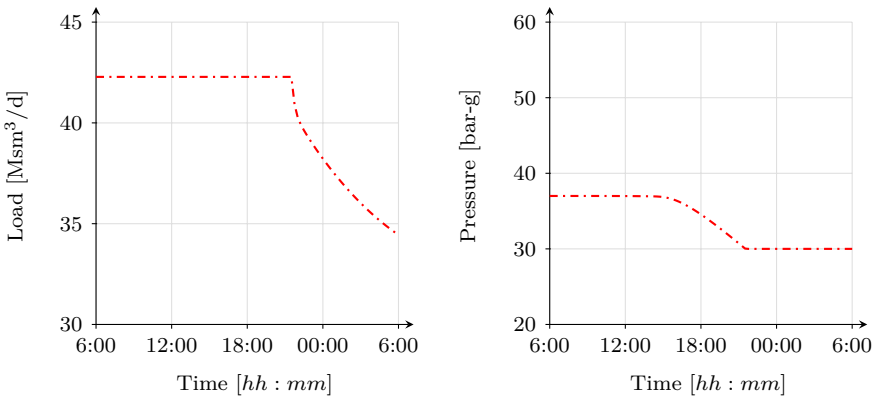


Fig. 4.16.: Load and pressure profile of CBE_1 for scenario 1.

difference between scenario 0 and scenario 2 shows the gas system reaction to the electric side disruption. In Fig. 4.10, it can be seen that the flow balance of the gas network in scenario 2 is more negative (the gas system loses more gas) than in scenario 0 until 18:00. This is caused by the increase in gas demand of GFPPs due to the disruption of the lignite

power plant and the loss of power generation from wind turbines. The increase in gas demand of GFPPs leads to a pressure drop in two GFPPs, followed by the disconnection of the power plants from the network (see Fig. 4.6 and 4.13). The pressure and load profiles for failed GFPPs are given in Fig. 4.13. The disconnection of the generators affects the loading of the gas system in a positive way. Moreover, the linepack starts to recover after 18:00 (see Fig. 4.10).

The scenario results indicate clearly that the disruptions taking place in the gas network that affect GFPPs also affected the operability of the power network. After failure of each GFPP, the power model calculates the new generating profiles for all power plants and sends these profiles to the gas model. In scenario 1, the closure of four GFPPs due to low pressure levels in the gas system caused voltage violations in the electricity network at peak demand hour (19:00–20:00) because of the high amount of power transmission from relatively distant generators in order to compensate the missing generating capacity. This violation in voltage levels caused 954 MW of load shedding during 2 h (see Fig. 4.5 and 4.14). In scenario 2, the cascading effects are more severe including three line overloads and load shedding of 1607 MW at the peak demand hours (19:00–20:00, see Fig. 4.6 and 4.15). The initial failure of large capacity lignite power plant together with lack of power generation from wind power caused an increase in power generation from GFPPs. This increase results in pressure drops at two GFPPs followed by the closure of both facilities. The system has to implement these cascading effects in order to avoid a complete blackout in the overall network.

Furthermore, the results show that the impact of disruptions introduced in both scenarios is much higher for the power system than for the gas system.

4.6. Conclusions

In this chapter, we developed an integrated co-simulation framework for cascading outage contingency analysis in combined gas and power system networks and demonstrated the capabilities of the implemented framework by applying it to a realistic, combined electricity and gas transmission network of an European region.

The simulation framework is composed of a transient hydraulic model for the gas system and a steady state AC-OPF model for the power system. Both models, are derived from the physical laws governing the flow of gas and electric power, respectively. Moreover, the most important facilities and their technical constraints are considered.

The gas and power system models are coupled through coupling equations describing the fuel gas offtake of GFPPs for power generation and the power supply to LNG terminals, UGS facilities and electric driven compressor stations. The model application was divided into three scenarios, namely, scenario 0 with no disruption, scenario 1 with gas side disruptions and scenario 2 with power side disruptions.

The results of these scenarios show how disruption events triggered in one system propagate to the other system. In scenario 1, for instance, three major gas supply stations are disrupted and as a result a number of GFPPs are shut-down due to insufficient fuel gas pressure. This contingency propagates further to other buses in the power system, where load shedding is implemented in order to maintain the voltage levels above the minimum voltage threshold. Similar observations are made in scenario 2, where a drastic reduction in renewable energy generation together with a shut-down of a large power plant triggered a large increase in gas demand of GFPPs, leading to a rapid pressure drop in the gas network and the subsequent shut-down of GFPPs. Eventually, this circumstance increased the stress on the power system leading to minimum bus voltage violations in a couple of buses, which is remedied by applying load shedding at the affected buses.

Based on these key findings, it can be concluded that there is a need for close collaboration and coordination between gas and power TSOs. Data concerning pressures, flows, voltages etc., efficiently handled and communicated may introduce resilience on the integrated network. This has to be done via well-structured protocols that inform the other TSO about the grace periods and support that each network may grant the other. The use of models like the one proposed in this study may be of much help for getting part of this information to share with the other operator.

In this chapter, the following sub-research questions elaborated for the gas system in Chapters 2 and 3 was addressed for the electric power system:

- *What are the most important facilities in the gas and electricity transmission networks in terms of security of supply?*
- *How can we develop a mathematical model that reflects appropriately their physical behaviour and their technical and contractual constraints?*

Furthermore, the following sub-research questions regarding the interconnections between gas and electricity networks were discussed:

- *What are the most crucial interconnection points between the gas and electric power system?*

- *How can these interconnections be represented in the mathematical model?*
- *How do disruptions originating in the gas and/or electric network propagate from one network to the other and even back to the network where the disruption originated?*
- *How do disruptions triggered in one system affect the operation of the other system?*

The co-simulation framework developed in this chapter is able to capture the propagation of disruptions from one energy system to the other. However, there are a number of aspects that could not be reflected appropriately due to the nature of the model.

Firstly, the coupling between the two energy systems are simulated in two different simulation time frames. Thus, there is no immediate feedback from one system as a result of a disruption in the other system.

Secondly, the curtailment of power system loads were directly applied to buses that were affected by voltage violations based on a predefined rule. Priority levels between different power system customers were not considered, which may have an effect on the results. Finally, time transitional constraints of power system generators in terms of maximum ramp rates, start-up and shut down times were neglected, which may restrict the available generation capacities to balance the power system loads.

In the next chapter, we develop a combined simulation model for interdependent gas and electricity networks that considers these aspects.

5. Combined Simulation of integrated Gas and Electricity Networks

This chapter is based on the following peer reviewed journal article and peer reviewed conference paper:

- K. A. Pambour, B. Cakir Erdener, R. Bolado-Lavin, and G. P. Dijkema, “**SAInt - A novel quasi-dynamic Model for assessing Security of Supply in coupled Gas and Electricity Transmission Networks**,” in *Applied Energy*, vol. 203, pp. 829 – 857, 2017.
- K. A. Pambour, B. Cakir Erdener, R. Bolado-Lavin, and G. P. J. Dijkema, “**An integrated simulation tool for analyzing the operation and interdependency of natural gas and electric power systems**,” in *Pipeline Simulation Interest Group (PSIG) Conference 2016*.

5.1. Introduction

The ongoing integration of RES into existing energy supply systems is connected with an increased coupling between natural gas and electric power transmission systems.

On the power side, the installation of variable RES, such as wind and solar, is increasing, which require flexible and reliable back up generation units with short start-up and shut down times and large ramping rates in order to provide the flexibility needed in the electricity system to cover the variability and uncertainties provided by wind and solar power. Gas fired power plants connected to gas and electricity networks, which are known for their reliability, short start-up time and shut down time can provide such flexibility to the electric power system [110].

On the gas side, an increased use of electric power to operate facilities in the gas system such as LNG terminals and electric driven compressors installed in gas compressor stations and UGS facilities, can be noticed [10]. Electric drivers outperform traditional gas turbines

with a higher mechanical efficiency, lower maintenance costs and less impact on the environment [11].

In addition to these interconnections, the power to gas (P2G) technology will significantly contribute to the coupling between the two systems [48, 49], where excess electric energy production (e.g. during variable RES curtailment) is used in an electro-chemical process to produce hydrogen and SNG, which can be injected and stored in gas pipelines or UGS facilities for later use at peak electricity demand periods. As more P2G facilities are installed, the dependence of electric power systems on gas network systems as a provider for energy storage will increase.

These developments stress the need to

- (1.) examine the depth and scope of these interdependencies,
- (2.) how they may affect the operation of the two systems and
- (3.) how to proactively approach the bottlenecks and challenges that may emerge.

The traditional co-simulation approach, where the physical equations for the gas and electric power system are solved in independent time frames [15, 57, 60, 126, 127] and/or a steady state model is used for the gas system [15, 29, 40, 126, 127], can only give qualitative information on how a contingency may affect security of supply in coupled gas and electric power systems. For instance, a steady state approach for the gas system cannot quantify appropriately the time evolution of the quantity of gas stored in pipelines, also referred to as linepack, which is a key indicator [60] for how much flexibility the gas system can provide to GFPPs for electric power generation (e.g. available ramping capacity for fuel gas extraction at start-up of spinning reserves, which have to deliver electric energy within 10-30 minutes in case of a contingency [61]).

Furthermore, the co-simulation approach cannot estimate accurately the grace period for gas and power TSOs to coordinate and deploy counter measures to mitigate a contingency. In order to examine the issues raised in (1.)-(3.) in a quantitative way, a dynamic model of the coupled gas and electric power system is needed that can reflect appropriately how disruptions triggered in one system propagate to the other system and affect the operation of facilities in both systems. This will allow gas and power system stakeholders to suggest modifications, that may help prevent and/or mitigate the consequences of disruptions. Some of these modifications that can be implemented are, for instance:

- (a) The curtailment of gas and electric power loads at specific locations and times to reduce the stress on the system and to prevent insufficient pipeline pressures

- (b) The installation of UGS facilities at strategic locations to increase the flexibility to react to loss or shortage of gas supply
- (c) The increase of withdrawal capacity of existing UGS facilities
- (d) The shut-down of specific power plants to maintain the operation of the system in degraded mode
- (e) The expansion of the network to increase transmission capacities and line pack
- (f) The availability of reverse flow at cross-border-points to increase the flexibility and resilience of the gas system

In this chapter, the simulation tool **SAInt** (Scenario Analysis Interface for Energy Systems) [128, 129] is extended by a novel combined quasi-dynamic model composed of the transient hydraulic simulation model for the gas system presented in Chapters 2 & 3, which considers the constraints and control of the most important facilities in the gas system, such as compressor stations and UGS facilities, and a steady state model for the electric power system based on AC-OPF, where the operational costs and key electric power system constraints such as thermal capacity limits of electric lines, active and reactive power generation limits and upper and lower limits on bus voltage magnitudes are considered. The bi-directional coupling between the two systems is established by synchronizing the fuel gas offtake from the gas system for power generation in GFPPs and the electric power supply to electric driven compressors installed in gas transport systems. Moreover, the power supply to LNG terminals is also modelled as an additional gas system dependence on the electric power system.

The scope of the proposed model is primarily on the technical operation of the integrated energy system in a contingency scenario, assuming that market based measures have been fully exploited but were insufficient to mitigate the impact of a disruption. Therefore, aspects related to the energy market are only considered partly in this studies⁸. Moreover, aspects related to the transient stability of the power system in case of a contingency (e.g. voltage stability, rotor angular or synchronous stability, frequency stability [112]), which may play a role in case of a disturbance in the power system, are not considered. However, we assume that the automatic generation control (AGC) system is capable of returning the system to a balanced and stable steady state within a short time frame (less than 5 minutes) after a disturbance [112]. Thus, we describe the operation of the power system by a succession of steady state model.

⁸operational costs for each power plant are considered

To the best of our knowledge, there is currently no commercial or open source simulation software on the market that allows the coupled simulation of gas and electric power systems in a single time frame and simulation environment. Thus, **SAInt** is the first published software tool to offer this type of functionality.

The model presented in this chapter and implemented into **SAInt** is intended to assist governments, gas and power TSOs, regulatory agencies and researchers to address the challenges connected with the ongoing transformation of critical energy infrastructures (CEIs). In particular, **SAInt** can be used to examine potential threats to security of energy supply and to develop strategies to prevent and mitigate the consequences of undesired disruption events in multi-vector energy systems with high penetrations of variable RES. Moreover, the capability of **SAInt** to quantify the impact of a disruption on security of supply can be utilized to perform a risk assessment of CEIs as postulated by EU Regulation 994/2010 [12], which involves, the identification of critical scenarios, the probability of their occurrence and the impact of the identified scenarios on security of supply, which can be estimated by **SAInt** [129].

To achieve these goals, this chapter follows the following structure. In Section 5.2.1, the AC-OPF model presented in Chapter 4 is extended by additional time transitional constraints and a model for dispatchable loads for modelling the curtailments of power system loads based on priority levels. In Section 5.2.2, the coupling equations developed in Chapter 4 are extended.

Next, the algorithm for solving the resulting system of equations for the combined energy system is elaborated, followed by the definition of parameters to evaluate and quantify the impact of disruptions on security of energy supply in Section 5.3. Finally, in Section 5.4, the functionality of the simulation tool and the capability of the implemented simulation model are demonstrated in a case study of a sample combined gas and electric power transmission network.

5.2. Methodology

The operation of gas and electric power systems is increasingly interdependent, due to an increased physical interconnection between the facilities installed in the two systems. A change in one system may propagate to the other system and even back to the triggering system. For instance, an increase in power generation from a GFPP, will cause the gas offtake from the gas grid to increase. This, in turn, may result in an increased power offtake of electric driven compressor stations to recover the pressure and line pack level

in the area affected by the gas offtake. The additional power offtake, again, will have to be balanced by the power generation units including GFPPs, by increasing the power output. This cycle may continue until an equilibrium state is reached. The equilibrium state in such a bidirectionally coupled system cannot be captured appropriately with the traditional co-simulation approach, where the two systems are analysed in independent time frames. Rather an integrated simultaneous solution of the physical equations describing the operation of the coupled energy supply systems at each simulation time step is needed.

The first challenge that arises when modelling the coupled power-gas system is to find a simulation model that describes the dynamic behaviour of the individual systems appropriately. The dynamics in gas transport systems, for instance, are much slower than the ones in electric power systems. Electricity travels almost instantaneously (with speed of light $3 \cdot 10^8$ m/s) and cannot be stored economically in large quantities in current electric power systems⁹ [15]. In case of a disruption, the response time of the electric power system is quite fast and basically the transmission line flows satisfy the steady-state algebraic equations. On the contrary, natural gas pipeline flow is a much slower process, with gas flow velocities typically below 10 m/s and the propagation of pressure and flow changes (speed of sound) around 340 m/s, resulting in a longer response time in case of a large fluctuation. In particular, high-pressure transmission pipelines have much slower dynamics due to the large quantities of natural gas stored in the pipelines.

In order to consider the different characteristics of the two systems, we propose a transient hydraulic model for the gas system and a succession of steady state AC-OPF model for the electric power system. The reason for using an optimal power flow instead of a power flow model is to be able to reflect appropriately the real time power dispatch of generation units, the curtailment of power system loads and important power system constraints, such as thermal capacity limits of transmission lines, reactive and active power limits of generation units and voltage limits of electric buses, which are not considered in AC power flow models.

We couple the power and gas model to a combined simulation model by defining coupling equations reflecting the physical interlink between the two systems at each simulation time step.

⁹with the only exception of hydraulic pumping power stations, whose availability is very much limited in a significant number of countries

5.2.1. Extended Power System Model

The operation of an electric power system is restricted by a number of constraints, which if violated can lead to severe contingencies. Transmission lines, for instance, have a maximum transmission capacity S^{max} , which if exceeded can lead to outages. Generation units, in turn, can only operate within a specific operating envelope (generator capability curve), which is restricted by the upper and lower limits on active and reactive power generation P_G^{max} , P_G^{min} , Q_G^{max} and Q_G^{min} , respectively. Moreover, electric power delivered to directly served customers and local distribution systems must satisfy a contracted minimum voltage level $|V^{min}|$, to avoid legal penalties and outages in the subsystems connected to the transmission grid.

In order to operate the electric power system in an economic and secure way, power TSOs are equipped with a number of simulation models to schedule the operation and control of generation units, in order to minimize total operation costs and to ensure security of supply, taking into account the changes in the electricity market and the legal and technical constraints imposed by stakeholders and power system components. The determination of an optimal generation schedule usually involves a successive solution of three different optimisation problems, namely, the unit commitment (UC), economic dispatch (ED) and reserve allocation (RA) [5, 61, 63]. The UC, which is described by a mixed integer linear optimisation model, determines a cost optimal schedule of when to operate which generation unit, taking into account its fixed and marginal operating costs, its ramp rate and its start-up and shut-down times and costs. The solution of the UC is used as input to the ED to compute the cost-optimal power dispatch schedule for each committed unit. The ED typically involves solving a (non-)linear constrained optimisation problem, where the objective is to find a solution for the state variables (voltage angle δ , voltage magnitude $|V|$, active and reactive power generation P_G and Q_G) that satisfies the electric power system constraints and minimizes the operational costs, which is typically expressed as a function of the active power generation $P_{G,i}$ for each committed unit i . The UC and ED are complemented by the RA, which ensures that a minimum amount of generation capacity is reserved and available to mitigate any unexpected contingency in the electric power system. The UC and ED are typically solved one day ahead of the actual operating day as well as in real-time intra-day operation, while the spinning reserves are typically allocated in the day-ahead scheduling. In real-time operation the UC is normally computed every 15 minutes, while the real time power dispatch is executed every 5-15 minutes [61]. Thus, the ED reflects reasonably well the operation of the electric power system, in particular, real-time power generation dispatch. Therefore, we will use the ED to determine the changes of the state variables to the time varying electric power system

loads for each simulation time step. In order to keep the complexity of the combined simulation model at a moderate level, we assume that all generation units in the model are involved in the real-time power dispatch. Thus, we omit solving the UC. However, for the transition between two consecutive simulation time steps t_{n+1} and t_n we consider key parameters that are typically included in the UC model, such as the ramp rate ω_r and the start-up T_s and shut-down T_d time for each generation unit, which we integrate into the ED model.

The basic ED, which is described by the AC-OPF model elaborated in Section 4.2.3 (see eq. (4.13)-(4.23)), can be solved for each simulation time step t_n to capture the behaviour of the electric power system. However, for the assessment of security of supply in coupled gas and electric power systems in scenarios where the two systems operate close to their limits, this basic formulation of the ED described above may not be suitable. For instance, in a contingency scenario, where total power demand exceeds total available power generation capacity, due to a disruption in a major power plant, the basic ED would not converge to a feasible solution. However, in practice in such a situation the power TSO will deploy demand side measures, like for instance, load shedding at specific locations based on a contingency protocol¹⁰, in order to maintain a secure operation of the electric power system. To account for such scenarios, we introduce the concept of dispatchable loads [116] as depicted in Fig. 5.1. The set of active power demand \mathbf{P}_D at buses is added to the vector of decision variables \mathbf{X} for the basic ED (see eq. (5.1)) as follows:

$$\mathbf{X} = \begin{bmatrix} \Delta & \mathbf{V}_m & \mathbf{P}_G & \mathbf{Q}_G & \mathbf{P}_D \end{bmatrix}^T \quad (5.1)$$

In addition, the objective function in eq. (4.13) is extended by a linear penalty function with respect to $\mathbf{P}_{D,i}$ and the upper and lower limits on the new decision variables are added to the linear inequality constraints of the basic ED:

$$\min_{\mathbf{X}} f(\mathbf{X}) = f(\mathbf{P}_G) - \sum_{i=1}^{N_b} \pi_i P_{D,i} \quad (5.2)$$

$$P_{D,i}^{min} \leq P_{D,i} \leq P_{D,i}^{set}, \quad i = 1 \dots N_b \quad (5.3)$$

The penalty function for dispatchable loads is subtracted from the total active power generation costs $f(\mathbf{P}_G)$ which are always greater zero. Thus, the solution for $P_{D,i}$ will tend to fulfil the scheduled electric power demand $P_{D,i}^{set}$ if generation and transmission

¹⁰which depends on the contractual agreements with each customer, e.g. agreements on firm and interruptible loads, penalties in case of unserved electric power

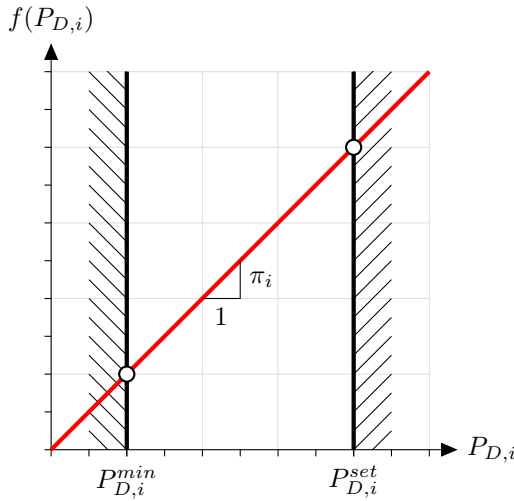


Fig. 5.1.: Linear penalty function $f(P_{D,i})$ and constraints for dispatchable loads. The active power load can vary between the scheduled load $P_{D,i}^{set}$, which is typically given by the load profile, and the minimum load $P_{D,i}^{min}$ which is greater or equal zero. The coefficient π_i of the penalty function is the slope of the penalty curve and is referred to as the penalty factor. The penalty factor can be used to assign priority levels to the different customers connected to the power grid. The higher the penalty factor the less likely a facility will be affected by demand side measures

capacities are sufficient to balance the power system loads and if bus voltage limits are not active. $P_{D,i}^{set}$ is set as the upper limit for the active power load $P_{D,i}$, while the lower limit $P_{D,i}^{min}$ can be set according to the contractual agreement with the customer (e.g. agreement on firm capacity and interruptible loads). As illustrated in Fig. 5.1 the slope of the linear penalty function is represented by the penalty factor π_i , which we define as follows:

$$\pi_i = \xi \cdot \max_{P_{G,k}^{min} \leq P_{G,k} \leq P_{G,k}^{max}} \left\{ \left\| \frac{\partial f_k(P_{G,k})}{\partial P_{G,k}} \right\| \right\} \cdot \lambda_i, \quad k = 1 \dots N_g, \quad 1 \leq \xi \leq 2 \quad (5.4)$$

where λ_i is the priority factor for the corresponding load $P_{D,i}$, which can be used to assign different priority levels to each individual customer connected to the power grid. This way, in cases where load shedding is required to balance the power system, customers with high priority factors are less likely to be affected by such demand side measures than customers with low priority factors. The priority factor is multiplied with the largest possible absolute value of the first derivative of the cost function for active power generation in order to ensure that the solution for dispatchable loads converges to the scheduled load $P_{D,i}^{set}$ as

long as power system constraints are not active (e.g. generation capacity covers scheduled loads and power losses and minimum voltage limits are not active).

The solution of the extended ED for a time step t_n is independent of the solution of a previous or future time step t_{n-1} or t_{n+1} , respectively. However, in real time power system operation there are specific transitional constraints between consecutive time steps, which restrict the operation and flexibility of the power system. In this study, we consider the following three transitional constraints, which are key constraints in the UC model, namely, the ramp rate, the start-up time and the shut-down time, which we define similar to [130] and integrate into the extended ED model, as follows:

(1.) Ramp rate (ω_r):

The ramp rate is the speed in [MW/min] at which the active power generation $P_{G,i}^{n+1}$ at simulation time t_{n+1} can be increased or decreased between the minimum and maximum active power generation limit $P_{G,i}^{min}$ and $P_{G,i}^{max}$, respectively. Hence, the upper ($P_{G,i}^{max,n+1}$) and lower limit ($P_{G,i}^{min,n+1}$) on active power generation of plant i at each simulation time step t_{n+1} can be expressed as follows:

$$P_{G,i}^{max,n+1} = \min \{ P_{G,i}^{max}; P_{G,i}^n + \omega_r \cdot \Delta t \} \quad (5.5)$$

$$P_{G,i}^{min,n+1} = \max \{ P_{G,i}^{min}; P_{G,i}^n - \omega_r \cdot \Delta t \} \quad (5.6)$$

(2.) Start-up time (T_s):

The start-up time is the time span between activating the power plant and the time after which the power plant reaches its minimum active power generation level $P_{G,i}^{min}$. The start-up time depends on the plant type and the time duration between the last shut-down time and the requested start-up time (i.e. cold start, warm start or hot start [130]). To account for this characteristic, we assume the following exponential function to determine the start-up time in respect to the last offline time t_o and the time t_n at which the start-up of the power plant is requested:

$$T_s(t_n, t_o) = T_s^{min} + (T_s^{max} - T_s^{min}) \left[1 - \exp \left(-5 \frac{t_n - t_o}{T_o} \right) \right] \quad (5.7)$$

where T_s^{min} is the minimum start-up time for a hot start, T_s^{max} the maximum start-up time for a cold start and T_o is the time duration after which a station is offline and thus regarded as in cold start state. Similar to [130] we set $T_o = 72$ h.

(3.) Shut-down time (T_d):

We define the shut-down time as the time for the power plant to reduce its active power generation to minimum active power generation $P_{G,i}^{min}$ before finally going offline. The shut-down time depends on the ramp rate and the active power generation at the time the shut-down is requested.

The presented power system model can be solved with an interior point method, which is explained in Appendix B.1. The interior point method and the algorithm for solving the power system model are implemented into the simulation tool **SAInt**.

5.2.2. Extended Coupling Equations

The coupling equation developed in Section 4.3 for the coupling between GFPPs in the electric power systems and demand nodes in the gas system (see eq. (4.27)) assume a constant thermal efficiency to determine the equivalent fuel gas offtake for a specific active power generation level. However, the thermal efficiency of a GFPP typically changes in respect to its active power generation. This dependency is reflected by the heat rate curve of the GFPP.

The required fuel gas $L_{p,i}$ for active power generation $P_{G,i}$ at plant i can be expressed in terms of the heat rate $HR_i(P_{G,i})$ of the GFPP and the gross calorific value GCV of the fuel gas, as follows [59]:

$$L_{GFPP,i} = \frac{HR_i(P_{G,i}) \cdot P_{G,i}}{GCV}, \quad i = 1 \dots N_{GFPP} \quad (5.8)$$

The heat rate describes the amount of heat needed in MJ to generate and inject 1 kWh of electric energy into the power transmission grid. It is an indicator of the efficiency of the power plant to convert chemical energy stored in natural gas into electrical energy. It is typically expressed as a quadratic function of the active power generation $P_{G,i}$, as follows [59, 115]:

$$HR_i(P_{G,i}) = \alpha_i + \beta_i \cdot P_{G,i} + \gamma_i \cdot P_{G,i}^2 \quad [\text{MJ/kWh}] \quad (5.9)$$

The heat rate is the reciprocal of the thermal efficiency η_T , thus, $HR = 3.6 \text{ MJ/kWh}$ corresponds to $\eta_T = 100 \%$.

Moreover, the linear coupling equation (see Section 4.3 eq. (4.26)) describing the power offtake of LNG terminals in terms of the regasification rate is modified to the following quadratic function:

$$P_{D,i}^{LNG} = k_{i,0} + k_{i,1} \cdot L_{reg,i} + k_{i,2} \cdot L_{reg,i}^2, \quad i = 1 \dots N_{LNG} \quad (5.10)$$

5.2.3. Algorithm for solving the Combined Simulation Model

The coupling equations can be integrated into the gas and electric power system model by extending the external nodal load L_i in the integral continuity equation (2.39) to

$$L_i = L_{GS,i} + L_{GFPP,i} \quad (5.11)$$

and the active power demand $P_{D,i}$ in the active power balance equation (4.6) to

$$P_{D,i} = P_{D,i}^{PS} + P_{D,i}^{CS} + P_{D,i}^{LNG} \quad (5.12)$$

where $L_{GS,i}$ is the gas offtake or supply at non-GFPP facilities and $P_{D,i}^{PS}$ power offtake of non-gas facilities in the power grid. The resulting set of equations (2.46), (4.14)-(4.23), (4.25), (5.2)-(5.12) describe the equilibrium state of the coupled gas and electric power system at each time step t_n . The time steps for the time integration are chosen according to the dynamic time step method for the gas model. Additional time steps are introduced if specific events in the power model occur such as the shut-down of a generation unit or outages of transmission lines.

The coupled model can be solved as a single combined system by extending the ED with additional decision variables, namely, the state variables p , Q and L from the gas model and additional equality constraints expressed by the transient hydraulic gas equations (2.41) & (2.2). While the computational costs for this approach may be acceptable for problems of smaller size, its application to large scale combined gas and electric power systems is connected with high computation time and storage. Thus, to speed up the solution process, we propose an iterative boundary condition adaptation method, which allows a parallel multi-threaded solution of the linearised equations (2.41) & (B.7). The coupling equations are treated as boundary conditions, which are adapted after each iteration step k until a converged integrated solution is obtained.

In order to start the combined dynamic gas and electric power system simulation, an initial state for the coupled system at time step t_0 is required, which can be obtained

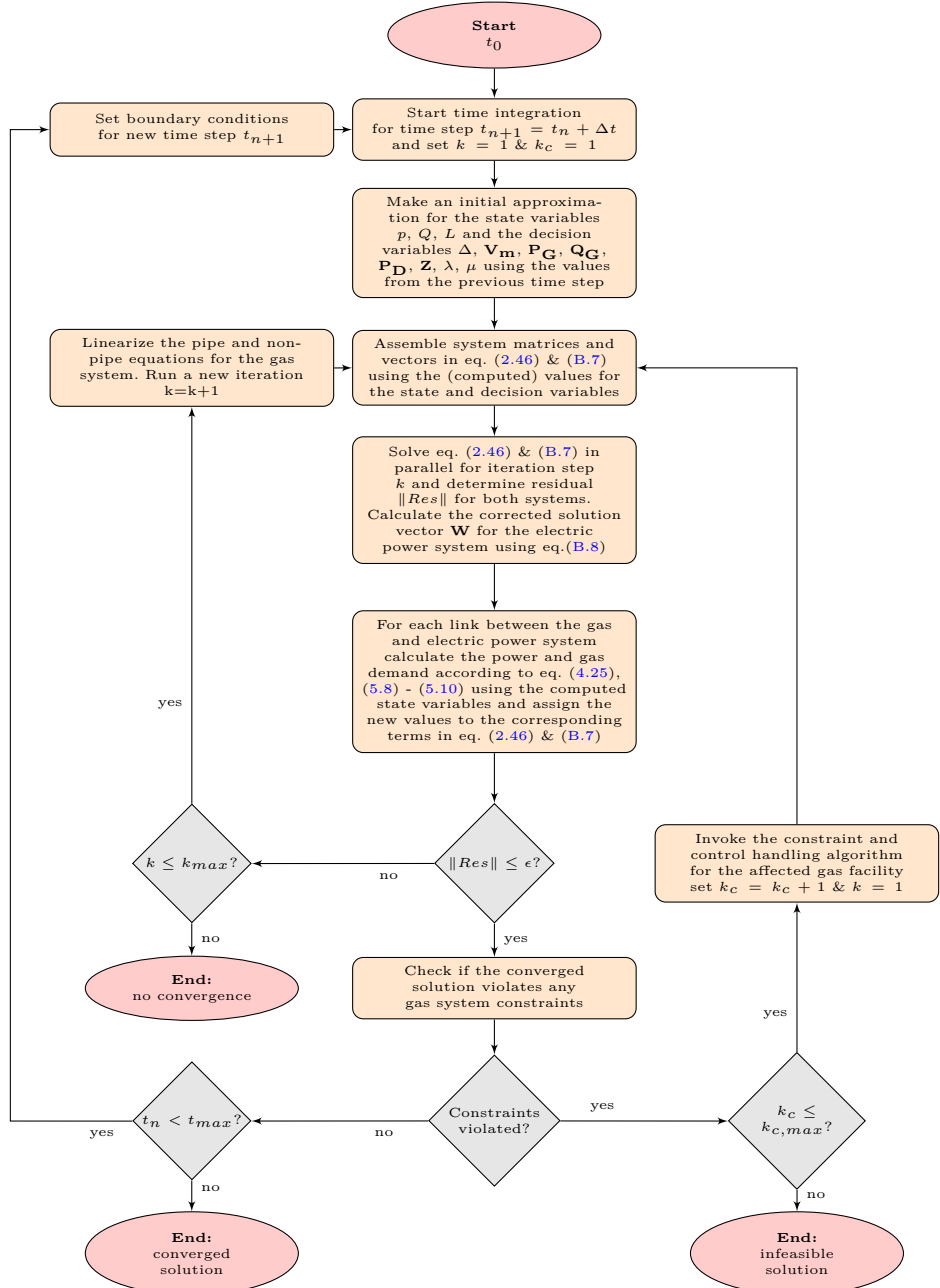


Fig. 5.2.: Flow chart of the algorithm for solving the coupled gas and electric power system model

from the solution of a combined steady state simulation or from the terminal state of a combined dynamic simulation. The algorithm for solving the coupled system is described in the flow chart depicted in Fig. 5.2. It contains three major loops, namely, the time integration loop with the step variable t_n , the iteration loop with step variable k and the CCH loop with step variable k_c . The CCH loop is entered, if a constraint in a gas system facility is violated (e.g. minimum pressure, maximum compression ratio violation etc.) after exiting the iterative loop. The control of the affected facility is set to the active constraint and the iterative loop is repeated.

The ramp rate for each power plant is considered by adapting the value of the upper and lower limits of the active power generation (see eq. (4.22)) for each simulation time step t_n such that the change in active power generation between two consecutive time steps does not exceed the ramping limits. Furthermore, we make use of the simulation control object introduced in Section 3.4 to control the start-up and shut down of a power plant in the course of the time integration. The combined simulation is terminated successfully if a converged and feasible solution is obtained for each simulation time step t_n .

5.3. Security of Energy Supply Parameters

The algorithm for the combined model is designed for assessing the impact of disruptions on security of energy supply in combined gas and electric power systems. In order to estimate quantitatively

- how a disruption affects the operation of a facility or the total system,
- to compare the impact of different contingency scenarios and
- to evaluate different mitigation measures and their effectiveness,

we define the following parameters that serve as indicators for quantifying the impact of contingencies on security of supply:

(1.) Quantity of gas or (electric) energy not supplied (GNS/ENS):

In case of a disruption, the quantity of gas or (electric) energy demanded by customers may not be available, due to insufficient fuel gas pressure, line pack, voltage magnitude or limited transmission capacity. The difference between the scheduled or demanded quantity of gas or (electric) energy and the actual quantity delivered to a customer (see Fig. 5.3) can be utilized as a quantitative indicator for the impact of a disruption on security of energy supply for a group of customers connected to the

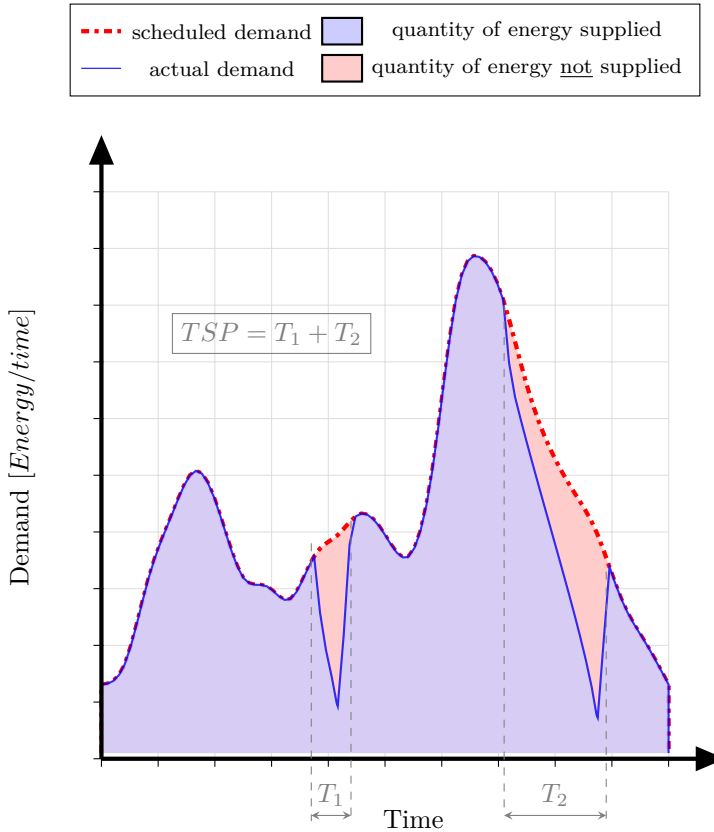


Fig. 5.3.: Security of supply indicators

affected facility or as a means of checking whether the terms of service are appropriate. We refer to this quantity as gas or (electric) energy not supplied (GNS/ENS), respectively. The total GNS and ENS for a gas offtake station (CGS,IND, CBE) or an electric load bus i at simulation time t_n can be determined by the following integral equations:

$$GNS_i(t_n) = \int_{t_0}^{t_n} [L_i^{set}(t) - L_i(t)] dt \quad (5.13)$$

$$ENS_i^g(t_n) = \int_{t_0}^{t_n} [L_i^{set}(t) - L_i(t)] \cdot GCV dt \quad (5.14)$$

$$ENS_i^e(t_n) = \int_{t_0}^{t_n} [P_{D,i}^{set}(t) - P_{D,i}(t)] dt \quad (5.15)$$

The ENS is reflected by the size of the red area depicted in Fig. 5.3. $L_i^{set}(t)$ and $P_{D,i}^{set}(t)$ correspond to the load profiles prescribed to demand nodes in the gas system (e.g. CGS, CBE, IND) and load buses in the electric power system, respectively.

(2.) Percentage of gas or (electric) energy not supplied (PENS):

The GNS and ENS of a facility gives an absolute value of the gas or energy not supplied, respectively. To evaluate the severity of the supply disruption for a facility or the total network we set the GNS/ENS in relation to the scheduled or expected energy supply and define an additional parameter referred to as percentage of scheduled energy not supplied due to a contingency, which we denote PENS. The PENS of a facility can be expressed as follows:

$$PENS_i^g(t_n) = \frac{ENS_i^g(t_n)}{\int_{t_0}^{t_n} L_i^{set}(t) \cdot GCV dt} \quad (5.16)$$

$$PENS_i^e(t_n) = \frac{ENS_i^e(t_n)}{\int_{t_0}^{t_n} P_{D,i}^{set}(t) dt} \quad (5.17)$$

The PENS can be graphically interpreted as the ratio between the red area and the sum of the red and blue area depicted in Fig. 5.3.

(3.) Survival time (SVT):

The indicators defined so far do not provide information on the propagation and timing of contingencies, which may be crucial for the coordination between gas and power TSOs. For instance, the time between the start time of a disruption and the time of an undesired shut down of a GFPP due to insufficient fuel gas pressure is a good indicator of the grace period for a TSO to react and deploy counter measures to mitigate and to avoid cascading effects. Hence, a generic indicator for the resilience and the grace period to react to a contingency can be defined as the time span between the occurrence of the initial disruption t_d and the point in time at which a facility i is affected, i.e. the time t_a at which the ENS or PENS of the affected facility is greater than a predefined tolerance ϵ_{svt} . We refer to this indicator as the survival time (SVT).

(4.) Time span of energy not Supplied (TSP):

The survival time indicates how long it takes until a facility is affected by a

disruption, but not how long the disruption affected the facility. To account for this crucial information, we define the parameter Time Span of Energy not Supplied (TSP), which is the sum of all time intervals, where the ENS of a facility is greater than zero (see Fig. 5.3). The TSP is an indicator of how severe a facility is affected by a contingency in terms of time.

(5.) Energy not supplied per time span (ENSTSP):

The TSP can be interpreted wrongly if a facility is affected by a disruption for a long time period, but the ENS in this time period is relatively small. To avoid this misinterpretation, we define an additional indicator for security of supply, which we refer to as energy not supplied per time span (ENSTSP), which is the ratio between ENS and TSP of a facility. The ENSTSP is the average rate of energy not supplied per time during the time intervals the facility is affected by the disruption.

The indicators presented in this section have been implemented into **SAInt** and are defined for each demand facility and for the total network system. In Chapter 3, we implemented into **SAInt** the functionality to group the facilities in the network model into subsystems, which can then be analysed independently¹¹. Thus, we can use this option to determine the value of each indicator for a specific area or group of facilities or customers, such as GFPPs and protected customers [12] (e.g. households, public services) connected to the gas or power grid. Moreover, the parameters of the subsystem can be used to declare conditional expressions for a specific action or event during the simulation. For instance, we can invoke the shut-down of a GFPP if the minimum pressure in a specific subsystem is below a certain pressure threshold or if the total ENS of the subsystem is greater than zero. In the next section, we apply the developed models to a case study of a sample combined energy system.

5.4. Model Application

The algorithm explained in Fig. 5.2 has been implemented into **SAInt**, a simulation software designed for analysing security of supply in (coupled) critical energy infrastructures.

In this section, we apply **SAInt** to perform a case study on the sample coupled gas and electric power system model depicted in Fig. 5.4 and 5.5, respectively. By doing this, we

¹¹subsystems in **SAInt** are referred to as GSUB for gas subsystems and ESUB for subsystems of the electric network

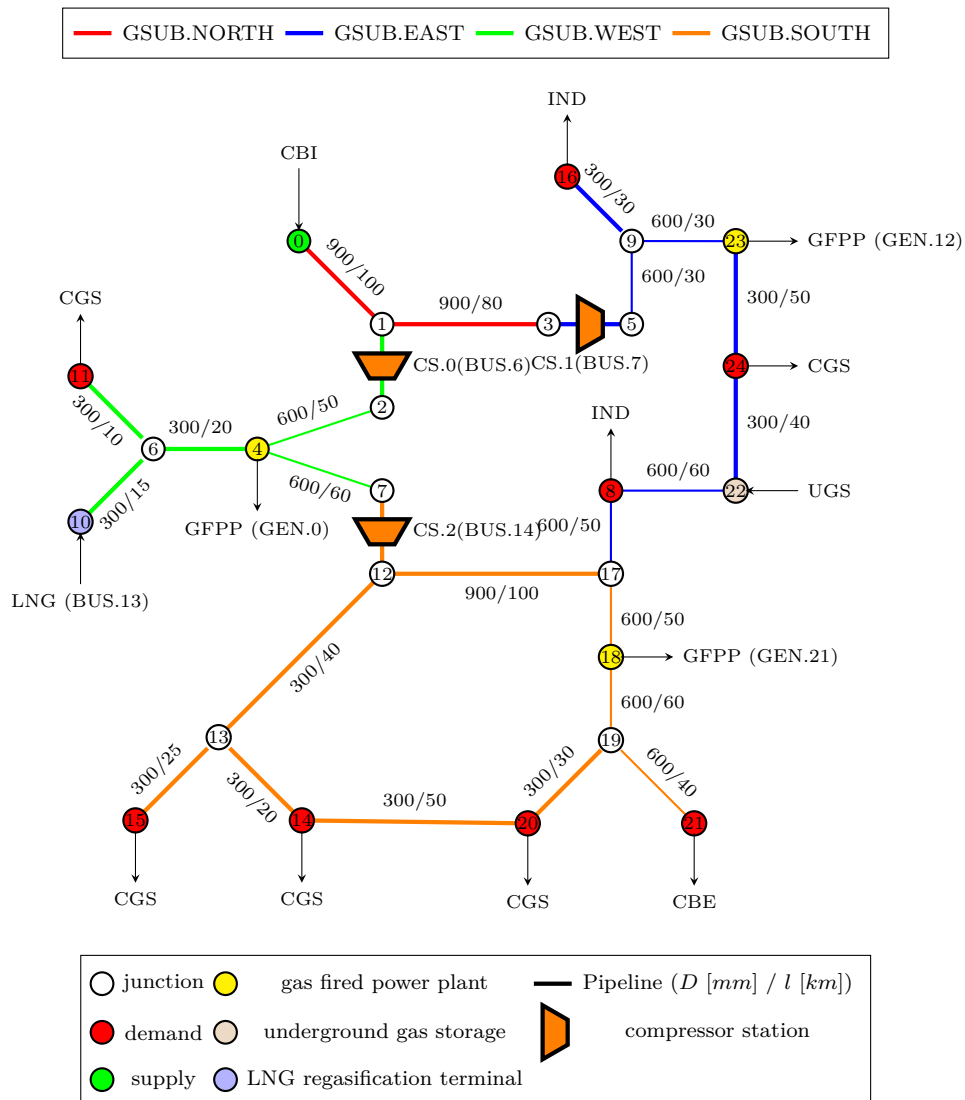


Fig. 5.4.: 25-Node gas model used for the case studies

intend to demonstrate the functionality of the simulation software and capabilities of the developed model to estimate and quantify

- (1.) how disruptions triggered in one system affect the operation of facilities in the two systems,
- (2.) how disruptions propagate from one system to the other,

- (3.) the grace period for gas and power TSOs to coordinate and react to contingencies, and
- (4.) how effective are specific counter measures to mitigate the impact of disruptions.

The gas and electric network used in the case study are bidirectionally coupled through three GFPPs (NO.4 <-> GEN.12, NO.18 <-> GEN.21, NO.23 <-> GEN.0), three ED-CSs (CS.0 <-> BUS.6, CS.1 <-> BUS.7, CS.2 <-> BUS.14) and one LNG terminal (NO.10 <-> BUS.13). Two of the GFPPs (NO.18 <-> BUS.21 & NO.23 <-> BUS.0) use combined cycle gas turbines (CCGTs), while the third GFPP (NO.4 <-> GEN.12)

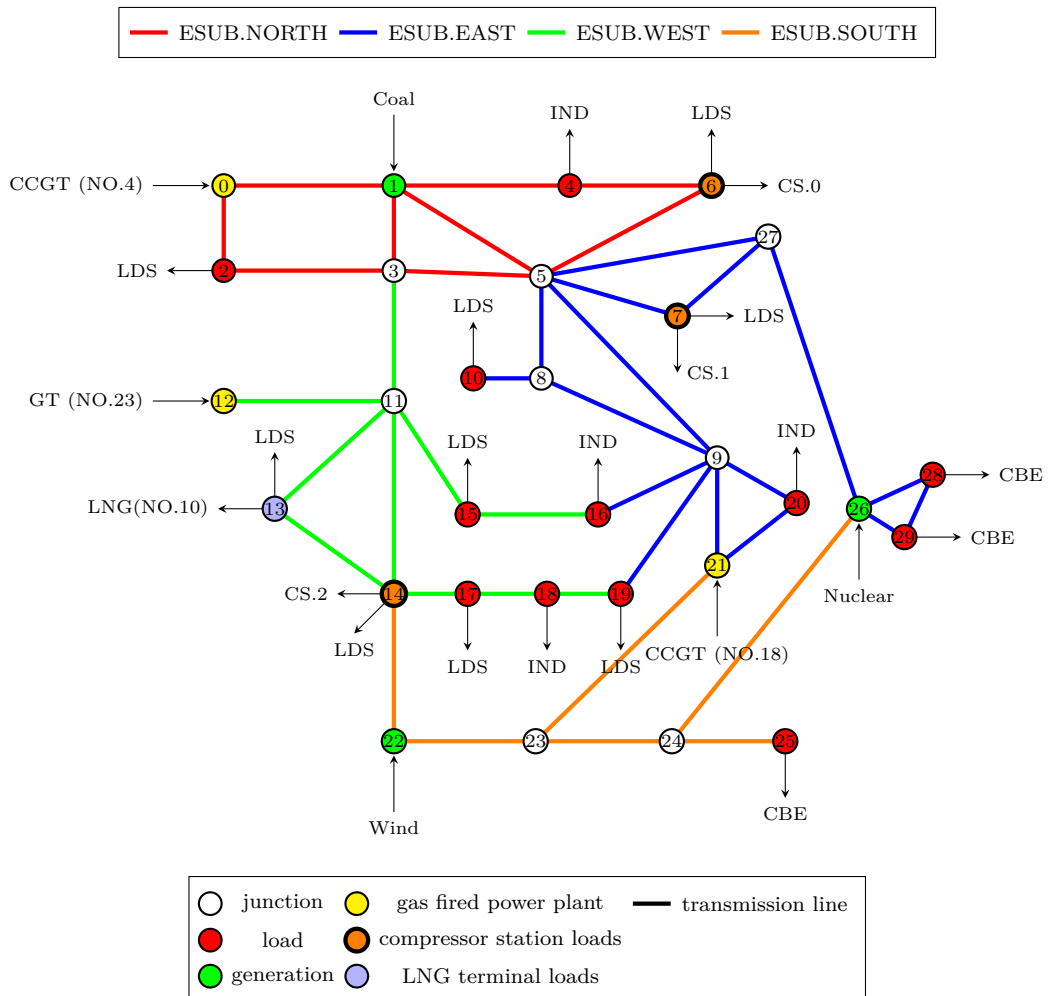


Fig. 5.5.: Modified version of IEEE 30-Bus power system model

Parameter	Symbol	Value	Unit
reference time step	Δt	900	[s]
total simulation time	T_{max}	24	[h]
gas temperature	T_g	288.15	[K]
dynamic viscosity ¹	η	$1.1 \cdot 10^{-5}$	[kg/m · s]
isentropic coefficient	κ	1.3	[\cdot]
reference pressure	p_n	1.01325	[bar]
reference temperature	T_n	273.15	[K]
critical pressure ²	p_{crit}	45	[bar]
critical temperature	T_{crit}	193.7	[K]
relative density	d	0.6	[\cdot]
gross calorific value	GCV	41.215	[MJ/sm ³]
nominal power	BaseMVA	100	[MVA]

¹ the dynamic viscosity of the gas is needed for calculating the Reynolds number, which, in turn is needed for computing the friction factor λ using Hofer's equation as described in Chapter 2

² the critical pressure and temperature of the gas is needed for calculating the compressibility factor based on the equation developed by Papay as described in Chapter 2

Tab. 5.1.: Input parameter for the sample combined gas and power transmission network

uses conventional gas turbines (GTs) to generate electricity. The third GFPP serves as a reserve and backup for intermittent wind power generation at generation bus GEN.22. Thus, the GFPP is offline unless the electric power generated by the wind turbines is below a certain threshold. The input data for the nodes, pipes, compressor stations and the LNG terminal in the gas network are given in Tables B.1 - B.4, while the data for the buses, transmission lines and generators in the electric network are listed in Tables B.5-B.7. The simulation properties for the case study are given in Table 5.1¹². The simulation time window for all studied scenarios is set to $T_{max} = 24$ h (one operating day, from 6:00 AM to 6:00 AM) for the sake of keeping the result data and discussion at a moderate size. However, the time window can be extended as desired in order to study long-term contingency scenarios. The reference time step is set to $\Delta t = 15$ min, however, the time resolution may be adapted by the dynamic time step adaptation (DTA) method in case of control changes or changes in active constraints during the time integration process. The DTA is explained in detail in a previous publication [129].

In order to run a combined quasi-dynamic simulation, an initial state of the combined network is required, which can either be the solution of a combined steady state or the terminal state of a combined quasi-dynamic simulation. For the case study, we compute

¹²All data used for the gas and power network are available as native **SAInt** input files in the electronic version of this chapter and are described further in B.4.1. The properties of the power plants (see Table B.7), were chosen according to the data provided by [130, 131]

initially a combined steady state scenario and use the solution as an initial state for the combined quasi-dynamic scenarios studied in this chapter. The results of the combined steady state simulation are plotted in Fig. 5.7 and listed in Tables B.8-B.11. The simulation protocol, which includes information of the residual for the gas model, power model and coupling equations for each step of the sequential linearisation is attached to the electronic version of this thesis ([SAInt-Log-SteadyState](#)).

In the following sections, we simulate three scenarios and discuss their results. All three scenarios were computed on an Intel Core i7-3630QM 2.4 GHz CPU with 8GB RAM and a 64-Bit Windows 10 Operating System.

5.4.1. Case 0 - Base case scenario with intermittent wind power generation and backup by spinning reserve GFPP

In case 0, we study a base case scenario, where wind power generation at bus GEN.22 is not available for some time intervals, due to insufficient wind velocity. We use the functionality to define conditional scenario parameters in **SAInt** to enforce the start-up of the backup GFPP connected to bus GEN.12 in case wind power generation at bus GEN.22 falls below 1 MW within two consecutive simulation time steps (see Fig. 5.4). However, the start-up of the backup GFPP, is only possible if there is enough linepack in subsystem GSUB.EAST and if the pressure in the corresponding fuel gas node (NO.23) is above 35 bar-g, in order to avoid a minimum pressure violation at start-up ($p^{min} = 30$ bar-g). For all CGSs in the gas network, we assign the relative load profile depicted in the left plot of Fig. 5.8 and scale the value with the computed steady state loads. For all active and reactive loads at substations connected to the local distribution system (LDC) we factor the relative load profile depicted in the right plot of Fig. 5.8 with the steady state power system loads. All other loads in both networks are assumed constant (i.e. loads of IND & CBE). The relative profile for wind generation visualized in Fig. 5.9 is assigned to the wind power generator connected to bus GEN.22 and is scaled with the steady state active wind power generation (60 MW). Fig. 5.10 shows a snapshot of the **SAInt**-electric network scenario table, where the boundary conditions and the implementation of the start-up and shut down of GFPPs is implemented.

For the given settings in case 0, we do not expect any significant impact on security of supply for both networks, since the available generation capacity provided by the backup GFPP should be sufficient to cover the system loads at times of missing wind power generation.

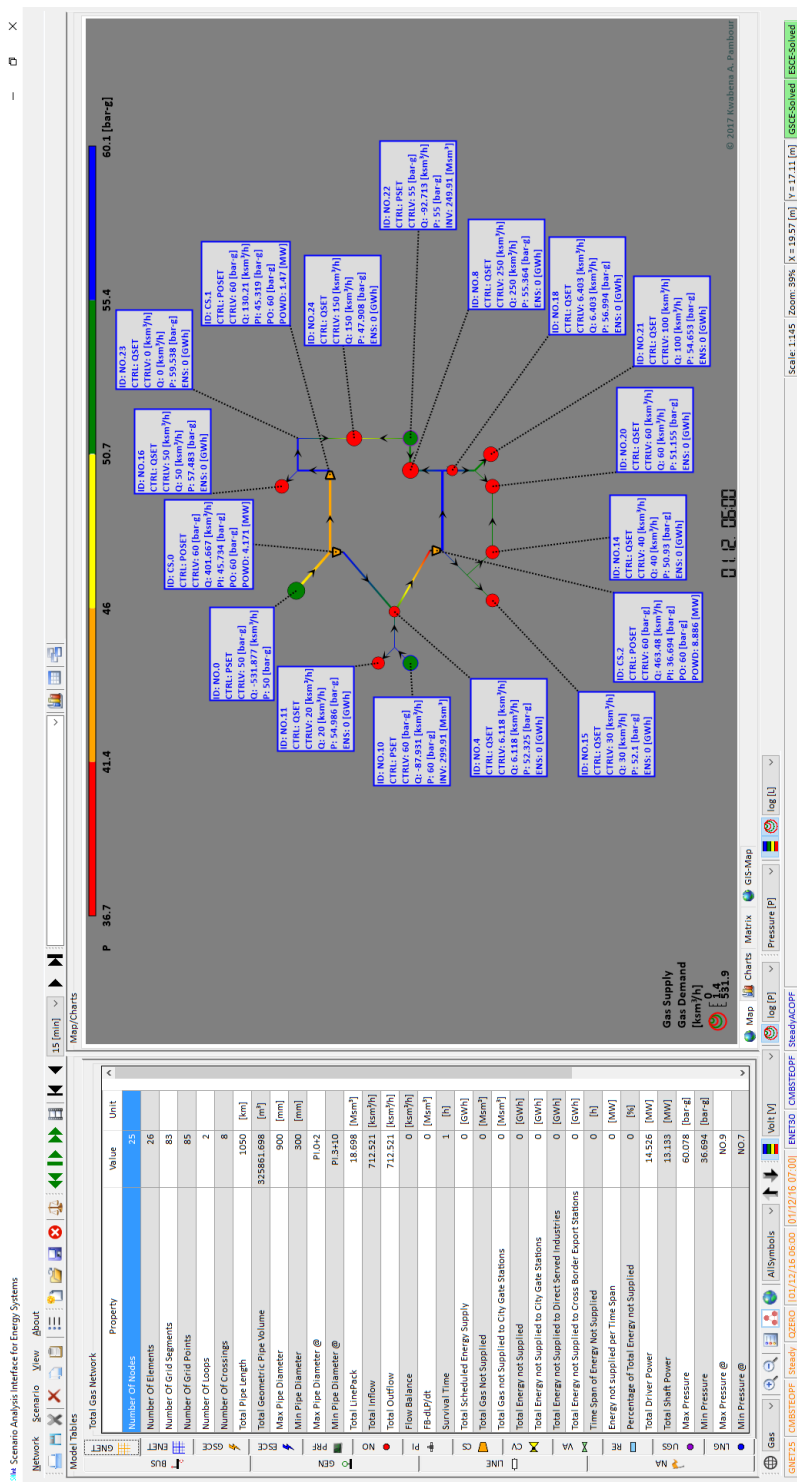


Fig. 5.6: Snapshot of SAInt-GUI showing results of the combined steady state computation for the gas network in the case study. Diameter of the circles representing demand (red) and supply (green) nodes in the top plot correspond to the magnitude of the steady state loads in logarithmic scale, as can be seen from the legend in the bottom left corner. Colors of the pipe elements correspond to the pressure levels as indicated by the top color bar. Pipe arrows indicate gas flow direction.

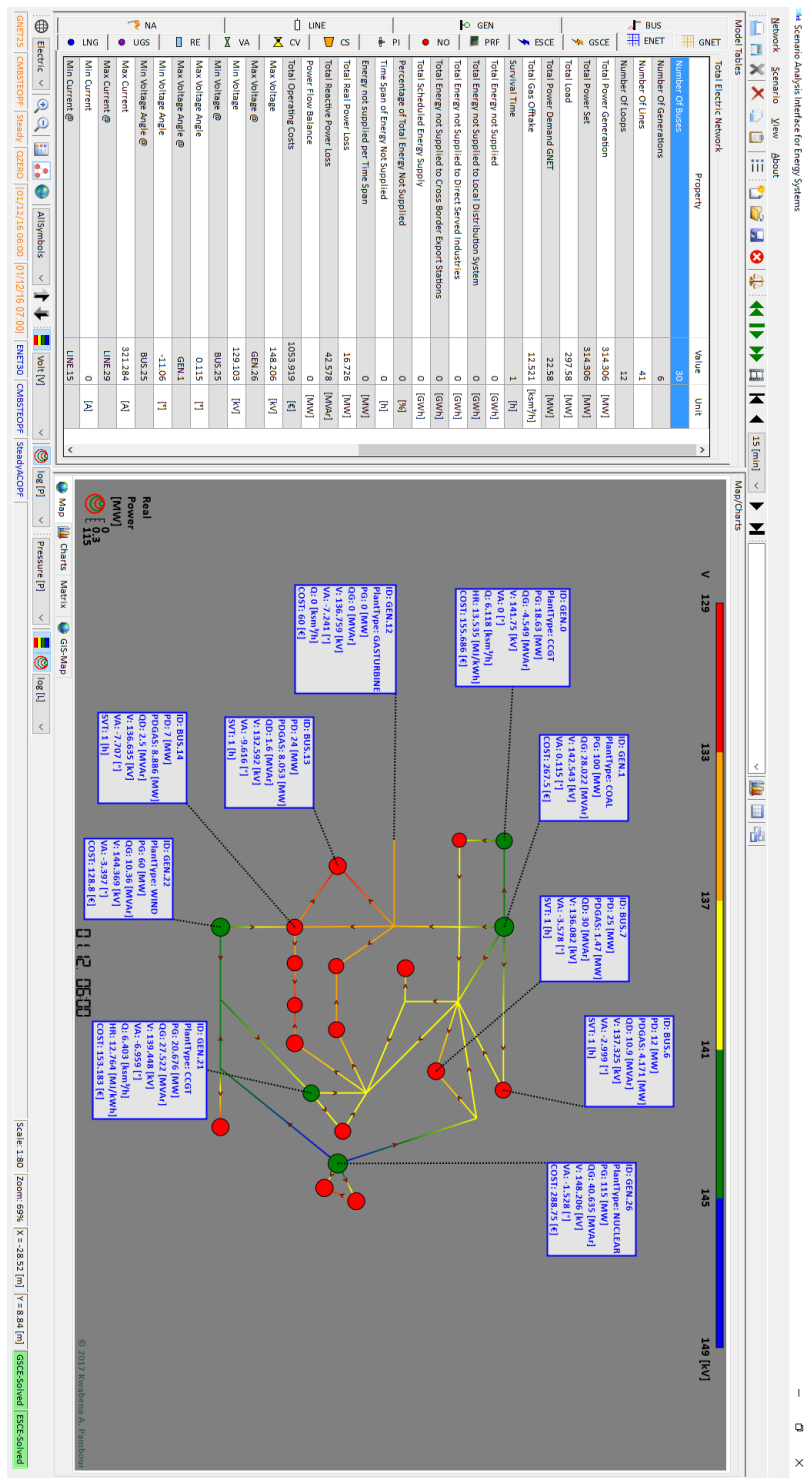


Fig. 5.7.: Snapshot of SAInt-GUI showing results of the combined steady state computation for the electric network in the case study. Diameter of the circles representing load (red) and generation (green) buses in the bottom plot correspond to the magnitude of active power in logarithmic scale, as can be seen from the legend in the bottom left corner. Colours of the line elements correspond to the voltage levels as indicated by the top color bar. Line arrows indicate flow direction of electric current. Labels describe the results and properties for selected objects in the combined system.

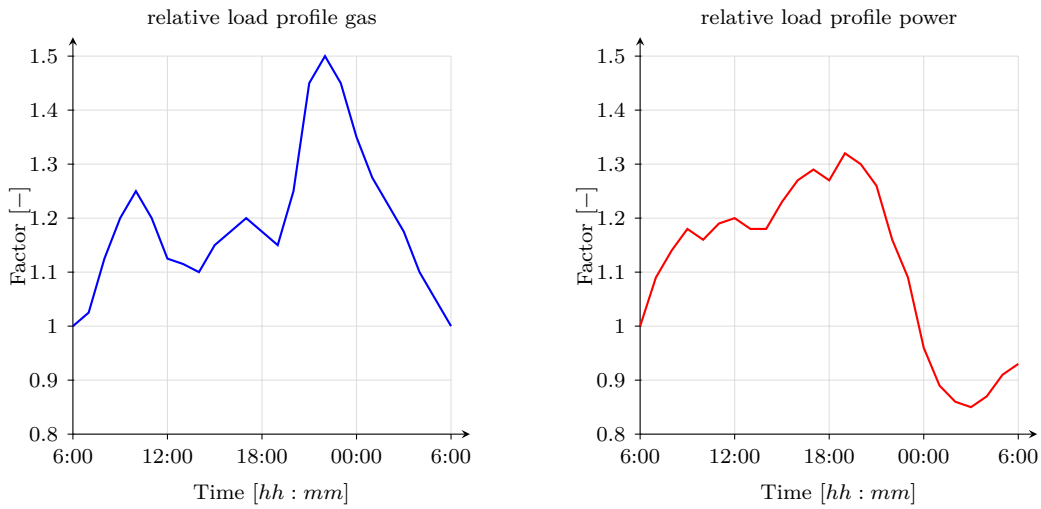


Fig. 5.8.: Load profile assigned to CGS in gas network (left side) and active power load at buses in electric power network (right side)

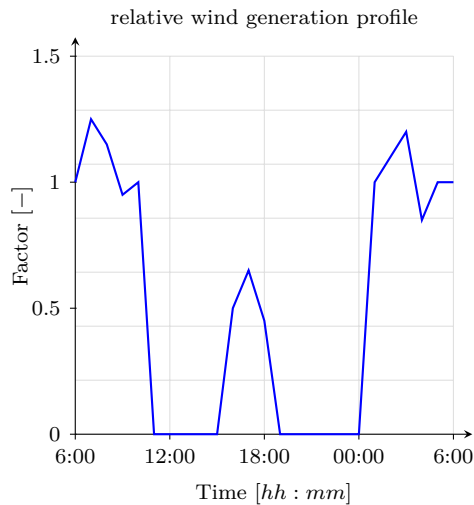


Fig. 5.9.: Relative profile for variable and intermittent wind power generation assigned to bus GEN.22

The results for case 0 are illustrated in the time plots depicted in Fig. 5.11 & 5.14 and in the animation video [SAInt_Case0](#) generated with **SAInt** and attached to the electronic version of the thesis. The simulation protocol for case 0 [SAInt-Log-Case0](#), which contains information on the residual for each simulation time step and the changes in control and

The SAInt - Table for ESE									
Active	Time	Object	^ Nr	Condition	Evaluation	Name	Parameter	Profile	Value
<input checked="" type="checkbox"/>	01/12 06:00	BUS	15			Bus015	P0	LOADPRF	9 [MW]
<input checked="" type="checkbox"/>	01/12 06:00	BUS	16			Bus016	P0	CONST	15 [MW]
<input checked="" type="checkbox"/>	01/12 06:00	BUS	17			Bus017	Q0	LOADPRF	9 [MW]
<input checked="" type="checkbox"/>	01/12 06:00	BUS	14			Bus014	P0	LOADPRF	7 [MW]
<input checked="" type="checkbox"/>	01/12 06:00	BUS	29			Bus029	P0	CONST	35 [MW]
<input checked="" type="checkbox"/>	01/12 06:00	BUS	15			Bus015	Q0	LOADPRF	18 [MW]
<input checked="" type="checkbox"/>	01/12 06:00	BUS	17			Bus017	P0	LOADPRF	10 [MW]
<input checked="" type="checkbox"/>	01/12 06:00	BUS	20			Bus020	P0	CONST	16 [MW]
<input checked="" type="checkbox"/>	01/12 06:00	BUS	25			Bus025	P0	CONST	30 [MW]
<input checked="" type="checkbox"/>	01/12 06:00	BUS	28			Bus028	P0	CONST	30 [MW]
<input checked="" type="checkbox"/>	01/12 06:00	BUS	18			Bus018	P0	CONST	8 [MW]
<input checked="" type="checkbox"/>	01/12 06:00	BUS	19			Bus019	Q0	LOADPRF	7 [MW]
<input checked="" type="checkbox"/>	01/12 06:00	BUS	19			Bus019	P0	LOADPRF	25 [MW]
<input checked="" type="checkbox"/>	01/12 06:00	BUS	13			Bus013	Q0	LOADPRF	16 [MW]
<input checked="" type="checkbox"/>	01/12 06:00	BUS	6			Bus005	Q0	LOADPRF	10.9 [MW]
<input checked="" type="checkbox"/>	01/12 06:00	BUS	6			Bus005	P0	LOADPRF	12 [MW]
<input checked="" type="checkbox"/>	01/12 06:00	BUS	7			Bus007	Q0	LOADPRF	30 [MW]
<input checked="" type="checkbox"/>	01/12 06:00	BUS	14			Bus014	Q0	LOADPRF	2.5 [MW]
<input checked="" type="checkbox"/>	01/12 06:00	BUS	2			Bus002	Q0	LOADPRF	1.2 [MW]
<input checked="" type="checkbox"/>	01/12 06:00	BUS	2			Bus002	P0	LOADPRF	5 [MW]
<input checked="" type="checkbox"/>	01/12 06:00	BUS	10			Bus010	P0	LOADPRF	24 [MW]
<input checked="" type="checkbox"/>	01/12 06:00	BUS	13			Bus013	P0	LOADPRF	24 [MW]
<input checked="" type="checkbox"/>	01/12 06:00	BUS	7			Bus007	P0	LOADPRF	25 [MW]
<input checked="" type="checkbox"/>	01/12 06:00	BUS	10			Bus010	Q0	LOADPRF	1.75 [MW]
<input checked="" type="checkbox"/>	01/12 06:00	GEN	22			Bus022	P0	WINDPRF	60 [MW]
<input checked="" type="checkbox"/>	01/12 06:00	GEN	0	NO 4 P[bus02]>35 and GSUB/WEST[Lp]Mem3>1.5		Bus000	ON	-	
<input checked="" type="checkbox"/>	01/12 06:00	GEN	0	NO 4 P[bus02]<30 or GSUB/WEST[Lp]Mem3>1.5		Bus000	OFF	-	
<input checked="" type="checkbox"/>	01/12 06:00	GEN	12	(GEN 22 PG [MW] < 1 and GEN 22 PG [time=dt] [MW] > 1) and (NO 23 P[bus02]>35 and GSUB/EAST[Lp]Mem3>3)		Bus012	ON	-	
<input checked="" type="checkbox"/>	01/12 06:00	GEN	12	(GEN 22 PG [MW] > 1 and GEN 22 PG [time=dt] [MW] > 1) or GSUB/EAST[Lp]Mem3<3		Bus012	OFF	-	
<input checked="" type="checkbox"/>	01/12 06:00	GEN	21	NO 18 P[bus02]>35 and GSUB/SOUTH[Lp]Mem3>6		Bus021	ON	-	
<input checked="" type="checkbox"/>	01/12 06:00	GEN	21	NO 18 P[bus02]<30 or GSUB/SOUTH[Lp]Mem3>6		Bus021	OFF	-	

Fig. 5.10.: SAInt scenario definition table showing the defined boundary conditions for the electric network for case 0 and the conditional expression for the shut-down and, start-up of GFPs in respect to their corresponding nodal gas pressure and linepack in the corresponding subsystem. Each boundary condition is composed of a simulation time (i.e. time at which the boundary condition is evaluated by the solver for the first time), a reference object, a parameter and its value (the value can also be an IronPython expression referring to properties of objects in the model) and a conditional expression and its evaluation type (choice of how often the condition should be evaluated by the solver in the course of the simulation). For some parameters a profile can be assigned by specifying the profile name, after the profile is created in the SAInt-profile editor introduced in Chapter 3. The variable "time" in the conditional IronPython expression denotes the elapsed simulation time in hours at which the expression is evaluated, while the variable "dt" denotes the time duration in hours between the last two consecutive simulation time steps, i.e. $dt = t_n - t_{n-1}$.

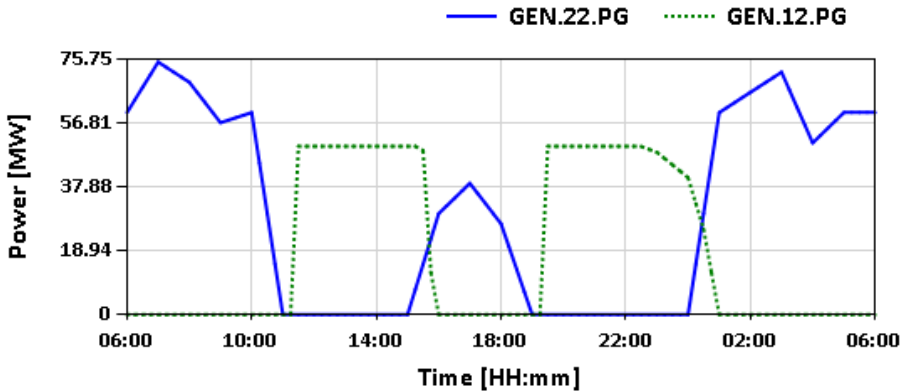


Fig. 5.11.: Case 0 - Time plot for active power generation (P_G) at buses GEN.12 and GEN.22

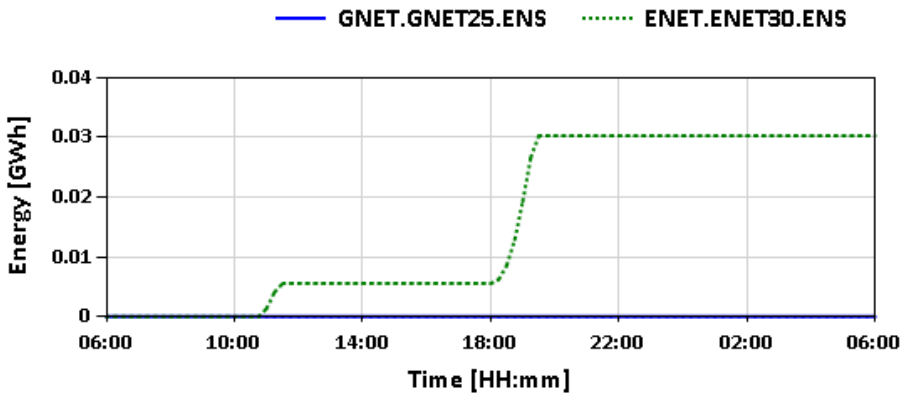


Fig. 5.12.: Case 0 - Time plot for Energy Not Supplied (ENS) for the total gas (blue curve) and total electric network (green curve)

active constraints of active gas facilities, is also available in the electronic version of the thesis. The computation for case 0 took approximately 10 s for 96 time steps.

Figure 5.11 shows the time evolution of the active power generation (P_G) at buses GEN.22 (blue curve, wind generation) and GEN.12 (green curve, backup GFPP). As can be seen, the GFPP starts-up whenever wind power generation is zero and shuts down whenever it is above zero. The start-up of the GFPP, however, is always delayed by approx. 30 min after loss of wind power generation, due to the transitional constraints (limit for start-up time is ≥ 15 min for GFPPs, see Table B.7) explained in Section 5.2.1 and defined in Table B.7

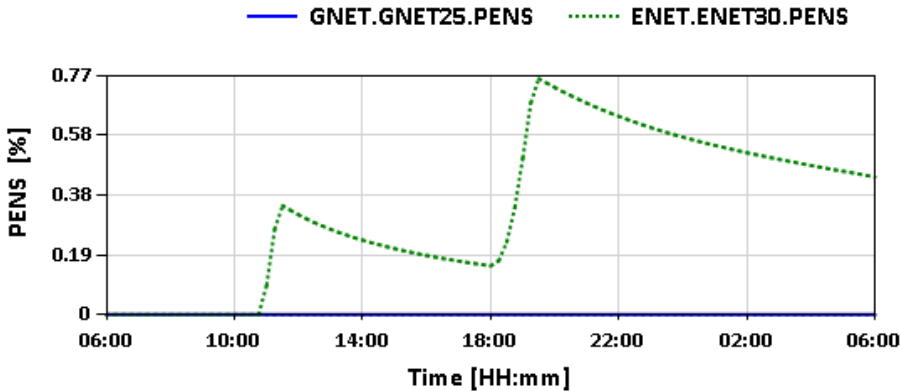


Fig. 5.13.: Case 0 - Time plot for Percentage of Energy not Supplied (ENS) for the total gas (blue curve) and total electric network (green curve)

and the conditional expression for starting-up and shutting down GFPPs after the active power generation is below or above 1 MW for two consecutive time steps, respectively. The impact of the delay in backup power on security of energy supply is visible in the time plot for ENS and PENS for the total gas and total electric power system depicted in Fig. 5.12 & 5.13. While the ENS and PENS for the gas system remain zero, security of supply in the electric power system is affected exactly at times, where there is a delay in backup power generation by the backup GFPP connected to GEN.12. The power system implements load shedding in order to balance the reduced generation capacity, which is visible by the increase in ENS and PENS at approx. 10:45 and 18:15. However, the impact of the load shedding is relatively small, since the PENS is less than 1 %. One way to avoid load shedding would be to set the wind power generation threshold for starting-up the GFPP to a higher value. However, this may also result in an increased number of start-up and shut down cycles, which, in turn, is connected to higher operational costs.

Besides, without the extension of the basic ED by the dispatchable load model derived in Section 5.2.1, the combined model would not have converged to a feasible solution, due to insufficient generation capacity to balance the power system loads. The ramping of the backup GFPP is possible, because there is enough pressure at the corresponding fuel gas offtake node in the gas system and sufficient linepack in the corresponding subsystem GSUB.EAST, as can be seen in Fig. 5.14, where the time plot of the unit state at GEN.12, the fuel gas offtake and pressure at gas node NO.23 and the linepack in subsystem GSUB.EAST is illustrated.

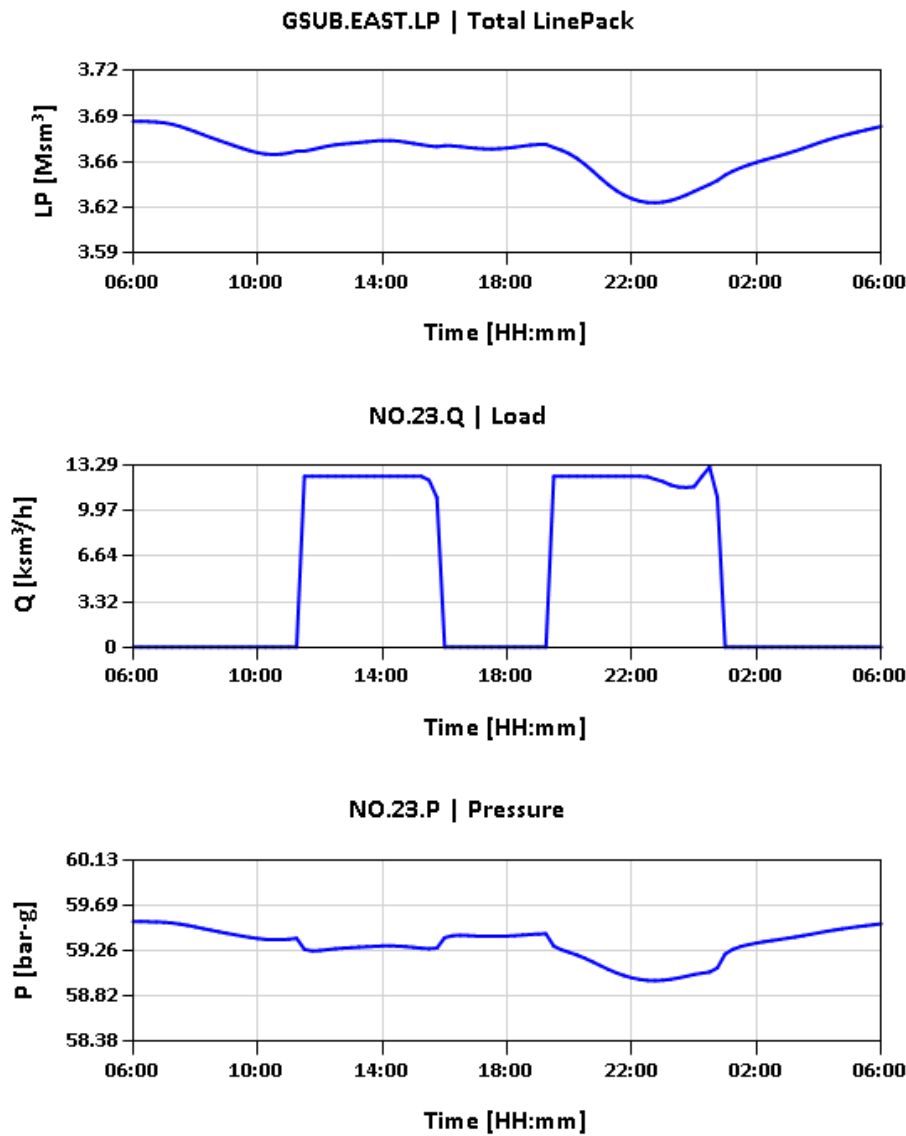


Fig. 5.14.: Case 0 - Time plot for linepack in subsystem GSUB.EAST (LP), nodal pressure (P) and fuel gas offtake for power generation (Q) at node NO.4

5.4.2. Case 1 - Disruption in compressor station CS.1

In this section, we examine how a disruption in compressor station CS.1 affects security of supply in the combined system. The gas flow through CS.1 is interrupted completely (OFF) at 14:00 for 8 hours, due to a failure in the compressor station¹³. At 22:00, the failure in the station is remedied, but the start-up of the station is delayed for another 4 hours. However, in this time the flow can bypass (BP) the station without gas compression until the station returns to its original control set point at 02:00 (outlet pressure control of 60 bar-g). The described events are visualized in Fig. 5.15, where the time evolution of the control of compressor station CS.1 is depicted. All boundary conditions and settings from case 0 are carried over to case 1.

We expect a stronger impact of the disruption on security of supply in the gas network than in the electricity network. For the gas network, the disruption in CS.1 may cause the pressure and line pack in the downstream hydraulic area to drop. Therefore, the scheduled gas demand in the area may not be covered due to insufficient gas pressure. This in turn, may also influence the start-up of the backup GFPP for balancing the missing wind power generation, which requires a specific fuel gas pressure and available linepack to operate.

The results for case 1 are illustrated in the time plots depicted in Fig. 5.15 & 5.22 and in the animation video [SAInt_Case1](#) attached to the electronic version of the thesis. The simulation protocol for case 1 ([SAInt-Log-Case1](#)) is also available in the electronic version of the thesis. The computation for case 1 took approximately 22 s for 100 time steps.

Figure 5.16 shows the reaction of the inlet and outlet pressure to the disruption and the control changes at compressor station CS.1. The interruption of gas flow through the station at 14:00 caused a rapid decrease in outlet pressure and a slight increase in inlet pressure. The inlet pressure stabilizes to a constant pressure due to the pressure control at the CBI station connected to node NO.0. As can be seen in the animation video for case 1 ([SAInt_Case1](#)), the gas supply from NO.0 decreases right after the interruption of gas flow at CS.1 to avoid an overpressure in the subsystem GSUB.NORTH. The reduction of the outlet pressure is a result of an imbalance between gas offtake (IND at NO.16 & CGS at NO.24) and gas supply (UGS at NO.22) to the downstream hydraulic area (area in GSUB.EAST separated by the outlet node of CS.1 and the pressure controlled UGS node NO.22). Thus, the linepack and the average pressure in the hydraulic area decreases

¹³Case 1 is a hypothetical scenario to demonstrate the capability of the developed model to simulate and estimate the impact of supply disruptions. In practice, a failure in a compressor station would not necessarily result in a complete shut-down and stop of flow, but rather the flow will bypass the station without compression through a designated bypass valve system. However, in this case study, we assume the bypass valve cannot be opened, due to a technical failure

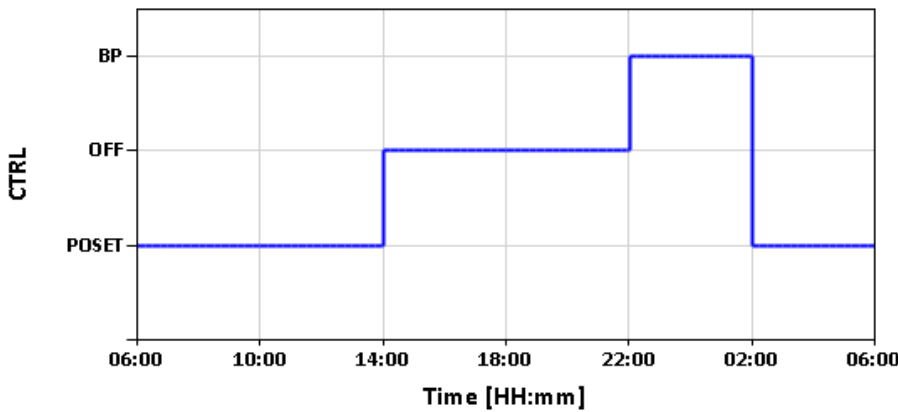


Fig. 5.15.: Case 1 - Time plot of the station control (*CTRL*) of compressor station CS.1

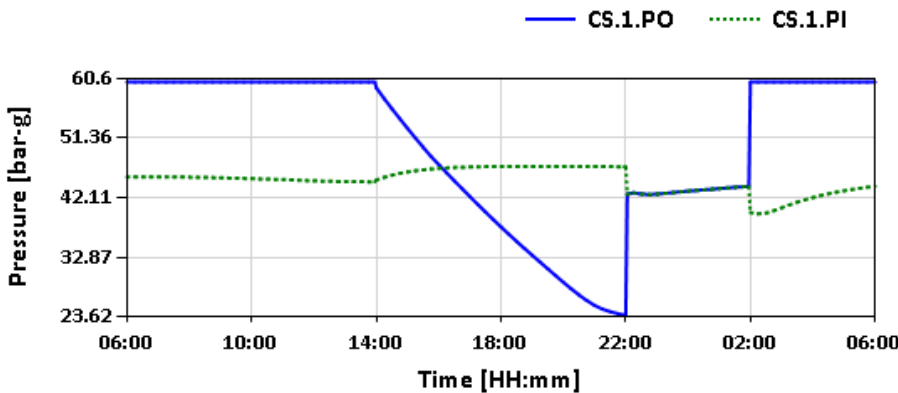


Fig. 5.16.: Case 1 - Time plot of the inlet and outlet pressure of compressor station CS.1

rapidly (the flow imbalance between NO.16, NO.24 and NO.22 right after the disruption can be seen in the animation video for case 1 ([SAInt_Case1](#)). The pressure and linepack in the hydraulic area decreases to an extend that at a certain simulation time the gas offtake at NO.16 and NO.24 are curtailed in order to maintain the minimum operating pressure of 25 bar-g and 16 bar-g, respectively (see simulation protocol [SAInt-Log-Case1](#) and animation video [SAInt_Case1](#) for more details). The simulation time at which the curtailment of gas demand is initiated is shown in the time plot of the TSP for the gas network depicted in Fig. 5.20 (blue curve). The TSP starts increasing linearly at approx. 20:00, 6 hours after the disruption in CS.1. This is the grace period for the gas TSO to react to the contingency, by deploying an emergency plan to mitigate or avoid the impact

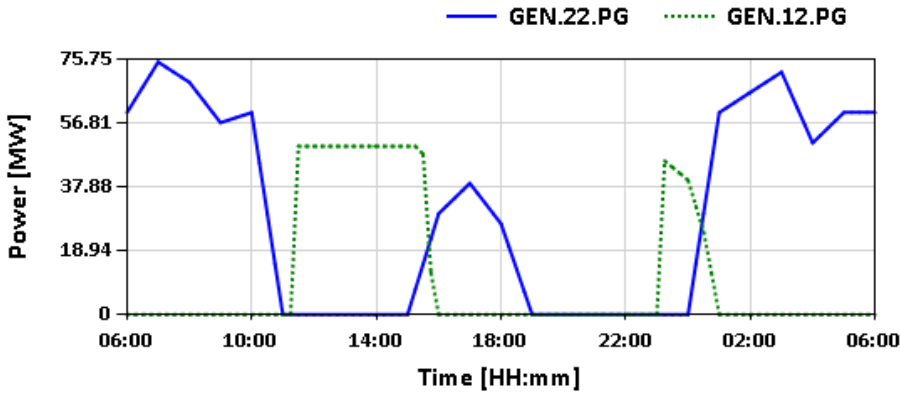


Fig. 5.17.: Case 1 - Time plot for active power generation (PG) at buses GEN.12 and GEN.22

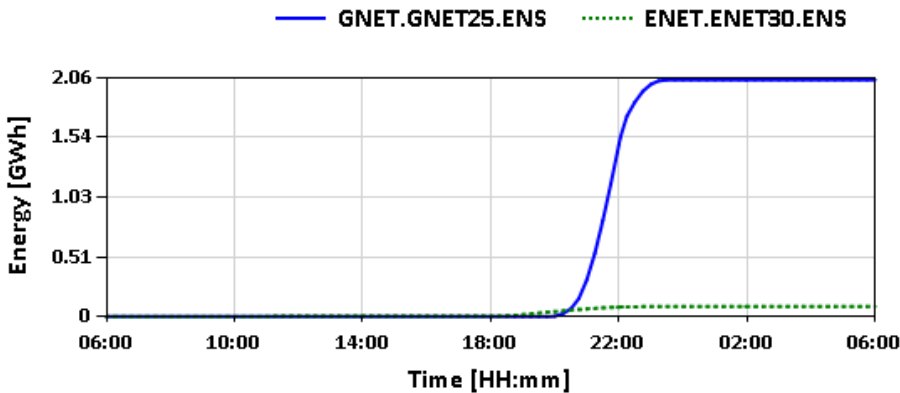


Fig. 5.18.: Case 1 - Time plot for Energy Not Supplied (ENS) for the total gas (blue curve) and total electric network (green curve)

of the disruption on security of supply. A counter measure could be for instance, to set the withdrawal from the UGS facility connected to node NO.23 to maximum withdrawal capacity. The information obtained for the grace period would not be available if instead of a dynamic model a steady state gas model was used, since the imbalance between supply and demand and, thus, the change in pressure and linepack cannot be reflected with the steady state approach.

The disruption in the gas system propagates also to the electric power system and affects security of supply in the power system, as can be seen in Fig. 5.17 & 5.22, where the active

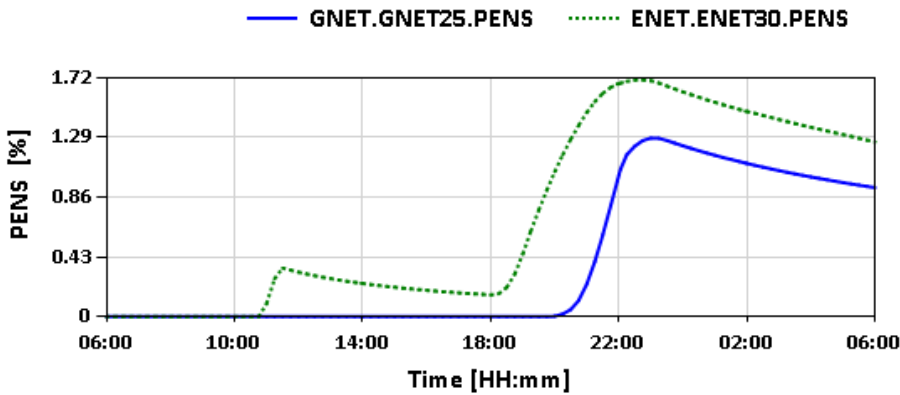


Fig. 5.19.: Case 1 - Time plot for Percentage of Energy Not Supplied (PENS) for the total gas (blue curve) and total electric network (green curve)

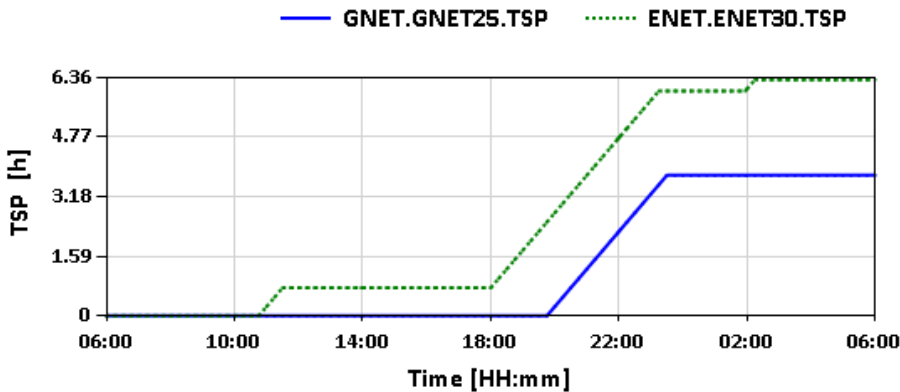


Fig. 5.20.: Case 1 - Time plot for Time Span of Energy Not Supplied (TSP) for the total gas (blue curve) and total electric network (green curve)

power generation at buses GEN.22 and GEN.12, the linepack in subsystem GSUB.EAST and the fuel gas offtake and pressure at node NO.23 are depicted. The start-up of the backup GFPP connected to bus GEN.12 after the loss of wind power generation at approximately 19:00 is delayed for approximately 4 hours (compare Fig. 5.11 to 5.11), due to insufficient fuel gas pressure at node NO.23 and linepack in subsystem GSUB.EAST. Because of this delay, the generation capacity in the electricity system is insufficient to balance the power system loads. Thus, some loads in the power system are curtailed in respect to the priority factors assigned to the different load buses in Table B.5.

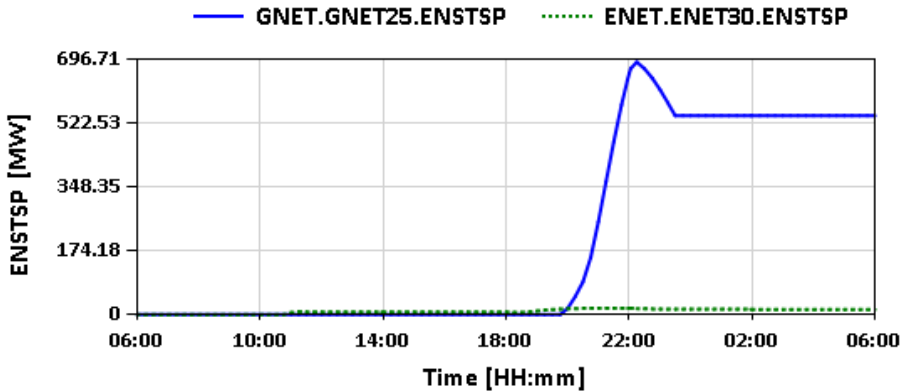


Fig. 5.21.: Case 1 - Time plot for Energy Not Supplied per Time Span of Energy Not Supplied (ENSTSP) for the total gas (blue curve) and total electric network (green curve)

The impact of the disruption on security of supply for the total gas and electricity network is depicted in Fig. 5.18 - 5.21. In absolute terms, the gas system is more affected by the disruption than the electricity system (see Fig. 5.18), since the ENS for the gas network is significantly higher than the ENS for the electricity network (ca. 2 GWh compared to ca. 0.1 GWh), while in relative terms, the impact is slightly higher for the electricity network than for the gas network as can be seen in Fig. 5.19. Furthermore, the survival time for the total gas system is 6 h and for the electricity system 8 h (see Fig. 5.19), assuming a survival time tolerance of $\epsilon_{svt} = 1\%$ for the PENS of the total system. This means that the time span between the disruption event and the point in time at which the total ENS is about to exceed 1 % of the expected or scheduled total energy supply is 6 h or 8 h, respectively. This crucial time information can be regarded as the grace period for gas and power TSOs to coordinate and react to the contingency.

Figures 5.20 & 5.21 show how long the disruption affected the total gas and electricity system (TSP) and the average rate of energy not supplied per time span (ENSTSP). As can be seen, the power system was affected by the disruption for a longer time period than the gas system (6.3 h compared to 3.75 h). However, due to the relatively large magnitude of the ENS for the gas system compared to the ENS for the electric power system (see. Fig. 5.18) the ENSTSP for the gas system is significantly greater than the one for the power system.

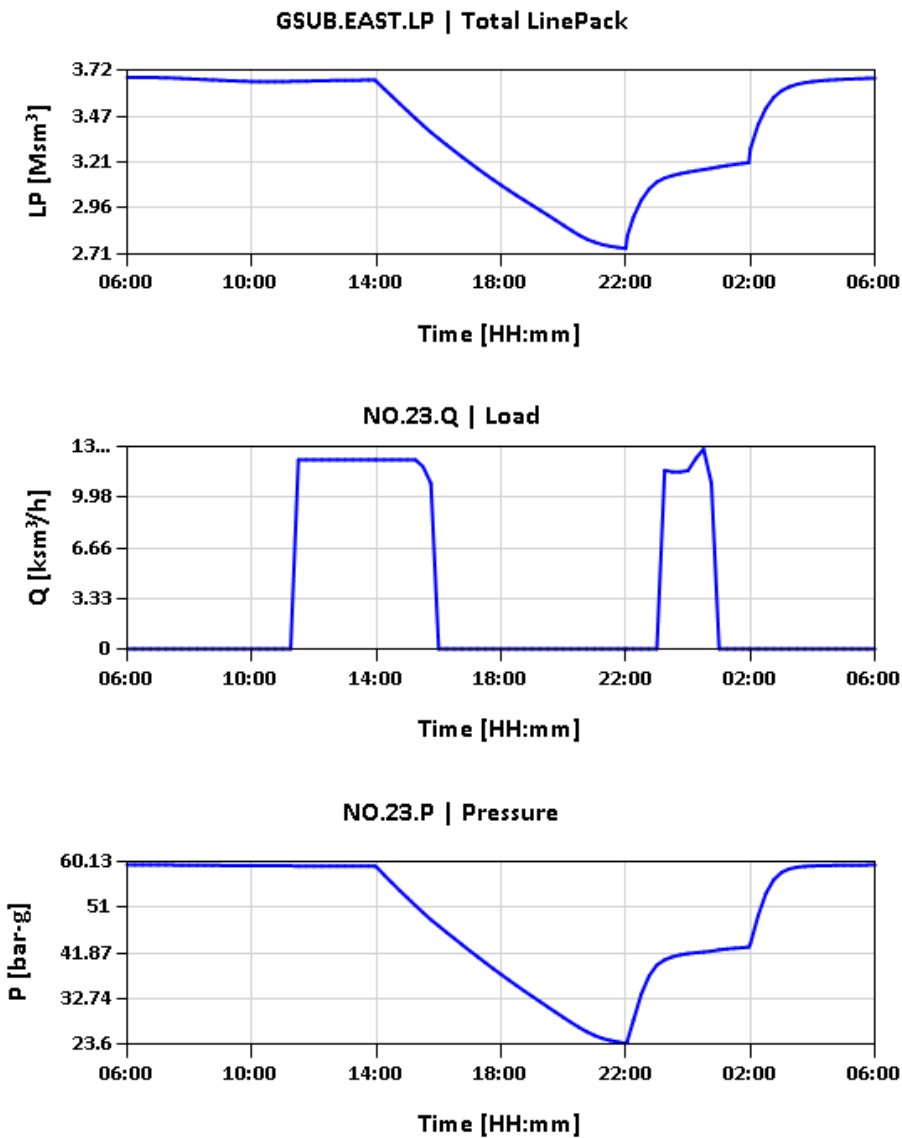


Fig. 5.22.: Case 1 - Time plot for linepack in subsystem GSUB.EAST (LP), nodal pressure (P) and fuel gas offtake for power generation (Q) at node NO.4

5.4.3. Case 2 - Full withdrawal capacity at gas storage facility to mitigate the impact of compressor station disruption

In this section, we investigate the effectiveness of a countermeasure to mitigate the impact of the disruption in compressor station CS.1, by enforcing the UGS facility connected to node NO.23 to increase its pressure set point to maximum operating pipeline pressure of 60 bar-g if the linepack in subsystem GSUB.EAST is below 3.3 Msm³. All boundary conditions and events defined in case 1 are carried over to case 2.

We expect this countermeasure to reduce the impact on security of supply in the gas and electricity system. However, we expect the gas system to benefit more from the countermeasure than the electricity system, since the countermeasure is applied in the gas system.

The results for case 2 are illustrated in the time plots depicted in Fig. 5.23 & 5.27 and in the animation video [SAInt_Case2](#) attached to the electronic version of the thesis. The simulation protocol for case 2 ([SAInt-Log-Case2](#)) is also available in the electronic version of the thesis. The computation for case 2 took approximately 23 s for 101 time steps. Figure 5.23 shows the time plot of gas offtake (Q) gas pressure (P) station control ($CTRL$)

GNET	$ENS(T_{max})$	$PENS(T_{max})$	$TSP(T_{max})$	$ENSTSP(T_{max})$	$SVT(1\%)$
	[GWh]	[%]	[h]	[MW]	[h]
Case 1	2.04	0.93	3.75	543.09	8
Case 2	1.31	0.60	3.25	403.23	-
Δ	-35.68 [%]	-35.48 [%]	-13.33 [%]	-25.75 [%]	-

Tab. 5.2.: Summary of results for security of supply parameters for gas network

ENET	$ENS(T_{max})$	$PENS(T_{max})$	$TSP(T_{max})$	$ENSTSP(T_{max})$	$SVT(1\%)$
	[GWh]	[%]	[h]	[MW]	[h]
Case1	0.09	1.26	6.30	14.02	6
Case2	0.05	0.66	4.45	10.41	-
Δ	-47.57 [%]	-47.62[%]	-29.37[%]	-25.76[%]	-

Tab. 5.3.: Summary of results for security of supply parameters for electric network

and the storage envelope showing the working points for the UGS facility connected to node NO.4. As can be seen, the UGS facility reacts to the disruption at approximately 16:45 when the linepack in subsystem GSUB.EAST is lower than 3.3 Msm³. The pressure set point is increased to 60 bar-g, however, this set point cannot be maintained at all

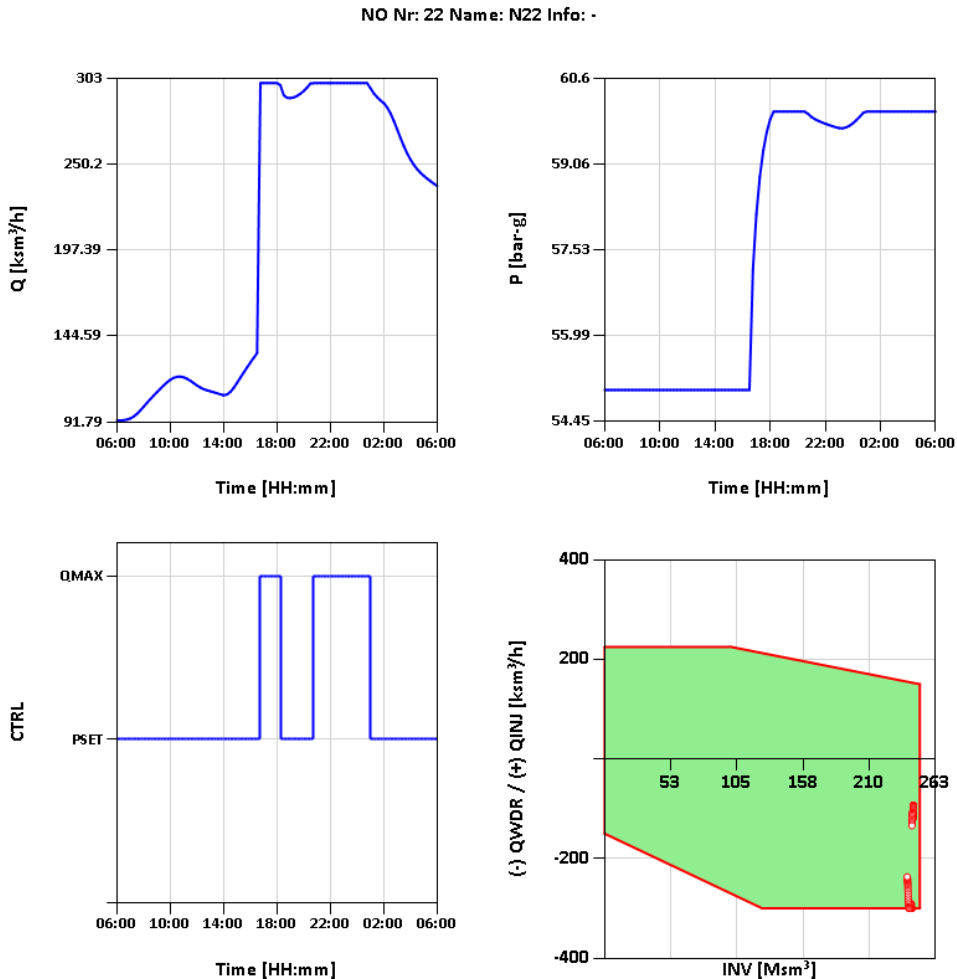


Fig. 5.23.: Case 2 - Time plot of gas offtake (Q) gas pressure (P) station control ($CTRL$) and the operating gas storage envelope (withdrawal and injection rate versus working inventory) for the UGS facility connected to node NO.4

time, due to the maximum withdrawal capacity limit of 300 ksm^3/h illustrated in the operating envelope of the UGS facility.

The increased withdrawal from storage has a positive effect on security of supply in the gas and electricity network, which is visible, if we compare the time plots from case 1 for ENS, PENS, TSP and ENSTSP (see Fig. 5.18-5.21) to the time plots for case 2 shown in Fig. 5.24-5.27. The values of the security of supply parameters at the end of the simulation

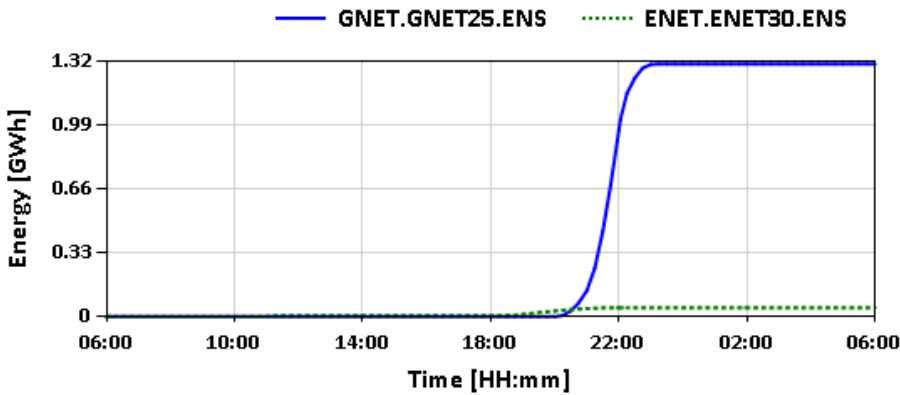


Fig. 5.24.: Case 2 - Time plot for Energy Not Supplied (ENS) for the total gas (blue curve) and total electric network (green curve)

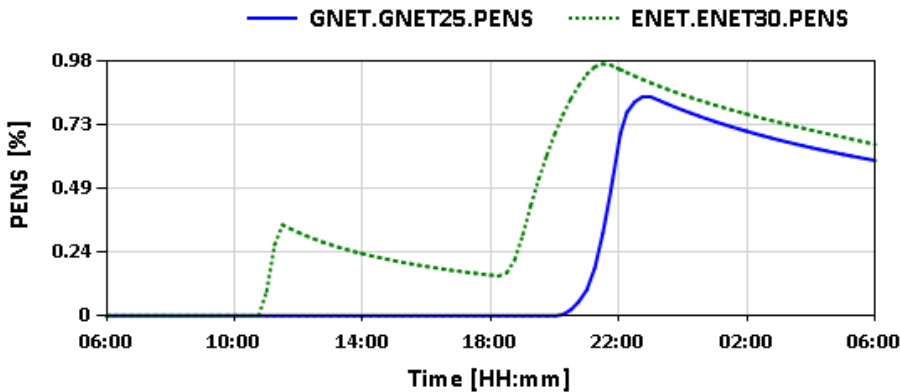


Fig. 5.25.: Case 2 - Time plot for Percentage of Energy Not Supplied (PENS) for the total gas (blue curve) and total electric network (green curve)

(T_{max} are summarized in Tables 5.2 & 5.3. The ENS for the gas system is reduced by more than 35 % and for the electricity system by almost 48 %. In addition, the SVT for both systems is increased to unlimited, since the total PENS for case 2 is always lower than the survival time tolerance of 1 %. Moreover, the TSP for the gas system is reduced by almost 30 % and for the electricity system by more than 13 %. Finally, the ENSTSP for both systems is reduced by roughly 26 %. Therefore, we can conclude that the countermeasure deployed in the gas system reduced the impact of the disruption triggered in compressor station CS.1 on security of supply in the combined gas and electric power

system. Moreover, the countermeasure was more effective for the electricity network than for the gas network, even though, it was deployed in the gas network.

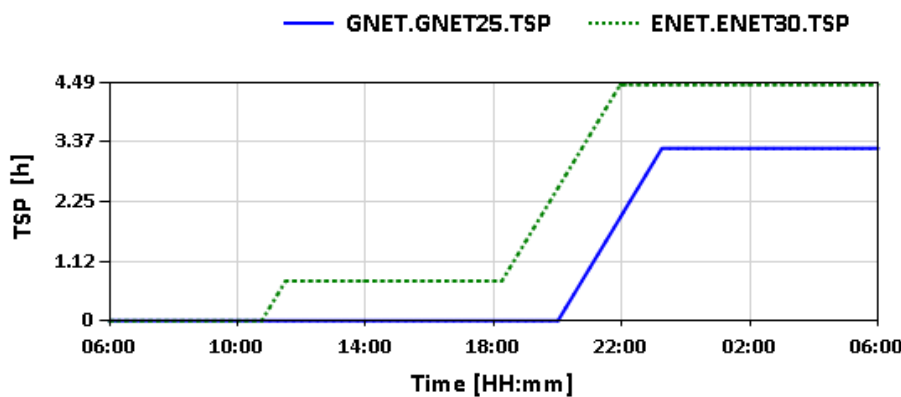


Fig. 5.26.: Case 2 - Time plot for Time Span of Energy Not Supplied (TSP) for the total gas (blue curve) and total electric network (green curve)

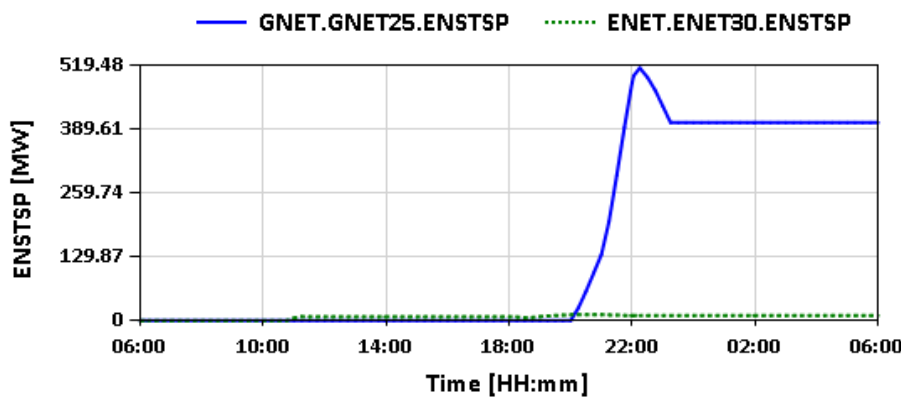


Fig. 5.27.: Case 2 - Time plot for Energy Not Supplied per Time Span of Energy Not Supplied (ENSTSP) for the total gas (blue curve) and total electric network (green curve)

5.5. Conclusion

In this chapter, we presented a novel quasi-dynamic simulation model for assessing security of supply in interconnected gas and electric transmission networks. The model consists of a transient hydraulic model for the gas system, which includes sub models of all important facilities and an extended ED for the electric power system, which contains a model for dispatchable loads and considers time transitional constraints such as the ramp rate and the start-up time of generation units. The models for the individual energy systems were combined through coupling equations describing the power supply to EDCSs and LNG terminals and the fuel gas offtake for power generation in GFPPs. The resulting system of equations describing the state change of the combined system between two consecutive time steps is solved iteratively by a sequential linearisation method, which updates the boundary conditions expressed by the coupling equations at each iteration step. In order to quantify the impact of contingencies on security of supply, we proposed five security of supply parameters, namely, (1) the energy not supplied, (2) the percentage of energy not supplied, (3) the survival time, (4) the time span of energy not supplied, and (5) the energy not supplied per time span.

The security of supply parameters together with the algorithm for the combined energy system were implemented into a novel simulation software named **SAInt**, the first published simulation tool that allows the combined simulation of interconnected gas and electric power systems in single time frame and simulation environment. The capabilities of the combined model and the functionality of the software tool were demonstrated in a case study of a sample combined gas and electric power system. The case studies were composed of three scenarios with supply disruptions triggered by the loss of wind power generation in the electric network (in all three cases 0, 1 & 2) and loss of gas compression and interruption of gas flow at a major compressor station (in case 1 and 2).

In case 0 the loss of wind power generation is compensated by a backup GFPP. However, due to the start-up time limits, which causes a short delay in power generation from GFPPs after the loss of wind power generation, some power system loads are curtailed, in order to balance the reduced generation capacity. The curtailment of the power system loads was enabled by the dispatchable load model added to the basic ED.

In case 1, the disruption in a compressor station affected gas offtake stations in the gas system and active power demand at load buses in the electric power system. The disruption caused the nodal gas pressure at the GFPP node and the linepack in the hydraulic area downstream the disrupted compressor station to fall below the threshold for starting-up and operating the GFPP. Thus, the start-up of the reserve GFPP to backup

the loss of wind power generation is delayed a couple of hours. During this time period the generation capacity in the electric network was insufficient to balance the scheduled or expected power system loads. Thus, the loads at a number of power system buses were curtailed based on a priority factor assigned to each load bus, in order to balance supply and demand in the electric network.

Finally, in the last case, we demonstrated how a countermeasure can be implemented to mitigate the impact of the disruption triggered in the compressor station and how the developed security of supply parameters can be utilized to evaluate the effectiveness of this countermeasure. The countermeasure consisted of increasing the withdrawal rate from a neighboring UGS facility to full withdrawal capacity by setting the pressure control set point of the facility to maximum operating pipeline pressure if the linepack in the affected hydraulic area goes below a certain threshold. The results for case 2 show that the countermeasure helped mitigate the impact of the disruption on security of supply in both energy networks, since all security of supply parameters were significantly reduced. Remarkably, the countermeasure had a stronger effect on the electric power system than on the gas system, though it was deployed in the gas system.

In summary, the case study demonstrate the very detailed level of information that can be obtained from the presented combined model implemented into **SAInt**. The type of information provided in this chapter cannot be obtained by a steady state approach for the gas system or by the co-simulation approach adopted in many scientific publications, due to their limitations. The provided information cannot only be used to analyse the propagation of contingencies, but also to develop and test strategies to react to contingencies, such as those described in the preventive action and emergency plan postulated in Regulation 994/2010 [12]. This may help gas and power TSOs, energy research institutes, policy makers, such as, competent authorities of EU-Member States, regulatory agencies etc. to take the right decisions on how to increase the resilience and security of supply in critical energy infrastructures. Furthermore, the security of supply parameters developed in this chapter, can be used for further analysis of gas and electric power system networks, such as sensitivity analysis, risk assessment or Monte Carlo simulation.

This chapter addressed the main research question of the thesis, namely, *how the consequences of disruptions in interconnected gas and electricity systems can be estimated*. The combined gas and electricity model together with the security of supply parameters developed in this chapter enable the estimation of consequences of different disruptions. The combined model was also used to assess the following sub-questions:

- *How can we quantify and compare the impact of supply disruptions on different gas customers?*
- *How can we quantify the grace period for gas and power TSOs to coordinate and react to supply disruptions?*
- *How can we evaluate the effectiveness of different countermeasures to mitigate supply disruptions?*

6. Conclusion

In this thesis, different simulation models for analysing the impacts of disruptions on security of supply in interdependent gas and electricity systems were developed.

In Chapter 2, a transient hydraulic gas model for simulating the operation of real world natural gas transport systems in terms of security of supply was developed. The model considers the physical equations describing the gas flow in pipelines and the most important facilities (e.g. compressor stations, entry and exit stations, underground storage facilities and LNG terminals) and their technical constraints. The set of equations describing the dynamics in gas transport systems were obtained by simplifying and adapting the full set of PDEs to the prevailing conditions in gas transport systems. The resulting equation system was discretised and linearised using an implicit time integration method. Furthermore, the gas model was validated against results from the literature and the commercial software package SIMONE. The comparison of the results confirmed the capability of the model to reflect the dynamic behaviour of gas transport networks in an adequate and accurate manner.

In Chapter 3, the transient gas simulation model developed and validated in Chapter 2, was extended by additional algorithms, for modelling the transition between different control mode changes and their interactions with different constraints imposed by controlled facilities in the gas network. Furthermore, the developed models, were implemented into a simulation tool named **SAInt**, which is divided into an Application Programming Interface (API), which is the main simulation engine of the software and a Graphical User Interface (GUI), which enables a visual communication between the user and the simulation engine. The software is designed for setting up and running simulations of different scenarios for a predefined gas network model. A dynamic scenario, for instance, contains the definition of a time window, an initial network state and a set of control settings for the different facilities in the gas network. The control settings are translated by the simulation engine into boundary conditions in order to solve the mathematical equations reflecting the physical operation of gas transport systems. The evaluation of each defined control setting may be triggered in respect to a predefined evaluation time and/or condition in the gas network model, which can be defined by a logical or arithmetic expression.

This enables the user to define an individual control logic for each controlled facility and the option to implement curtailments based on specific rules. Furthermore, the concept of subsystems was introduced, which allows dividing the gas network model into different network sections. The aggregated properties for each subsystem can be used to define conditional control settings for each facility. The capabilities of the developed software application to simulate gas supply disruptions and to model and asses demand and supply side measures to mitigate the impact of gas supply disruptions were demonstrated in a case study of a real world example.

After developing the gas network model and implementing it into the software application, the next step (Chapter 4) was dedicated to defining a model for the electric power system and to combine this model with the dynamic gas model to develop an integrated co-simulation platform for cascading outage contingency analysis in interconnected gas and power system networks. The model for the electricity system is based on steady state AC-optimal power flow simulation (AC-OPF) and includes sub models for the most important power system facilities such as transmission lines, transformers, buses, generation units as well as shunt capacitors and reactors. The AC-OPF model is implemented into the Matlab based open source power system library MATPOWER and considers the active and reactive power flow balance as well as the constraints of power system components such as the thermal capacity limits of transmission lines, the reactive power capability curves of generation units and the voltage limits at buses.

The gas and electricity model are integrated to a co-simulation platform by identifying the most important physical interconnections between the two systems and defining mathematical equations reflecting this interlink. These power gas interconnections include the fuel gas offtake of GFPPs for power generation in the electricity system and the power offtake from the electricity system for electric power supply to LNG terminals, and electric driven compressors installed in UGS facilities and gas compressor stations.

The co-simulation framework is divided into two separate simulation environments, namely, the gas system simulator (**SAInt**) and the power system simulator (MATPOWER). The communication and data exchange between **SAInt** and MATPOWER is established through an interface implemented into **SAInt** that makes use of the Matlab Automation Server to execute Matlab scripts, to exchange input and output data with Matlab workspace variables and to enable the visualisation of power system topologies and simulation results. Furthermore, the co-simulation interface is responsible for respecting the coupling equations between the two simulation models.

The co-simulation framework was applied to perform a case study on a realistic combined gas and power system network of an European region. The model application was divided

into three different scenarios, where different gas and power system contingencies were studied. In the first scenario, the normal operation of the combined system with no disruptions was studied and the results were compared to the second scenario with gas side disruptions and the third scenario with power side disruptions.

The simulation results demonstrated, how disruptions triggered in one system propagate to the other system. In the second scenario, for instance, three major gas supply stations were disrupted and as a result a number of GFPPs were shut-down due to insufficient fuel gas pressure. This contingency propagates further to other buses in the power system, where load shedding is implemented in order to maintain the voltage levels above the minimum voltage threshold. Similar observations are made in scenario 2, where a drastic reduction in renewable energy generation together with a shut-down of a large power plant triggered a large increase in gas demand of GFPPs, leading to a rapid pressure drop in the gas network and the subsequent shut-down of GFPPs. Eventually, this circumstance increased the stress on the power system leading to minimum bus voltage violations in a couple of buses, which is remedied by applying load shedding at the affected buses.

The co-simulation framework, was able to capture the propagation of disruptions from one energy system to the other, however, there were a number of aspects that could not be reflected appropriately due to the nature of the model.

Firstly, the coupling between the two energy systems were simulated in two different simulation time frames, thus there was no immediate feedback from one system as a result of a disruption in the other system. The power system was simulated for one operating day (24 hours) and the results computed for gas fired generators were used for calculating the corresponding fuel gas offtakes in the gas system. The gas offtakes, in turn, were used to simulate the gas system and to check if the gas system can operate under these conditions in terms of pressure limits at delivery points. If pressure limits were violated the gas system curtailed the computed fuel offtakes from the power system and the power system was simulated again using the fuel offtake constraints computed by the gas system and additional power requirements of electric driven compressors and LNG terminals. The fuel offtake constraints computed by the gas system reduces the generation capacities in the power system, thus, power system loads were curtailed in order to balance the system. The above iteration was repeated until a feasible solution for the two systems was found. In reality the changes in one system has immediate effect on physical properties (e.g. pressures, linepack, voltages, supply and demand) in the other system, which may cascade back to the system were it originated. However, these cascading effects cannot be captured by the co-simulation concept, where the time frames between the two systems are inherently different.

Secondly, the curtailment of power system loads were directly applied to buses that were affected by voltage violations based on a predefined rule. Priority levels between different power system customers were not considered, which may have an effect on the results. Finally, time transitional constraints of power system generators in terms of maximum ramp rates, start-up and shut down times were neglected, which may restrict the available generation capacities to balance the power system loads.

To overcome these deficiencies, in Chapter 5, a novel combined quasi-dynamic simulation model was developed and implemented into the simulation tool **SAInt**. The combined simulation model consists of the transient gas system model developed in Chapters 2 & 3, an extended steady state AC-OPF model and the coupling equations describing the physical interconnections between the two energy systems. The three model elements are integrated into one combined model which is solved in a single simulation time frame and environment. The extended AC-OPF model considers time transitional constraints of power system generators, such us ramp up/down limits as well as start up and shut down times and includes a model for dispatchable power system loads, which allows the consideration of priority levels in the event of load curtailments. The concepts for subsystems and scenarios developed for the gas model in Chapter 3 as well as the definition of conditional control mode changes for gas system facilities were extended to the electric power system model. Thus, the control logic of gas fired generators in the power system model could be designed based on the conditions in the gas system model. For instance, the start up and shut down of a gas fired power plant could be scheduled based on the pressure and linepack level in a specific section (subsystem) in the gas network model. In order to quantify the impact of contingencies on security of supply, and to compare the effectiveness of different countermeasures to mitigate the impacts of disruptions on security of supply a number of security of supply parameters were defined, such as energy not supplied, percentage of energy not supplied and survival time.

The capabilities of the combined simulation model were demonstrated in a case study of a sample combined gas and power system network. The case study consisted of three scenarios with gas and power side contingencies as well as mitigation measures to react to these disruptions.

In the first scenario, the operation of a gas generator was simulated, which serves as reserve and back up for variable and intermittent power generation from a wind turbine. In the second scenario a disruption in a gas compressor station was simulated which led to curtailments in the gas system and eventually to a delayed start up of the back up gas generator due to pressure restrictions in the gas system. The delayed start up of the gas generator caused a reduced generation capacity in the power system, which eventually led

to load curtailments in the power system based on a predefined priority level for each load bus. The impacts on security of supply in the two energy systems were compared using the security of supply parameters developed and implemented into **SAInt**. In terms of energy not supplied to customers, the impact of the disruption was higher for the gas system than for the power system. However, in terms of the ratio between energy not supplied and total scheduled energy supply (i.e. percentage of energy not supplied) the impact of the disruption was higher for the power system than for the gas system. Finally, in the last scenario the effectiveness of a countermeasure to mitigate the impact of the disruption in the gas compressor station was examined. The countermeasure was to increase the withdrawal rate from a neighbouring underground storage facility to maximum capacity if the linepack in the affected region goes below a specific value. Simulation results indicated a reduction of the impact on security of supply as a result of the implementation of the countermeasure.

The models and tools developed in this thesis demonstrate the importance of considering the interdependencies between gas and electricity systems when assessing the reliability of critical energy infrastructures. The information provided by the simulation models can be used to improve the coordination between gas and power system operators. For instance, gas and power system operators may develop strategies to coordinate and react to different contingencies affecting the reliability of the two systems. The developed strategies can be assessed using the simulation models and tools presented in this thesis to compare the effectiveness of different strategies and their potential vulnerabilities and bottlenecks. The estimation of consequences on security of supply computed by the developed models can also be used to perform a risk assessment of combined gas and power systems, which would enable the detection of potential risks affecting security of energy supply. The results from the risk assessment can be used to develop preventive action plans and emergency plans, which can also be tested using the simulation model.

Furthermore, the developed models can be used to address future research questions in the area of gas and power system interdependencies. One potential future research question concerns the integration and operation of P2G facilities in combined gas and electricity systems and how these facilities may impact the operation of the gas system if different gas qualities are injected at different locations. Analysing these questions requires an extension of the presented simulation models by a model for tracking the gas qualities in the gas model.

A. Input Data for 30-Nodes Gas Network

Parameter	Symbol	Value	Unit
time step	Δt	900	[s]
total simulation time	t_{max}	24	[h]
gas temperature	T	288.15	[K]
dynamic viscosity	η	$1.1 \cdot 10^{-5}$	[kg/m · s]
pipe roughness	k	0.012	[mm]
standard pressure	p_n	1.01325	[bar]
standard temperature	T_n	273.15	[K]
relative density	d	0.6	[·]
calorific value	CV	41.215	[MJ/sm ³]

Tab. A.1.: Input parameter for the dynamic simulation of the 30-Nodes sample network and the combined model

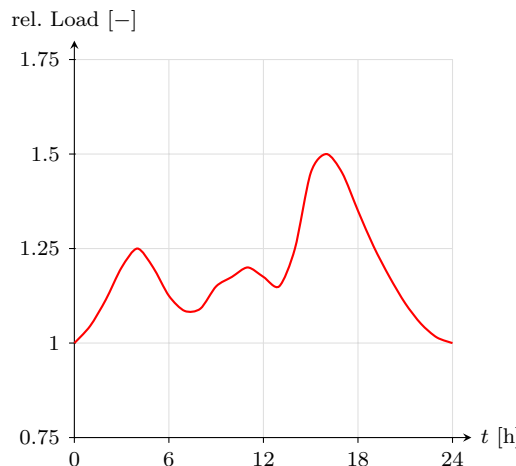


Fig. A.1.: Relative Load profile assigned to demand nodes of the sample network

Pipe	Node					Node	QSET [ksm ³ /s]	PSET [bar-g] [bar-g]
	inlet	outlet	L [km]	D [m]				
1	1	2	24	0.7		1	-	50 (supply)
2	1	3	25	0.7		2	90	-
3	1	4	20	0.7		3	29	-
4	4	3	30	0.7		4	75	-
5	3	2	40	0.7		5	0	-
6	2	22	45	0.7		6	55	-
7	2	5	70	0.6		7	85	-
8	5	6	60	0.6		8	28	-
9	22	21	52	0.7		9	90	-
10	6	21	30	0.6		10	41	-
11	4	10	40	0.7		11	39	-
12	4	11	35	0.6		12	20	-
13	4	12	25	0.7		13	0	-
14	12	13	70	0.6		14	80	-
15	12	11	30	0.7		15	45	-
16	11	10	50	0.6		16	0	-
17	13	14	60	0.6		17	120	-
18	10	14	100	0.6		18	42	-
19	14	15	80	0.7		19	18	-
20	10	9	75	0.6		20	35	-
21	15	9	80	0.7		21	29	-
22	15	16	75	0.6		22	71	-
23	16	17	80	0.7		23	0	-
24	10	6	40	0.6		24	0	-
25	9	17	65	0.7		25	0	-
26	9	8	40	0.6	Compressor	POSET [bar-g]		
27	8	17	55	0.6		1	55	
28	9	7	45	0.6		2	55	
29	8	18	30	0.7		3	55	
30	7	18	42	0.6				
31	6	7	20	0.7				
32	18	19	30	0.6				
33	7	20	40	0.7				
34	20	19	32	0.6				
35	20	21	45	0.7				

Tab. A.2.: Input data for the reference network taken from [92]

B. Combined Simulation of Gas and Electricity Networks

B.1. Primal Dual Interior Point Method

The extended ED model is solved with the Primal Dual Interior Point Method (PDIPM) described in [116, 132–134] by applying the Karush-Kuhn-Tucker (KKT) optimality condition to the Lagrangian function of the following augmented ED:

$$\min_{\mathbf{X}, \mathbf{Z}} f(\mathbf{X}, \mathbf{Z}) = \sum_{i=1}^{N_g} f_i(P_{G,i}) - \sum_{i=1}^{N_b} f_i(P_{D,i}) - \gamma \sum_{i=1}^{N_{iq}} \ln(Z_i) \quad (\text{B.1})$$

$$s. t. \quad \mathbf{G}(\mathbf{X}) = \mathbf{0}, \quad \mathbf{H}(\mathbf{X}) + \mathbf{Z} = \mathbf{0}, \quad \mathbf{Z} > \mathbf{0} \quad (\text{B.2})$$

where a set of positive slack variables \mathbf{Z} is added to the set of inequality constraints and for each slack variable Z_i a logarithmic barrier function is subtracted from the cost function. The resulting Lagrangian function of the augmented ED yields:

$$L(\mathbf{X}, \mathbf{Z}, \lambda, \mu) = f(\mathbf{X}, \mathbf{Z}) + \boldsymbol{\lambda}^T \cdot \mathbf{G}(\mathbf{X}) + \boldsymbol{\mu}^T \cdot [\mathbf{H}(\mathbf{X}) + \mathbf{Z}] \quad (\text{B.3})$$

where λ and μ are the vector of Lagrange multipliers for the set of equality $\mathbf{G}(\mathbf{X})$ and inequality $\mathbf{H}(\mathbf{X})$ constraints, respectively. The optimal solution of the augmented ED must fulfil the first order optimality conditions (KKT-conditions):

$$\mathbf{F}(\mathbf{X}, \mathbf{Z}, \lambda, \mu) = [L_X, L_Z, L_\lambda, L_\mu]^T = \mathbf{0} \quad (\text{B.4})$$

$$L_X = \frac{\partial L}{\partial \mathbf{X}}, \quad L_Z = \frac{\partial L}{\partial \mathbf{Z}}, \quad L_\lambda = \frac{\partial L}{\partial \lambda}, \quad L_\mu = \frac{\partial L}{\partial \mu} \quad (\text{B.5})$$

$$\boldsymbol{\mu} > \mathbf{0}, \quad \mathbf{Z} > \mathbf{0} \quad (\text{B.6})$$

which yields a non-linear equation system eq. (B.4) that can be solved for the solution variables $\mathbf{W} = [\mathbf{X}, \mathbf{Z}, \lambda, \mu]^T$ using a Newton-Raphson approach

$$-\mathbf{F}^k = \frac{\partial \mathbf{F}}{\partial \mathbf{W}} \Big|_k \cdot \Delta \mathbf{W} \quad (\text{B.7})$$

where the Newton updates for the primal (\mathbf{X}, \mathbf{Z}) and dual (λ, μ) variables are truncated as follows, in order to maintain feasibility of the solution:

$$\mathbf{X}^{k+1} = \mathbf{X}^k + \alpha_p \cdot \Delta \mathbf{X}, \mathbf{Z}^{k+1} = \mathbf{Z}^k + \alpha_p \cdot \Delta \mathbf{Z} \quad (\text{B.8})$$

$$\lambda^{k+1} = \lambda^k + \alpha_d \cdot \Delta \lambda, \mu^{k+1} = \mu^k + \alpha_d \cdot \Delta \mu \quad (\text{B.9})$$

with

$$\alpha_p = \min \left(\zeta \cdot \min_{\Delta Z_i < 0} \left(-\frac{Z_i}{\Delta Z_i} \right), 1 \right), \quad \alpha_d = \min \left(\zeta \cdot \min_{\Delta \mu_i < 0} \left(-\frac{\mu_i}{\Delta \mu_i} \right), 1 \right) \quad (\text{B.10})$$

$$i = 1 \dots N_{iq}, \quad 0.9 \leq \zeta \leq 1 \quad (\text{B.11})$$

The optimal solution obtained for the augmented ED coincides with the optimal solution of the initial extended ED if the perturbation factor γ converges to zero during the iterative solution process. Thus, at each Newton step k the perturbation factor γ is modified using the average primal dual distance as follows:

$$\gamma = \sigma \left(\frac{\mu^T \cdot \mathbf{Z}}{N_{iq}} \right), \quad 0 \leq \sigma \leq 1 \quad (\text{B.12})$$

The Newton-Raphson iterations are completed successfully, if the infinity norm of the residual vector \mathbf{F}^k and the perturbation factor γ are below a specified tolerance ϵ_f and ϵ_γ , respectively. The process is aborted if after a specified number of iterations k_{max} a converged solution is not reached. The presented PDIPM is designed for solving large scale problems with reasonable computation times [116], however, the method belongs to the class of Newton methods, which are known to be not globally convergent, i.e. convergence depends on the initial guess for the solution variables. However, results show good convergence [116] if a flat start ($\delta_i = 0$ & $|U_i| = 1$) or an available solution from a previous time step is chosen as an initial guess, as it is done in the algorithm for the combined gas and electric power system simulation (see Figure 5.2) explained in Section 5.2.2.

The presented PDIPM has been implemented into **SAInt** using the complex matrix notations for the derivatives of the Langrangian function (see eq. (B.4)-(B.7)) given in [134].

The accuracy of the implemented model has been confirmed by benchmarking the results against the Matlab-based power system library MATPOWER [116]. The results of an AC-OPF simulation conducted with **SAInt** and MATPOWER for the sample electric network are attached as supplementary data to the electronic version of the thesis (see [B.4.4](#)).

B.2. Data for sample gas and electricity network used in the case study

The gas and electric network data used for the case study are given in Tables [B.1-B.7](#). The actual native input files used in **SAInt** for the computations are available in the electronic version of this thesis and are explained further in [B.4.1](#).

Nr	ID	Type	X [-]	Y [-]	H [m]	p^{min} [bar-g]	p^{max} [bar-g]	Q^{max} [ksm ³ /h]	I^{max} [Msm ³]
0	NO.0	CBI	-2.5	4.1	50	20	60	600	
1	NO.1		-0.1	2	100				
2	NO.2		-0.1	1.2	100				
3	NO.3		4.4	2	150				
4	NO.4	GFPP	-3.8	-2	125	30	60	500	
5	NO.5		5	2	150				
6	NO.6		-6	-2	110				
7	NO.7		0	-4.2	75				
8	NO.8	IND	5	-3	50	25	60	250	
9	NO.9		5	4	40				
10	NO.10	LNG	-7	-3	70	40	60	375	510
11	NO.11	CGS	-7	-1	300	20	60	400	
12	NO.12		0	-5	75				
13	NO.13		-1.5	-6.5	120				
14	NO.14	CGS	-0.1	-8.1	215	16	50	250	
15	NO.15	CGS	-3.1	-8.1	45	30	50	275	
16	NO.16	IND	4	5	50	25	50	240	
17	NO.17		5	-5	60				
18	NO.18	GFPP	5	-5.6	60	30	60		
19	NO.19		5	-7	170				
20	NO.20	CGS	4	-8.1	160	16			
21	NO.21	CBE	6	-8	150	30	60		
22	NO.22	UGS	7	-3	140	30	60	120	450
23	NO.23	GFPP	7	4	110	30	60		
24	NO.24	CGS	7	0.5	80	16	50		

Tab. B.1.: Input data for nodes in gas model

ID	FrNr	ToNr	<i>D</i>	<i>l</i>	<i>k</i>
			[mm]	[km]	[mm]
PI.0	0	1	900	100	0.012
PI.1	1	3	900	80	0.012
PI.2	2	4	600	50	0.01
PI.3	4	6	300	20	0.02
PI.4	6	11	300	10	0.0112
PI.5	6	10	300	15	0.01
PI.6	4	7	600	60	0.012
PI.7	5	9	600	30	0.01
PI.8	9	23	600	30	0.012
PI.9	23	24	300	50	0.012
PI.10	24	22	300	40	0.01
PI.11	22	8	600	60	0.09
PI.12	8	17	600	60	0.012
PI.13	12	13	300	40	0.012
PI.14	13	15	300	25	0.012
PI.15	13	14	300	20	0.011
PI.16	14	20	300	50	0.012
PI.17	18	19	600	60	0.01
PI.18	19	20	300	30	0.012
PI.19	19	21	600	40	0.012
PI.20	9	16	300	30	0.012
PI.21	12	17	900	100	0.01
PI.22	17	18	600	50	0.012

Tab. B.2.: Input data for pipelines in gas model

ID	FrNr	ToNr	<i>D</i>	η_{ad}	η_m	<i>f</i>
			[mm]	[-]	[-]	[-]
CS.0	1	2	600	0.78	0.9	1
CS.1	3	5	600	0.76	0.88	1
CS.2	7	12	600	0.79	0.91	1

ID	PI^{min} [bar-g]	PO^{max} [bar-g]	Π^{max} [-]	PWD^{max} [MW]	Q_{vol}^{max} [m ³ /s]	Q^{max} [ksm ³ /h]
CS.0	25	60	2.5	55	50	1000
CS.1	25	60	2	40	50	1500
CS.2	20	60	2.5	45	50	1000

Tab. B.3.: Input data for compressor stations

Facility	ID	<i>k</i> ₀	<i>k</i> ₁	<i>k</i> ₂
		[MW]	$\left[\frac{\text{MW}}{\text{sm}^3/\text{s}}\right]$	$\left[\frac{\text{MW}}{(\text{sm}^3/\text{s})^2}\right]$
LNG terminal	NO.10	5	0.208	-0.000723

Tab. B.4.: Input data for electric power supply to LNG terminal

Nr	ID	BasekV	V_m^{min}	V_m^{max}	λ	ϵ_{svt}	X	Y
		[kV]	[p.u.]	[p.u.]	[-]	[%]	[-]	[-]
0	GEN.0	135	0.95	1.05	-	-	-27.6	1.3
1	GEN.1	135	0.95	1.1	-	-	-24.6	1.3
2	BUS.2	135	0.95	1.05	10	1	-27.6	-0.2
3	BUS.3	135	0.95	1.05	1	1	-24.6	-0.2
4	BUS.4	135	0.95	1.05	1	1	-21.5	1.3
5	BUS.5	135	0.95	1.05	1	1	-22	-0.3
6	BUS.6	135	0.95	1.05	10	1	-19	1.3
7	BUS.7	135	0.95	1.05	10	1	-19.6	-1
8	BUS.8	135	0.95	1.05	1	1	-22	-2.1
9	BUS.9	135	0.95	1.05	1	1	-18.9	-3.5
10	BUS.10	135	0.95	1.05	10	1	-23.2	-2.1
11	BUS.11	135	0.95	1.05	1	1	-24.6	-2.5
12	GEN.12	135	0.95	1.1	-	-	-27.6	-2.5
13	BUS.13	135	0.95	1.05	10	1	-26.7	-4.4
14	BUS.14	135	0.95	1.05	10	1	-24.6	-5.9
15	BUS.15	135	0.95	1.05	10	1	-23.3	-4.5
16	BUS.16	135	0.95	1.05	1	1	-21	-4.5
17	BUS.17	135	0.95	1.05	10	1	-23.3	-5.9
18	BUS.18	135	0.95	1.05	1	1	-21.9	-5.9
19	BUS.19	135	0.95	1.05	10	1	-20.6	-5.9
20	BUS.20	135	0.95	1.05	1	1	-17.5	-4.3
21	GEN.21	135	0.95	1.1	-	-	-18.9	-5.4
22	GEN.22	135	0.95	1.1	-	-	-24.6	-8.5
23	BUS.23	135	0.95	1.05	1	1	-22.1	-8.5
24	BUS.24	135	0.95	1.05	1	1	-19.7	-8.5
25	BUS.25	135	0.95	1.05	1	1	-17.7	-8.5
26	GEN.26	135	0.95	1.1	-	-	-16.4	-4.4
27	BUS.27	135	0.95	1.05	5	1	-18	0.4
28	BUS.28	135	0.95	1.05	5	1	-15.1	-3.8
29	BUS.29	135	0.95	1.05	5	1	-15.6	-4.9

Tab. B.5.: Input data for buses in power network. Priority factor λ is chosen such that buses connected to LDSs are less likely to be affected by load shedding than buses connected to INDs and CBEs.

ID	FrNr	ToNr	<i>R</i>	<i>X</i>	<i>b</i>	<i>S</i> ^{max}
			[p.u.]	[p.u.]	[p.u.]	[MVA]
LINE.0	0	1	0.02	0.06	0.03	100
LINE.1	0	2	0.05	0.19	0.02	100
LINE.2	1	3	0.06	0.17	0.02	100
LINE.3	2	3	0.01	0.04	0	100
LINE.4	1	4	0.05	0.2	0.02	100
LINE.5	1	5	0.06	0.18	0.02	100
LINE.6	3	5	0.01	0.04	0	100
LINE.7	4	6	0.05	0.12	0.01	100
LINE.8	5	6	0.03	0.08	0.01	100
LINE.9	5	7	0.01	0.04	0	100
LINE.10	5	8	0	0.21	0	100
LINE.11	5	9	0	0.56	0	100
LINE.12	8	10	0	0.21	0	100
LINE.13	8	9	0	0.11	0	100
LINE.14	3	11	0	0.26	0	100
LINE.15	11	12	0	0.14	0	100
LINE.16	11	13	0.12	0.26	0	100
LINE.17	11	14	0.07	0.13	0	100
LINE.18	11	15	0.09	0.2	0	100
LINE.19	13	14	0.22	0.2	0	100
LINE.20	15	16	0.08	0.19	0	100
LINE.21	14	17	0.11	0.22	0	100
LINE.22	17	18	0.06	0.13	0	100
LINE.23	18	19	0.03	0.07	0	100
LINE.24	9	19	0.09	0.21	0	100
LINE.25	9	16	0.03	0.08	0	100
LINE.26	9	20	0.03	0.07	0	100
LINE.27	9	21	0.07	0.15	0	100
LINE.28	20	21	0.01	0.02	0	100
LINE.29	14	22	0.1	0.2	0	100
LINE.30	21	23	0.12	0.18	0	100
LINE.31	22	23	0.13	0.27	0	100
LINE.32	23	24	0.19	0.33	0	100
LINE.33	24	25	0.25	0.38	0	100
LINE.34	24	26	0.11	0.21	0	100
LINE.35	27	26	0	0.4	0	100
LINE.36	26	28	0.22	0.42	0	100
LINE.37	26	29	0.32	0.6	0	100
LINE.38	28	29	0.24	0.45	0	100
LINE.39	7	27	0.06	0.2	0.02	100
LINE.40	5	27	0.02	0.06	0.01	100

Tab. B.6.: Input data for transmission lines in power network

ID	P_G^{max} [MW]	P_G^{min} [MW]	Q_G^{max} [MVAr]	Q_G^{min} [MVAr]	ω_r [MW/min]	T_s^{min} [h]	T_s^{max} [h]
GEN.0	60	15	48	-36	3	2	4
GEN.1	100	25	80	-60	2.5	2	8
GEN.12	50	12.5	40	-30	7.5	1/4	1/2
GEN.21	60	15	48	-36	3	2	4
GEN.22	60	15	48	-36	3	3	20
GEN.26	115	28.75	92	-69	5.75	3	20

ID	c_0 [€]	c_1 $\left[\frac{\text{€}}{\text{MW}}\right]$	c_2 $\left[\frac{\text{€}}{\text{MW}^2}\right]$	α $\left[\frac{\text{MJ}}{\text{kWh}}\right]$	β $\left[\frac{\text{MJ}}{\text{kWh} \cdot \text{MW}}\right]$	γ $\left[\frac{\text{MJ}}{\text{kWh} \cdot \text{MW}^2}\right]$
GEN.0	65	3.75	0.06	22.3590	-0.5607	0.0047
GEN.1	55	1.125	0.01	-	-	-
GEN.12	60	4.5	0.04	56.0000	-1.8286	0.0183
GEN.21	50	3.75	0.06	22.3590	-0.5607	0.0047
GEN.22	55	1.05	0.003	-	-	-
GEN.26	30	1.1	0.01	-	-	-

Tab. B.7.: Input data for generation units in power model

B.3. Simulation results for combined steady state simulation

The results for the combined steady state simulation are given in Tables B.8-B.11.

B.4. Description of supplementary data available in the electronic version

All supplementary files are available for download online at <http://www.sciencedirect.com/science/article/pii/S0306261917307018>. In the following sections, we give a description of the different files:

B.4.1. SAInt Project files

The input files provided as supplementary data to the electronic version of this thesis include all input data used for the network and for the case studies. All files are original SAInt input files and are provided in xml format. A SAInt-Project is generally divided into the following four types of files:

ID	CTRL	CTRLV	Q	p
			[ksm ³ /h]	[bar-g]
NO.0	PSET	50 [bar-g]	-531.877	50
NO.1	OFF		0	45.734
NO.2	OFF		0	60
NO.3	OFF		0	45.319
NO.4	QSET	6.118 [ksm ³ /h]	6.118	52.325
NO.5	OFF		0	60
NO.6	OFF		0	56.013
NO.7	OFF		0	36.694
NO.8	QSET	250 [ksm ³ /h]	250	55.364
NO.9	OFF		0	60.078
NO.10	PSET	60 [bar-g]	-87.931	60
NO.11	QSET	20 [ksm ³ /h]	20	54.986
NO.12	OFF		0	60
NO.13	OFF		0	52.674
NO.14	QSET	40 [ksm ³ /h]	40	50.93
NO.15	QSET	30 [ksm ³ /h]	30	52.1
NO.16	QSET	50 [ksm ³ /h]	50	57.483
NO.17	OFF		0	58.319
NO.18	QSET	6.403 [ksm ³ /h]	6.403	56.994
NO.19	OFF		0	54.99
NO.20	QSET	60 [ksm ³ /h]	60	51.155
NO.21	QSET	100 [ksm ³ /h]	100	54.653
NO.22	PSET	55 [bar-g]	-92.713	55
NO.23	QSET	0 [ksm ³ /h]	0	59.538
NO.24	QSET	150 [ksm ³ /h]	150	47.908

Tab. B.8.: Nodal control set points and results for initial combined steady state computation. Negative Q means gas supply, positive Q gas offtake.

ID	CTRL	CTRLV	Q	PI	PO	PWD
			[ksm ³ /h]	[bar-g]	[bar-g]	[MW]
CS.0	POSET	60 [bar-g]	401.667	45.734	60	4.171
CS.1	POSET	60 [bar-g]	130.21	45.319	60	1.47
CS.2	POSET	60 [bar-g]	463.48	36.694	60	8.886

Tab. B.9.: Compressor stations control set points and results for initial combined steady state computation.

1. SAIInt-Network files (with extensions *.net, *.enet):

Network files contain all topological information of the individual network and its static properties, which typically do not change in the course of a simulation (e.g. transmission line and pipeline properties). Each network in a project has its own file and the network type is expressed by the its file extension (e.g. *.net for gas network, *.enet for electric network).

ID	δ [°]	V_m [kV]	V_m [p.u.]	PD [MW]	PDGAS [MW]	QD [MVAr]
GEN.0	0	141.75	1.05	0	0	0
GEN.1	0.115	142.543	1.056	0	0	0
BUS.2	-2.359	138.707	1.027	5	0	1.2
BUS.3	-2.762	138.185	1.024	0	0	0
BUS.4	-1.87	139.741	1.035	0	0	0
BUS.5	-3.224	137.514	1.019	0	0	0
BUS.6	-2.999	137.325	1.017	12	4.171	10.9
BUS.7	-3.578	136.082	1.008	25	1.47	30
BUS.8	-6.962	137.015	1.015	0	0	0
BUS.9	-7.457	137.343	1.017	0	0	0
BUS.10	-9.78	136.358	1.01	24	0	1.75
BUS.11	-7.241	136.759	1.013	0	0	0
GEN.12	-7.241	136.759	1.013	0	0	0
BUS.13	-9.616	132.592	0.982	24	8.053	1.6
BUS.14	-7.707	136.635	1.012	7	8.886	2.5
BUS.15	-8.11	135.577	1.004	9	0	1.8
BUS.16	-8.056	135.955	1.007	15	0	5.8
BUS.17	-9.796	133.445	0.988	10	0	0.9
BUS.18	-10.337	132.718	0.983	8	0	3.4
BUS.19	-10.359	133.009	0.985	25	0	0.7
BUS.20	-7.151	138.57	1.026	16	0	11.2
GEN.21	-6.959	139.448	1.033	0	0	0
GEN.22	-3.397	144.369	1.069	0	0	0
BUS.23	-5.347	141.75	1.05	0	0	0
BUS.24	-4.871	141.75	1.05	0	0	0
BUS.25	-11.06	129.103	0.956	30	0	2.3
GEN.26	-1.528	148.206	1.098	0	0	0
BUS.27	-3.251	138.546	1.026	0	0	0
BUS.28	-9.218	135.13	1.001	30	0	0.9
BUS.29	-10.654	132.639	0.983	35	0	1.9

Tab. B.10.: Results for power system buses for initial combined steady state simulation

ID	PG [MW]	QG [MVAr]	Q [ksm ³ /h]	COST [€]	HR [MJ/kWh]	η_T [-]
GEN.0	18.63	-4.549	6.118	155.686	13.535	0.266
GEN.1	100	28.022	0	267.5	-	-
GEN.12	0	0	0	60	-	-
GEN.21	20.676	27.522	6.403	153.183	12.764	0.282
GEN.22	60	10.36	0	128.8	-	-
GEN.26	115	40.635	0	288.75	-	-

Tab. B.11.: Results for power system generation units for initial combined steady state simulation

2. SAInt-Scenario files (with extensions *.sce, *.esce):

For each network file, we can define an unlimited number of scenarios or cases, which include all boundary conditions, conditional expressions, load profiles etc..

Each scenario file is associated to a network (file). The type of network a scenario is connected to is expressed by its file extension, analogous to the network file extensions (e.g. *.sce for gas network, *.esce for electric network).

3. **SAInt-State** or condition files (with extensions *.con, *.econ):

The network and scenario files are both input files generated by **SAInt**. The state or condition files, in contrast, are result files generated after each simulation run. The state file contains the solution for all state variables for the terminal state of a simulation. It can be regarded as a snapshot of the network at the end of the simulation. The state file is needed as a initial state of the network for computing a (combined) dynamic simulation. Each state file is associated to a scenario (file). The type of network a state is connected to is expressed by its file extension, analogous to the network file extensions (e.g. *.con for gas network state file, *.econ for electric network state file).

4. and **SAInt-Solution** files (with extensions *.sol, *.esol):

The simulation results for a scenario are saved in a solution file. The result of a dynamic simulation is a sequence of network states (snapshots) for each simulation time step. To limit the size of the solution files the result for each state contains only fundamental parameters that cannot be calculated or derived from a combination of other parameters such as nodal gas pressure, voltage angle and magnitude. The type of network a solution file is connected to is expressed by its file extension, analogous to the network file extensions (e.g. *.sol for gas network solution file, *.esol for electric network solution file).

In the following, we list all network, scenario, state and solution files used for the case study and provided as supplementary data and give a short description of their content:

1. [**GNET25.net**](#) - Gas network file for sample 25 Node gas network
2. [**ENET30.enet**](#) - Electric network file for sample 30 Bus IEEE power network
3. [**CMBSTEOPF.sce**](#) - Gas network scenario file for the combined steady state scenario
4. [**CMBSTEOPF.esce**](#) - Electric network scenario file for the combined steady state scenario
5. [**CMBSTEOPF.con**](#) - Gas network state file for the combined steady state scenario
6. [**CMBSTEOPF.econ**](#) - Electric network state file for the combined steady state scenario
7. [**Case0.sce**](#) - Gas network scenario file for the combined dynamic scenario for case 0

8. [Case0.esce](#) - Electric network scenario file for the combined dynamic scenario for case 0
9. [Case0.sol](#) - Gas network solution file for the combined dynamic scenario for case 0
10. [Case0.esol](#) - Electric network solution file for the combined dynamic scenario for case 0
11. [Case1.sce](#) - Gas network scenario file for the combined dynamic scenario for case 1
12. [Case1.esce](#) - Electric network scenario file for the combined dynamic scenario for case 1
13. [Case1.sol](#) - Gas network solution file for the combined dynamic scenario for case 1
14. [Case1.esol](#) - Electric network solution file for the combined dynamic scenario for case 1
15. [Case2.sce](#) - Gas network scenario file for the combined dynamic scenario for case 2
16. [Case2.esce](#) - Electric network scenario file for the combined dynamic scenario for case 2
17. [Case2.sol](#) - Gas network solution file for the combined dynamic scenario for case 2
18. [Case2.esol](#) - Electric network solution file for the combined dynamic scenario for case 2

B.4.2. Animation videos for the case studies generated with SAInt

The animation videos for the three cases were generated by **SAInt** and provided as animated GIF-files, which can be played in any web browser. The videos show the time evolution of the state variables, the direction of gas flow and electric currents, and the state changes of controlled facilities in the gas and power system. The description of the different symbols in the video are given in the caption of Figure 5.7. The digital clock in the bottom mid-section indicates the current simulation time.

B.4.3. Simulation protocol for the case studies generated with SAInt

The simulation protocols were exported from the **SAInt**-log window and contain information on the total simulation time, the number of iterations in the successive linearisation loop, time integration loop, and the CCH-loop (as explained in section 5.2.2 and the flow

chart depicted in Figure 5.2), the residual for the gas and power system equations and the residual for the value of the coupling equations for the last two consecutive steps of the successive linearisation loop. Furthermore, the protocol contains a number of action implemented by the solver to avoid constraints violations in the gas network.

B.4.4. Comparison between **SAInt & **MATPOWER** [134] for AC-OPF**

The comparison between **SAInt** and **MATPOWER** were conducted for a single AC-OPF simulation for the sample electric network used in the case study. The input data and results obtained with **SAInt** are included in the Excel file [ComparisonSAInt.xls](#) while the ones for **MATPOWER** are given in [ComparisonMatpowerResult.log](#). A comparison of the results confirms the accuracy of the AC-OPF model implemented into **SAInt**.

Bibliography

- [1] IPCC, “Climate change 2014 - mitigation of climate change.contribution of working group iii to the fifth assessment report of the intergovernmental panel on climate change,” tech. rep., Intergovernmental Panel on Climate Change, 2014.
- [2] European Commission, “A roadmap for moving to a competitive low carbon economy in 2050,” *COM(2011) 112 final*, 2011.
- [3] Die Bundesregierung, “Energiekonzept für eine umweltschonende, zuverlässige und bezahlbare Energieversorgung.” https://www.bundesregierung.de/ContentArchiv/DE/Archiv17/_Anlagen/2012/02/energiekonzept-final.pdf?__blob=publicationFile&v=5, September 2010.
- [4] R. Wallooppilai and M.-L. Laud, “Planning for power: Pipeline design to meet gas-fired power plant needs,” in *PSIG Pipeline Simulation Interest Group*, 2003.
- [5] R. Carter, S. Backhaus, A. Hollis, A. Zlotnik, M. Chertkov, A. Giacomoni, and D. A., “Impact of regulatory change to coordinate gas pipelines and power systems,” in *Pipeline Simulation Interest Group*, 2016.
- [6] C. Jaworsky, C. Spataru, and K. Turitsyn, “Vulnerability assessment of interdependent gas and electricity networks,” in *HICSS48, USA*, 2015.
- [7] U.S. Energy Information Administration , “International energy outlook 2016,” Report DOE/EIA-0484(2016), U.S. Energy Information Administration , May 2016.
- [8] enea consulting, “The potential of power-to-gas - technology review and economic potential assessment,” 2016.
- [9] European Power to Gas Platform, 2017.
- [10] N. Judson, “Interdependence of the electricity generation system and the natural gas system and implications for energy security,” tech. rep., Massachusetts Institute of Technology Lincoln Laboratory, 2013.
- [11] J. B. Greenblatt, “Opportunities for efficiency improvements in the u.s. natural gas transmission, storage and distribution system,” 05/2015 2015.

-
- [12] European Union, “Regulation (EU) No 994/2010 of the european parliament and the council of 20 october 2010 concerning measures to safeguard security of gas supply and repealing council directive 2004/67/ec,” *Official Journal of the European Union*, 2010, <http://eur-lex.europa.eu/legal-content/EN/TXT/PDF/?uri=CELEX:32010R0994&from=EN>, August 7, 2018.
 - [13] NERC, “Accommodating an increased dependence on natural gas for electric power, phase ii: A vulnerability and scenario assessment for the north american bulk power,” tech. rep., North American Electric Reliability Corporation (NERC), 2013.
 - [14] R. Rubio Barros, D. Ojeda-Estebar, A. Ano, and A. Vargas, “Combined operational planning of natural gas and electric power systems: state of the art,” in *Potocnik P, editor. Natural gas, Sciyo*, 2010.
 - [15] B. Cakir Erdener, K. A. Pambour, R. B. Lavin, and B. Dengiz, “An integrated simulation model for analysing electricity and gas systems,” *International Journal of Electrical Power & Energy Systems*, vol. 61, no. 0, pp. 410 – 420, 2014.
 - [16] J. Abrell and H. Weigt, “Combining energy networks,” TU Dresden, Electricity markets working papers WP-EM-38 2010., 2010.
 - [17] O. Özdemir, K. Veum, J. Joode, G. Migliavacca, A. Grassi, and A. Zani, “The impact of large-scale renewable integration on europe’s energy corridors,” *Proceedings of IEEE Trondheim PowerTech*, p. 1–8, 2011.
 - [18] D. Möst and H. Perlwitz, “Prospect of gas supply until 2020 in europe and its relevance of the power sector in the context of emissions trading energy,” vol. 34, p. 1510–1522, 2008.
 - [19] M. Lienert and S. Lochner, “The importance of market interdependencies in modelling energy systems – the case of european electricity generation market,” *International Journal of Electric Power and Energy Systems*, vol. 34, pp. 99–113, 2012.
 - [20] H. Chen and R. Baldick, “Optimizing short-term natural gas supply portfolio for electric utility companies,” *IEEE Transactions on Power Systems*, vol. 22, pp. 232–239, Feb 2007.
 - [21] U. Asif and P. Jirutitijaroen, “An optimization model for risk management in natural gas supply and energy portfolio of a generation company,” in *Proceedings of TENCON 2009–2009 IEEE region 10 conference*, 2009.
 - [22] O. Kittithreerapronchai, P. Jirutitijaroen, S. Kim, and J. Prina, “Optimizing natural gas supply and energy portfolios of a generation company,” in *Proceedings of*

- PMAPS 2010 – IEEE 11th international conference on probabilistic methods applied to power systems*, pp. 231–237, 2010.
- [23] P. Duenas, J. Barquin, and J. Reneses, “Strategic management of multi-year natural gas contracts in electricity markets,” *IEEE Transactions on Power Systems*, vol. 27, pp. 771–779, May 2012.
 - [24] S. Spiecker, “Analyzing market power in a multistage and multiarea electricity and natural gas system,” in *Proceedings of EEM – 8th IEEE international conference on the European energy market*, pp. 313–320, 2011.
 - [25] H. Weigt and J. Abrell, “Investments in a combined energy network model: Substitution between natural gas and electricity,” 2014.
 - [26] M. Gil, P. Dueñas, and J. Reneses, “Electricity and natural gas interdependency: Comparison of two methodologies for coupling large market models within the european regulatory framework,” *IEEE Transactions on Power Systems*, vol. 31, pp. 361–369, Jan 2016.
 - [27] M. Shahidehpour, Y. Fu, and T. Wiedman, “Impact of natural gas infrastructure on electricity power system security,” *Proc IEEE*, vol. 93(5), pp. 1042–56, 2005.
 - [28] C. Li, M. Eremia, and M. Shahidehpour, “Interdependency of natural gas network and power system security,” *IEEE Trans Power Sys*, vol. 23(4), pp. 1817–24, 2008.
 - [29] C. Liu, M. Shahidehpour, Y. Fu, and Z. Li, “Security-constrained unit commitment with natural gas transmission constraints,” *IEEE Trans Power Syst*, 2009.
 - [30] G. Li, R. Zhang, H. Chen, T. Jiang, H. Jia, Y. Mu, and X. Jin, “Security-constrained economic dispatch for integrated natural gas and electricity systems,” *Energy Procedia 88*, pp. 330–335, 2016.
 - [31] S. An, Q. Li, and T. Gedra, “Natural gas and electricity optimal power flow,” *Proceedings of IEEE transmission and distribution conference and exposition*, vol. 1, pp. 138–43, 2003.
 - [32] C. Unshuay, J. Marangon Lima, and A. Zambroni de Souza, “Modelling the integrated natural gas and electricity optimal power flow,” *Proceedings of IEEE PES general meeting*, 2007.
 - [33] A. Martínez-Mares and C. Fuerte-Esquivel, “Integrated energy flow analysis in natural gas and electricity coupled systems.,” in *Proceedings of IEEE NAPS – North American power symposium*, p. 1–7, 2011.

-
- [34] C. Liu, M. Shahidehpour, and J. Wang, “Coordinated scheduling of electricity and natural gas infrastructures with a transient model for natural gas flow,” 2011.
 - [35] M. Chaudry, N. Jenkins, and G. Strbac, “Multi-time period combined gas and electricity network optimisation,” *Electr Power Syst Res*, vol. 78, pp. 1265–79, 2008.
 - [36] S. Clegg and P. Mancarella, “Integrated electrical and gas network modelling for assessment of different power-and-heat options,” in *Power Systems Computation Conference (PSCC)*, pp. 1–7, 2014.
 - [37] M. Qadrdan, M. Chaudry, J. Wu, N. Jenkins, and J. Ekanayake, “Impact of a large penetration of wind generation on the {GB} gas network,” *Energy Policy*, vol. 38, no. 10, pp. 5684 – 5695, 2010. The socio-economic transition towards a hydrogen economy - findings from European research, with regular papers.
 - [38] M. Qadrdan, N. Jenkins, and J. Ekanayake, “Operating strategies for a gb integrated gas and electricity network considering the uncertainty in wind power forecasts,” *IEEE Transactions on Sustainable Energy*, vol. 5, no. 1, pp. 128–138, 2014.
 - [39] M. Chertkov, S. Backhaus, and V. Lebedev, “Cascading of fluctuations in interdependent energy infrastructures: Gas-grid coupling,” *Applied Energy*, vol. 160, pp. 541 – 551, 2015.
 - [40] A. Alabdulwahab, A. Abusorrah, X. Zhang, and M. Shahidehpour, “Coordination of interdependent natural gas and electricity infrastructures for firming the variability of wind energy in stochastic day-ahead scheduling,” *IEEE Transactions on Sustainable Energy*, vol. 6, pp. 606–615, April 2015.
 - [41] H. Cui, F. Li, Q. Hu, L. Bai, and X. Fang, “Day-ahead coordinated operation of utility-scale electricity and natural gas networks considering demand response based virtual power plants,” *Applied Energy*, vol. 176, pp. 183 – 195, 2016.
 - [42] L. Bai, F. Li, H. Cui, T. Jiang, H. Sun, and J. Zhu, “Interval optimization based operating strategy for gas-electricity integrated energy systems considering demand response and wind uncertainty,” *Applied Energy*, vol. 167, pp. 270 – 279, 2016.
 - [43] X. Zhang, M. Shahidehpour, A. Alabdulwahab, and A. Abusorrah, “Hourly electricity demand response in the stochastic day-ahead scheduling of coordinated electricity and natural gas networks,” *IEEE Transactions on Power Systems*, vol. 31, pp. 592–601, Jan 2016.
 - [44] M. Qadrdan, M. Cheng, J. Wu, and N. Jenkins, “Benefits of demand-side response in combined gas and electricity networks,” *Applied Energy*, pp. –, 2016.

- [45] C. A. Saldarriaga, R. A. Hincapié, and H. Salazar, “A holistic approach for planning natural gas and electricity distribution networks,” *IEEE Transactions on Power Systems*, vol. 28, pp. 4052–4063, Nov 2013.
- [46] M. Chaudry, N. Jenkins, M. Qadrdan, and J. Wu, “Combined gas and electricity network expansion planning,” *Applied Energy*, vol. 113, pp. 1171 – 1187, 2014.
- [47] M. Qadrdan, M. Abeysekera, M. Chaudry, J. Wu, and N. Jenkins, “Role of power-to-gas in an integrated gas and electricity system in great britain,” *International Journal of Hydrogen Energy*, vol. 40, no. 17, pp. 5763 – 5775, 2015.
- [48] S. Clegg and P. Mancarella, “Integrated modeling and assessment of the operational impact of power-to-gas (p2g) on electrical and gas transmission networks,” *IEEE Transactions on Sustainable Energy*, vol. 6, pp. 1234–1244, Oct. 2015.
- [49] S. Clegg and P. Mancarella, “Storing renewables in the gas network: Modelling of power-to-gas seasonal storage flexibility in low-carbon power systems,” *IET Generation Transmission & Distribution*, 2016.
- [50] M. Urbina and Z. Li, “A combined model for analysing the interdependency of electrical and gas systems,” *Proceedings of NAPS, 39th IEE North American power symposium*, 2007.
- [51] M. Urbina and Z. Li, “Modeling and analysing the impact of interdependency between natural gas and electricity infrastructures,” *Proceedings of IEEE PES general meeting*, 2008.
- [52] R. Carvalho, L. Buzna, F. Bono, E. Gutierrez, W. Just, and D. Arrowsmith, “Robustness of trans-european gas networks,” *Physical Review E* 80, 2009.
- [53] J. Munoz, N. Jimenez-Redondo, J. Perez-Ruiz, and J. B. J., “Natural gas network modeling for power systems reliability studies,” in *Proceedings of PowerTech conference*, vol. 3, p. 6, 2003.
- [54] C. Liu, M. Shahidehpour, and J. Wang, “Application of augmented lagrangian relaxation to coordinated scheduling of interdependent hydrothermal power and natural gas systems,” *IET Generation, Transmission Distribution*, vol. 4, pp. 1314–1325, December 2010.
- [55] G. Li, R. Zhang, T. Jiang, H. Chen, L. Bai, and X. Li, “Security-constrained bi-level economic dispatch model for integrated natural gas and electricity systems considering wind power and power-to-gas process,” *Applied Energy*, pp. –, 2016.

-
- [56] J. Qiu, Z. Y. Dong, J. H. Zhao, Y. Xu, Y. Zheng, C. Li, and K. P. Wong, "Multi-stage flexible expansion co-planning under uncertainties in a combined electricity and gas market," *IEEE Transactions on Power Systems*, vol. 30, pp. 2119–2129, July 2015.
 - [57] J. Devlin, K. Li, P. Higgins, and A. Foley, "A multi vector energy analysis for interconnected power and gas systems," *Applied Energy*, pp. –, 2016.
 - [58] Q. Zeng, J. Fang, J. Li, and Z. Chen, "Steady-state analysis of the integrated natural gas and electric power system with bi-directional energy conversion," *Applied Energy*, pp. –, 2016.
 - [59] S. Chen, Z. Wei, G. Sun, K. W. Cheung, and Y. Sun, "Multi-linear probabilistic energy flow analysis of integrated electrical and natural-gas systems," *IEEE Transactions on Power Systems*, vol. PP, no. 99, pp. 1–1, 2016.
 - [60] S. Clegg and P. Mancarella, "Integrated electrical and gas network flexibility assessment in low-carbon multi-energy systems," *IEEE Transactions on Sustainable Energy*, vol. 7(2), pp. 718–731, 2016.
 - [61] A. Zlotnik, M. Chertkov, R. Carter, A. Hollis, A. Daniels, and S. Backhaus, "Using power grid schedules in dynamic optimization of gas pipelines," in *Pipeline Simulation Interest Group.*, 2016.
 - [62] N.-Y. Chiang and V. M. Zavala, "Large-scale optimal control of interconnected natural gas and electrical transmission systems," *Applied Energy*, vol. 168, pp. 226 – 235, 2016.
 - [63] A. Zlotnik, L. Roald, S. Backhaus, M. Chertkov, and G. Andersson, "Coordinated scheduling for interdependent electric power and natural gas infrastructures," *IEEE Transactions on Power Systems*, vol. PP, no. 99, pp. 1–1, 2016.
 - [64] EUROGAS, "Statistical report 2014." http://www.eurogas.org/uploads/media/Eurogas_Statistical_Report_2013.pdf, December 2014.
 - [65] J. Szoplik, *The Gas Transportation in a Pipeline Network, Advances in Natural Gas Technology*. InTEch, 2012.
 - [66] A. D. Woldeyohannes and M. A. Abd Majid, "Simulation model for natural gas transmission pipeline network system," *Simulation Modelling Practice and Theory - Elsevier B.V.*, vol. 19, pp. 196–212, 2011.

- [67] J. Mohring, J. Hoffmann, T. Halfmann, A. Zemitis, and G. Basso, “Automated model reduction of complex gas pipeline networks,” Pipeline Simulation Interest Group (PSIG), 2003.
- [68] D. W. Schroeder Jr., “A tutorial on pipe flow equations,” August 2001.
- [69] T. van der Hoeven, *Math in Gas and the art of linearization*. Energy Delta Institute, April 2004.
- [70] A. Herrán-González, J. D. L. Cruz, B. D. Andrés-Toro, and J. Risco-Martín, “Modeling and simulation of a gas distribution pipeline network,” *Applied Mathematical Modelling*, vol. 33, no. 3, pp. 1584 – 1600, 2009.
- [71] E. Ebrahimzadeh, M. N. Shahrak, and B. Bazoooyar, “Simulation of transient gas flow using the orthogonal collocation method,” *Chemical Engineering Research and Design*, vol. 90, no. 11, pp. 1701 – 1710, 2012.
- [72] H. P. Reddy, S. Narasimhan, and S. M. Bhallamudi, “Simulation and state estimation of transient flow in gas pipeline networks using a transfer function model,” *Industrial & Engineering Chemistry Research*, vol. 45, no. 11, pp. 3853–3863, 2006.
- [73] W. Hai, L. Xiaojing, and Z. Weiguo, “Transient flow simulation of municipal gas pipelines and networks using semi implicit finite volume method,” *Procedia Engineering*, vol. 12, no. 0, pp. 217 – 223, 2011. 2011 SREE Conference on Engineering Modelling and Simulation (CEMS 2011).
- [74] M. Herty, J. Mohring, and S. V., “A new model for gas flow in pipe networks,” *Mathematical Methods in the Applied Sciences*, 2009.
- [75] L. Gato and J. Henriques, “Dynamic behaviour of high-pressure natural-gas flow in pipelines,” *International Journal of Heat and Fluid Flow*, vol. 26, no. 5, pp. 817 – 825, 2005.
- [76] M. Behbahani-Nejad and A. Bagheri, “The accuracy and efficiency of a matlab-simulink library for transient flow simulation of gas pipelines and networks,” *Journal of Petroleum Science and Engineering*, vol. 70, pp. 256 – 265, 2010.
- [77] M. Behbahani-Nejad and Y. Shekari, “The accuracy and efficiency of a reduced-order model for transient flow analysis in gas pipelines,” *Journal of Petroleum Science and Engineering*, vol. 73, pp. 13 – 19, 2010.
- [78] C. Dorao and M. Fernandino, “Simulation of transients in natural gas pipelines,” *Journal of Natural Gas Science and Engineering*, vol. 3, no. 1, pp. 349 – 355, 2011.

- [79] R. Alamian, M. Behbahani-Nejad, and A. Ghanbarzadeh, “A state space model for transient flow simulation in natural gas pipelines,” *Journal of Natural Gas Science and Engineering*, vol. 9, no. 0, pp. 51 – 59, 2012.
- [80] A. Lewandowski, “New numerical methods for transient modeling of gas pipeline networks,” Pipeline Simulation Interest Group, 1995.
- [81] S. Grundel, N. Hornung, B. Klaassen, P. Benner, and T. Clees, “Computing surrogates for gas network simulation using model order reduction,” in *Surrogate-Based Modeling and Optimization* (S. Koziel and L. Leifsson, eds.), pp. 189–212, Springer New York, 2013.
- [82] A. J. Osiadacz, “Transient flow models - limitations, advantages, and disadvantages,” *Pipeline Simulation Interest Group*, no. 9606, 1996.
- [83] M. Chaczykowski, “Transient flow in natural gas pipeline - the effect of pipeline thermal model,” *Applied Mathematical Modelling*, vol. 34, no. 4, pp. 1051 – 1067, 2010.
- [84] M. Chaczykowski, “Sensitivity of pipeline gas flow model to the selection of the equation of state,” *Chemical Engineering Research and Design*, vol. 87, no. 12, pp. 1596 – 1603, 2009.
- [85] A. J. Osiadacz and M. Chaczykowski, “Comparison of isothermal and non-isothermal pipeline gas flow models,” *Chemical Engineering Journal*, vol. 81, no. 1, pp. 41 – 51, 2001.
- [86] S. Ke and H. Ti, “Transient analysis of isothermal gas flow in pipeline network,” *Chemical Engineering Journal*, vol. 76, no. 2, pp. 169 – 177, 2000.
- [87] T. van der Hoeven, “Gas transport pipe,” No. PSIG 0710, Pipeline Simulation Interest Group, 2007.
- [88] J. L. Modisette and J. P. Modisette, “Transient and succession-of-steady-states pipeline flow models,” Pipeline Simulation Interest Group (PSIG), 2001.
- [89] S. K. Bachman and M. J. Goodreau, “Steady state - is the solution realistic for the piping network?,” Pipeline Simulation Interest Group (PSIG), 2003.
- [90] P. Hofer, “Beurteilung von fehlern in rohrnetzberechnungen,” *gwf-gas/erdgas*, vol. 114, no. 3, 1973.
- [91] I. Papay, *OGIL Musz. Tud. Kozl.* 1968.
- [92] A. J. Osiadacz, *Simulation and Analysis of Gas Networks*. E. & F.N. SPON, 1987.

- [93] G. Cerbe, *Grundlagen der Gastechnik*. HANSER, 2008.
- [94] K. H. van Dam and E. J. L. Chappin, “Coupling agent-based models of natural gas and electricity markets.” http://nextgenerationinfrastructures.eu/catalog/file/548235/ATES_10_VanDam.pdf.
- [95] naturalgas.org, “Storage of natural gas,” 01 2015.
- [96] S. Barry, “Natural gas storage is not as boring as you think,” 06 2012.
- [97] S. Lochner and C. Dieckhoener, “Tiger infrastructure and dispatch model of the european gas market,” *EWI - Institute of Energy Economics at the University of Cologne*, 2010.
- [98] E.ON GAS STORAGE GmbH, “Characteristic curves.” <http://www.eon-gas-storage.de/cps/rde/xchg/egs/hs.xsl/3051.htm?rdeLocaleAttr=en&rdeCOQ=SID-6B2D2800-99ED0905>, August 7, 2018.
- [99] J. Králik, *Dynamic modeling of large-scale networks with application to gas distribution*. Studies in automation and control, Elsevier, 1988.
- [100] S. Kaplan and B. Garrick, *On the Quantitative Definition of Risk, Risk Analysis*, vol. 1. 1981.
- [101] P. Praks, V. Kopustinskas, and M. Masera, “Probabilistic modelling of security of supply in gas networks and evaluation of new infrastructure,” *Reliability Engineering & System Safety*, vol. 144, pp. 254 – 264, 2015.
- [102] A. Sziksza and F. Monforti, “Gemflow: A time dependent model to assess responses to natural gas supply crises,” *Energy Policy*, vol. 39, no. 9, pp. 5129 – 5136, 2011.
- [103] N. Voropai, S. Senderov, and A. Edelev, “Detection of “bottlenecks” and ways to overcome emergency situations in gas transportation networks on the example of the european gas pipeline network,” *Energy*, vol. 42, no. 1, pp. 3 – 9, 2012. 8th World Energy System Conference, {WESC} 2010.
- [104] F. Monforti and A. Sziksza, “A montecarlo approach for assessing the adequacy of the european gas transmission system under supply crisis conditions,” *Energy Policy*, vol. 38, no. 5, pp. 2486 – 2498, 2010. Greater China Energy: Special Section with regular papers.
- [105] R. Carvalho, L. Buzna, F. Bono, M. Masera, D. K. Arrowsmith, and D. Helbing, “Resilience of natural gas networks during conflicts, crises and disruptions,” *PLoS ONE*, vol. 9, p. e90265, 03 2014.

-
- [106] S. Lochner, “Modeling the european natural gas market during the 2009 russia–ukrainian gas conflict: Ex-post simulation and analysis,” *Journal of Natural Gas Science and Engineering*, vol. 3, no. 1, pp. 341 – 348, 2011.
 - [107] X. S. Li and J. W. Demmel, “A scalable distributed-memory sparse direct solver for unsymmetric linear systems.” http://crd-legacy.lbl.gov/~xiaoye/toms_slud.pdf, ACM Transactions on Mathematical Software, Vol. 29, No. 2, June 2003, Pages 110–140.
 - [108] I. S. Duff and J. K. Reid, “A code for the direct solution of sparse unsymmetric linear systems of equations,” *ACM Transactions on Mathematical Software*, vol. 22, pp. 187–226, 1996.
 - [109] I. S. Duff and J. A. Scott, “The design of a new frontal code for solving sparse unsymmetric systems,” *ACM Transactions on Mathematical Software*, vol. 22, no. 1, pp. 30–45, 1996.
 - [110] I. Pearson, P. Zeniewski, F. Gracceva, P. Zastera, C. McGlade, and S. Sorrell, “Unconventional gas: potential energy market impacts in the european union,” tech. rep., JRC scientific and policy reports EUR 25305 EN, 2012.
 - [111] J. D. Glover, M. S. Sarmar, and T. J. Overbye, *Power Systems and Analysis Design*. Global Engineering, fifth ed., 2010.
 - [112] G. Andersson, “Modelling and analysis of electric power systems.” Lecture 227-0526-00, ITET ETH Zurich, September 2008.
 - [113] S. Tong, M. Kleinberg, and K. Miu, “A distributed slack bus model and its impact on distribution system application techniques,” *IEEE*, 2005.
 - [114] S. Tong, *Slack Bus Modeling for Distributed Generation and Its Impacts on Distribution System Analysis, Operation and Planning*. PhD thesis, Drexel University, 2006.
 - [115] A. Martinez-Mares and C. R. Fuerte-Esquivel, “A unified gas and power flow analysis in natural gas and electricity coupled networks,” *IEEE Transactions on Power Systems*, vol. 27, November 2012.
 - [116] R. D. Zimmerman, C. E. Murillo-Sanchez, and R. J. Thomas, “Matpower: Steady-state operations, planning and analysis tools for power systems research and education,” *Power Systems, IEEE Transactions*, vol. 26, pp. 12–19, February 2011.

- [117] B. A. Carreras, V. E. Lynch, I. Dobson, and D. E. Newman, “Critical points and transitions in an electric power transmission model for cascading failure blackouts,” *Chaos: Interdiscipl. J. Nonlin. Sci.*, vol. 12, no. 4, pp. 985–994, 2002.
- [118] R. Baldick, B. Chowdhury, I. Dobson, Z. Dong, B. Gou, D. Hawkins, H. Huang, M. Joung, D. Kirschen, F. Li, J. Li, Z. Li, C.-C. Liu, L. Mili, S. Miller, R. Podmore, K. Schneider, K. Sun, D. Wang, Z. Wu, P. Zhang, W. Zhang, and X. Zhang, “Initial review of methods for cascading failure analysis in electric power transmission systems ieee pes cams task force on understanding, prediction, mitigation and restoration of cascading failures,” in *Power and Energy Society General Meeting - Conversion and Delivery of Electrical Energy in the 21st Century, 2008 IEEE*, pp. 1–8, July 2008.
- [119] M. Papic, K. Bell, Y. Chen, I. Dobson, L. Fonte, E. Haq, P. Hines, D. Kirschen, X. Luo, S. S. Miller, N. Samaan, M. Vaiman, M. Varghese, and P. Zhang, “Survey of tools for risk assessment of cascading outages,” in *2011 IEEE Power and Energy Society General Meeting*, pp. 1–9, July 2011.
- [120] H. Ren, X. Fan, D. Watts, and X. Lv, “Early warning mechanism for power system large cascading failures,” in *Power System Technology (POWERCON), 2012 IEEE International Conference on*, pp. 1–6, Oct 2012.
- [121] M. Vaiman, K. Bell, Y. Chen, B. Chowdhury, I. Dobson, P. Hines, M. Papic, S. S. Miller, and P. Zhang, “Risk assessment of cascading outages: Part i 2014; overview of methodologies,” in *2011 IEEE Power and Energy Society General Meeting*, pp. 1–10, July 2011.
- [122] Vaiman, Bell, Chen, Chowdhury, Dobson, Hines, Papic, Miller, and Zhang, “Risk assessment of cascading outages: Methodologies and challenges,” *IEEE Transactions on Power Systems*, vol. 27, pp. 631–641, May 2012.
- [123] C. J. Mozina, “Power plant protection and control strategies for blackout avoidance,” in *Georgia Tech Protective Relay Conference*, 2005.
- [124] NERC, “System disturbance report,” tech. rep., North American Electric Reliability Council, 1998.
- [125] IEEE Power System Relaying Committee Report, “Summary of system protection and voltage stability,” *Transactions on Power Delivery*, vol. 10, no. 2, 1995.

-
- [126] X. Zhang, L. Che, and M. Shahidehpour, “Impact of natural gas system on short-term scheduling with volatile renewable energy,” in *2015 IEEE Power Energy Society General Meeting*, pp. 1–5, July 2015.
 - [127] I. G. Sardou, M. E. Khodayar, and M. Ameli, “Coordinated operation of natural gas and electricity networks with microgrid aggregators,” *IEEE Transactions on Smart Grid*, vol. PP, no. 99, pp. 1–1, 2016.
 - [128] K. A. Pambour, B. Cakir Erdener, R. Bolado-Lavin, and G. P. J. Dijkema, “An integrated simulation tool for analyzing the operation and interdependency of natural gas and electric power systems,” in *Pipeline Simulation Interest Group (PSIG) Conference 2016*, 2016.
 - [129] K. A. Pambour, R. Bolado-Lavin, and G. P. Dijkema, “SAInt – A simulation tool for analysing the consequences of natural gas supply disruptions,” in *Pipeline Technology Conference (PTC) 2016*, 2016.
 - [130] A. S. Brouwer, M. van den Broek, A. Seebregts, and A. Faaij, “Operational flexibility and economics of power plants in future low-carbon power systems,” *Applied Energy*, vol. 156, pp. 107 – 128, 2015.
 - [131] S. A. . Soman, S. A. Khaparde, and S. Pandit, *Computational Methods for Large Sparse Power Systems Analysis*. Springer, 2002.
 - [132] H. Wang, *On the computation and application of multi-period security-constrained optimal power flow for real-time electricity market operations*. PhD thesis, Cornell University, 2007.
 - [133] R. D. Zimmerman and C. E. Murrillo-Sanchez, *Matpower 5.1 User’s Manual*. Power Systems Engineering Research Center (Pserc), March 2015.
 - [134] R. D. Zimmerman, *AC Power Flows, Generalized OPF Costs and their Derivatives using Complex Matrix Notation - Matpower Technical Note 2*. Power Systems Engineering Research Center (Pserc), March 2011.

Summary

Background

The integration of renewable energy sources (RES) into existing energy supply systems has increased the coupling between different critical energy infrastructures. The operation of natural gas and electricity transmission networks, for instance, is increasingly interdependent, due to a growing use of natural gas fired generators in the electricity system and the use of electric driven compressor stations in the gas system. Moreover, new evolving technologies such as power to gas (P2G) are expected to further increase the coupling between both energy vectors.

Gas fired power plants (GFPP) are electricity producers in power systems and at the same time gas consumers in natural gas networks. Due to their flexibility, manoeuvrability and short response time, they are mainly used as peak shavers and as a backup for variable and intermittent RES. Gas fired generators need a certain minimum delivery gas pressure in order to operate. The fuel offtake from gas pipeline networks may be subject to curtailments if the desired offtake would violate the minimum delivery pressure limits. In the worst case, these curtailments may lead to a complete shut down of the GFPP, which in turn may affect the operation of the electricity system, due to reductions in total generation capacity. Thus, it is extremely important to investigate how the pressure constraints in the gas system may affect the operation of gas generators in the electricity system.

Electric driven compressor stations, in contrast, use electricity from the power grid to increase the downstream gas pressure for gas transportation in pipelines and for meeting contracted delivery pressures at offtake points. They are particularly attractive in situations, where the use of conventional gas turbines may be limited by emission restrictions or other environmental regulations. Furthermore, electric drivers have higher mechanical efficiencies, lower operating and maintenance costs and are more flexible and controllable than conventional gas turbines.

The growing interdependence between gas and electricity systems is connected to challenges concerning security of energy supply, i.e. the uninterrupted supply of energy to customers, particularly, in difficult climatic conditions and in the event of an unexpected disruption. A disruption in one energy system may cascade to the other system and even back to the system where it originated. For instance, a rapid increase in power generation from a GFPP due to loss of renewable generation may be connected to an increase in fuel gas offtake from the gas grid, which in turn may cause a pressure reduction in the gas system. This pressure reduction may be compensated for by an electric driven compressor station, which requires additional power offtake from the electricity network. The additional power offtake, again, will have to be balanced by the power generation units including GFPPs, by increasing the power output. This cycle may continue until an equilibrium state of the coupled energy system is reached.

The above example demonstrates the importance of investigating and understanding the interactions between gas and electricity systems, how they may affect the operation of the two systems and how to proactively approach the bottlenecks and challenges that may emerge. Traditionally, gas and electric power systems were operated independently, due to the relatively weak coupling between both infrastructures, thus, most mathematical models examine the two systems individually without paying much attention to the interactions between them. However, the growing interdependence between both energy systems suggests the need for simulation models that are capable of examining both systems in an integrated manner considering the physical equations describing the operation and interactions between the two systems.

Research Questions

In this thesis, simulation models for analysing the operation and interdependencies between interconnected natural gas and electricity transmission networks in terms of security of energy supply are developed. The developed simulation models are implemented into a novel simulation tool named **SAInt** - Scenario Analysis Interface for Energy Systems. **SAInt** is intended to support gas and power transmission system operators, regulatory agencies, governments, energy consultants and researchers, to examine the interactions between gas and electric power systems and to assess the impact of disruptions on security of supply in integrated gas and electric power systems. The tool can be used to answer the main research questions of this thesis, namely, how to quantify the consequences of disruption events originating in gas and/or electricity transmission networks and how to

implement and compare the effectiveness of countermeasures to mitigate the impact of these undesired events.

Answering these questions, requires the development of mathematical models, that reflect the physical behaviour and constraints of the gas and electricity system and the coupling between both energy vectors.

Methodology

When modelling the interdependencies between gas and electricity systems, there are several aspects to be considered mainly due to the differences in the structure and physical characteristics of both systems. For instance, the failure response of both infrastructures is significantly different. A technical failure in the power system can result in an immediate loss of service from a generation plant or transmission line. Under some extreme conditions, this can propagate and eventually result in loss of service to electric customers due to cascading effects. On the contrary, most technical failures in gas systems (e.g. pipeline rupture, failure in compressor station or storage facilities etc.) result in a locally or regionally reduced network capacity rather than an entire loss of service to gas consumers [13]. This capacity reduction might result in curtailments of gas delivery to customers according to their priority level. Another important distinction between the two systems is the different dynamic behaviour. Electricity travels almost instantaneously and cannot be stored economically in large quantities in current power systems. In case of disruptions, the response time of the power system is quite small and the transmission line flows can be described by a steady-state approach. On the contrary, the gas flow in pipelines is a much slower process, with gas velocities below 15 m/s, resulting in a longer response time in case of disruptions. In particular, high-pressure transmission pipelines have much slower dynamics due to the large volumes of gas stored in pipelines. This quantity of gas cannot be neglected when simulating the dynamics in gas transmission systems; in fact the linepack in the pipeline increases the flexibility of the gas system to react to short term fluctuations in demand and supply. This information is important especially in the modelling stage, since different timing of the systems need to be considered during the simulation process.

Considering these aspects the following approach is adopted for developing the combined simulation model for assessing security of supply in interconnected gas and electricity transmission networks. Firstly, the complete models for the individual energy systems is developed, which includes sub models of the most important facilities and components,

that may play a vital role in the event of a disruption. Secondly, the individual models are integrated by identifying and modelling the most important interconnections between the two systems. Finally, parameters for quantifying the consequences of disruptions on security of supply are elaborated and applied to the integrated model to examine the impact of disruptions and the effectiveness of countermeasures to mitigate the consequences of such undesired events.

Gas System Model

The gas system model includes sub models for pipelines, compressor stations, regulator stations, valves, underground gas storage facilities, LNG regasification terminals and other entry and exit stations.

The pipeline model is based on the isothermal, one dimensional, transient hydraulic equations describing the gas flow in pipelines. It considers the basic physical properties of transport pipelines such as pressure drop, friction, gravity and inertia. The transient pipeline model is able to capture the pressure changes at entry and exit points of pipelines as well as the changes in linepack, i.e. the quantity of gas stored in pipelines at any instant of time.

Furthermore, the models for compressor stations and regulator stations consider the control modes and constraints that are inherently present in such automatic controlled facilities. The constraints are modelled as generic constraints reflecting the overall limits of all units and components in the respective facility. Some of the constraints that are considered are, for instance, the maximum discharge pressure, the minimum suction pressure, the maximum shaft and driver power and the maximum volumetric and mass flow rate constraints. The modelling of constraints are extremely important for security of supply studies, since these limits define whether the system may be able to cope with a disruption or not. Furthermore, the open or closed state of valve stations are also modelled as control modes.

In addition, the model for underground gas storage facilities considers the withdrawal and injection process as well as the available working gas inventory in the reservoir. The constraints of a storage facility is modelled by its storage envelope, which describes the operating region of the facility in terms of withdrawal/injection rate and working gas inventory. Different storage types, such as depleted gas fields, salt cavern or aquifer storages can be modelled by assigning the respective parameters for the storage envelope.

Moreover, the model for LNG regasification terminals takes the maximum regasification rate as well as the working gas inventory into account. Moreover, the arrival of LNG

vessels to the terminal can be modelled and scheduled considering the time and size of arriving vessels and the vessel discharge rate for relocating the LNG from the vessel to the storage tanks at the terminal. LNG regasification terminals as well as underground gas storage facilities can be assigned a flow rate or pressure control, which is respected as long as other facility constraints are not violated.

Finally, the model for exit and entry stations, such as production fields, GFPPs, city gate stations (CGS), cross border import /export stations, which are typically equipped with control devices such as control valves and meters, respects the maximum and minimum delivery pressure limits as well as the maximum supply limits, respectively. Each entry or exit station can be assigned a pressure or flow rate control, which is respected as long as constraints are not violated.

The individual sub models for each gas system facility are interconnected to a total gas system model by applying the integral form of the continuity equation, which yields a system of non-linear equations, which can be linearised and solved for a discretised spatio-temporal simulation grid using an implicit time integration method.

Development of a Simulation Tool

The gas simulation model is implemented into a simulation tool named **SAInt**, which enables the visualization of the gas network topology, the set up of scenarios, the execution of simulation models and the visualization of simulation results. **SAInt** is divided into two separate modules, namely, **SAInt-API** (Application Programming Interface) and **SAInt-GUI** (Graphical User Interface). The API, is the main library of the software and contains all solvers and classes for instantiating the different objects comprising the gas system model (nodes, pipes, compressors etc.). The API is independent of the GUI and can be used separately in other environments supporting .NET libraries (e.g. MS Excel, Visual Studio, IronPython etc.). **SAInt-GUI** is the graphical interface, which enables a visual communication between the API and the user. The GUI uses the classes and solvers provided by the API to perform the simulation tasks requested by the user.

Electricity System Model

The electric power system model is based on steady state AC-optimal power flow (AC-OPF) and includes sub models for the most important power system facilities such as transmission lines, transformers, buses, generation units, loads as well as shunt capacitors

and reactors. The basic AC-OPF model considers the active and reactive power balance for the entire network as well as the constraints of power system components such as the thermal capacity limits of transmission lines, the reactive power capability curves of generation units and the voltage limits at buses.

The basic AC-OPF model is extended by a model for dispatchable power system loads and transitional constraints, such as the maximum ramp rate and the start-up and shut-down times of generation units. The model for dispatchable power system loads enables the curtailment of power system loads based on predefined priority levels assigned to each power system customer.

Coupling of Gas and Electricity Systems

The gas and power system model are interconnected at gas fired power plants, electric driven compressor stations and LNG regasification terminals. Gas fired power plants represent generation units in the power system model and at the same time offtake points in the gas system. The energy transfer between both networks is described by a quadratic heat rate function and the gross calorific value of the extracted fuel gas. Electric driven compressor stations, in contrast, extract electric power from a load bus to increase the gas pressure for transportation. The extracted load is equivalent to the required driver power for compressing a quantity of natural gas from a given upstream pressure to a desired downstream pressure. The coupling at LNG regasification terminals is described by a quadratic function which yields the active power demand of the LNG terminal in respect to the regasification rate of the terminal.

Co-Simulation Framework for assessing Security of Supply

The transient gas simulation model, the basic AC-OPF model for electric power system and the coupling equations describing their physical interlink are integrated to develop a co-simulation framework for assessing security of supply in integrated gas and electricity transmission network. The co-simulation framework is divided into two separate simulation environments, namely, the gas system simulator (**SAInt**) and the power system simulator (**MATPOWER**). The communication and data exchange between **SAInt** and **MATPOWER** is established through an interface implemented into **SAInt** that makes

use of the Matlab Automation Server to execute Matlab scripts, to exchange input and output data with Matlab workspace variables and to enable the visualisation of power system topologies and simulation results. Furthermore, the co-simulation interface is responsible for respecting the coupling equations between both simulation models.

The co-simulation framework is applied to perform a case study on a realistic combined gas and power system network of an European region. The model application is divided into three different scenarios, where different gas and power system contingencies are studied. In the first scenario, the normal operation of the combined system with no disruptions is studied and the results are compared to the second scenario with gas side disruptions and the third scenario with power side disruptions.

The simulation results demonstrate, how disruptions triggered in one system propagate to the other system. In the second scenario, for instance, three major gas supply stations are disrupted and as a result a number of GFPPs are shut-down due to insufficient fuel gas pressure. This contingency propagates further to other buses in the power system, where load shedding is implemented in order to maintain the voltage levels above the minimum voltage threshold. Similar observations are made in scenario 2, where a drastic reduction in renewable energy generation together with a shut-down of a large power plant triggered a large increase in gas demand of GFPPs, leading to a rapid pressure drop in the gas network and the subsequent shut-down of GFPPs. Eventually, this circumstance increased the stress on the power system leading to minimum bus voltage violations in a couple of buses, which is remedied by applying load shedding at the affected buses.

Combined Simulation of Gas and Electricity Networks

The co-simulation framework, was able to capture the propagation of disruptions from one energy system to the other, however, there were a number of aspects that could not be reflected appropriately due to the nature of the model.

Firstly, the coupling between the two energy systems is simulated in two different simulation time frames, thus, there is no immediate feedback from one system as a result of a disruption in the other system. The power system is simulated for one operating day (24 hours) and the results computed for the gas fired generators are used for calculating the corresponding fuel gas offtakes in the gas system. The gas offtakes, in turn, are used to simulate the gas system and to check if the gas system can operate under these conditions in terms of pressure limits at delivery points. If pressure limits are violated the gas system curtails the computed fuel offtakes from the power system and the power system is simulated again using the fuel offtake constraints computed by the gas system and

additional power requirements of electric driven compressors and LNG terminals. The fuel offtake constraints computed by the gas system reduces the generation capacities in the power system, thus, power system loads are curtailed in order to balance the system. The above iteration is repeated until a feasible solution for both systems is found. In reality the changes in one system will have immediate effect on the physical properties (e.g. pressures, linepack, voltages, supply and demand), which may cascade back to the system where it originated. However, these cascading effects cannot be captured appropriately by a co-simulation concept, where the time frames between both systems are inherently different.

Secondly, the curtailment of power system loads are directly applied to buses that are affected by voltage violations based on a predefined rule. Priority levels between different power system customers are not considered, which may have an effect on the results. Finally, time transitional constraints of power system generators in terms of maximum ramp rates, start-up and shut down times are neglected, which may restrict the available generation capacities to balance the power system loads.

To overcome these deficiencies, a combined quasi-dynamic simulation model is developed and implemented into the simulation tool **SAInt**. The combined simulation model consists of the transient gas system model, the extended AC-OPF model and the coupling equations. The three model elements are integrated into one combined model, which is solved in a single simulation time frame and environment.

Furthermore, the two energy networks can interact with each other through conditional control mode definitions. Thus, the control logic of gas fired generators in the power system model could be designed based on the conditions in the gas system model. For instance, the start up and shut down of a gas fired power plant could be scheduled based on the pressure and linepack level in a specific section in the gas network model.

In order to quantify the impact of contingencies on security of supply, and to compare the effectiveness of different countermeasures to mitigate the impacts of disruptions on security of supply a number of security of supply parameters are defined, such as energy not supplied, percentage of energy not supplied and survival time.

The capabilities of the combined simulation model are demonstrated in a case study of a sample combined gas and power system network. The case study consists of three scenarios with gas and power side contingencies as well as mitigation measures to react to these disruptions.

In the first scenario, the operation of a gas generator is simulated, which serves as reserve and back up for variable and intermittent power generation from a wind turbine. In the second scenario a disruption in a gas compressor station is simulated which leads to

curtailments in the gas system and eventually to a delayed start up of the back up gas generator due to pressure restrictions in the gas system. The delayed start up of the gas generator caused a reduced generation capacity in the power system, which eventually leads to load curtailments in the power system based on a predefined priority level for each load bus. The impacts on security of supply in both energy systems are compared using the security of supply parameters. In terms of energy not supplied to customers, the impact of the disruption is higher for the gas system than for the power system. However, in terms of the ratio between energy not supplied and total scheduled energy supply (i.e. percentage of energy not supplied) the impact of the disruption is higher for the power system than for the gas system. Finally, in the last scenario the effectiveness of a countermeasure to mitigate the impact of the disruption in the gas compressor station is examined. The countermeasure involves the increase of the withdrawal rate from a neighbouring underground storage facility to maximum capacity if the linepack in the affected region goes below a specific value. Simulation results indicated a reduction of the impact on security of supply as a result of the implementation of the countermeasure.

Conclusion

The models and tools developed in this thesis demonstrate the importance of considering the interdependencies between gas and electricity systems when assessing the reliability of critical energy infrastructures. The information provided by the simulation models can be used to improve the coordination between gas and power system operators. For instance, gas and power system operators may develop strategies to coordinate and react to different contingencies affecting the reliability of the two systems. The developed strategies can be assessed using the simulation models and tools presented in this thesis to compare the effectiveness of different strategies and their potential vulnerabilities and bottlenecks. The estimation of consequences on security of supply computed by the developed models can also be used to perform a risk assessment of combined gas and power systems, which would enable the detection of potential risks affecting security of energy supply. The results from the risk assessment can be used to develop preventive action plans and emergency plans, which can also be tested using the simulation model.

Furthermore, the developed models can be used to address future research questions in the area of gas and power system interdependencies. One potential future research question concerns the integration and operation of P2G facilities in combined gas and electricity systems and how these facilities may impact the operation of the gas system if different gas qualities are injected at different locations.

Samenvatting

Achtergrond

De integratie van duurzame energie in bestaande energiesystemen vergroot de koppeling tussen die energiesystemen. Het besturen van gas- en elektriciteitsnetwerken is in toenemende mate onderling afhankelijk. Dit komt door het gebruik van gas gestookte centrales in elektriciteitsnetwerken en elektrisch aangedreven compressoren in gasnetwerken. Bovendien zullen nieuw opkomende technologieën zoals Power-to-Gas de koppeling tussen de energie netwerken verder vergroten.

Een gascentrale is enerzijds een bron van energie in het elektriciteitsnetwerk en anderzijds een gasleverantie in het gasnetwerk. Dankzij de flexibiliteit, manoeuvreerbaarheid en snelle inzetbaarheid worden gascentrales vooral gebruikt voor piekafvlakking en intermitterende duurzame energie bronnen.

Gascentrales hebben een minimale druk nodig om te kunnen functioneren. Als de druk van het brandstofafnamepunt in het gasnetwerk onder een minimum waarde dreigt te komen kan de levering gekort worden. In het ergste geval kan dit leiden tot afschakeling van de gascentrale, hetgeen van invloed is op de totale stroomvoorziening van een elektriciteitsnetwerk. Het is dus van groot belang te onderzoeken hoe de drukgrenzen in het gasnetwerk de besturing van gascentrales in het elektriciteitsnetwerk beïnvloeden.

Omgekeerd gebruiken elektrisch aangedreven compressoren vermogen van het elektriciteitsnetwerk om ten behoeve van gastransport de druk in leidingen op niveau te houden, teneinde tegemoet te komen aan de minimale druk op afleverpunten. Elektrisch aangedreven compressoren zijn vooral van belang als het gebruik van conventionele gas turbines beperkt is vanwege milieumaatregelen. Bovendien hebben elektrisch aangedreven compressoren een hoger mechanisch rendement, lagere gebruiks- en onderhoudskosten en zijn flexibeler en eenvoudiger te besturen dan conventionele gas turbines.

De groeiende onderlinge afhankelijkheid van gas- en elektriciteitsnetwerken staat in verband met energie leveringszekerheid: de ononderbroken levering van energie aan gebruikers, vooral onder moeilijke klimaatomstandigheden en onverwachte onderbrekingen. Een

onderbreking in één energie systeem kan een domino effect hebben in het andere systeem en weer terug slaan op het systeem waar het begon.

Als een duurzame energiebron plotseling uitvalt moet een gasgenerator snel ingezet worden met als gevolg toename van een brandstofvraag in het gasnetwerk met een er bij horende druk verlaging. Als deze lagere druk gecompenseerd wordt door een elektrisch aangedreven compressor vergt dit weer extra vermogen van het elektriciteitsnetwerk. Deze additionele vermogensvraag moet onder andere gecompenseerd worden door extra gasgeneratoren. Deze cirkelgang kan doorgaan totdat een evenwichtssituatie van het gekoppelde systeem is bereikt.

Bovenstaand voorbeeld laat zien dat het belangrijk is om de interactie tussen gas- en elektriciteitsystemen te onderzoeken en te begrijpen, hoe zij de besturing van beide systemen beïnvloeden en hoe knelpunten benaderd moeten worden. Tot nu toe werden gas en elektriciteitsystemen onafhankelijk van elkaar gestuurd hetgeen mogelijk was omdat beide systemen slechts zwak aan elkaar gekoppeld waren. Dit gold ook voor de mathematische modellen. Door de groeiende onderlinge afhankelijkheid tussen beide energie systemen groeit de noodzaak tot het gebruik van modellen waarmee beide systemen in een geïntegreerde manier beschouwd kunnen worden en waaraan de natuurkundige vergelijkingen van beide systemen ten grondslag liggen.

Onderzoeksvraag

Voor dit proefschrift zijn modellen ontwikkeld waarmee het sturen en de onderlinge afhankelijkheid van aardgas- en elektriciteitstransportnetwerken geanalyseerd kunnen worden in termen van leveringszekerheid. De ontwikkelde simulatie modellen zijn geïmplementeerd in een nieuw simulatie programma, genaamd SAInt – Scenario Analysis Interface for Energy Systems. SAInt is bedoeld ter ondersteuning van gas- en elektriciteitstransportbedrijven, toezichthouders van de energemarkt, energieconsultanten en -onderzoekers; teneinde de interactie tussen gas- en elektriciteitsnetwerken en de impact van verstoring van de leveringszekerheid in geïntegreerde systemen te kunnen onderzoeken. SAInt kan gebruikt worden om de belangrijkste onderzoeksvragen van dit proefschrift te beantwoorden, namelijk: hoe ernstig is een verstoring in het gas en/of het elektriciteit transport systeem en hoe effectief zijn de maatregelen om de impact van deze verstoringen te verhelpen.

Het beantwoorden van deze vragen vereist de ontwikkeling van wiskundige modellen die het natuurkundige gedrag en de beperkingen van het gas- en elektriciteitsysteem weer-spiegelen en de koppeling gestalte geven.

Methodologie

Bij het modelleren van de onderlinge afhankelijkheden van gas- en elektriciteitsystemen, zijn er verschillende aspecten waarmee rekening gehouden moet worden, vooral vanwege de verschillen in de structuur en de natuurkundige eigenschappen van beide systemen. De manier waarop beide systemen op fouten reageren is significant verschillend. Een technische fout in een elektriciteitssysteem kan resulteren in een uitval van een generator of elektriciteitsleiding. In extreme omstandigheden kan dit zelfs leiden tot leveringsproblemen vanwege domino effect [13]. Technische fouten in gas-systemen daarentegen (b.v. leiding breuk, storing bij compressorstation of bering) resulteren in lokale of regionale reductie van de netwerkcapaciteit en niet tot een volledige uitval. Deze capaciteitsreductie kan leiden tot een vermindering van gas levering op bases van een prioriteit. Een ander verschil tussen beide systemen is het dynamisch gedrag. Het transport van elektriciteit is instantaan en elektrische energie kan in de huidige generatie niet op grote schaal worden opgeslagen. Bij een onderbreking reageert een elektriciteitssysteem direct en kan de nieuwe situatie benaderd worden door een stabiele toestand. De gasstroom in leidingen, met snelheden lager dan 15 m/s, is daarentegen een veel langzamer proces het-geen bij een verstoring tot een langere reactietijd leidt. Voor hogedruktransportleidingen geldt dat zeker vanwege het grote volume aan gas dat in de leidingen opgeslagen is. Deze hoeveelheid gas kan niet verwarloosd worden als een gastransportsysteem dynamisch gesimuleerd wordt; in feite vergroot de leidingbuffer de flexibiliteit van het gastransport-systeem om te kunnen reageren op korte fluctuaties in vraag en aanbod. Deze informatie is belangrijk bij het modelleren, omdat de verschillen in dynamische respons meegenomen moeten worden in het simulatie proces.

Om tot een gecombineerd simulatiemodel te komen waarmee de leveringszekerheid van gekoppelde gas- en elektriciteitstransportnetwerken bepaald kan worden is met in acht name van het voorgaande de volgende benadering gevolg'd. Eerst zijn de complete modellen voor de individuele energie systemen ontwikkeld met inbegrip van de deel modellen van de componenten die een belangrijke rol spelen bij uitval. Vervolgens zijn de individuele modellen geïntegreerd door de koppelingen tussen beide systemen vorm te geven. Tenslotte worden in het geïntegreerde model verstoringen in het aanbod aangebracht om

de invloed van deze verstoringen en het effect van maatregelen om het effect van de verstoringen te lenigen, te onderzoeken.

Gas-systeem model

Het gas-systeem model bevat deelmodellen voor leidingen, compressorstations, reduceerstations, afsluiters, ondergrondse berging, LNG-hervergassingsinstallatie en andere voeding- en leveringstations. Het pijpleiding model is gebaseerd op de isotherme, één dimensionale dynamisch hydraulische vergelijking die de gasstroom in pijpleidingen beschrijft. Het betreft de basis natuurkundige eigenschappen van gastransport pijpleidingen zoals drukval, weerstand, zwaartekracht en massatraagheid. Het dynamische leiding model reageert op druk wisselingen aan beide zijden en houdt ook rekening met leiding-buffer: de hoeveelheid gas opgeslagen in de pijp op een zeker moment. Verder nemen de modellen voor compressor en reduceer stations, de besturingsmodus en het regelbereik in aanmerking, die wezenlijk zijn bij een automatische regelaar. Het regelbereik is gemodelleerd in termen van grenzen op de variabelen van het betreffende onderdeel. De grenzen zijn bijvoorbeeld: maximum uitlaatdruk, minimum inlaatdruk, maximum as- en aandrijfvermogen en maximum volume- en massa stroom. Het modelleren van deze grenzen is buitengewoon belangrijk voor leveringszekerheid studies, daar deze grenzen bepalend zijn of het systeem om kan gaan met een verstoring of niet. Verder zijn de toestand open en dicht van afsluiterstations ook gemodelleerd als besturingsmodi.

Het model voor ondergrondse gasopslag houdt rekening met het injectie- en zendproces, en de hoeveelheid opgeslagen gas in de berging. De beperkingen van injectie- en zendstroom wordt gemodelleerd middels een contour die de operationele mogelijkheden aangeeft in termen van injectie- en zendstroom en vulling. Verschillende buffer-types, zoals uitgeputte gasvelden, zoutcavernes of aquiferopslag kunnen gemodelleerd worden middels parameters van de contour. De LNG-hervergassingsinstallatie neemt ook de maximum hervergassingstroom en het werkgasvolume mee. Het arriveren van LNG schepen kan worden ingepland waarbij de aankomst-tijd en de grootte van het schip en de maximale ontlaadstroom van het schip naar de terminal, meegegenomen wordt. LNG-hervergassingsinstallaties en ondergrondse bergen kunnen gestuurd worden op druk- of gasstroom zolang de andere stationsgrenzen niet overschreven worden. Er zijn voedings- en leveringstations zoals: productie velden, gascentrales, stadslevering en import en export stations, waarvan de laatste meestal uitgevoerd zijn met reduceers en gasstroom meters. De druk bij deze stations moet binnen grenzen blijven en ook de stroom is beperkt. Voeding- en leveringstations zijn gestuurd op druk- of gasstroom zolang de stationsgrenzen

niet overschreden worden. De individuele deelmodellen zijn met elkaar verbonden tot een totaal gas-systeemmodel door toepassing van de integrale vorm van de continuïteitsvergelijking. Door plaats-discretisatie verkrijgt men een verzameling differentiaalvergelijkingen in tijd. Deze kunnen opgelost worden met een impliciete tijdsintegratiemethode. Het dan verkregen stelsel niet lineaire vergelijkingen kan iteratief opgelost worden waarbij er bij iedere iteratie gelineariseerd wordt.

Ontwikkeling van de simulator

Het gas-simulatiemodel is vorm gegeven in het simulatieprogramma met de naam SAInt (Scenario Analysis Interface for Energy Systems). Met SAInt kan het netwerk gevisualiseerd worden, er kunnen scenario's opgesteld worden en een netwerk met een scenario kan doorgerekend worden, waarbij de resultaten getoond worden. SAInt is opgedeeld in twee modules, SAInt-API (Application Programming Interface) en SAInt-GUI (Graphical User Interface). De API is de hoofd bibliotheek met modules voor het oplossen van al de vergelijkingen op netwerk niveau en voor de verschillende onderdelen (knooppunten, leidingen, compressors, enz.). De API is onafhankelijk van de GUI en kan afzonderlijk gebruikt worden in andere .NET omgevingen (b.v. MS Excel, Visual Studio, IronPython, enz.). SAInt-GUI is de grafische gebruikersomgeving waarmee de gebruiker op een visuele manier de API kan gebruiken. De GUI gebruikt de modules van de API om door de gebruiker gewenste simulaties uit te voeren.

Elektrisch systeem model

Het model van het elektrische systeem is gebaseerd op optimale wisselstroom netwerk berekening met de naam AC-OPF (AC-optimal power flow). AC-OPF bevat deelmodellen voor de belangrijkste onderdelen zoals elektriciteitsleidingen, transformatoren, knooppunten, generatoren, leveringen en tevens capacitieve en reactieve belastingen. Het basis AC-OPF model voldoet aan de actieve en reactieve vermogenbalans. De beperkingen van de elektriciteitsleidingen, reactief vermogen contouren van de generatoren en spanningen op knooppunten worden meegenomen. Het basis AC-OPF model is uitgebreid met afschakelbare leveringen en overgangsbeperkingen zoals maximale toenamesnelheid en de benodigde tijd om aan of uit te zetten. Het model voor afschakelbare leveringen maakt het mogelijk dat leveringen gekort worden op basis van individuele prioriteiten.

Koppeling van het gas- en elektriciteitssysteem

De modellen van het gas- en elektriciteitsysteem zijn aan elkaar gekoppeld via gascentrales, elektrisch aangedreven compressoren en LNG hervergassingsinstallaties. Een gascentrale is tegelijkertijd een generator in het elektriciteitsysteem en een gaslevering vanuit het gas-systeem. De gaslevering in termen van chemische vermogen is een kwadratische functie van het generator vermogen. Omgekeerd is een elektrisch aangedreven compressor, die de druk voor transport in het gas-systeem verhoogt, een levering vanuit het elektrische systeem. Het geleverde elektrische vermogen is equivalent aan het gevraagde vermogen om een gas-stroom van de inlaat druk tot de uitlaatdruk te brengen. De koppeling via de LNG hervergassingsinstallatie wordt beschreven met een kwadratische functie die aangeeft hoe het elektrisch vermogen afhangt van de hervergassings-stroom van de LNG-installatie.

Co-Simulatie raamwerk om de leveringszekerheid vast te stellen

Door het dynamische gas-simulatiemodel en het AC-OPF model voor een elektrische systemen en de koppelingsvergelijkingen samen te voegen ontstaat een raamwerk waarmee de leveringszekerheid van een geïntegreerd gas- en elektriciteitsysteem kan worden vastgesteld. Het co-simulatie raamwerk bestaat uit twee gesepareerde omgevingen, te weten de gassimulator (SAInt) en de simulator voor het elektrische systeem (MATPOWER). De communicatie en data uitwisseling tussen SAInt en MATPOWER is vorm gegeven middels een koppeling die geïmplementeerd is in SAInt en gebruik maakt van de "Matlab Automation Server". Hiermee worden MATLAB commando's uitgevoerd, data uitgewisseld middels "Matlab workspace variables" en is het mogelijk de topologie van een elektriciteitsnetwerk en de simulatieresultaten weer te geven. Deze co-simulatie koppeling zorgt ook voor de koppelingsvergelijkingen tussen beide simulatie modellen. Met het co-simulatie raamwerk is het mogelijk een casus te bestuderen van een gecombineerd gas- en elektriciteitsnetwerk van een Europese regio. Om het effect van onvoorzien omstandigheden te onderzoeken worden drie verschillende scenario's doorgerekend. Het eerste scenario komt overeen met normale sturing zonder uitval. De resultaten daarvan kunnen dienen ter vergelijk met die van het tweede scenario met gas uitval en derde scenario met elektrische uitval. De resultaten van de simulatie tonen aan hoe een verstoring in één systeem doordringt in het andere systeem. In het tweede scenario worden bij voorbeeld drie grote gasvoedingstations afgeschakeld zodat een aantal gascentrales automatisch uitgaan, vanwege onvoldoende druk op het brandstofgas punt. Deze verstoring zet zich door in andere knooppunten van het elektriciteitssysteem met als gevolg dat elektriciteitsleveringen gekort worden teneinde de spanning op die knooppunten niet onderuit te laten

gaan. Gelijksoortige verschijnselen zijn opgetreden bij het derde scenario waar het wegvalLEN van duurzame energie en het afschakelen van een grote elektriciteitscentrale er toe leiden dat een gascentrale moet opschakelen, hetgeen op zijn beurt er weer toe leidt dat de druk in het gas-systeem onderuitgaat, met als gevolg dat gascentrales uitgeschakeld worden. De belasting van het elektriciteitsysteem kan er zelfs toe leiden dat de spanning in knooppunten te laag zouden worden hetgeen voorkomen wordt door de leveringen op die knooppunten te korten.

Gecombineerde simulatie van Gas- en Elektriciteitsnetwerken

Met het co-simulatie raamwerk kan de verbreiding van een verstoring van het ene energiesysteem naar het andere vorm gegeven worden. Vanwege de opzet van het framework zijn er echter een aantal aspecten die niet goed doorwerken. Er is geen directe terugkoppeling tussen beide energie systemen omdat de simulaties separaat worden uitgevoerd. Het elektriciteitsysteem wordt gesimuleerd over een dag (24 uur) en de vermogens van de gascentrales worden gebruikt om de brandstoflevering uit het gassysteem te berekenen. Deze gasleveringen worden op hun beurt weer gebruikt bij de simulatie van het gas-systeem om te kunnen testen of de druk op afleverpunten binnen de grenzen blijft. Als druk op deze afleverpunten onderuit dreigt te gaan worden de brandstofleveringen in het gas-systeem gekort. Bij een volgende simulatie van het elektriciteitsysteem zijn de generatoren minder inzetbaar vanwege lagere brandstof stromen en worden de berekende vermogensten behoeve van elektrisch aangedreven compressoren en LNG installaties gebruikt. De beperkingen die voortvloeien uit een gas-systeemsimulatie reduceren de capaciteit van de generatoren in het elektriciteitsysteem met als gevolg dat leveringen van het elektriciteitssysteem gekort worden om het systeem in balans te houden. Het bovenstaande wordt herhaald tot er een aanvaardbare oplossing is gevonden voor beide systemen.

In werkelijkheid hebben de veranderingen in één systeem onmiddellijk effect of de waarden van de variabelen in het andere systeem (b.v. druk, leidingbuffer, spanning, voeding en levering) hetgeen direct terug kan slaan op het systeem waar de verandering begon. Dit domino-effect kan niet adequaat met co-simulatie behandeld worden, omdat het separate simulaties zijn. Een ander punt is dat het korten van leveringen van het elektriciteitsysteem direct plaats vindt bij knooppunten waarbij de spanning onderuit dreigt te gaan. Onderlinge prioriteiten tussen leveringen van het elektriciteitsysteem worden niet meegenomen. Ten slotte worden overgangsbegrenzingen van elektrische generatoren, zoals opschakeltijd en de tijd nodig om aan en uit te zetten niet meegenomen, waardoor de beschikbare generatorcapaciteit overschat wordt.

Om aan deze bezwaren tegemoet te komen is een quasi-dynamisch simulatiemodel ontwikkeld en geïmplementeerd in SAInt. Het gecombineerde simulatiemodel bestaat uit het dynamische gas-systeem-model, het uitgebreide AC-OPF model en de koppelingsvergelijkingen. Deze drie model elementen zijn geïntegreerd in een gecombineerd model met gemeenschappelijke tijdstappen.

Bovendien kunnen de beide systemen op elkaar reageren op basis van vooraf gestelde voorwaarde. De besturing van een gasgenerator in het elektriciteitsysteem kan afhankelijk zijn van de toestand in het gas-systeem. Het opstarten of uitschakelen van een gascentrale kan bij voorbeeld gebaseerd zijn op het volume in een leidingbuffer.

Leveringszekerheidparameters kunnen gedefinieerd worden, zoals absolute of relatieve niet geleverde energie of overlevingstijd. Hiermee kan de invloed van een verstoring gemeten worden en het effect van maatregelen om de verstoring te verhelpen. De mogelijkheden van gecombineerde simulatie wordt duidelijk gemaakt aan de hand van een casus van een gecombineerd gas- en elektriciteitsnetwerk. De casus bestaat uit drie scenario's met verstoringen en maatregelen om de verstoringen te verhelpen.

In het eerste scenario wordt een gasgenerator gesimuleerd die als reserve staat en als back-up fungeert voor variërende en uitvallende elektriciteit gegenereerd door een windturbine. In het tweede scenario wordt uitval van een gascompressor gesimuleerd wat leidt tot verminderde leveranties vanuit het gas-systeem en mogelijk tot een vertraagde start van een back-up generator vanwege drukbeperkingen in het gas-systeem. Deze vertraagde start van de gasgenerator zorgt ervoor dat het totaal opgewekte vermogen beperkt is wat aanleiding kan geven tot beperkingen van leveringen op basis van prioriteiten.

De invloed op de leveringszekerheid per systeem wordt vergeleken met behulp van de leveringszekerheidsparameters. In termen van niet geleverd vermogen is de invloed van een verstoring groter voor het gas-systeem dan voor het elektriciteitsysteem. De relatieve invloed van een verstoring is echter groter in het elektriciteitsysteem dan in het gas-systeem. Ten slotte wordt in het laatste scenario de effectiviteit van maatregelen om een verstoring van een gascompressor station te verhelpen, bekeken. Als maatregel wordt de zendcapaciteit van een naburige berging maximaal ingezet als het leidingbuffervolume van de door de compressor belevereide regio beneden een bepaalde waarde komt. De simulatie resultaten tonen aan dat de invloed van verstoringen door de genomen maatregelen beperkt kunnen worden.

Conclusie

Met de modellen en programma's uit dit proefschrift is het belang aangetoond om de wederzijdse afhankelijkheden tussen gas- en elektriciteitsystemen mee te nemen als men de betrouwbaarheid van deze kritische infrastructuren wil kunnen inschatten. De informatie die men met deze modellen verkrijgt kan gebruikt worden om de coördinatie tussen gas- en elektriciteitsstelseloperators te kunnen verbeteren. Gas- en elektriciteitsstelseloperators kunnen bij voorbeeld een strategie ontwikkelen om samen te werken bij een reactie op verstoringen die effect hebben op beide systemen. Strategieën kunnen ontwikkeld worden met behulp van de simulatiemodellen en programma's die in dit proefschrift ontwikkeld zijn, en de effectiviteit, risico's en knelpunten kunnen vergeleken worden. De ingeschatte gevolgen op de leveringszekerheid, die met deze modellen berekend zijn, kunnen ook gebruikt worden voor risicoanalyse van gecombineerde systemen zodat potentiële risico's ten aanzien van leveringszekerheid duidelijk worden. De resultaten van een risicoanalyse kunnen gebruikt worden om preventieve acties en noodplannen te ontwikkelen die weer getest kunnen worden met het simulatie model. Bovendien kunnen de ontwikkelde modellen gebruikt worden om toekomstige vraagstukken op het gebied van wederzijdse afhankelijkheden van gas- en elektriciteitsstelselen te beantwoorden. Eén van deze vraagstukken betreft Power-to-Gas. Hoe moeten deze installaties ingezet en bestuurd worden in een geïntegreerd gas- en elektriciteitsstelsel en wat is de invloed als er gasinjecties zijn met verschillende kwaliteiten op verschillende punten.

List of Publications

Peer-Reviewed Journal Articles

- K. A. Pambour, R. T. Sopgwı, B.-M. Hodge, and C. Brancucci, “**The Value of Day-Ahead Coordination of Power and Natural Gas Network Operations**,” in *Energies*, vol. 11, no. 7, pp. 1628, 2018.
- K. A. Pambour, B. Cakir Erdener, R. Bolado-Lavin, and G. P. Dijkema, “**SAInt - A novel quasi-dynamic Model for assessing Security of Supply in coupled Gas and Electricity Transmission Networks**,” in *Applied Energy*, vol. 203, pp. 829 – 857, 2017.
- K. A. Pambour, B. Cakir Erdener, R. Bolado-Lavin, and G. P. Dijkema, “**Development of a simulation framework for analyzing Security of Supply in integrated gas and electricity systems**,” *Applied Sciences*, vol. 7, no. 1, pp. 47, 2017.
- K. A. Pambour, R. Bolado-Lavin, and G. P. Dijkema, “**An integrated transient model for simulating the operation of natural gas transport systems**,” in *Journal of Natural Gas Science and Engineering*, vol. 28, pp. 672 – 690, 2016.
- B. Cakir Erdener, K. A. Pambour, R. B. Lavin, and B. Dengiz, “**An integrated simulation model for analysing electricity and gas systems**,” in *International Journal of Electrical Power & Energy Systems*, vol. 61, no. 0, pp. 410 – 420, 2014.

Peer-Reviewed Conference Paper

- K. A. Pambour, B. Cakir Erdener, R. Bolado-Lavin, and G. P. J. Dijkema, “**An integrated simulation tool for analyzing the operation and interdependency of natural gas and electric power systems**,” in *Pipeline Simulation Interest Group (PSIG) Conference 2016*.

Conference Papers

- K. A. Pambour, R. Bolado-Lavin, and G. P. Dijkema, “**SAInt – A simulation tool for analysing the consequences of natural gas supply disruptions**,” in *Pipeline Technology Conference (PTC) 2016*.
- N. Zaccarelli, N. Rodríguez-Gomez, K. A. Pambour, R. Bolado-Lavin, “**Towards EUGas-26: The European gas assessment model for EU Directive 2008/14/EC and EU regulation no 994/2010**,” in *International Gas Union Research Conference 2014*.
- N. Rodríguez-Gomez, N. Zaccarelli, K. A. Pambour, R. Bolado-Lavin, “**Scenario analysis of gas crisis using the European Gas Assessment Model (EU-Gas)**,” in *International Gas Union Research Conference 2014*.

Science and Policy Reports

- B. Cakir Erdener, K. A. Pambour, R. Bolado-Lavin, “**Interdependencies between Natural Gas and Power - Development of a Strategy for Modelling Interdependencies**,” in *European Union - JRC Science Hub, 2015*.
- B. Cakir Erdener, K. A. Pambour, R. Bolado-Lavin, “**Interdependencies between Natural Gas and Power - Scenario Analysis and Recommendations to MS**,” in *European Union - JRC Science Hub, 2015*.

Author Biography

Kwabena Addo Pambour was born on December 13, 1983 in Accra, Ghana. In August 1992, he moved to city of Essen in Germany, where he attended primary school at Krainbruch Grundschule Essen-Dellwig, and secondary and high school at [Gesamtschule Essen-Borbeck](#). In June 2003 he graduated from high school and joined the German military to complete his nine month national military service with the 3. Wachbataillon BMVg located in Siegburg/Bonn, Germany. After his military service, he was awarded a six year scholarship by [Evangelisches Studienwerk e.V. Villigst](#) for his achievements in high school (Abitur) and his engagement in the Pentecostal Church Community.

In October 2014, he started studying Mechanical Engineering at [Ruhr-University in Bochum](#), Germany and continued his studies in October 2006 at [RWTH Aachen University](#), in Aachen, Germany, where he specialized in Aeronautical Engineering. From September 2007 to June 2008, he completed part of his studies in a study-abroad program at [University of California, Davis](#), United States (UC Davis), which was sponsored by [Evangelisches Studienwerk e.V. Villigst](#).

After his study-abroad, he continued his studies at [RWTH Aachen University](#), where he graduated with the German degree Diplom-Ingenieur in Mechanical Engineering (Dipl.-Ing., equivalent to M.Sc.) in June 2010. In June 2011, he was awarded the prestigious [Springorum-Medal](#) by [RWTH Aachen University](#). In parallel, Kwabena studied Business Administration at [RWTH Aachen University](#), which he completed in September 2011 with the German degree Diplom-Wirtschaftsingenieur (Dipl.- Wirt.Ing., equivalent to MBA).

After his studies, he was employed by the [European Commission \(EC\) - Joint Research Centre \(JRC\) - Directorate \(C\) for Energy, Transport and Climate](#), in Petten, the Netherlands, from May 2011 to May 2014 as a scientific researcher to conduct research in the area of security of energy supply. After his employment at [EC-JRC](#), he worked as a software consultant and engineer for [LIWACOM](#), the vendor of the gas network simulation software [SIMONE](#).

In December 2014, he started his PhD research as an external PhD student at [University of Groningen](#), the Netherlands, in the [Energy and Sustainability Research Institute](#) of the Faculty of Science and Engineering.

In January 2017, Kwabena founded [cleaNRGi Solutions GmbH](#), a energy startup devoted to providing software and engineering solutions to the challenges connected to the integration of renewable energy sources into existing energy infrastructures.

During his research, Kwabena developed the simulation software [SAInt](#), which is used by the [EC-JRC](#), the [National Renewable Energy Laboratory \(NREL\)](#), situated in Golden, Colorado, USA and many other organisations. Furthermore, he wrote and presented several papers at international conferences. He published five peer-reviewed journal articles and a peer-reviewed conference paper.